

**UNIVERSIDADE DE SÃO PAULO
INSTITUTO DE QUÍMICA**

Programa de Pós-Graduação em Ciências Biológicas (Bioquímica)

ERICH BIRELLI TAHARA

**Influência da Restrição Calórica no Metabolismo
Bioenergético e Estado Redox de *Saccharomyces
cerevisiae* e *Kluyveromyces lactis***

Versão original da Tese defendida

São Paulo

Data do Depósito na SPG:
09/12/2011

ERICH BIRELLI TAHARA

**Influência da Restrição Calórica no Metabolismo
Bioenergético e Estado Redox de *Saccharomyces
cerevisiae* e *Kluyveromyces lactis***

Tese apresentada ao Instituto de Química da
Universidade de São Paulo para obtenção do Título de
Doutor em Ciências (Bioquímica)

Orientadora: Prof^a. Dr^a. Alicia Juliana Kowaltowski

Co-orientador: Mario Henrique de Barros

São Paulo

2011

Para meu pai, Koya Tahara, e minha mãe, Olivia Birelli Tahara, com todo meu amor e a mais afetuosa gratidão.

AGRADECIMENTOS

À minha orientadora, Prof^a Alicia Juliana Kowaltowski – que em um dia de fevereiro de 2003 aceitou em seu laboratório um jovem cheio de dúvidas e sonhos – pela atenção, amizade e, sobretudo, paciência ao longo de quase uma década.

Ao Prof. Mario Henrique de Barros, que em outro dia do mesmo mês, do mesmo ano, apresentou ao mesmo jovem cheio de dúvidas e sonhos o fascinante mundo das leveduras – o mundo delas, e o meu também, nunca mais seriam os mesmos. (Aliás, o mundo do Mario também não.)

Ao Prof. Luis Eduardo Soares Netto, Prof^a. Gisele Monteiro de Souza e Simone Vidigal Alves, pela ajuda com o protocolo de quantificação de glutatona e com os mutantes de *S. cerevisiae*.

À Profa. Nadja Cristhina de Souza-Pinto e ao Prof. José Ribamar dos Santos Ferreira Júnior pelo suporte, atenção e pelas frutíferas conversas sobre DNA mitocondrial.

Ao Prof. Andreas Karoly Gombert, Thiago Olitta Basso e Bianca Eli Della Bianca, pela inestimável ajuda com as quantificações dos metabólitos extracelulares de *S. cerevisiae*.

À Prof^a. Sayuri Miyamoto, Priscilla Bento Matos Cruz Derogis e Tatiana Harumi Yamaguti pelo excelente tratamento dispensado a mim desde o início de nossa colaboração.

Ao Prof. Frederico José Gueiros Filho, por também ter-me permitido utilizar as dependências de seu laboratório, e à Theopi Varvakis Rados pela incomparável ajuda com a aquisição das imagens de mitocôndrias de *S. cerevisiae*.

À Prof^a Iolanda Midea Cuccovia, à Prof^a Clélia Terra e ao Prof. Bayardo Baptista Torres, responsáveis pela disciplina de Bioquímica na minha graduação.

Ao Prof. Francisco Rafael Martins Laurindo e à Dra. Denise de Castro Fernandes.

À Prof^a. Patrícia Fernanda Schuck;

Ao pessoal da Secretaria da Pós-Graduação, da Secretaria do Departamento de Bioquímica e da Secretaria da Sociedade Brasileira de Bioquímica e Biologia Molecular.

À Camille Caldeira Ortiz, Edson Alves Gomes e Doris Dias Araújo pela amizade e excelente apoio técnico.

Aos meus tantos amigos de laboratório, em ordem (quase) cronológica: Renato Ferranti, Eduardo Belisle, Miriam Mateus da Silva, Dino Gabrielli Santesso, Douglas Vasconcelos Cancherini, Juliana Gabriela de Paula, Heberty Di Tarso Fernandes Facundo, Raquel de Sousa Carreira, Maynara Fornazari, Bruno Barros Queliconi, Ariel Rodrigues Cardoso, Fernanda Menezes Cerqueira, João Victor Cabral Costa, Fabiana Dutra Esquivel, Bruno Chaussê de Freitas, Thire Baggio Marazzi, Phillippe Pessoa de Santana e Luis Alberto Luévano Martínez. Em especial, à Graciele Almeida de Oliveira, Felipe Donizeti Teston Navarete, Kizzy Cezário e Norton Felipe dos Santos Silva pela ajuda com inúmeros experimentos.

Também, não menos especialmente, à Profª. Fernanda Marques da Cunha, pela preciosa amizade e atenção.

Aos amigos espalhados pela Universidade de São Paulo: Julio Henrique Kravcuks Rozenfeld, Cleverson Busso, Viviane Cristina dos Santos Carmo Baptista, Mariana Alba Zampol, Fernando Gomes, Mateus Prates Mori, Carolina Domeniche Romagna, Renata Fernandes de Campos, Paulo Newton Tonolli, Amanda Rabelo Crisma, Karina Nakajima, Anderson Arndt, Lilian de Carvalho, Indrani Majumder.

Aos amigos espalhados fora da Universidade de São Paulo (porque também há vida fora dela): Fabio Gonçalves Monteiro, Adilson de Oliveira Coelho, Audrey Navarro Pulice, Rodrigo Benha, Luciana Benha, Natália Moreno Conceição, Cintia Kawai, Ederson Cristiano Correia, Sonia Correia, Silvana Faria de Almeida, Simone Faria de Almeida.

E também aos amigos que foram aqui cruelmente esquecidos.

À Fundação de Amparo à Pesquisa do Estado de São Paulo pelo financiamento concedido, e também ao Conselho Nacional de Desenvolvimento Científico e Tecnológico e à John Simon Guggenheim Foundation.

E à Deus, pelo dom da vida e pelo amor sem igual.

*O poeta é um fingidor.
Finge tão completamente
Que chega a fingir que é dor
A dor que deveras sente.*

*E os que lêem o que escreve,
Na dor lida sentem bem,
Não as duas que ele teve,
Mas só a que eles não têm.*

*E assim nas calhas de roda
Gira, a entreter a razão,
Esse comboio de corda
Que se chama coração.*

Fernando Pessoa (1888 – 1935)

RESUMO

Tahara, E.B. **Influência da Restrição Calórica no Metabolismo Bioenergético e Estado Redox de *Saccharomyces cerevisiae* e *Kluyveromyces lactis*.** 2011. 94p. Tese - Programa de Pós-Graduação em Bioquímica. Instituto de Química, Universidade de São Paulo, São Paulo.

O envelhecimento envolve um progressivo declínio na eficiência metabólica dos sistemas biológicos ao longo do tempo. Embora não possa ser evitado, o envelhecimento pode ter seus fenótipos típicos mitigados em organismos submetidos à restrição calórica, um regime dietético que consiste em uma oferta diminuída de calorias. Ao longo do tempo, a levedura *Saccharomyces cerevisiae* mostrou-se um importante organismo modelo para o estudo de importantes marcas relacionadas ao envelhecimento, sobretudo por ser responsável à restrição calórica. Através de uma abordagem do metabolismo energético e do estado de óxido-redução celular, nós temos buscado identificar quais são os fatores imprescindíveis para a exibição do aumento do tempo de vida cronológico dessa levedura. Nós verificamos que defeitos específicos na síntese de nicotinamida adenina dinucleotídeo aumentam a geração mitocondrial de espécies reativas de oxigênio pela enzima dihidrolipoil desidrogenase, porém não suprimem o aumento da taxa de perda do DNA mitocondrial de *S. cerevisiae*. Por outro lado, os mutantes dessa levedura irreponsáveis à restrição calórica são aqueles que possuem defeitos no metabolismo aeróbico, mais especificamente na montagem da cadeia de transporte de elétrons. Também verificamos que diferentes mutações em enzimas do ciclo dos ácidos tricarboxílicos alteram a taxa de perda do DNA mitocondrial de *S. cerevisiae* numa forma dependente da concentração inicial de glicose nos meios de cultura e também do tempo de cultivo. Também observamos que a eficiência energética em *S. cerevisiae* cultivada sob restrição calórica é aumentada em relação à levedura cultivada em condição controle. Finalmente, também observamos que a morfologia mitocondrial é alterada pelo estado metabólico celular e se correlaciona com a geração de espécies reativas de oxigênio nesse organismo. Assim sendo, em conjunto, esses dados revelam importantes modificações metabólicas e no estado de óxido redução proporcionadas pela restrição calórica e como os fenótipos típicos do envelhecimento podem ser mitigados em *S. cerevisiae*, assim como quais são os fatores imprescindíveis para a resposta dessa levedura à restrição calórica.

Palavras-chave: *Saccharomyces cerevisiae*; metabolismo; mitocôndria; envelhecimento; restrição calórica.

ABSTRACT

Tahara, E.B. **Influence of Caloric Restriction on Energy Metabolism and Redox State of *Saccharomyces cerevisiae* e *Kluyveromyces lactis*.** 2011. 94p. PhD Thesis. Graduate Program in Biochemistry. Instituto de Química, Universidade de São Paulo, São Paulo.

Aging involves a progressive decline in metabolic efficiency of biological systems over time. Although it cannot be avoided, aging phenotypes are delayed in organisms undergoing caloric restriction, a dietary regimen consisting of a reduced availability of calories. The yeast *Saccharomyces cerevisiae* has proved to be an important model organism for studying important characteristics related to aging, and is responsive to caloric restriction. We sought to identify factors essential for increased chronological lifespan in yeast by investigating changes in energy metabolism and redox state. We found that defects in the synthesis of nicotinamide adenine dinucleotide increased mitochondrial generation of reactive oxygen species by the enzyme dihidrolipoil dehydrogenase, but did not suppress the increase in chronological life span. On the other hand, mutants of this yeast which do not respond to caloric restriction are those that have defects in aerobic metabolism, specifically in the assembly of the electron transport chain. We also found that different mutations in enzymes of the citric acid cycle alter the rate of loss of mitochondrial in a manner dependent on the initial concentration of glucose in culture media and culture time. We also observed that energy efficiency in *S. cerevisiae* grown under caloric restriction is increased compared to yeast grown under control conditions. Finally, we also observed that mitochondrial morphology is altered by the cellular metabolic state and correlates with the generation of reactive oxygen species in this organism. Thus, altogether, these data reveal significant changes in metabolism and redox state promoted by caloric restriction, how phenotypes typical of aging can be prevented in *S. cerevisiae*, as well as what factors are required for the response of yeast to caloric restriction.

Keywords: *Saccharomyces cerevisiae*, metabolism, mitochondria, aging, calorie restriction.

ÍNDICE DE ILUSTRAÇÕES

Figura 1. 1. Tempo de vida cronológico de <i>S. cerevisiae</i> WT, <i>npt1Δ</i> e <i>bna6Δ</i>	20
Figura 1. 2. Consumo de oxigênio induzido por substratos exógenos em <i>S. cerevisiae</i> WT, <i>npt1Δ</i> e <i>bna6Δ</i>	22
Figura 1. 3. Liberação de peróxido de hidrogênio induzida por substratos exógenos em <i>S. cerevisiae</i> WT, <i>npt1Δ</i> e <i>bna6Δ</i>	23
Figura 1. 4. Estado de óxido-redução da glutationa em <i>S. cerevisiae</i> WT, <i>npt1Δ</i> e <i>bna6Δ</i>	24
Figura 1. 5. Consumo de oxigênio e liberação de peróxido de hidrogênio induzidos por substratos exógenos em <i>S. cerevisiae</i> WT, <i>npt1Δlpd1D</i> e <i>bna6Δlpd1D</i>	26
Figura 2. 1. Tempo de vida cronológico de <i>S. cerevisiae</i> <i>lpd1Δ</i> , <i>npt1Δlpd1Δ</i> e <i>bna6Δlpd1Δ</i>	30
Figura 2. 2. Tempo de vida cronológico de <i>S. cerevisiae</i> <i>aco1Δ</i> , <i>kgd1Δ</i> e <i>sdh1Δ</i>	32
Figura 2. 3. Tempo de vida cronológico de <i>S. cerevisiae</i> ρ^0 e <i>abf2Δ</i>	34
Figura 2. 4. Tempo de vida cronológico de <i>S. cerevisiae</i> <i>cyt1Δ</i>	35
Figura 2. 5. Tempo de vida cronológico de <i>S. cerevisiae</i> <i>atp2Δ</i>	37
Figura 2. 6. Capacidade de crescimento em meio seletivo rico e meio seletivo sintético para respiração.....	38
Figura 2. 7. Progressão temporal da porcentagem de células respiratório-competentes durante o envelhecimento cronológico de <i>S. cerevisiae</i> WT, <i>aco1Δ</i> , <i>kgd1Δ</i> , <i>lpd1Δ</i> e <i>sdh1Δ</i>	41
Figura 2. 8. Tempo de vida cronológico de <i>K. lactis</i>	43
Figura 3. 1. Consumo de oxigênio ao longo do tempo de vida cronológico em <i>S. cerevisiae</i> WT.....	47
Figura 3. 2. Curvas de biomassa ao longo do tempo de vida cronológico de <i>S. cerevisiae</i> WT e ρ^0	48
Figura 3. 3. Curvas de pH extracelular ao longo do tempo de vida cronológico de <i>S. cerevisiae</i> WT e ρ^0	49
Figura 3. 4. Curvas de exaustão de glicose, e de formação e exaustão de etanol, glicerol, acetato, piruvato e succinato ao longo do tempo de vida cronológico de <i>S. cerevisiae</i> WT.	50
Figura 3. 5. Curvas de exaustão de glicose, e de formação e exaustão de etanol, glicerol, acetato, piruvato e succinato ao longo do tempo de vida cronológico de <i>S. cerevisiae</i> ρ^0	51
Figura 3. 6. Velocidade específica máxima de crescimento celular em glicose e velocidade específica máxima de consumo de glicose em <i>S. cerevisiae</i> WT e ρ^0	52
Figura 3. 7. Fator de conversão de glicose a células, de glicose a etanol e de glicose a glicerol em <i>S. cerevisiae</i> WT e ρ^0	54
Figura 3. 8. Velocidades específicas máximas de formação de etanol, de crescimento celular em etanol, de consumo de etanol e fator de conversão de etanol a células em <i>S. cerevisiae</i> WT e ρ^0	55
Figura 3. 9. Velocidade específica máxima de crescimento celular de <i>S. cerevisiae</i> WT em etanol e glicerol.....	56
Figura 4. 1. Liberação de peróxido de hidrogênio induzida por substratos exógenos ao longo do tempo de vida cronológico de <i>S. cerevisiae</i> WT.	61
Figura 4. 2. Estado de óxido-redução da glutationa ao longo do tempo de vida cronológico de <i>S. cerevisiae</i> WT.....	62
Figura 4. 3. Tolerância ao estresse oxidativo ambiental ao longo do tempo de vida cronológico de <i>S. cerevisiae</i> WT..	63
Figura 4. 4. Morfologia mitocondrial ao longo do tempo de vida cronológico de <i>S. cerevisiae</i> WT.	64

ÍNDICE DE TABELAS

Tabela 1. 1. Valores da viabilidade celular de <i>S. cerevisiae</i> WT, <i>npt1Δ</i> e <i>bna6Δ</i> cultivadas em condição controle.....	20
Tabela 1. 2. Valores da viabilidade celular de <i>S. cerevisiae</i> WT, <i>npt1Δ</i> e <i>bna6Δ</i> cultivadas em restrição calórica.....	21
Tabela 2. 1. Valores da viabilidade celular de <i>S. cerevisiae</i> <i>lpd1Δ</i> , <i>npt1Δlpd1Δ</i> e <i>bna6Δlpd1Δ</i> cultivadas em condição controle.....	30
Tabela 2. 2. Valores da viabilidade celular de <i>S. cerevisiae</i> <i>lpd1Δ</i> , <i>npt1Δlpd1Δ</i> e <i>bna6Δlpd1Δ</i> cultivadas em restrição calórica.....	31
Tabela 2. 3. Valores da viabilidade celular de <i>S. cerevisiae</i> <i>aco1Δ</i> , <i>kgd1Δ</i> e <i>sdh1Δ</i> cultivadas em condição controle.....	32
Tabela 2. 4. Valores da viabilidade celular de <i>S. cerevisiae</i> <i>aco1Δ</i> , <i>kgd1Δ</i> e <i>sdh1Δ</i> cultivadas em restrição calórica.....	33
Tabela 2. 5. Valores da viabilidade celular de <i>S. cerevisiae</i> ρ^0 e <i>abf2Δ</i> cultivadas em condição controle.....	34
Tabela 2. 6. Valores da viabilidade celular de <i>S. cerevisiae</i> <i>cyt1Δ</i> cultivada em condição controle.....	36
Tabela 2. 7. Valores da viabilidade celular de <i>S. cerevisiae</i> <i>atp2Δ</i> cultivada em condição controle.....	37
Tabela 3. 1. Relação numérica entre os percentuais de alteração de $\mu_{\text{Glu}}^{\text{max}}$ e $r_{c\text{Glu}}^{\text{max}}$ promovida pela ausência do DNA mitocondrial na condição controle e em restrição calórica.	53
Tabela 1. Tempos de retenção aproximados e canais de detecção dos metabólitos extracelulares de <i>S. cerevisiae</i> cultivada em YPD.....	76
Tabela 2. Intervalos de tempo utilizados para o cálculo da $\mu_{\text{Glu}}^{\text{max}}$ e da $\mu_{\text{EtOH}}^{\text{max}}$ e intervalo de tempo decorrido para o início da metabolização do etanol após a exaustão total da glicose em <i>S. cerevisiae</i>	78

SUMÁRIO

INTRODUÇÃO	15
OBJETIVO.....	17
Seção 1 – Importância do metabolismo de nicotinamida adenina dinucleotídeo no tempo de vida cronológico e no estado de óxido-redução celular de <i>Saccharomyces cerevisiae</i> : dihidrolipoil desidrogenase como fonte de espécies reativas de oxigênio	18
1.1. Metabolismo de nicotinamida adenina dinucleotídeo e tempo de vida em <i>S. cerevisiae</i>	19
1.2. Tempo de vida cronológico de <i>S. cerevisiae npt1Δ e bna6Δ</i>	19
1.3. Consumo de oxigênio e liberação de peróxido de hidrogênio induzidos por substratos exógenos em <i>S. cerevisiae npt1Δ e bna6Δ</i>	21
1.4. Estado de óxido-redução da glutationa em <i>S. cerevisiae npt1Δ e bna6Δ</i>	23
1.5. Consumo de oxigênio e liberação de peróxido de hidrogênio induzidos por substratos exógenos em <i>S. cerevisiae npt1Δlpd1Δ e bna6Δlpd1Δ</i>	25
1.6. Conclusões	27
Seção 2 – Aptidão respiratória e atividade de enzimas do metabolismo aeróbico como moduladores do tempo de vida cronológico, da responsividade à restrição calórica e da estabilidade do DNA mitocondrial de <i>Saccharomyces cerevisiae</i>	28
2.1. Aptidão respiratória e tempo de vida cronológico em <i>S. cerevisiae</i>	29
2.2. Tempo de vida cronológico de <i>S. cerevisiae lpd1Δ, npt1Δlpd1Δ e bna6Δlpd1Δ</i>	29
2.3. Tempo de vida cronológico de <i>S. cerevisiae aco1Δ, kgd1Δ e sdh1Δ</i>	31
2.4. Tempo de vida cronológico de <i>S. cerevisiae ρ⁰ e abf2Δ</i>	33
2.5. Tempo de vida cronológico de <i>S. cerevisiae cyt1Δ</i>	35
2.6. Tempo de vida cronológico de <i>S. cerevisiae atp2Δ</i>	36
2.7. Capacidade de crescimento de <i>S. cerevisiae</i> em meio seletivo rico e meio seletivo sintético para respiração	37
2.8. Progressão temporal da porcentagem de células respiratório-competentes durante o envelhecimento cronológico de <i>S. cerevisiae</i>	39
2.9. Tempo de vida cronológico de <i>Kluyveromyces lactis</i>	42
2.10. Conclusões	43
Seção 3 – Restrição calórica e DNA mitocondrial como moduladores da história metabólica de <i>Saccharomyces cerevisiae</i>	45
3.1. Estudo de parâmetros fisiológicos em <i>S. cerevisiae</i>	46
3.2. Consumo de oxigênio em <i>S. cerevisiae</i> WT	46
3.3. Curvas de biomassa e de pH ao longo do tempo de vida cronológico de <i>S. cerevisiae</i> WT e ρ^0	47
3.4. Curvas de exaustão de glicose e de formação e exaustão de etanol, glicerol, acetato, piruvato e succinato em <i>S. cerevisiae</i> WT e ρ^0	50
3.5. Velocidade específica máxima de crescimento celular em glicose e velocidade específica máxima de consumo de glicose de <i>S. cerevisiae</i> WT e ρ^0	52

3.6. Fator de conversão de glicose a células, de glicose a etanol e de glicose a glicerol de <i>S. cerevisiae</i> WT e ρ^0	53
3.7. Velocidade específica máxima de formação de etanol/glicerol; de crescimento celular em etanol/glicerol; de consumo de etanol/glicerol; e fator de conversão de etanol/glicerol a células.....	54
3.8. Velocidade específica máxima de crescimento celular em etanol e em glicerol	56
3.9. Conclusões	57
Seção 4 – Metabolismo de espécies reativas de oxigênio ao longo do tempo de vida cronológico de <i>Saccharomyces cerevisiae</i>.....	58
4.1. Espécies reativas de oxigênio no envelhecimento.....	59
4.2. Liberação de peróxido de hidrogênio induzida por substratos exógenos ao longo do tempo de vida cronológico de <i>S. cerevisiae</i> WT	60
4.3. Estado de óxido-redução da glutationa ao longo do tempo de vida cronológico de <i>S. cerevisiae</i> WT	61
4.4. Tolerância ao estresse oxidativo ambiental ao longo do tempo de vida cronológico de <i>S. cerevisiae</i> WT.....	63
4.5. Morfologia mitocondrial ao longo do tempo de vida cronológico de <i>S. cerevisiae</i> WT	64
4.6. Conclusões	65
CONCLUSÕES FINAIS.....	67
MATERIAIS E MÉTODOS.....	70
1. Linhagem parental e mutantes de <i>S. cerevisiae</i>	70
2. Linhagem parental de <i>K. lactis</i>	70
3. Meios de cultura, armazenamento e cultura celular.....	70
4. Determinação do tempo de vida cronológico de <i>S. cerevisiae</i> e <i>K. lactis</i>	71
5. Obtenção de esferoplastos de <i>S. cerevisiae</i>	71
6. Quantificação de proteína	72
7. Determinação da quantidade de digitonina necessária para permeabilização de esferoplastos de <i>S. cerevisiae</i>	72
8. Determinação do consumo de oxigênio induzido por substratos exógenos em esferoplastos de <i>S. cerevisiae</i>	73
9. Determinação da liberação de peróxido de hidrogênio induzido por substratos exógenos em esferoplastos de <i>S. cerevisiae</i>	73
10. Quantificação de glutationa total, oxidada e reduzida em <i>S. cerevisiae</i>	74
11. Construção dos mutantes <i>npt1Δlpd1Δ</i> e <i>bna6Δlpd1Δ</i>	74
12. Isolamento de <i>S. cerevisiae</i> ρ^0	75
13. Determinação da capacidade de crescimento em meio seletivo rico e sintético para respiração	75
14. Determinação da porcentagem de colônias respiratório-competentes em <i>S. cerevisiae</i>	75

15. Determinação do consumo de oxigênio em células intactas de <i>S. cerevisiae</i> WT	76
16. Separação, análise e quantificação dos metabólitos extracelulares de <i>S. cerevisiae</i> WT e ρ^0	76
17. Determinação da curva de crescimento celular e de pH do meio extracelular	77
18. Determinação do fator de conversão de Abs ₆₀₀ para biomassa.....	77
19. Cálculo dos parâmetros fisiológicos associados aos cultivos	77
20. Determinação da velocidade específica máxima de crescimento em glicose e etanol/glicerol.....	78
21. Determinação do fator de conversão de substrato a biomassa	78
22. Determinação do fator de conversão de substrato a produto	79
23. Determinação da velocidade específica máxima de consumo de substrato e de geração de produto	79
24. Estimativa da velocidade específica de crescimento em etanol e glicerol	79
25. Determinação da tolerância a estresse oxidativo ambiental	80
26. Determinação da morfologia mitocondrial.....	80
27. Geração de gráficos e análise estatística	80
BIBLIOGRAFIA	81

Introdução

O envelhecimento é um complexo processo multifatorial ao longo do qual os sistemas biológicos exibem alterações progressivas em suas funções metabólicas, em sua eficiência e em seu comportamento, e está fortemente associado à diminuição das respostas ao estresse, ao declínio da fertilidade e também, em última análise, ao aumento da mortalidade tempo-dependente (Kenyon, 2001; Kirkwood, 2002; Jazwinski, 2002; Viña *et al.*, 2007).

A literatura ocidental é prolífica em apresentar personagens que definitivamente não foram em nada beneficiados pelo envelhecimento e suas consequências – Homero, em sua *Odisséia*, retrata o Odisseu idoso como fraco, sendo um inepto ao trabalho e um peso sobre a terra; William Shakespeare, em *O Rei Lear*, associa a velhice de Lear à fraqueza, à doença, à melancolia e à perda da capacidade de discernimento; em um dos seus poemas, T.S. Eliot faz seu personagem Gerontian (“pequeno homem idoso”, em grego) esperar com ansiedade a refrescante chuva, já que tudo o que nele havia estava seco: seu tato, seu paladar, seu olfato, sua visão e sua audição. Não é surpreendente, portanto, que a relutância humana em aceitar naturalmente os fenótipos típicos do envelhecimento tenha resultado na crença – presente no imaginário das mais variadas culturas, nos mais diversos tempos – da existência de uma fonte cujas águas restaurariam a juventude e a vitalidade daqueles que dela fizessem uso (Post e Binstock, 2004).

Embora a mítica fonte da juventude nunca tenha sido descoberta, em 1935, quando McCay e colaboradores separaram-se com o achado de que roedores submetidos a um regime de oferta calórica diminuída em relação àquela oferecida ao grupo controle haviam exibido uma maior sobrevivência ao final de três anos (McCay *et al.*, 1935), foi observado, pela primeira vez, o resultado de uma intervenção dirigida capaz de aumentar o tempo de vida de um organismo. Atualmente, a restrição calórica é definida como um regime dietético de baixa oferta de calorias que, porém, atende às mínimas necessidades energéticas e de nutrientes essenciais diárias de um determinado organismo, retardando a exibição de fenótipos típicos do envelhecimento – o que se correlaciona positivamente com o aumento do tempo de vida (Walford *et al.*, 1987; Weindruch e Walford, 1988; Roth *et al.*, 1999; Hursting *et al.*, 2003; Fontana *et al.*, 2010).

Devido a uma série de facilidades operacionais – tais como o baixo custo de cultivo, o domínio da manipulação genética e, principalmente, os curtos tempos de vida – a utilização de sistemas mais simples, como a levedura *Saccharomyces cerevisiae*, o nematóide *Caenorhabditis elegans* e o artrópode *Drosophila melanogaster* tem decisivamente contribuído para o entendimento das características mais relevantes e dos mecanismos moleculares envolvidos no processo de envelhecimento de eucariotos (Sinclair *et al.*, 1998; Jazwinski, 2002; Bitterman *et al.*, 2003; Fabrizio *et al.*, 2005; Grotewiel *et al.*, 2005; Piper, 2006; Artal-Sanz e Tavernarakis, 2008; Barros *et al.*, 2010).

Os primeiros pesquisadores a considerar a utilização de *S. cerevisiae* como organismo modelo para estudar o envelhecimento foram Mortimer e Johnston, em meados do século passado (Mortimer e Johnston, 1959). Em seu trabalho seminal, eles propuseram a definição do tempo de vida dessa levedura como sendo o número de gerações pelas quais passa uma célula, *i.e.*, a contabilização do número total de células-filhas geradas por uma única célula-mãe. Duas décadas mais tarde, Müller e colaboradores revisitaram o conceito de longevidade em *S. cerevisiae* e, por sua vez, escolheram acessar o tempo de vida dessa levedura através da determinação da sua atividade metabólica em fase estacionária de crescimento, propondo, então, que o tempo de vida dessa levedura seria o período total em que uma célula apresenta-se metabolicamente ativa (Müller *et al.*, 1980). Assim sendo, da proposta de Mortimer e Johnston, e daquela de Müller e colaboradores, atualmente temos o que são chamados de *tempo de vida replicativo* e *tempo de vida cronológico*, respectivamente (MacLean *et al.*, 2001; Fabrizio e Longo, 2003; Jazwinski, 2004; Minois *et al.*, 2005; Barros *et al.*, 2010). Dessa forma, é interessante perceber que, enquanto o tempo de vida replicativo *quantifica a capacidade reprodutiva* de *S. cerevisiae*, o tempo de vida cronológico *quantifica a viabilidade dessa levedura, ao longo do tempo, em sua fase pós-mitótica*.

Com o passar dos anos, *S. cerevisiae* provou ser um organismo modelo conveniente para estudos de envelhecimento, atraindo intenso interesse depois de Jiang e colaboradores (Jiang *et al.*, 2000) e Lin e colaboradores (Lin *et al.*, 2000) terem independentemente demonstrado que essa levedura exibe aumento do tempo de vida replicativo em resposta à restrição calórica – cuja aplicação é realizada reduzindo-se a quantidade inicial de glicose em meio de cultura YPD dos usuais 2,0% para 0,5%, ou ainda menos (Jiang *et al.*, 2000; Lin *et al.*, 2000). Pouco tempo depois, outros trabalhos adicionalmente demonstraram que este mesmo protocolo é capaz de também aumentar o tempo de vida cronológico de *S. cerevisiae* (Reverter-Branchat *et al.*, 2004; Barros *et al.*, 2004; Smith *et al.*, 2007).

Desta forma, a descoberta da plena responsividade de *S. cerevisiae* à restrição calórica, há menos de uma década atrás, proporcionou a abertura de novas e promissoras possibilidades quanto à exploração e estudo das características intrínsecas a essa levedura, em diversas situações e com diferentes abordagens, com a finalidade de se determinar os mecanismos pelos quais essa intervenção aumenta os seus dois tipos de tempo de vida.

Objetivo

O objetivo central deste trabalho foi a pesquisa dos mecanismos pelos quais a restrição calórica aumenta o tempo de vida de *S. cerevisiae*, bem como os demais fenótipos por ela promovidos, através (i) da determinação da importância do metabolismo de nicotinamida adenina dinucleotídeo no tempo de vida cronológico e no estado de óxido-redução celular (Seção 1); (ii) do estudo do impacto de diferentes inativações gênicas no tempo de vida cronológico com o objetivo de reconhecer os fatores essenciais para a responsividade de *S. cerevisiae* à restrição calórica, bem como a determinação da viabilidade do uso de *Kluyveromyces lactis* como modelo alternativo para estudos da influência desta intervenção no envelhecimento de levedura (Seção 2); (iii) da determinação da influência da restrição calórica e do genoma mitocondrial em parâmetros fisiológicos relacionados ao metabolismo energético de *S. cerevisiae* (Seção 3); e (iv) da investigação do impacto da restrição calórica na liberação de espécies reativas de oxigênio e no estado de óxido-redução celular ao longo do envelhecimento cronológico dessa levedura (Seção 4).

Seção 1 – Importância do metabolismo de nicotinamida adenina dinucleotídeo no tempo de vida cronológico e no estado de óxido-redução celular de *Saccharomyces cerevisiae*: dihidrolipoil desidrogenase como fonte de espécies reativas de oxigênio

1.1. Metabolismo de nicotinamida adenina dinucleotídeo e tempo de vida em *S. cerevisiae*

Os estudos de longevidade de *S. cerevisiae* situados no período compreendido entre o início da década de 1990 e meados da seguinte apresentaram como principal foco a intensiva busca e a análise fenotípica de diversos genes potencialmente envolvidos na determinação do tempo de vida replicativo dessa levedura (D'Mello *et al.*, 1994; Sun *et al.*, 1994; Kennedy *et al.*, 1995; Jazwinski, 1996; Kennedy e Guarente, 1996; Sinclair *et al.*, 1997; Sinclair e Guarente, 1997; Kim *et al.*, 1999; Kaeberlein *et al.*, 1999; Jiang *et al.*, 2000; Lin *et al.*, 2000; Jazwinski, 2001; Saffi *et al.*, 2001; Hoopes *et al.*, 2002; Chen *et al.*, 2003; Kaeberlein *et al.*, 2005a e 2005b). Embora o seu papel no envelhecimento tenha sido recentemente questionado (Kaeberlein e Powers, 2007), à época particular destaque foi dado ao gene *SIR2* uma vez que (i) a sua inativação diminui marcadamente a duração do tempo de vida replicativo de *S. cerevisiae* (Kim *et al.*, 1999), e que (ii) a sua presença é necessária para o aumento desse mesmo tipo de tempo de vida quando essa levedura é cultivada em condições de restrição calórica (Lin *et al.*, 2000; Lin *et al.*, 2002; Blander e Guarente, 2004; Guarente e Picard, 2005).

SIR2 codifica a proteína Sir2p, uma desacetilase de histonas dependente da nicotinamida adenina dinucleotídeo oxidada (NAD^+), altamente conservada ao longo da escala filogenética, envolvida no silenciamento telomérico e do DNA ribossômico (Gottlieb e Esposito, 1989; Gottschling *et al.*, 1990; Brachmann *et al.*, 1995; Bryk *et al.*, 1997; Smith e Boeke, 1997; Landry *et al.*, 2000). De fato, uma diminuição da quantidade intracelular de NAD^+ decorrente da inativação do gene *NPT1* em *S. cerevisiae* previne o aumento do tempo de vida replicativo promovido pela restrição calórica (Lin *et al.*, 2000). A enzima fosforibosil nicotinato transferase (Npt1p), codificada pelo gene *NPT1*, é responsável pela última etapa da via sintética de recuperação de NAD^+ , *i.e.*, a conversão de nicotinato a ribonucleotídeo nicotinato – o intermediário para o qual convergem esta via e a via sintética *de novo* de NAD^+ em *S. cerevisiae* (Panozzo *et al.*, 2002).

1.2. Tempo de vida cronológico de *S. cerevisiae npt1Δ* e *bna6Δ*

Uma vez que o tempo de vida replicativo e o tempo de vida cronológico em *S. cerevisiae* têm suas durações determinadas por mecanismos distintos – embora haja certa sobreposição entre eles (Fabrizio *et al.*, 2001; Barros *et al.*, 2004; Barea e Bonato, 2009) – decidimos determinar a viabilidade celular do mutante *npt1Δ* na 16^a h, e no 7^º, 14^º, 21^º e 28^º dia de cultivo com o objetivo de verificar se a inativação do gene *NPT1* também suprime o aumento do tempo de vida cronológico mediado pela restrição calórica. Também objeto de estudo foi o mutante *bna6Δ*, que não apresenta atividade de quinolato fosforibosil transferase (Bna6p), enzima que é responsável pela produção de ribonucleotídeo nicotinato na via sintética *de novo* de NAD^+ a partir de ácido quinolínico (Panozzo *et al.*, 2002). Diferentemente da ausência de atividade da Npt1p, a inativação

de *BNA6* não impede o aumento do tempo de vida replicativo promovido pela restrição calórica em *S. cerevisiae* (Lin *et al.*, 2000).

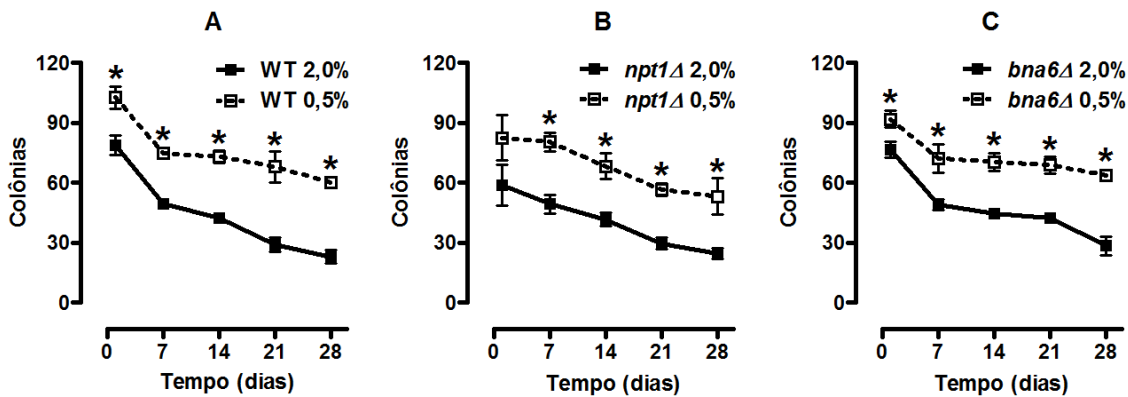


Figura 1.1. Tempo de vida cronológico de *S. cerevisiae* WT, *npt1Δ* e *bna6Δ*. A determinação das viabilidades celulares de *S. cerevisiae* WT (Painel A), *npt1Δ* (Painel B) e *bna6Δ* (Painel C) na 16^a h, e no 7^o, 14^o, 21^o e 28^o dia de cultivo foi realizada conforme descrição em *Materiais e Métodos* (Item 4). **p* < 0,05 vs. 2,0% (teste *t* de Student não-pareado).

Observamos que, diferentemente do que acontece em relação ao tempo de vida replicativo (Lin *et al.*, 2000), a ausência de Npt1p não suprime o aumento do tempo de vida cronológico mediado pela restrição calórica em *S. cerevisiae* (Figura 1.1, Painel B). Essa observação é mais uma evidência que corrobora a existência de mecanismos de regulação distintos na determinação dos dois tempos de vida dessa levedura. Além disso, verificamos que a inativação do gene *BNA6* também não possui influência sobre a resposta de *S. cerevisiae* à restrição calórica, uma vez que essa intervenção também promove o aumento da viabilidade celular do mutante *bna6Δ* em todos os dias de cultivo investigados (Figura 1.1, Painel C).

Tabela 1.1. Valores da viabilidade celular de *S. cerevisiae* WT, *npt1Δ* e *bna6Δ* cultivadas em condição controle. Os valores abaixo estão expressos em média do número de colônias ± erro médio. Para determinação do valor de *p* foi utilizado one-way ANOVA seguido do pós-teste de Bonferroni, no qual todas as médias foram comparadas entre si.

	WT 2,0%	<i>npt1Δ 2,0%</i>	<i>bna6Δ 2,0%</i>	<i>p < 0,05</i>
16^a h	78,71 ± 4,85	58,67 ± 10,13	76,42 ± 4,05	-
7^o dia	49,42 ± 2,06	49,29 ± 4,77	48,93 ± 2,75	-
14^o dia	42,36 ± 2,54	41,57 ± 3,24	44,53 ± 2,33	-
21^o dia	29,11 ± 3,64	29,58 ± 2,81	42,33 ± 1,23	<i>bna6Δ vs. WT</i>
28^o dia	22,99 ± 3,18	24,58 ± 2,69	28,42 ± 4,56	-

Os dados de viabilidade celular obtidos ao longo do tempo de cultivo também nos permitiu verificar qual o impacto da ausência da Npt1p e da Bna6p na duração do tempo de vida cronológico em *S. cerevisiae*. Notamos que os dois defeitos metabólicos específicos na via de recuperação e na via *de novo* de síntese de NAD⁺ não diminuem a viabilidade cronológica dos dois mutantes em

relação à célula selvagem em condição controle de cultivo; há, inclusive, um aumento significativo da viabilidade celular do mutante *bna6Δ* no 21º dia de cultivo em comparação à *S. cerevisiae* WT (Tabela 1.1).

Tabela 1.2. Valores da viabilidade celular de *S. cerevisiae* WT, *npt1Δ* e *bna6Δ* cultivadas em restrição calórica. Os valores abaixo estão expressos em média do número de colônias ± erro médio. Para determinação do valor de *p* foi utilizado one-way ANOVA seguido do pós-teste de Bonferroni, no qual todas as médias foram comparadas entre si.

	WT 0,5%	<i>npt1Δ</i> 0,5%	<i>bna6Δ</i> 0,5%	<i>p</i> < 0,05
16ª h	102,70 ± 5,61	82,53 ± 11,45	91,87 ± 4,20	-
7º dia	74,56 ± 1,91	80,37 ± 4,83	72,18 ± 7,23	-
14º dia	73,00 ± 3,28	68,20 ± 6,48	70,39 ± 4,50	-
21º dia	67,89 ± 7,64	56,58 ± 3,01	68,78 ± 4,27	-
28º dia	60,02 ± 2,37	60,02 ± 9,15	63,67 ± 2,66	-

Observamos também que o tempo de vida cronológico de ambos os mutantes cultivados em restrição calórica é igual àquele observado na célula selvagem, demonstrando que as inativações de *NPT1* e de *BNA6* também não interferem na amplitude do aumento do tempo de vida cronológico de *S. cerevisiae* (Tabela 1.2).

1.3. Consumo de oxigênio e liberação de peróxido de hidrogênio induzidos por substratos exógenos em *S. cerevisiae* *npt1Δ* e *bna6Δ*

Interrupções específicas na via de síntese *de novo* e na de recuperação de NAD⁺ (i) não suprimiram o aumento do tempo de vida cronológico desses mutantes em resposta à restrição calórica (Figura 1.1) e (ii) tampouco alteraram significativamente os valores de viabilidade celular dos mutantes *npt1Δ* e *bna6Δ* em relação à célula selvagem (Tabelas 1.1 e 1.2). Entretanto, NAD⁺ é um cofator cujo papel é essencial para reações de óxido-redução celulares e para o metabolismo energético. Assim, esperaríamos que *S. cerevisiae* com inativações em *NPT1* e *BNA6*, apresentasse, ao menos, alguns fenótipos distintos daqueles exibidos pela célula selvagem. Portanto, levando em consideração o papel final que NAD⁺ possui no metabolismo energético – *i.e.*, atuar como molécula doadora de elétrons para a cadeia de transporte de elétrons mitocondrial – investigamos o consumo de oxigênio induzido por malato 1 mM, glutamato 1 mM e etanol 2% em esferoplastos de *S. cerevisiae* WT, *npt1Δ* e *bna6Δ* permeabilizados com uma quantidade adequada de digitonina – para garantir a preservação da integridade da membrana mitocondrial (Item 7 em *Materiais e Métodos*) – após 16 h e 64 h de cultivo, para a obtenção desses valores em duas fases de crescimento distintas (Figura 3.2, Painel A; Tabela 2).

Observamos então que os mutantes *npt1Δ* e *bna6Δ* exibiram um menor consumo de oxigênio induzido por substratos exógenos do que aquele apresentado pela célula selvagem na fase logarítmica tardia de crescimento – *i.e.*, na 16^a h de crescimento, em nossas condições de cultivo (Figura 3.2) – tanto em condição controle como em restrição calórica (Figura 1.2, Painel A). Porém, surpreendentemente, a restrição calórica foi capaz de elevar o consumo de oxigênio induzido por substratos exógenos em ambos os mutantes quando comparado àquele da condição controle (Figura 1.2, Painel A) e, também, de aumentar esse parâmetro a níveis comparáveis aos da célula selvagem na fase estacionária de crescimento, *i.e.*, após 64 h de cultivo (Figura 1.2, Painel B). Entretanto, nessa mesma fase, o consumo de oxigênio induzido por substratos exógenos dos mutantes *npt1Δ* e *bna6Δ* cultivados em condição controle foi significativamente menor do que a da célula selvagem (Figura 1.2, Painel B). A diminuição da concentração inicial de glicose nos meios de cultura caloricamente restritos e a consequente modificação no padrão de expressão dos genes respiratórios em *S. cerevisiae* devido à mitigação do fenômeno da repressão por glicose (Rolland *et al.*, 2002; Item 2.9) explicam essa marcante diferença no consumo de oxigênio induzido por substratos exógenos existente entre a fase logarítmica tardia e a fase estacionária de crescimento dos mutantes *npt1Δ* e *bna6Δ* cultivados sob condição controle e restrição calórica.

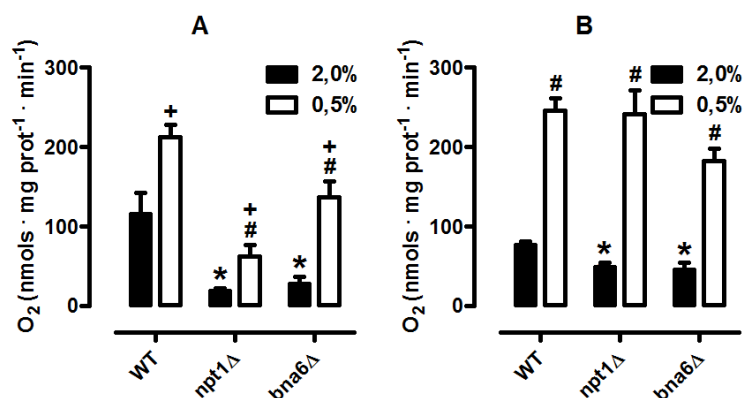


Figura 1.2. Consumo de oxigênio induzido por substratos exógenos em *S. cerevisiae* WT, *npt1Δ* e *bna6Δ*. A determinação do consumo de oxigênio em esferoplastos (800 µg/mL) de *S. cerevisiae* WT, *npt1Δ* e *bna6Δ* induzido por malato 1 mM, glutamato 1 mM e etanol 2% na fase logarítmica tardia (16 h de cultivo; Painel A) e estacionária de crescimento (64 h de cultivo; Painel B) foi realizada segundo descrição em *Materiais e Métodos* (Item 8). Uma quantidade de digitonina que variou entre 0,004% e 0,006% foi utilizada para proporcionar o aumento da permeabilidade dos esferoplastos aos substratos exógenos. Painel A: **p* < 0,05 vs. WT 2,0% e #*p* < 0,05 vs. WT 0,5% (one-way ANOVA/Bonferroni); **p* < 0,05 vs. 2,0% (teste *t* de Student não-pareado). B: **p* < 0,05 vs. WT 2,0% (one-way ANOVA/Bonferroni); #*p* < 0,05 vs. WT 2,0% (teste *t* de Student não-pareado).

Uma vez que nosso grupo havia previamente demonstrado a existência de uma correlação negativa entre o consumo de oxigênio e a geração mitocondrial de espécies reativas de oxigênio induzida por substratos exógenos em *S. cerevisiae* (Barros *et al.*, 2004), a verificação de alterações nos valores do consumo de oxigênio induzido por substratos exógenos nos mutantes *npt1Δ* e *bna6Δ* sugeriu a existência de diferenças quanto à taxa geração de oxidantes por esses mutantes em relação à célula selvagem. Desta forma, determinamos a liberação de peróxido de hidrogênio

induzida por malato 1 mM, glutamato 1 mM e etanol 2% em esferoplastos de *S. cerevisiae* WT, *npt1Δ* e *bna6Δ* também permeabilizados com uma quantidade adequada de digitonina.

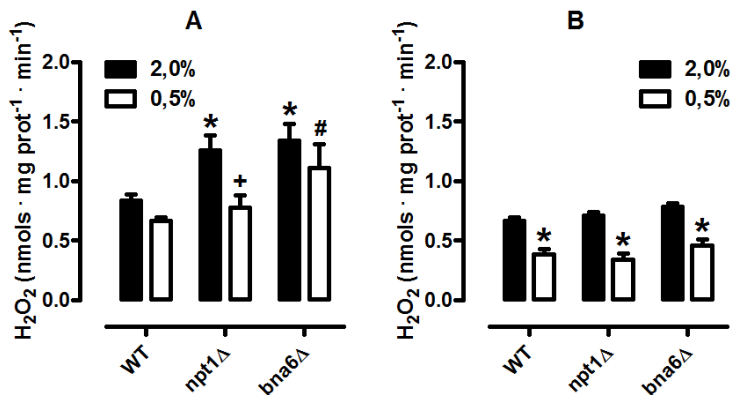


Figura 1.3. Liberação de peróxido de hidrogênio induzida por substratos exógenos em *S. cerevisiae* WT, *npt1Δ* e *bna6Δ*. A determinação da liberação de peróxido de hidrogênio em esferoplastos (100 µg/mL) de *S. cerevisiae* WT, *npt1Δ* e *bna6Δ* induzida por malato 1 mM, glutamato 1 mM e etanol 2% na fase logarítmica tardia (16 h de cultivo; Painel A) e estacionária de crescimento (64 h de cultivo; Painel B) foi realizada segundo descrição em *Materiais e Métodos* (Item 9). Uma quantidade de digitonina que variou entre 0,002% e 0,003% foi utilizada para proporcionar o aumento da permeabilidade dos esferoplastos à peroxidase de raiz forte – necessária para a oxidação da sonda fluorescente *Amplex Red* pelo peróxido de hidrogênio – e aos substratos exógenos. Painel A: * $p < 0,05$ vs. WT 2,0% e # $p < 0,05$ vs. WT 0,5% (one-way ANOVA/Bonferroni); + $p < 0,05$ vs. *npt1Δ* 2,0% (teste t de Student não-pareado). Painel B: * $p < 0,05$ vs. 2,0% (teste t de Student não-pareado).

Podemos observar que a liberação de peróxido de hidrogênio induzida por substratos exógenos em *S. cerevisiae* *npt1Δ* e *bna6Δ* é significativamente maior do que a observada na célula selvagem na fase logarítmica tardia de crescimento (Figura 1.3, Painel A), mas não na fase estacionária (Figura 1.3, Painel B). Além disso, quando em restrição calórica e na fase logarítmica tardia de crescimento, a ausência da Npt1p não promove um aumento da liberação de peróxido de hidrogênio induzida por substratos exógenos em *S. cerevisiae*, ao contrário do que é observado no mutante *bna6Δ* (Figura 1.3, Painel A).

Finalmente, na fase estacionária de crescimento, a restrição calórica diminui significativamente a liberação de peróxido de hidrogênio induzida por substratos exógenos nos mutantes *npt1Δ* e *bna6Δ*, assim como na célula selvagem (Figura 1.3, Painel B). Em conjunto, esses resultados demonstram que a inativação de *NPT1* e *BNA6* alteram, paralelamente, o consumo de oxigênio e a liberação de peróxido de hidrogênio induzidos por substratos exógenos em *S. cerevisiae*.

1.4. Estado de óxido-redução da glutationa em *S. cerevisiae* *npt1Δ* e *bna6Δ*

A glutationa – ou γ-glutamilcisteinilglicina – é um tripeptídeo envolvido em uma série de processos celulares tais como (i) a manutenção da comunicação celular de metazoários através de

gap junctions (Barhoumi *et al.*, 1993); (ii) o metabolismo de ascorbato – na conversão de dehidroascorbato a ascorbato, seja atuando como substrato da dehidroascorbato redutase, seja reagindo com o dehidroascorbato sem mediação enzimática (Foyer e Mullineaux, 1998); e (iii) a prevenção da oxidação de grupos tiólicos e a consequente ligação cruzada entre resíduos de aminoácidos (Pompella *et al.*, 2003). Uma vez que a glutationa é substrato das glutationa peroxidases e das glutationa-S-transferases celulares, além de ser capaz de conjugar-se não-enzimaticamente com moléculas reativas, a sua atividade antioxidante é considerada de grande importância para a prevenção da oxidação descompensada de componentes celulares (Grant, 2001; Pompella *et al.*, 2003). Além disso, a razão entre a quantidade de glutationa oxidada (GSSG) e reduzida (GSH) é aceita como uma medida confiável do *estado de óxido-redução celular* – conceito que deve ser entendido como o quão deslocado para a geração de oxidantes ou para a detoxificação destes está o *steady-state* celular. Em outras palavras, uma razão aumentada entre GSSG e GSH indica a existência de um balanço deslocado à maior geração e/ou menor detoxificação de oxidantes celulares. Assim, determinando as quantidades celulares de GSSG, GSH e glutationa total (GSSG + GSH) nos mutantes *npt1Δ* e *bna6Δ*, pudemos verificar se os estados fisiológicos de óxido-redução celular desses dois mutantes de *S. cerevisiae* estavam em concordância com aqueles sugeridos pela liberação de peróxido de hidrogênio induzida por substratos exógenos (Figura 1.3).

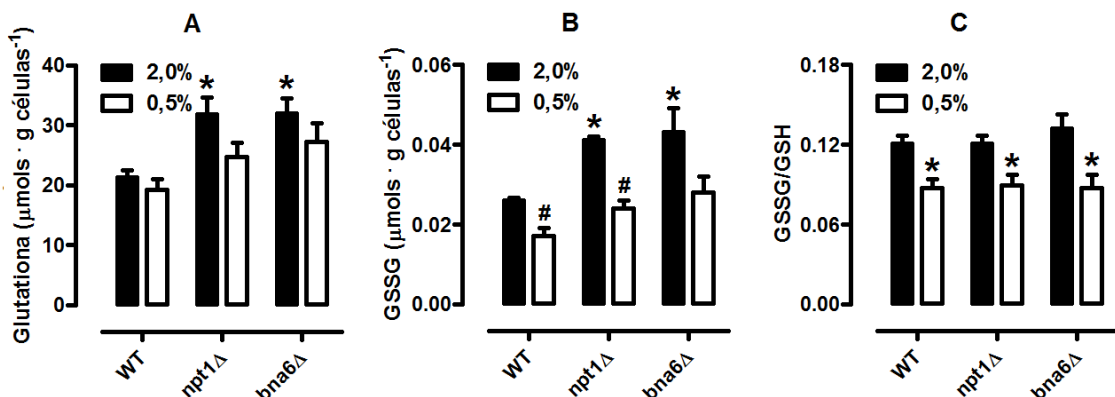


Figura 1.4. Estado de óxido-redução da glutationa em *S. cerevisiae* WT, *npt1Δ* e *bna6Δ*. As concentrações intracelulares de glutationa total (Painel A), oxidada (Painel B) e a razão entre GSSG e GSH (Painel C) na fase estacionária tardia de crescimento (86 h de cultivo) foram determinadas conforme descrição em *Materiais e Métodos* (Item 10). Painel A: * $p < 0,05$ vs. WT 2,0% (one-way ANOVA/Bonferroni). Painel B: * $p < 0,05$ vs. WT 2,0% (one-way ANOVA/Bonferroni); # $p < 0,05$ vs. 2,0% (teste t de Student não-pareado). Painel C: * $p < 0,05$ vs. 2,0% (teste t de Student não-pareado).

Verificamos que a quantidade de GSSG na célula selvagem e no mutante *npt1Δ* (Figura 1.4, Painel B), assim como a razão entre GSSG e GSH em *S. cerevisiae* WT, *npt1Δ* e *bna6Δ* (Figura 1.4, Painel C), são significativamente menores quando em restrição calórica. De fato, *S. cerevisiae* caloricamente restrita exibe uma menor liberação de peróxido de hidrogênio induzida por substratos exógenos em fase estacionária quando comparada à condição controle (Figura 1.3, Painel B). Além disso, tanto as quantidades de glutationa total como as de GSSG nos mutantes

npt1Δ e *bna6Δ* são significativamente maiores em relação à célula selvagem (Figura 1.4, Painéis A e B). É interessante considerar que a síntese de glutatona é induzida em condições de estresse oxidativo em *S. cerevisiae* (Grant, 2001). Desta forma, podemos afirmar que os estados de óxido-redução celulares aqui verificados estão em concordância com aqueles previamente indicados pela determinação da liberação de peróxido de hidrogênio induzida por substratos exógenos, uma vez que os mutantes *npt1Δ* e *bna6Δ* possuem uma aumentada liberação de peróxido de hidrogênio induzida por substratos exógenos na fase logarítmica tardia de crescimento em relação à célula selvagem (Figura 1.3).

1.5. Consumo de oxigênio e liberação de peróxido de hidrogênio induzidos por substratos exógenos em *S. cerevisiae npt1Δlpd1Δ* e *bna6Δlpd1Δ*

Desde que Jensen, há quase 50 anos, reportou que peróxido de hidrogênio poderia ser formado a partir de preparações mitocondriais (Jensen, 1966), o conhecimento concernente sobre os mecanismos de geração de espécies reativas de oxigênio celulares, bem como a sua química e o seu papel na fisiologia e fisiopatologia, tem sido largamente ampliado (Davies, 1995; Beckamn e Ames, 1998; Harman, 2001; Golden, 2002; Sohal, 2002; Turrens, 2003; Balaban *et al.*, 2005; Miller *et al.*, 2006; Kowaltowski *et al.*, 2009).

Embora as espécies reativas de oxigênio sejam geradas em diversos compartimentos e enzimas celulares – tais como pelas oxidases presentes nos peroxissomos (Schrader e Fahimi, 2006); as NADPH oxidases localizadas na membrana plasmática (Lambeth, 2004); e pelas ciclooxygenases citosólicas (Pathak *et al.*, 2006) – a vasta maioria de seu total (aproximadamente 90%) possui origem na cadeia de transporte de elétrons mitocondrial (Balaban *et al.*, 2005).

Apesar de os resultados de consumo de oxigênio induzido por substratos exógenos (Figura 1.2) estarem coerentemente alinhados com a liberação de peróxido de hidrogênio induzida por substratos exógenos nos mutantes *npt1Δ* e *bna6Δ* (Figura 1.3) – considerando a correlação negativa existente entre o consumo de oxigênio e a geração de espécies reativas de oxigênio em *S. cerevisiae* (Barros *et al.*, 2004) – os defeitos metabólicos em vias de síntese de NAD⁺ faz com que estes dois mutantes possuam uma diminuída quantidade de NADH celular – a espécie responsável pela entrega dos elétrons à cadeia de transporte de elétrons mitocondrial. De fato, tanto na fase logarítmica tardia de crescimento, quanto na estacionária, o consumo de oxigênio induzido por substratos exógenos desses dois mutantes é menor do que o apresentado pela célula selvagem (Figura 1.2), evidenciando o menor aporte de elétrons à cadeia de transporte de elétrons em *S. cerevisiae npt1Δ* e *bna6Δ* quando em uma condição de excesso de substratos exógenos. Dessa forma, o aumento da liberação de peróxido de hidrogênio induzida por substratos exógenos em ambos os mutantes somente poderia ser explicado em termos mecanísticos desde que existisse em

S. cerevisiae, além da cadeia de transporte de elétrons, outra fonte mitocondrial de espécies reativas de oxigênio.

Interessantemente, em 2004, foram publicados dois trabalhos demonstrando que a flavoenzima dihidrolipoil desidrogenase, um dos componentes do sistema enzimático glicina descarboxilase (Douce *et al.*, 2001) e dos complexos piruvato desidrogenase e α -cetoglutarato desidrogenase (Roy e Dawes, 1987; Pronk *et al.*, 1996) – todos localizados na matriz mitocondrial – é, em mamíferos, uma fonte mitocondrial de espécies reativas de oxigênio em um cenário em que há baixa disponibilidade de NAD⁺ celular (Tretter e Adam-Vizi, 2004; Starkov *et al.*, 2004). Para então investigarmos se a dihidrolipoil desidrogenase de *S. cerevisiae* (Lpd1p) era também uma importante fonte de espécies reativas de oxigênio em nos mutantes *npt1Δ* e *bna6Δ*, determinamos o consumo de oxigênio e a liberação de peróxido de hidrogênio induzidos por substratos exógenos em ambos os mutantes com a adicional inativação de *LPD1*, o gene responsável pela codificação da Lpd1p em *S. cerevisiae* (Roy e Dawes, 1987). Os mutantes *npt1Δlpd1Δ* e *bna6Δlpd1Δ* foram obtidos segundo descrição em *Materiais e Métodos* (Item 11).

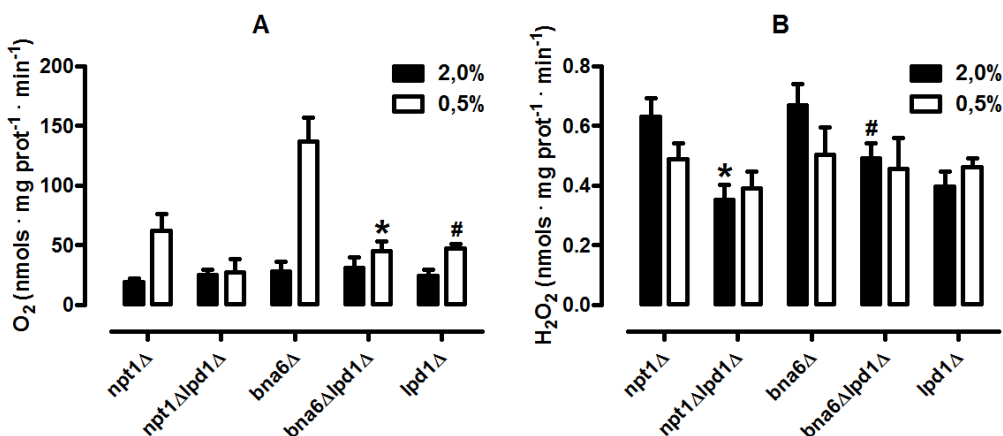


Figura 1.5. Consumo de oxigênio e liberação de peróxido de hidrogênio induzidos por substratos exógenos em *S. cerevisiae* WT, *npt1Δlpd1Δ* e *bna6Δlpd1Δ*. A determinação do consumo de oxigênio em esferoplastos de *S. cerevisiae* WT, *npt1Δlpd1Δ* e *bna6Δlpd1Δ* (800 µg/mL) induzido por malato 1 mM, glutamato 1 mM e etanol 2% na fase logarítmica tardia (16 h de cultivo; Painel A) e a determinação da liberação de peróxido de hidrogênio em esferoplastos de *S. cerevisiae* WT, *npt1Δlpd1Δ* e *bna6Δlpd1Δ* (100 µg/mL) induzido por malato 1 mM, glutamato 1 mM e etanol 2% na fase logarítmica tardia (16 h de cultivo; Painel B) foi realizada segundo descrição em *Materiais e Métodos* (Itens 8 e 9). Uma quantidade de digitonina que variou entre 0,004% e 0,006% (Painel A) e 0,002% e 0,003% (Painel B) foi utilizada para proporcionar o aumento da permeabilidade dos esferoplastos aos substratos exógenos e, além desses, à peroxidase de raiz forte (Painel B). Os resultados do consumo de oxigênio e da liberação de peróxido de hidrogênio induzidos por substratos exógenos dos mutantes *npt1Δ* e *bna6Δ* já haviam sido apresentados na Figuras 1.2 e 1.3, respectivamente, mas o estão sendo aqui novamente para o bem da clareza. Painel A: **p* < 0,05 vs. *bna6Δ* (one-way ANOVA/Bonferroni) e #*p* < 0,05 vs. *lpd1Δ* 2,0% (teste *t* de Student não-pareado). Painel B: **p* < 0,05 vs. *npt1Δ* e #*p* < 0,05 vs. *bna6Δ* (one-way ANOVA/Bonferroni).

Observamos que não há diferença entre o consumo de oxigênio induzido por substratos exógenos entre os mutantes *npt1Δ* e *npt1Δlpd1Δ* caloricamente restritos; entretanto, o mutante *bna6Δlpd1Δ* apresenta uma diminuição significativa no consumo de oxigênio induzido por

substratos exógenos em relação ao mutante *bna6Δ* em condições de restrição calórica, mas não em relação ao mutante *lpd1Δ* em nenhuma condição de cultivo (Figura 1.5, Painel A).

Além disso – e sobretudo – verificamos que a inativação do gene *LPD1* nos mutantes *npt1Δ* e *bna6Δ* é capaz de diminuir significativamente a liberação de peróxido de hidrogênio induzida por substratos exógenos em *S. cerevisiae* em relação aos mutantes *npt1Δ* e *bna6Δ* quando em condição controle (Figura 1.5, Painel B), mesmo a despeito de seu baixo consumo de oxigênio induzido por substratos exógenos (Figura 1.5, Painel A). Em outras palavras, a correlação negativa existente entre a respiração e a liberação de oxidantes em *S. cerevisiae* não é válida para os duplos mutantes em questão, os quais possuem, em comum, a inativação de *LPD1*. Desta forma, observando que alelo nulo *lpd1* é epistático sobre os alelos nulos *npt1* e *bna6*, demonstramos que a Lpd1p é uma importante fonte de espécies reativas em *S. cerevisiae*.

1.6. Conclusões

Podemos concluir, portanto, que as inativações de *NPT1* e *BNA6* não suprimem o aumento do tempo de vida cronológico devido à restrição calórica em *S. cerevisiae*; elas diminuem significativamente, porém, o consumo de oxigênio induzido por substratos exógenos dessa levedura, aumentando tanto a liberação de peróxido de hidrogênio como as quantidades de glutationa total e GSSG celulares. Os aumentos da liberação de oxidantes e da oxidação de GSH são revertidos pela restrição calórica. Finalmente, *em condição controle de cultivo*, a inativação do gene *LPD1* nos mutantes *npt1Δ* e *bna6Δ* promove a diminuição da liberação de peróxido de hidrogênio induzida por substratos exógenos em *S. cerevisiae*, provando ser a Lpd1p uma importante fonte de espécies reativas de oxigênio nessa levedura, em uma maneira sensível à restrição calórica.

Seção 2 – Aptidão respiratória e atividade de enzimas do metabolismo aeróbico como moduladores do tempo de vida cronológico, da responsividade à restrição calórica e da estabilidade do DNA mitocondrial de *Saccharomyces cerevisiae*

2.1. Aptidão respiratória e tempo de vida cronológico em *S. cerevisiae*

Uma característica da cultura em batelada – utilizada para a realização dos estudos de envelhecimento – é disponibilidade finita de substratos. Tanto em condição controle de cultivo como em restrição calórica, a glicose disponível é totalmente consumida em, no máximo, 24 h de cultivo (Figura 3.4, Painel A), enquanto *S. cerevisiae* permanece viável em fase estacionária de crescimento ao longo de várias semanas (Sinclair *et al.*, 1998; Reverter-Branchat *et al.*, 2004; Fabrizio e Longo, 2003; Figura 1.1, Painel A). Após o esgotamento da glicose, os substratos restantes (i) ou estavam presentes no início do cultivo – como por exemplo os aminoácidos – (ii) ou foram formados durante o metabolismo de glicose – como por exemplo o etanol, o ácido acético e o glicerol – e somente podem ser metabolizados aerobicamente (MacLean *et al.*, 2001; Frick e Wittmann, 2005). Portanto, a aptidão respiratória é uma exigência necessária para a manutenção da viabilidade de *S. cerevisiae* durante a fase estacionária (MacLean *et al.*, 2001; Fabrizio e Longo 2003; Samokhvalov *et al.*, 2004). De fato, durante o final da fase de crescimento suportada por uma fonte de carbono fermentável e o início da fase de crescimento suportada por substratos respiratórios, *S. cerevisiae* tem a expressão de enzimas do ciclo dos ácidos tricarboxílicos e dos componentes da cadeia de transporte de elétrons mitocondrial drasticamente alterada (DeRisi *et al.*, 1997). Os genes relacionados ao metabolismo aeróbico são desreprimidos à medida que a glicose é consumida, fazendo com que, durante a fase estacionária de crescimento, o metabolismo aeróbico seja predominante (MacLean *et al.*, 2001; Fabrizio Longo e 2003; Samokhvalov *et al.*, 2004).

2.2. Tempo de vida cronológico de *S. cerevisiae lpd1Δ, npt1Δlpd1Δ* e *bna6Δlpd1Δ*

Como já discutido anteriormente, a Lpd1p é componente do sistema enzimático glicina descarboxilase e também dos complexos enzimáticos piruvato desidrogenase e α -cetoglutarato desidrogenase. Ela é responsável pela conversão de dihidrolipoato a lipoato em uma reação que envolve a transferência de elétrons do substrato à sua flavina adenina dinucleotídeo, e desta para o NAD⁺, gerando NADH.

A inativação de *LPD1*, portanto, promove a interrupção da conversão de glicina em serina (Sinclair e Dawes, 1995); de piruvato a acetil-CoA e de α -cetoglutarato a succinil-CoA (Pronk *et al.*, 1996). Essas duas últimas reações são de grande importância para o metabolismo energético aeróbico já que (i) a primeira fornece o substrato que se condensa com o oxaloacetato, formando citrato – o primeiro intermediário do ciclo dos ácidos tricarboxílicos – e que (ii) a segunda é parte integrante dessa via.

Decidimos então determinar o tempo de vida cronológico dos mutantes *lpd1Δ*, bem como dos mutantes *npt1Δlpd1Δ* e *bna6Δlpd1Δ*, com o objetivo de investigarmos o impacto das inativações de *NPT1* e *BNA6* no mutante *lpd1Δ* na duração do tempo de vida cronológico e na responsividade de *S. cerevisiae* à restrição calórica.

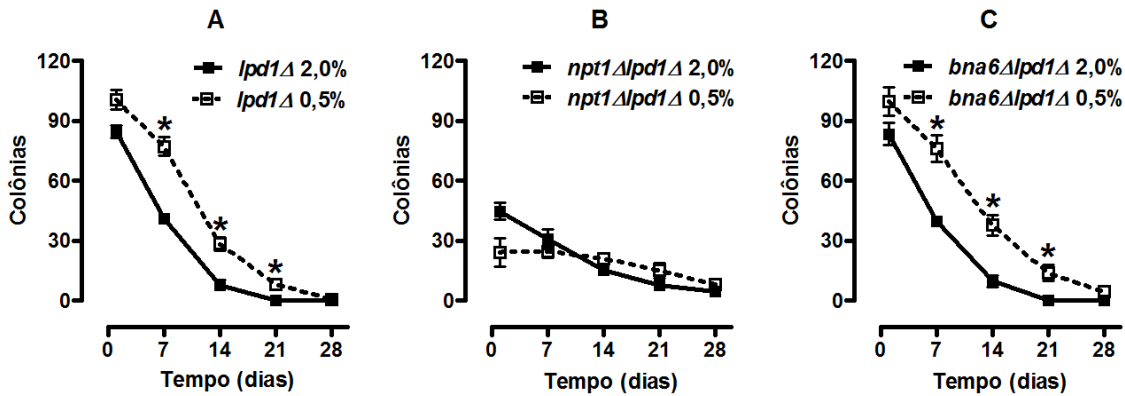


Figura 2.1. Tempo de vida cronológico de *S. cerevisiae* *lpd1Δ*, *npt1Δlpd1Δ* e *bna6Δlpd1Δ*. A determinação das viabilidades celulares de *S. cerevisiae* *lpd1Δ* (Painel A), *npt1Δlpd1Δ* (Painel B) e *bna6Δlpd1Δ* (Painel C) na 16^a h, e no 7^º, 14^º, 21^º e 28^º dia de cultivo foi realizada conforme descrição em *Materiais e Métodos* (Item 4). **p* < 0,05 vs. 2,0% (teste *t* de Student não-pareado).

Tabela 2.1. Valores da viabilidade celular de *S. cerevisiae* *lpd1Δ*, *npt1Δlpd1Δ* e *bna6Δlpd1Δ* cultivadas em condição controle. Os valores abaixo estão expressos em média do número de colônias ± erro médio. Para determinação do valor de *p* foi utilizado one-way ANOVA seguido do pós-teste de Bonferroni, no qual todas as médias foram comparadas entre si. Os valores da viabilidade celular de *S. cerevisiae* WT cultivada em condição controle já haviam sido apresentados na Tabela 1.1, e o são aqui novamente para o bem da clareza.

	WT 2,0%	<i>lpd1Δ</i> 2,0%	<i>npt1Δlpd1Δ</i> 2,0%	<i>bna6Δlpd1Δ</i> 2,0%	<i>p</i> < 0,05
16^a h	78,71 ± 4,85	84,60 ± 3,17	44,61 ± 4,21	83,33 ± 5,54	<i>npt1Δlpd1Δ</i> vs. WT, <i>lpd1Δ</i> e <i>bna6Δlpd1Δ</i>
7^º dia	49,42 ± 2,06	49,42 ± 1,93	30,76 ± 4,97	39,61 ± 2,30	<i>npt1Δlpd1Δ</i> vs. WT
14^º dia	42,36 ± 2,54	7,88 ± 2,65	15,38 ± 2,53	9,77 ± 2,77	WT vs. <i>lpd1Δ</i> , <i>npt1Δlpd1Δ</i> e <i>bna6Δlpd1Δ</i>
21^º dia	32,07 ± 2,61	0,16 ± 0,16	7,4 ± 1,46	0,25 ± 0,15	WT vs. <i>lpd1Δ</i> , <i>npt1Δlpd1Δ</i> e <i>bna6Δlpd1Δ</i>
28^º dia	22,99 ± 3,18	0,00 ± 0,00	4,46 ± 2,03	0,16 ± 0,16	WT vs. <i>lpd1Δ</i> , <i>npt1Δlpd1Δ</i> e <i>bna6Δlpd1Δ</i>

Observamos que os mutantes *lpd1Δ* e *bna6Δlpd1Δ*, apesar de apresentarem uma menor viabilidade celular a partir do 14^º dia de cultivo em relação à célula selvagem, tanto em condição controle de cultivo como em restrição calórica (Tabela 2.1), ainda foram capazes de responder à restrição calórica com o aumento do tempo de vida cronológico (Figura 2.1, Painéis A e C). Em todos os dias estudados, nas duas condições de cultivo, os mutantes *lpd1Δ* e *bna6Δlpd1Δ* não exibiram diferenças em suas viabilidades, demonstrando que a inativação de *BNA6* no mutante *lpd1Δ* não possui efeito adicional neste fenótipo (Tabelas 2.1 e 2.2). Por outro lado, a inativação de *NPT1* no mutante *lpd1Δ* provou possuir maior impacto no tempo de vida cronológico de *S. cerevisiae* dado que, (i) em condição controle de cultivo, na 16^a h existe uma diferença significativa

na viabilidade celular entre os mutantes *lpd1Δ* e *npt1Δlpd1Δ* (Tabela 2.1) e que (ii) em restrição calórica, essa diferença existe tanto na 16^a h como no 7º dia de cultivo (Tabela 2.2). Além disso, o mutante *npt1Δlpd1Δ*, em todos os dias estudados e em ambas condições de cultivo, exibiu uma viabilidade celular diminuída em relação à célula selvagem (Tabelas 2.1 e 2.2).

Tabela 2.2. Valores da viabilidade celular de *S. cerevisiae lpd1Δ, npt1Δlpd1Δ e bna6Δlpd1Δ* cultivadas em restrição calórica. Os valores abaixo estão expressos em média do número de colônias ± erro médio. Para determinação do valor de *p* foi utilizado one-way ANOVA seguido do pós-teste de Bonferroni, no qual todas as médias foram comparadas entre si. Os valores da viabilidade celular de *S. cerevisiae* WT cultivada em restrição calórica já haviam sido apresentados na Tabela 1.2, e o são aqui novamente para o bem da clareza.

	WT 0,5%	<i>lpd1Δ</i> 0,5%	<i>npt1Δlpd1Δ</i> 0,5%	<i>bna6Δlpd1Δ</i> 0,5%	<i>p < 0,05</i>
16^a h	102,70 ± 5,61	100,50 ± 4,78	24,25 ± 7,07	99,75 ± 7,17	<i>npt1Δlpd1Δ</i> vs. WT, <i>lpd1Δ</i> e <i>bna6Δlpd1Δ</i>
7º dia	74,56 ± 1,91	77,17 ± 4,55	24,69 ± 3,05	76,22 ± 6,56	<i>npt1Δlpd1Δ</i> vs. WT, <i>lpd1Δ</i> e <i>bna6Δlpd1Δ</i>
14º dia	73,00 ± 3,28	28,42 ± 3,42	21,10 ± 2,44	37,67 ± 5,11	WT vs. <i>lpd1Δ</i> , <i>npt1Δlpd1Δ</i> e <i>bna6Δlpd1Δ</i> , <i>npt1Δlpd1Δ</i> vs. <i>bna6Δlpd1Δ</i>
21º dia	67,89 ± 7,64	8,16 ± 2,36	17,33 ± 4,22	13,75 ± 4,02	WT vs. <i>lpd1Δ</i> , <i>npt1Δlpd1Δ</i> e <i>bna6Δlpd1Δ</i>
28º dia	60,02 ± 2,37	0,75 ± 0,75	8,00 ± 2,33	4,41 ± 2,57	WT vs. <i>lpd1Δ</i> , <i>npt1Δlpd1Δ</i> e <i>bna6Δlpd1Δ</i>

Em conjunto, esses dados indicam que, apesar de a inativação de *LPD1* na célula selvagem e nos mutantes *npt1Δ* e *bna6Δ* promover uma significativa diminuição do tempo de vida cronológico de *S. cerevisiae*, em dois desses cenários – a inativação de *LPD1* na célula selvagem e no mutante *bna6Δ* – ainda é observado o aumento do tempo de vida cronológico devido à restrição calórica (Figura 2.1, Painéis A e C). No terceiro – a inativação de *LPD1* no mutante *npt1Δ* – é verificada a ineeficácia da restrição calórica em aumentar o tempo de vida cronológico dessa levedura.

2.3. Tempo de vida cronológico de *S. cerevisiae aco1Δ, kgd1Δ e sdh1Δ*

A verificação da responsividade dos mutantes *lpd1Δ* e *bna6Δlpd1Δ*, assim como da irresponsividade do mutante *npt1Δlpd1Δ* à restrição calórica, indicou-nos que (i) a interrupção da rota sintética *de novo* de NAD⁺ não foi capaz de abolir o aumento do tempo de vida cronológico de *S. cerevisiae lpd1Δ* em virtude da restrição calórica (Figura 2.1, Painéis A e C) e que (ii) somente um defeito na via sintética de recuperação de NAD⁺ associada à ausência da atividade de Lpd1p foi capaz de prevenir o aumento do tempo de vida cronológico mediado pela restrição calórica nessa levedura (Figura 2.1, Painel B). Desta forma, iniciamos a busca por outros mutantes de *S. cerevisiae* que, assim como o mutante *npt1Δlpd1Δ*, também fossem irresponsivos à restrição calórica, já que a identificação de mutações que previnem fenótipos específicos da restrição calórica contribuiria sobremaneira com o entendimento de como esse regime de cultivo pode aumentar a longevidade dessa levedura.

Ainda com o foco voltado para o ciclo dos ácidos tricarboxílicos, elegemos *S. cerevisiae* com inativações em *ACO1*, *KGD1* e *SDH1*, os quais não exibem, nesta ordem, atividade de aconitase 1 (Gangloff *et al.*, 1990), de α -cetoglutarato desidrogenase – assim como o mutante *lpd1Δ* – (Repetto e Tzagoloff, 1989) e de succinato desidrogenase (Chapman *et al.*, 1992).

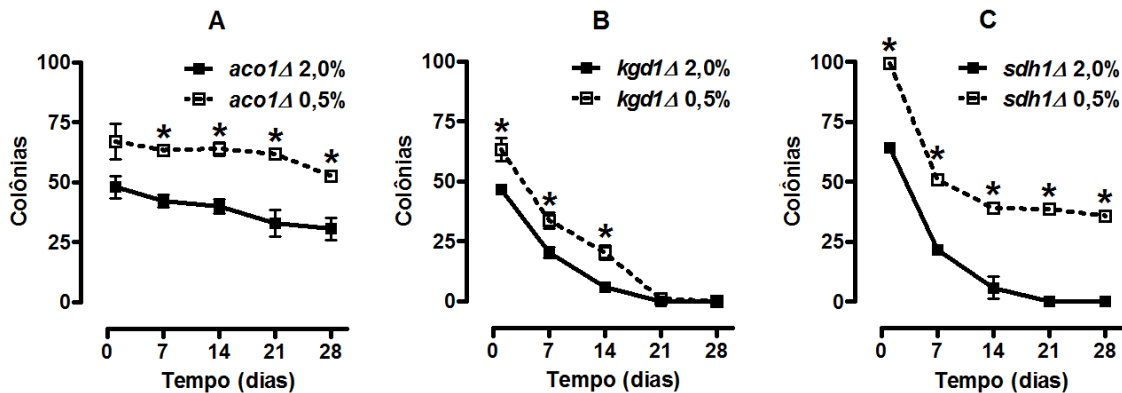


Figura 2.2. Tempo de vida cronológico de *S. cerevisiae aco1Δ, kgd1Δ e sdh1Δ*. A determinação das viabilidades celulares de *S. cerevisiae aco1Δ, kgd1Δ e sdh1Δ* na 16^a h, e no 7^o, 14^o, 21^o e 28^o dia de cultivo foi realizada conforme descrição em *Materiais e Métodos* (Item 4). * $p < 0,05$ vs. 2,0% (teste *t* de Student não-pareado).

Tabela 2.3. Valores da viabilidade celular de *S. cerevisiae aco1Δ, kgd1Δ e sdh1Δ* cultivadas em condição controle. Os valores abaixo estão expressos em média do número de colônias \pm erro médio. Para determinação do valor de p foi utilizado one-way ANOVA seguido do pós-teste de Bonferroni, no qual todas as médias foram comparadas entre si. Os valores da viabilidade celular de *S. cerevisiae* WT cultivada em restrição calórica já haviam sido apresentados na Tabela 1.1, e o são aqui novamente para o bem da clareza.

	WT 2,0%	<i>aco1Δ</i> 2,0%	<i>kgd1Δ</i> 2,0%	<i>sdh1Δ</i> 2,0%	<i>p < 0,05</i>
16^a h	$78,71 \pm 4,85$	$48,00 \pm 4,55$	$46,58 \pm 1,66$	$64,11 \pm 1,82$	WT vs. <i>aco1Δ</i> e <i>kgd1Δ</i>
7^o dia	$49,42 \pm 2,06$	$42,17 \pm 2,61$	$20,50 \pm 2,23$	$21,67 \pm 1,96$	WT vs. <i>aco1Δ</i> e <i>kgd1Δ</i> ; <i>aco1Δ</i> vs. <i>kgd1Δ</i> e <i>sdh1Δ</i>
14^o dia	$42,36 \pm 2,54$	$40,11 \pm 2,89$	$5,75 \pm 11,10$	$5,74 \pm 4,68$	WT vs. <i>sdh1Δ</i> e <i>kgd1Δ</i> ; <i>aco1Δ</i> vs. <i>kgd1Δ</i> e <i>sdh1Δ</i>
21^o dia	$32,07 \pm 2,61$	$33,00 \pm 5,67$	$0,00 \pm 0,00$	$0,00 \pm 0,00$	WT vs. <i>sdh1Δ</i> e <i>kgd1Δ</i> ; <i>aco1Δ</i> vs. <i>kgd1Δ</i> e <i>sdh1Δ</i>
28^o dia	$22,99 \pm 3,18$	$30,67 \pm 4,66$	$0,00 \pm 0,00$	$0,00 \pm 0,00$	WT vs. <i>sdh1Δ</i> e <i>kgd1Δ</i> ; <i>aco1Δ</i> vs. <i>kgd1Δ</i> e <i>sdh1Δ</i>

Podemos verificar que (i) o mutante *aco1Δ* apresentou uma viabilidade celular diminuída em relação à célula selvagem no 1^o e no 7^o dia de cultivo, porém não o fez a partir do 14^o dia, em ambas as condições de cultivo; que (ii) a inativação de *KGD1* diminuiu significativamente a viabilidade de *S. cerevisiae* em condição controle e em restrição calórica em todos os tempos estudados; e que (iii) o mutante *sdh1Δ* apresentou uma diminuição da viabilidade celular em relação à célula selvagem, em ambas as condições de cultivo, a partir do 7^o dia, tempo em que também passa a exibir valores de viabilidade comparáveis ao mutante *kgd1Δ* quando em condição controle (Tabelas 2.3 e 2.4).

Tabela 2.4. Valores da viabilidade celular de *S. cerevisiae* *aco1Δ*, *kgd1Δ* e *sdh1Δ* cultivadas em restrição calórica. Os valores abaixo estão expressos em média do número de colônias ± erro médio. Para determinação do valor de *p* foi utilizado one-way ANOVA seguido do pós-teste de Bonferroni, no qual todas as médias foram comparadas entre si. Os valores da viabilidade celular de *S. cerevisiae* WT cultivada em condição controle já haviam sido apresentados na Tabela 1.2, e o são aqui novamente para o bem da clareza.

	WT 0,5%	<i>aco1Δ</i> 0,5%	<i>kgd1Δ</i> 0,5%	<i>sdh1Δ</i> 0,5%	<i>p</i> < 0,05
16^a h	102,70 ± 5,61	67,09 ± 7,41	63,33 ± 4,86	99,33 ± 0,66	WT vs. <i>aco1Δ</i> e <i>kgd1Δ</i> ; <i>sdh1Δ</i> vs. <i>aco1Δ</i> e <i>kgd1Δ</i>
7º dia	74,56 ± 1,91	63,50 ± 0,87	63,50 ± 3,38	50,67 ± 2,03	WT vs. <i>aco1Δ</i> , <i>kgd1Δ</i> e <i>sdh1Δ</i> ; <i>aco1Δ</i> vs. <i>kgd1Δ</i> e <i>sdh1Δ</i> ; <i>kgd1Δ</i> vs. <i>sdh1Δ</i>
14º dia	73,00 ± 3,28	64,00 ± 2,72	20,33 ± 3,02	38,92 ± 2,28	WT vs. <i>kgd1Δ</i> e <i>sdh1Δ</i> ; <i>aco1Δ</i> vs. <i>kgd1Δ</i> e <i>sdh1Δ</i> ; <i>kgd1Δ</i> vs. <i>sdh1Δ</i>
21º dia	67,89 ± 7,64	61,84 ± 1,83	1,08 ± 0,67	38,54 ± 1,67	<i>sdh1Δ</i> vs. WT e <i>kgd1Δ</i>
28º dia	60,02 ± 2,37	52,67 ± 0,33	0,00 ± 0,00	35,75 ± 2,06	WT vs. <i>kgd1Δ</i> e <i>sdh1Δ</i> ; <i>aco1Δ</i> vs. <i>kgd1Δ</i> e <i>sdh1Δ</i> ; <i>kgd1Δ</i> vs. <i>sdh1Δ</i>

Quanto à responsividade à restrição calórica, observamos que, os três mutantes do ciclo dos ácidos tricarboxílicos estudados apresentaram aumento da viabilidade celular quando cultivados em restrição calórica (Figura 2.2.). Esses achados indicam que as interrupções pontuais promovidas pela inativação de *ACO1*, *KGD1* e *SDH1* não impedem o aumento do tempo de vida cronológico de *S. cerevisiae* quando caloricamente restrita.

2.4. Tempo de vida cronológico de *S. cerevisiae* ρ^0 e *abf2Δ*

Uma vez que os mutantes do ciclo dos ácidos tricarboxílicos *aco1Δ*, *kgd1Δ* e *sdh1Δ* mostraram-se responsivos à restrição calórica (Figura 2.2), decidimos investigar se a interrupção do metabolismo respiratório a jusante desta via metabólica impede o aumento do tempo de vida cronológico em *S. cerevisiae* promovido por esta condição de cultivo. Desta forma, decidimos estudar a responsividade à restrição calórica de mutantes de *S. cerevisiae* que apresentam deficiências em seu DNA mitocondrial.

Em *S. cerevisiae*, o DNA mitocondrial é responsável pela codificação das subunidades 1, 2 e 3 da citocromo *c* oxidase, do apocitocromo *b* e das subunidades 6, 8 e 9 da ATP sintase (Foury *et al.*, 1998). Desta forma, mutantes com ausência funcional do DNA mitocondrial *per se* ou com defeitos na manutenção de sua integridade e funcionalidade apresentam importantes deficiências no metabolismo aeróbico. Para isso, isolamos e caracterizamos um mutante ρ^0 (Seção 2; Item 12 em *Materiais e Métodos*), além de também termos escolhido outro, com inativação no gene *ABF2*, para ser objeto de estudo. O mutante *abf2Δ* não possui a proteína de ligação *ars*, um membro da família de proteínas mitocondriais de alta mobilidade, importante para a replicação, a recombinação e a estabilidade do DNA mitocondrial de *S. cerevisiae* (Diffley e Stillman, 1991 e 1992), não sendo capaz de crescer em meio seletivo para respiração quando previamente cultivado em glucose (Zelenaya-Troitskaya *et al.*, 1995).

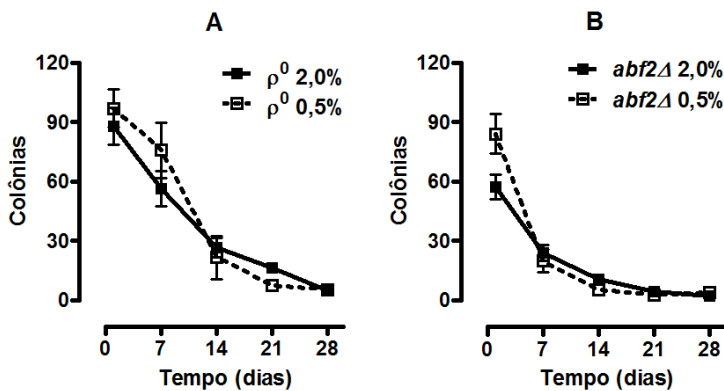


Figura 2.3. Tempo de vida cronológico de *S. cerevisiae* ρ^0 e $abf2\Delta$. A determinação das viabilidades celulares de *S. cerevisiae* ρ^0 (Painel A) e $abf2\Delta$ (Painel B) na 16^a h, e no 7º, 14º, 21º e 28º dia de cultivo foi realizada conforme descrição em *Materiais e Métodos* (Item 4).

Tabela 2.5. Valores da viabilidade celular de *S. cerevisiae* ρ^0 e $abf2\Delta$ cultivadas em condição controle. Os valores abaixo estão expressos em média do número de colônias \pm erro médio. Para determinação do valor de p foi utilizado one-way ANOVA seguido do pós-teste de Bonferroni, no qual todas as médias foram comparadas entre si. Os valores da viabilidade celular de *S. cerevisiae* WT cultivada em condição controle já haviam sido apresentados na Tabela 1.1, e o são aqui novamente para o bem da clareza.

	WT 2,0%	ρ^0 2,0%	$abf2\Delta$ 2,0%	$p < 0,05$
16^a h	$78,71 \pm 4,85$	$87,74 \pm 9,28$	$57,22 \pm 6,284$	-
7º dia	$49,42 \pm 2,06$	$56,41 \pm 8,79$	$24,11 \pm 4,05$	$abf2\Delta$ vs. WT e ρ^0
14º dia	$42,36 \pm 2,54$	$26,44 \pm 4,81$	$10,78 \pm 0,67$	WT vs. ρ^0 e $abf2\Delta$
21º dia	$32,07 \pm 2,61$	$16,15 \pm 1,96$	$4,44 \pm 1,17$	WT vs. ρ^0 e $abf2\Delta$; ρ^0 vs. $abf2\Delta$
28º dia	$22,99 \pm 3,18$	$4,78 \pm 2,19$	$2,22 \pm 0,77$	WT vs. ρ^0 e $abf2\Delta$

Verificamos que a ausência de atividade do DNA mitocondrial, seja em um mutante sem o genoma mitocondrial *per se* – ρ^0 – seja em um mutante com defeitos na manutenção de sua integridade e funcionalidade – $abf2\Delta$ – resulta em uma completa supressão da resposta de *S. cerevisiae* à restrição calórica (Figura 2.3). Esta observação demonstra que a interrupção do fluxo de elétrons pela cadeia de transporte de elétrons mitocondrial, e as consequências disso, tais como a perda da fosforilação oxidativa, do potencial de membrana mitocondrial e deficiências na importação de proteínas (Baker e Schatz, 1991; Stuart *et al.*, 1994) abolem totalmente o aumento do tempo de vida cronológico promovido pela restrição calórica em *S. cerevisiae*.

Podemos adicionalmente observar que o mutante $abf2\Delta$ também exibe uma viabilidade celular diminuída com relação àquela da linhagem parental em todos os dias de experimento (Tabela 2.5). Essa observação permite-nos concluir que a ausência da Afb2p, além de suprimir o aumento do tempo de vida cronológico das células cultivadas em restrição calórica, também limita o tempo de vida cronológico de *S. cerevisiae* quando esta é cultivada em condição controle. Interessantemente, já no 7º dia de cultivo os mutantes $abf2\Delta$ exibem uma viabilidade celular diminuída em relação à célula selvagem, o que só ocorre com o mutante ρ^0 a partir do 14º dia de

cultivo (Tabela 2.5). Essa observação sugere que a *Abf2p* exerce outros papéis além daquele de garantir a replicação, a recombinação e a estabilidade do DNA mitocondrial na determinação do tempo de vida cronológico em *S. cerevisiae*.

2.5. Tempo de vida cronológico de *S. cerevisiae cyt1Δ*

A adequada funcionalidade mitocondrial requer que haja uma concertada interação entre os genomas nuclear e mitocondrial (Linnane *et al.*, 1972; Falkenberg *et al.*, 2007). Uma vez que a ausência do DNA mitocondrial suprime o aumento do tempo de vida de *S. cerevisiae* mediado pela restrição calórica (Figura 2.3), decidimos investigar se a ausência de uma subunidade específica da cadeia de transporte de elétrons mitocondrial codificada pelo DNA nuclear poderia promover essa mesma irresponsividade. Desta forma, em ambas as condições de cultivo, determinamos o tempo de vida cronológico do mutante *cyt1Δ*, que não possui o citocromo *c₁*, um componente do complexo ubiquinol-citocromo *c* redutase, o primeiro transportador de prótons da cadeia de transporte de elétrons em *S. cerevisiae* (Sidhu e Beattie, 1983).

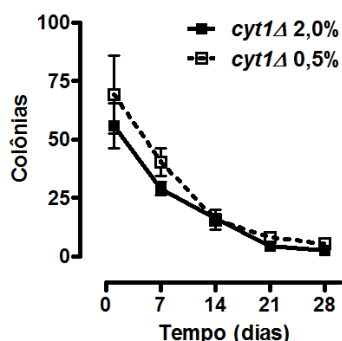


Figura 2.4. Tempo de vida cronológico de *S. cerevisiae cyt1Δ*. A determinação da viabilidade celular de *S. cerevisiae cyt1Δ* na 16^a h, e no 7^º, 14^º, 21^º e 28^º dia de cultivo foi realizada conforme descrição em *Materiais e Métodos* (Item 4).

Embora Kaeberlein e colaboradores tenham demonstrado que a restrição calórica é capaz de aumentar o tempo de vida replicativo do mutante *cyt1Δ* (Kaeberlein *et al.*, 2005), verificamos esse mesmo mutante não apresenta aumento do tempo de vida cronológico mediado pela restrição calórica (Figura 2.4), além de exibir uma viabilidade celular diminuída quando comparada à célula selvagem (Tabela 2.6). Essa observação indica que a inativação de um gene nuclear que codifica uma subunidade específica da cadeia de transporte de elétrons mitocondrial pode também promover a irresponsividade de *S. cerevisiae* à restrição calórica. Além disso – e sobretudo – esse achado, em conjunto com a ineeficácia da restrição calórica em aumentar o tempo de vida nos mutantes *ρ⁰* e *abf2Δ*, suporta a idéia de que a integridade da cadeia de transporte de elétrons é essencial para a viabilidade em fase estacionária de crescimento e também para o aumento do tempo de vida cronológico mediado pela restrição calórica.

Tabela 2.6. Valores da viabilidade celular de *S. cerevisiae cyt1Δ* cultivada em condição controle. Os valores abaixo estão expressos em média ± erro médio. Para determinação do valor de p foi utilizado o teste t de Student não-pareado. Os valores da viabilidade celular de *S. cerevisiae WT* cultivada em condição controle já haviam sido apresentados na Tabela 1.1, e o estão sendo aqui novamente para o bem da clareza.

	WT 2,0%	cyt1Δ 2,0%	$p < 0,05$
16^a h	$78,71 \pm 4,85$	$55,92 \pm 9,57$	não
7º dia	$49,42 \pm 2,06$	$29,00 \pm 2,67$	sim
14º dia	$42,36 \pm 2,54$	$16,33 \pm 1,07$	sim
21º dia	$32,07 \pm 2,61$	$4,58 \pm 0,41$	sim
28º dia	$22,99 \pm 3,18$	$2,66 \pm 1,00$	sim

2.6. Tempo de vida cronológico de *S. cerevisiae atp2Δ*

Os resultados até aqui obtidos indicam que a integridade da cadeia de transporte de elétrons mitocondrial é necessária para a responsividade de *S. cerevisiae* à restrição calórica (Figuras 2.3 e 2.4). No entanto, os mutantes ρ^0 também apresentam defeitos na ATP sintase, uma vez que as suas subunidades 6, 8 e 9 são codificadas pelo genoma mitocondrial (Foury *et al.*, 1998). Desta forma, com o objetivo de determinar isoladamente o impacto de um defeito na ATP sintase na determinação do tempo de vida cronológico e na resposta à restrição calórica, investigamos se o mutante *atp2Δ*, que não possui a subunidade β do componente F1 da ATP sintase (Saltzgaber-Muller *et al.*, 1983), é capaz responder à restrição calórica com o aumento do tempo de vida cronológico.

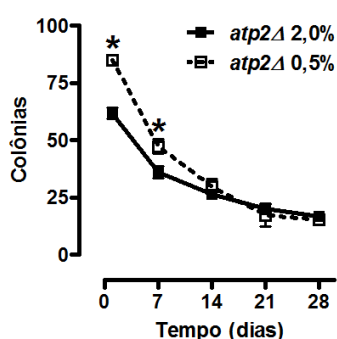


Figura 2.5. Tempo de vida cronológico de *S. cerevisiae atp2Δ*. A determinação das viabilidades celulares de *S. cerevisiae atp2Δ* na 16^a hora, e no 7º, 14º, 21º e 28º dia de cultivo foi realizada conforme descrição em *Materiais e Métodos* (Item 4) * $p < 0,05$ vs. 2,0% (teste t de Student não-pareado).

Podemos observar que o mutante *atp2Δ* caloricamente restrito apresenta maior viabilidade celular apenas na 16^a hora e no 7º dia de cultivo (Figura 2.5). A exibição de viabilidades celulares iguais a partir do 14º dia de cultivo entre este mutante cultivado em condição controle e em restrição calórica demonstra que defeitos advindos da ausência da Atp2p comprometem a resposta

a longo prazo de *S. cerevisiae* à restrição calórica. Também é interessante notar que até o 21º dia de cultivo, *S. cerevisiae* com inativação em *ATP2* possui uma viabilidade celular significativamente menor do que a célula selvagem, demonstrando a importância da síntese de ATP na determinação do tempo de vida cronológico de *S. cerevisiae* nas três primeiras semanas de cultivo (Tabela 2.7).

Tabela 2.7. Valores da viabilidade celular de *S. cerevisiae atp2Δ* cultivada em condição controle. Os valores abaixo estão expressos em média ± erro médio. Para determinação do valor de *p* foi utilizado o teste *t* de Student não-pareado. Os valores da viabilidade celular de *S. cerevisiae* WT cultivada em condição controle já haviam sido apresentados na Tabela 1.1, e o estão sendo aqui novamente para o bem da clareza.

	WT 2,0%	<i>atp2Δ</i> 2,0%	<i>p</i> < 0,05
16^a h	78,71 ± 4,85	61,67 ± 2,47	sim
7º dia	49,42 ± 2,06	35,87 ± 2,61	sim
14º dia	42,36 ± 2,54	26,42 ± 2,15	sim
21º dia	32,07 ± 2,61	20,27 ± 2,22	sim
28º dia	22,99 ± 3,18	16,78 ± 0,86	não

2.7. Capacidade de crescimento de *S. cerevisiae* em meio seletivo rico e meio seletivo sintético para respiração

Como já discutido anteriormente, a aptidão respiratória que confere a *S. cerevisiae* a habilidade de utilizar substratos que sejam metabolizados por vias aeróbicas é de fundamental importância para a manutenção da viabilidade dessa levedura em fase estacionária de crescimento dado que a quantidade de glicose disponível nos meios de cultura utilizados para a realização dos cultivos celulares para a determinação do tempo de vida cronológico é finita. Dessa forma, com o objetivo de investigar a capacidade de crescimento dos mutantes previamente estudados e correlacioná-la com a duração do tempo de vida cronológico e com a responsividade à restrição calórica, determinamos a aptidão respiratória da célula selvagem e dos mutantes em meio seletivo rico – YPEG – e sintético para respiração – SEG.

Observamos a existência de quatro grupos de *S. cerevisiae*, determinados segundo a sua capacidade de crescimento em meio seletivo rico e sintético para respiração: (i) o grupo que exibe crescimento em ambos os meios seletivos – WT e *aco1Δ*; (ii) o grupo que exibe crescimento residual, apenas no meio seletivo rico – *npt1Δlpd1Δ* e *atp2Δ*; (iii) o grupo capaz de exibir comparativamente maior extensão de crescimento em meio seletivo rico – *lpd1Δ*, *bna6Δlpd1Δ*, *kgd1Δ* e *sdh1Δ*; e (iv) o grupo que não exibe crescimento em nenhum deles – ρ^0 , *abf2Δ* e *cyt1Δ*.

Este último grupo é composto por mutantes que não apresentam aumento do tempo de vida cronológico mediado pela restrição calórica – ρ^0 , *abf2Δ* e *cyt1Δ*. (Figuras 2.3 e 2.4). Já os mutantes que apresentam um tempo de vida cronológico diminuído em relação à célula selvagem, mas que

ainda são capazes de responder à restrição calórica com seu aumento, estão reunidos no terceiro grupo – *lpd1Δ*, *bna6Δlpd1Δ*, *kgd1Δ* e *sdh1Δ* (Figura 2.1, Painéis A e C; Figura 2.2, Painéis B e C). No segundo grupo, estão os mutantes *npt1Δlpd1Δ* e *atp2Δ*: enquanto o primeiro não apresenta responsividade à restrição calórica e exibe uma severa diminuição no tempo de vida replicativo (Figura 2.1, Painel B), o segundo é parcialmente responsável à restrição calórica (Figura 2.5).

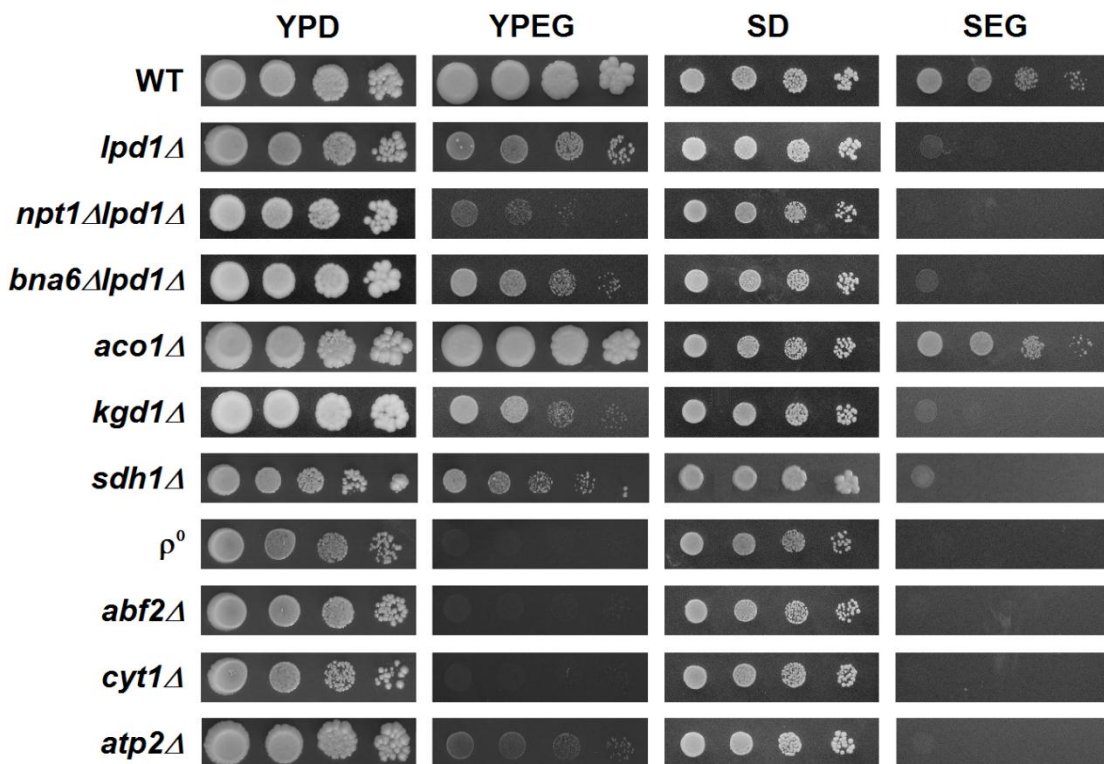


Figura 2.6. Capacidade de crescimento em meio seletivo rico e meio seletivo sintético para respiração. A determinação da capacidade de crescimento de *S. cerevisiae* WT, *lpd1Δ*, *npt1Δlpd1Δ*, *bna6Δlpd1Δ*, *aco1Δ*, *kgd1Δ*, *sdh1Δ*, ρ^0 , *abf2Δ*, *cyt1Δ* e *atp2Δ* em meio seletivo rico e meio seletivo sintético para respiração foi realizada conforme descrição em *Materiais e Métodos* (Item 13). A documentação fotográfica foi realizada após sete dias de crescimento a 30 °C. A figura acima é representativa de, no mínimo, duas repetições independentes. YPD (meio fermentativo rico): extrato de levedura 1%, peptona 2%, glicose 2%, ágar; YPEG (meio seletivo rico para respiração): extrato de levedura 1%, peptona 2%, etanol 2%, glicerol 2%, ágar 2%; SD (meio fermentativo sintético): base nitrogenada 0,17%, sulfato de amônio 0,5%, glicose 2% e ágar 2% suplementado com adenina e aminoácidos (Item 3 em *Materiais e Métodos*); SEG (meio seletivo sintético para respiração): base nitrogenada 0,17%, sulfato de amônio 0,5%, etanol 2%, glicerol 2% e ágar 2% suplementado com adenina e aminoácidos (Item 3 em *Materiais e Métodos*).

É interessante notar que, classicamente, mutantes do ciclo dos ácidos tricarboxílicos são considerados inaptos ao crescimento em meio que não contém fontes de carbono fermentáveis (Tzagoloff e Dieckmann, 1990). De fato, esses mutantes – que compõem o segundo e o terceiro grupos, exceção feita à *S. cerevisiae atp2Δ* – somente exibiram crescimento em meio seletivo rico para respiração devido à presença de intermediários do ciclo dos ácidos tricarboxílicos no extrato de levedura presente em sua composição. Na presença de extrato de levedura, NADH e FADH₂ podem ser gerados em reações dessa via à montante ou à jusante das disruptões promovidas pelas inativações gênicas e então ser oxidados pela cadeia de transporte de elétrons mitocondrial.

Portanto, em incubações a longo prazo como a realizada aqui, os mutantes ciclo dos ácidos tricarboxílicos são capazes de exibir crescimento em meio seletivo rico para respiração, mas não em meio seletivo sintético – que não possui extrato de levedura em sua composição. Além disso, é notável a extensão do crescimento do mutante *aco1Δ* – comparável à célula selvagem – tanto em meio seletivo rico para respiração quanto em meio seletivo sintético. De fato, a *ORF YJL200c (ACO2)*, presente no mutante *aco1Δ*, codifica uma segunda isoforma de aconitase em *S. cerevisiae* (Sickmann *et al.*, 2003).

Em suma, podemos concluir que, nessas condições, a capacidade de crescimento em meio seletivo rico e em meio seletivo sintético para respiração oferece a informação da aptidão respiratória a longo prazo de *S. cerevisiae*, a qual se correlaciona qualitativamente com a presença e a intensidade de resposta dessa levedura à restrição calórica e com a duração de seu tempo de vida cronológico.

2.8. Progressão temporal da porcentagem de células respiratório-competentes durante o envelhecimento cronológico de *S. cerevisiae*

O DNA mitocondrial é organizado sob a forma de estruturas denominadas *nucleóides*, complexos formados pela interação de proteínas empacotadoras e a dupla-fita de ácidos nucléicos (Kucej e Butow, 2007). Desde a descoberta da existência desses complexos nucleoprotéicos em *S. cerevisiae* (Rickwood *et al.*, 1981), muitos avanços quanto à natureza das proteínas nucleoidais e seu papel na manutenção da funcionalidade do mtDNA desse organismo foram alcançados (Miyakawa *et al.*, 1984, 1987 e 1995; Zelenaya-Troitskaya, 1995; Newman *et al.*, 1996; Meeusen *et al.*, 1999; Hoobs *et al.*, 2001; Brewer *et al.*, 2003; Kaufman *et al.*, 2003; Chen *et al.*, 2005; Nosek *et al.*, 2006).

Atualmente, tem-se uma lista contendo mais de vinte proteínas que são reconhecidas como participantes dos nucleóides. Curiosamente, a maioria delas exibe “funções primárias” no metabolismo do etanol, do piruvato, de intermediários do ciclo dos ácidos tricarboxílicos e de aminoácidos de cadeia ramificada (Chen *et al.*, 2005). Além disso, foi demonstrada, recentemente, a existência de um mecanismo de remodelamento do perfil do conjunto dessas proteínas empacotadoras do genoma mitocondrial, regulado pelo estado metabólico de *S. cerevisiae* (Kucej *et al.*, 2008). Dentre as proteínas portadoras de “funções primárias” em outras vias metabólicas de *S. cerevisiae* por nós estudadas, estão a Aco1p (Figura 2.2, Painel A e Figura 2.6), a Kgd1p (Figura 2.2, Painel B e Figura 2.6) e a Lpd1p (Figura 2.1, Painel A e Figura 2.6).

De fato, durante a realização das determinações do tempo de vida cronológico desses três mutantes, além do *sdh1Δ*, notamos a existência de diferentes tendências de esses mutantes espontaneamente formarem colônias do tipo *petite* – as quais são quase que exclusivamente relacionadas com a instabilidade e consequente perda da funcionalidade do DNA mitocondrial

(Linnane *et al.*, 1989; Ferguson e von Borstel, 1992). Portanto, decidimos quantificar a progressão temporal da porcentagem da população de células respiratório-competentes (ρ^+) em *S. cerevisiae* com inativações em *ACO1*, *KGD1*, *LPD1* e *SDH1* em condição controle de cultivo e em restrição calórica.

Pela análise da Figura 2.7, observamos que essas quatro inativações alteraram a estabilidade do DNA mitocondrial de forma dependente (i) do tempo e (ii) da condição de cultivo. Podemos verificar que na 16^a h de cultivo, em condição controle, as ausências da Aco1p e da Kgd1p diminuíram a estabilidade do DNA mitocondrial, enquanto a ausência da Lpd1p reduziu a porcentagem de células ρ^+ em restrição.

Comparando as porcentagens de células ρ^+ entre a 16 h e o 7º dia de cultivo – período em que a glicose é totalmente consumida (Figura 3.4, Painel A) – verificamos que, em condição controle, (i) a porcentagem de colônias ρ^+ no mutante *aco1Δ* no 7º dia foi maior do que na 16^a h [$60,67 \pm 3,62$ (16^a h) vs. $94,91 \pm 2,02$ (7º d), $p = 0,0007$]; e que (ii) esse parâmetro em *S. cerevisiae kgd1Δ* permaneceu inalterado [$58,02 \pm 4,85$ (16^a h) vs. $57,86 \pm 7,46$ (7º d), $p = 0,9865$]. Essa observação demonstra a importância da Kgd1p na manutenção da estabilidade do DNA mitocondrial de *S. cerevisiae* nessa etapa da longevidade cronológica. Já em restrição calórica, verificamos que a porcentagem de colônias ρ^+ no 7º dia de cultivo (i) permaneceu inalterada em relação à 16^a h no mutante *sdh1Δ* [$83,14 \pm 0,27$ (16^a h) vs. $79,39 \pm 3,25$ (7º d), $p = 0,4855$]; (ii) foi aumentada no mutante *lpd1Δ* [$59,83 \pm 4,84$ (16^a h) vs. $72,33 \pm 1,86$ (7º d), $p = 0,0422$]; e (iii) foi diminuída no mutante *kdg1Δ* [$69,65 \pm 2,82$ (16^a h) vs. $39,69 \pm 2,75$ (7º d), $p = 0,0016$], fazendo com que esses três mutantes exibam uma estabilidade do DNA mitocondrial significativamente diminuída quando comparada à célula selvagem.

É interessante notar a tendência geral ao aumento da porcentagem de células ρ^+ da 16^a h – tempo que ainda há a presença de glicose nos meios de cultura (Figura 3.2, Painel A) – até o 7º dia de cultivo. Embora essa observação possa ser justificada utilizando o argumento da existência de um mecanismo que exerce uma pressão seletiva sobre as células ρ^0 causado pela exaustão da glicose – o que promoveria a morte celular destas e, consequentemente, a diminuição percentual de sua presença nos cultivos ao longo do tempo – podemos observar que a viabilidade cronológica do mutante ρ^0 cultivado em condição controle é comparável àquela apresentada pela célula selvagem até o 14º dia de cultivo (Tabela 2.5).

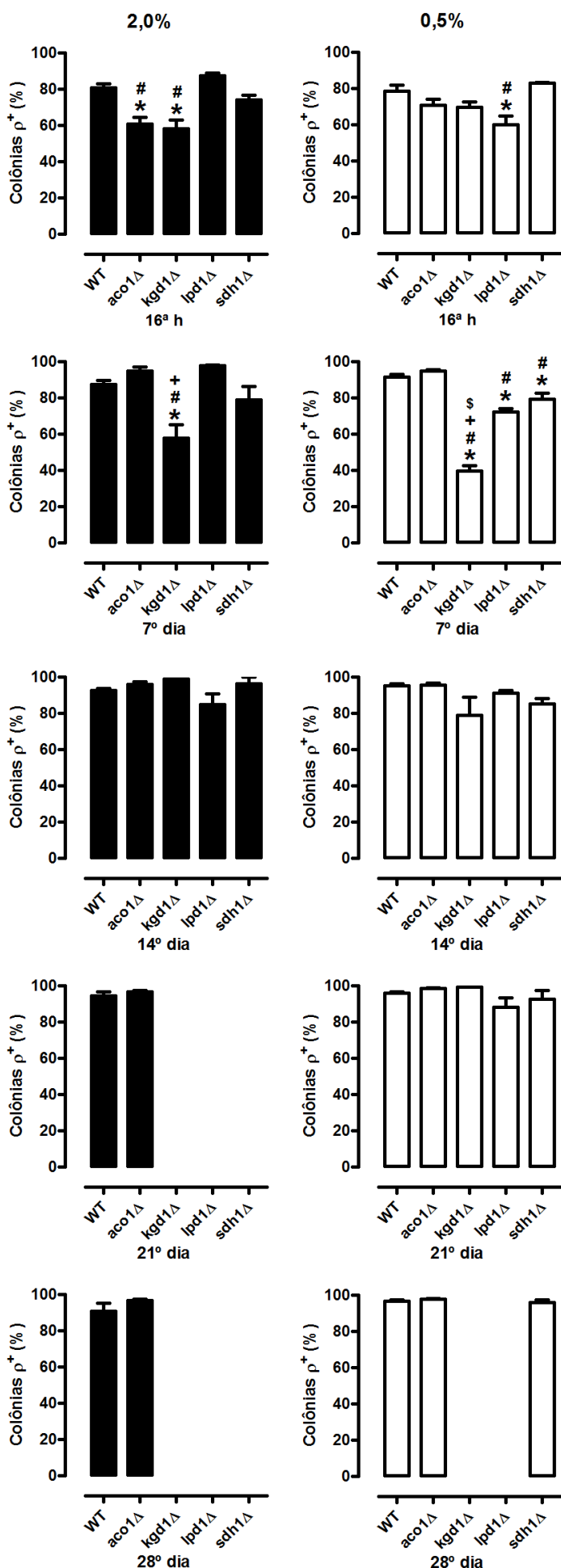


Figura 2.7. Progressão temporal da porcentagem de células respiratório-competentes durante o envelhecimento cronológico de *S. cerevisiae* WT, *aco1Δ*, *kgd1Δ*, *lpd1Δ* e *sdh1Δ*. A determinação da porcentagem de células respiratório-competentes (ρ^+) em *S. cerevisiae* WT, *aco1Δ*, *kgd1Δ*, *lpd1Δ* e *sdh1Δ* na 16^a h, e no 7^o, 14^o, 21^o e 28^o dia de cultivo através da replicação das colônias formadas em placas contendo YPD sólido em placas contendo meio seletivo rico para respiração (YPEG) sólido foi realizada conforme descrição em *Materiais e Métodos* (Item 14). O teste estatístico utilizado para a comparação das médias foi o one-way ANOVA seguido do pós-teste de Bonferroni. 16^a h, 2,0%: * $p < 0,05$ vs. WT; # $p < 0,05$ vs. *lpd1Δ*. 16^a h, 0,5%: * $p < 0,05$ vs. WT; # $p < 0,05$ vs. *sdh1Δ*. 7^o dia, 2,0%: * $p < 0,05$ vs. WT; * $p < 0,05$ vs. *aco1Δ*; * $p < 0,05$ vs. *lpd1Δ*. 7^o dia, 0,5%: * $p < 0,05$ vs. WT; # $p < 0,05$ vs. *aco1Δ*; + $p < 0,05$ vs. *lpd1Δ*; \$ $p < 0,05$ vs. *sdh1Δ*.

De fato, como previamente discutido, essa observação indica que a sobrevivência de uma célula ρ^0 em meio com ausência de uma fonte de carbono fermentável não é influenciada de forma significativa durante os primeiros 14 dias de cultivo. Porém, a incapacidade de os mutantes ρ^0 em utilizar substratos metabolizados aerobicamente (Figura 3.8, Painel C) e a consequente ausência do crescimento de biomassa promovida por esses substratos nesses mutantes (Figura 3.2, Painel C; Figura 3.8, Painel B), somadas ao fato de que as células selvagens possuem uma velocidade específica máxima de crescimento em glicose significativamente aumentada em relação ao mutante ρ^0 (Figura 3.6, Painel A), além de exibir crescimento de biomassa suportado por substratos metabolizados aerobicamente (Figura 3.8, Painel D), são os fatores que decisivamente contribuem para a observação da diminuição percentual das células ρ^0 da 16^a hora ao 7º dia de cultivo.

Ainda mais notável, portanto, é a diminuição da porcentagem de células ρ^+ no mutante *kgd1Δ* observada nos primeiros sete dias de cultivo quando cultivado em restrição calórica, demonstrando que, diferentemente das inativações de *LPD1* e *SDH1*, a inativação de *KGD1* promove uma instabilidade ao genoma mitocondrial sem paralelo dentre os mutantes estudados nesse período de cultivo.

Finalmente, é possível inferir que a Sdh1p – mesmo não tendo sido descrita como uma proteína participante do complexo nucleóide – participa indiretamente da regulação da estabilidade do DNA mitocondrial, uma vez que o mutante *sdh1Δ* apresentou uma diminuição da porcentagem de células ρ^+ aumentada em relação à célula selvagem em restrição calórica no 7º dia de cultivo. De fato, Lee e colaboradores predisseram uma provável interação desta com a Kgd1p em *S. cerevisiae* (Lee *et al.*, 2007).

2.9. Tempo de vida cronológico de *Kluyveromyces lactis*

A conclusão advinda dos resultados obtidos através das determinações do tempo de vida cronológico em condição controle e em restrição calórica nos diferentes mutantes de *S. cerevisiae* é a de que a integridade da cadeia de transporte de elétrons é estritamente necessária para que a redução da oferta inicial de glicose nos meios YPD possa aumentar o tempo de vida cronológico dessa levedura (Figuras 2.3 e 2.4).

É interessante considerar que a glicose diminui a expressão de uma série de enzimas relacionadas ao metabolismo aeróbico em *S. cerevisiae*, em um fenômeno denominado *repressão por glicose*, relatado na literatura desde os anos 1960 (Yotsuyanagi, 1962; Polakis e Bartley, 1965; Polakis *et al.*, 1965; Jayaraman *et al.*, 1966; Rolland *et al.*, 2002). De fato, *S. cerevisiae* é uma levedura Crabtree-positiva, a qual, quando presente em altas concentrações de glicose, tem o destino metabólico do piruvato direcionado à conversão a etanol em detrimento de sua conversão a acetil-CoA, independentemente da presença de oxigênio (De Deken, 1966; Fiechter *et al.*, 1981).

Desta forma, questionamos se a mitigação da repressão do metabolismo aeróbico por glicose em *S. cerevisiae* era um fator necessário para a eficácia do protocolo de restrição calórica em levedura. Para investigar esta possibilidade, decidimos verificar se o tempo de vida cronológico de *Kluyveromyces lactis*, uma levedura ascomiceta como *S. cerevisiae*, porém Crabtree-negativa (Kiers *et al.*, 1998), poderia ser aumentado quando esta fosse cultivada em restrição calórica.

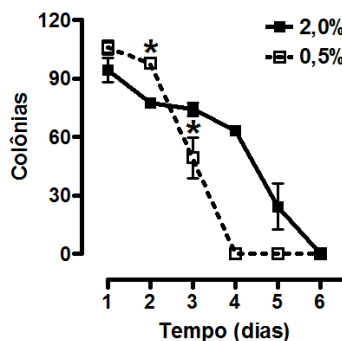


Figura 2.8. Tempo de vida cronológico de *K. lactis*. A determinação da viabilidade celular de *K. lactis* da 16^a h ao 6º dia de cultivo foi realizada conforme descrição em *Materiais e Métodos* (Item 4). * $p < 0,05$ vs. 2,0% (teste *t* de Student não-pareado).

Pela análise da Figura 2.8, podemos observar que, apesar de *K. lactis* caloricamente restrita ter exibido uma viabilidade celular maior do que a célula cultivada em condição controle no 2º dia de cultivo, a partir do 3º dia o inverso já era verdadeiro. Além disso, a restrição calórica promoveu uma total inviabilidade de *K. lactis* já no 4º dia de cultivo, enquanto as células cultivadas em condição controle apresentaram uma razoável viabilidade até o 5º dia de cultivo. Desta forma, concluímos que o protocolo de restrição calórica para levedura não é capaz de aumentar o tempo de vida cronológico de *K. lactis*, demonstrando ser a mitigação da repressão por glicose promovida pela diminuição da quantidade inicial de glicose nos meios YPD um fator determinante para a exibição do aumento do tempo de vida cronológico em *S. cerevisiae*.

Também é notável a diminuída longevidade cronológica desta levedura quando comparada à de *S. cerevisiae*: enquanto *K. lactis* em ambas as condições de cultivo já exibe uma completa inviabilidade em menos de uma semana, *S. cerevisiae*, por sua vez, é capaz de se manter viável por períodos mais longos (Sinclair *et al.*, 1998; Reverter-Branchat *et al.*, 2004; Fabrizio e Longo, 2003; Figura 1.1, Painel A). Assim sendo, dada a sua irresponsividade à restrição calórica e ao seu curto tempo de vida cronológico, o uso extensivo de *K. lactis* como modelo para estudos dos efeitos da restrição calórica envelhecimento não se torna, no momento, de considerável interesse.

2.10. Conclusões

Podemos concluir, portanto, que as (i) inativações concomitantes de *BNA6* e *LPD1*, além (ii) das inativações de *ABF2* e de *CYT1*, assim como (iii) a ausência do genoma mitocondrial *per se*,

diminuem a duração do tempo de vida cronológico de *S. cerevisiae* e também suprimem integralmente o aumento deste tempo de vida promovido pela restrição calórica. O defeito na subunidade β da ATP sintase faz com que *S. cerevisiae* exiba uma resposta parcial à restrição calórica. Inativações de genes que codificam enzimas participantes de etapas de conversão de intermediários do ciclo dos ácidos tricarboxílicos tais como *ACO1*, *KGD1*, *LPD1* e *SDH1*, por sua vez, não impedem o aumento do tempo de vida cronológico em virtude da restrição calórica. Desta forma, a integridade funcional da cadeia de transporte de elétrons mostrou ser um requisito estritamente necessário para que *S. cerevisiae* tenha o seu tempo de vida cronológico aumentado pela restrição calórica. Além disso, a mitigação do fenômeno da repressão por glicose em *S. cerevisiae* promovida pela diminuição da disponibilidade inicial de glicose no meio de cultura caloricamente restrito mostrou-se essencial para que o protocolo de restrição calórica tenha êxito em aumentar o tempo de vida cronológico de levedura.

Finalmente, também observamos que em condição controle e na presença de glicose no meio de cultura (Figura 3.4, Painel A), *Aco1p* e *Kgd1p* são importantes para a manutenção do DNA mitocondrial de *S. cerevisiae*, enquanto em restrição calórica e na presença de glicose no meio de cultura (Figura 3.4, Painel A), *Lpd1p* o é. No 7º dia de cultivo, quando a glicose já não está mais presente (Figura 3.4, Painel A), (i) *Kgd1p* – em condição controle – e (ii) *Lpd1p*, *Sdh1p* e, novamente, *Kgd1p* – em restrição calórica – são proteínas cuja ausência é refletida em uma diminuição da porcentagem de células ρ^+ em *S. cerevisiae*. Em conjunto, essas observações demonstram que não somente a presença ou a ausência da glucose nos meios de cultura como também a sua disponibilidade inicial afetam diferencialmente as atividades de proteínas participantes do complexo nucleóide, corroborando a existência de mecanismos de recrutamento dessas proteínas sensíveis ao estado metabólico celular.

**Seção 3 – Restrição calórica e DNA mitocondrial como moduladores da história metabólica de
*Saccharomyces cerevisiae***

3.1. Estudo de parâmetros fisiológicos em *S. cerevisiae*

O estudo da fisiologia de *S. cerevisiae* através da quantificação dos fluxos metabólicos centrais é de grande importância para o entendimento de como essa levedura responde a diferentes condições de cultivo ao longo do tempo. Essa pesquisa pode ser realizada (i) pela quantificação de substratos e metabólitos extracelulares e (ii) pelo balanço dos metabólitos intracelulares através do uso de traçadores isotópicos como substratos (Aiba e Matsuoka, 1979; Stephanopoulos *et al.*, 1998; Frick e Wittmann, 2005).

Embora uma descrição mais detalhada e uma quantificação mais acurada do metabolismo de *S. cerevisiae* sejam obtidas pela combinação desses dois métodos de determinação, a quantificação temporal da fonte de carbono primária fornecida e dos produtos gerados e exportados pela célula para o meio de cultura torna-se uma ferramenta bastante informativa para a pesquisa de determinadas vias metabólicas em *S. cerevisiae*, quando analisada em conjunto com dados de formação de biomassa e variação do pH extracelular ao longo do tempo (Basso *et al.*, 2010).

A análise da exaustão da glicose e da dinâmica de metabólitos extracelulares tais como etanol, glicerol, acetato, piruvato e succinato e seu tratamento matemático para a obtenção de parâmetros fisiológicos dá origem a dados quantitativos que auxiliam na explicação de como *S. cerevisiae* tem, por exemplo, o fluxo do metabolismo de glicose modulado pela restrição calórica e pela ausência do DNA mitocondrial. Portanto, a quantificação de glicose e de seus metabólitos extracelulares, bem como a geração de biomassa e o monitoramento do pH extracelular foram realizados com a finalidade de caracterizar as alterações fisiológicas induzidas pela restrição calórica em *S. cerevisiae* WT e p^o.

3.2. Consumo de oxigênio em *S. cerevisiae* WT

A variação das taxas de consumo de oxigênio é uma verificação indefectível em *S. cerevisiae*, dadas as mudanças metabólicas pelas quais essa levedura passa ao longo de sua história cronológica. Com o objetivo de se determinar quais são as diferenças dos perfis de respiração existentes entre as células controle e as caloricamente restritas ao longo do envelhecimento cronológico, realizamos medidas de consumo de oxigênio em células intactas de *S. cerevisiae* WT.

A análise da Figura 3.1 permite observar que as células em restrição calórica atingem uma taxa máxima de consumo de oxigênio significativamente maior do que as células controle [$27,18 \pm 1,50$ (0,5%) vs. $15,09 \pm 0,48$ (2,0%); $p = 0,0015$ (teste *t* de Student não-pareado)], e o fazem 12 h mais precocemente ($t = 33$ h para 0,5% e $t = 45$ h para 2,0%). Além disso, a partir da 24^a h de cultivo, quando as células caloricamente restritas já iniciaram a utilização de etanol e glicerol como fontes de carbono (Tabela 2 em *Materiais e Métodos*), até a 42^a h de cultivo, o consumo de

oxigênio pelas células em restrição calórica é maior do que o das células controle. De fato, a respiração celular destas somente supera aquela das células caloricamente restritas na 45^a h de cultivo, justamente o ponto máximo de respiração das células controle. Já na 48^a h de cultivo, a taxa de consumo de oxigênio das células cultivadas em ambas as condições volta a ser igual, assim permanecendo até a 168^a h, quando o consumo de oxigênio das células controle volta a ser maior do que as células cultivadas em restrição calórica. Interessantemente, na 672^a h de cultivo, a taxa de consumo de oxigênio das células em restrição calórica passa a ser novamente maior do que aquela apresentada pelas células controle.

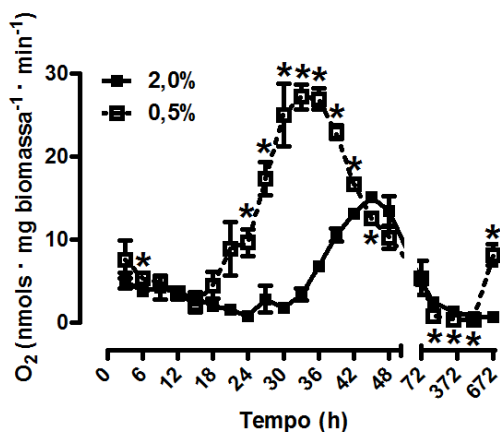


Figura 3.1. Consumo de oxigênio ao longo do tempo de vida cronológico em *S. cerevisiae* WT. A determinação do consumo de oxigênio em células intactas de *S. cerevisiae* WT foi realizada conforme descrição em *Materiais e métodos* (Item 15). * $p < 0,05$ vs. WT 2,0% (teste *t* de Student não-pareado).

As diferenças existentes entre as taxas máximas de respiração das células controle e caloricamente restritas seguramente advêm do efeito repressor que a glicose exerce sobre determinados genes que codificam proteínas que participam do metabolismo aeróbico, como já previamente discutido no Item 2.9. Notável é a observação de que mesmo após a sua exaustão (24 h na condição controle de cultivo e 18 h em restrição calórica; Figura 3.4, Painel A), a maior quantidade de glicose presente no início da cultura ainda exerce, ainda que indiretamente, um efeito fenotípico claramente distinto daquele observado nas células cujo início de cultivo foi realizado em uma condição de menor disponibilidade dessa fonte de carbono. Cabe aqui ressaltar que as quantidades relativas de etanol e glicerol – dois substratos oxidáveis de relevância para o metabolismo respiratório – atingem maiores concentrações na condição controle (Figura 3.4, Painéis B e C), excluindo a possibilidade de haver uma menor disponibilidade desses substratos por grama de biomassa nessa condição de cultivo.

3.3. Curvas de biomassa e de pH ao longo do tempo de vida cronológico de *S. cerevisiae* WT e ρ⁰

Para determinarmos a velocidade específica máxima de crescimento celular em glicose (Figura 3.6, Painel A) e em etanol/glicerol (Figura 3.8, Painel B), assim como os fatores de

conversão de glicose e de etanol/glicerol a biomassa (Figura 3.7, Painel A; Figura 3.8, Painel D), acompanhamos o crescimento celular de *S. cerevisiae* WT e ρ^0 através de sua absorbância a 600 nm (Abs_{600}) ao longo de 28 dias de cultivo em meio controle e em restrição calórica. Para posteriormente transformar os valores de Abs_{600} obtidos em valores de biomassa, determinamos o fator de conversão entre esses dois parâmetros segundo Olsson e Nielsen (1997), chegando ao valor de 0,194 mg/mL de biomassa seca por unidade de Abs_{600} (Item 18 em *Materiais e Métodos*).

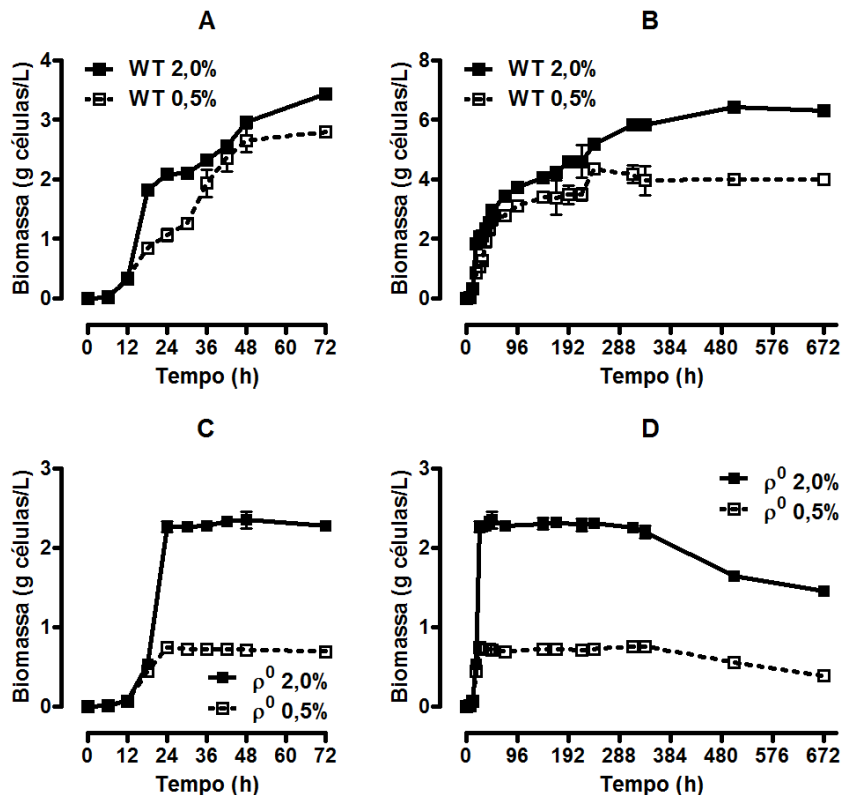


Figura 3.2. Curvas de biomassa ao longo do tempo de vida cronológico de *S. cerevisiae* WT e ρ^0 . As determinações da Abs_{600} e do fator de conversão de Abs_{600} a biomassa para a obtenção da curva de biomassa ao longo do tempo de vida cronológico de *S. cerevisiae* WT e ρ^0 foram realizadas conforme descrição em *Materiais e Métodos* (Itens 17 e 18). Os Paineis A e C apresentam uma escala de tempo diminuída para melhor visualização da fase exponencial de crescimento.

Analizando as curvas de biomassa em maior resolução (Figura 3.2, Painéis A e C), podemos observar qualitativamente a influência promovida pela ausência do DNA mitocondrial de *S. cerevisiae* sobre a geração de biomassa na fase pós-diáuxica (Monod, 1949): enquanto a célula selvagem apresenta crescimento celular promovido pela utilização de substratos oxidáveis – tais como o etanol e o glicerol – o mutante ρ^0 não o faz. Além disso, verificamos que, ao final dos 28 dias de cultivo, a biomassa formada pelas células cultivadas em condição controle ($6,32 \pm 0,12$ g biomasssa/L) é $38,50 \pm 1,64\%$ maior do que a formada pelas células cultivadas em restrição calórica ($3,88 \pm 0,14$ g biomasssa/L). Essa observação, somada ao fato de o meio caloricamente restrito possuir 75% menos glicose no início dos cultivos do que o meio controle, indica que a eficiência de conversão energética de *S. cerevisiae* cultivada em restrição calórica é maior do que a apresentada pelas células cultivadas em condição controle. De fato, há um aumento significativo do fator de conversão de etanol/glicerol a biomassa pelas células em restrição calórica (Figura 3.8,

Painel D), o que demonstra que este regime de cultivo promove um melhor aproveitamento energético do etanol e do glicerol em *S. cerevisiae*, ainda que estes substratos sejam produzidos em maior quantidade pelas células controle (Figura 3.4, Painéis B e C).

Outra diferença é a biomassa máxima formada pelos mutantes ρ^0 cultivados em condição controle (observada após 240 h de cultivo) em relação à linhagem parental no mesmo tempo (Figura 3.2, Painéis B e D): $55,42 \pm 0,92\%$ menor [$5,19 \pm 0,07$ g biomassa/L (WT) e $2,31 \pm 0,02$ g biomassa/L (ρ^0)]. Além disso, se compararmos a biomassa das duas células em restrição calórica (também em 240 h), verificamos nos mutantes ρ^0 uma diminuição de $83,29 \pm 1,28\%$ em seu valor [$4,35 \pm 0,05$ g biomassa/L (WT) e $0,72 \pm 0,01$ g biomassa/L (ρ^0)], sendo essa observação compatível com a menor disponibilidade de glicose nos meios de cultura de restrição calórica e com a impossibilidade de esses mutantes em utilizar, para a geração de biomassa, substratos metabolizados exclusivamente por vias aeróbicas. Portanto, essas diferenças percentuais quantificam a contribuição da integridade funcional do DNA mitocondrial para a geração de biomassa em *S. cerevisiae*. Além disso, a diminuição da biomassa em *S. cerevisiae* ρ^0 observada a partir do 14º dia de cultivo (Figura 3.2, Painel D), tanto em condição controle de cultivo como em restrição calórica, reflete o progressivo aumento da mortalidade (Figura 2.3, Painel A; Tabela 2.5) e da consequente degradação celular desse mutante, que são justificadas pela sua inabilidade de se manter viável na ausência de substratos fermentáveis a longo prazo (Figura 2.3; Tabela 2.5). Já o aumento de biomassa apresentado pela linhagem parental, também a partir do 14º dia de cultivo (Figura 3.2, Painel C), pode ser explicado pela evaporação de água do sistema, fator claramente observado em todas as repetições deste experimento – através de aferições por 28 dias das massas de erlemeyers contendo somente meio de cultivo, verificamos que o valor estimado para a evaporação de água é de 0,262 g por dia de cultivo.

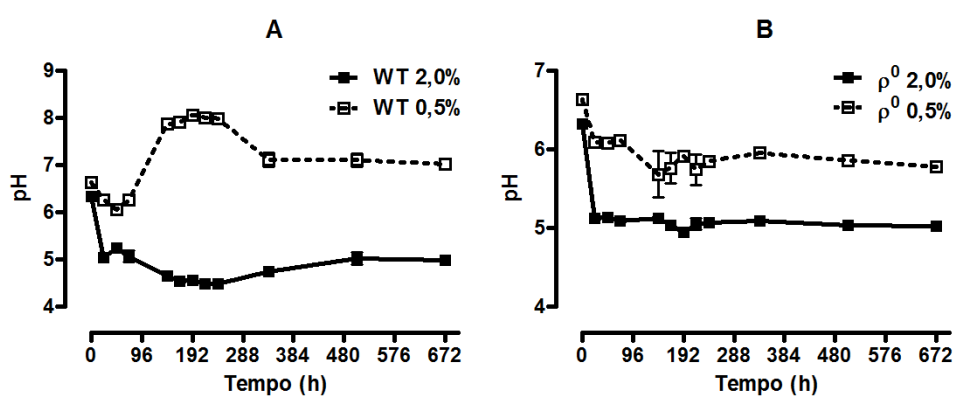


Figura 3.3. Curvas de pH extracelular ao longo do tempo de vida cronológico de *S. cerevisiae* WT e ρ^0 . As determinações do pH extracelular ao longo do tempo de vida cronológico de *S. cerevisiae* WT e ρ^0 foram realizadas conforme descrição em *Materiais e Métodos* (Item 17).

Com relação às curvas de pH do meio extracelular de *S. cerevisiae* WT, observamos grandes diferenças entre a concentração de íons hidrogênio entre os cultivos em condição controle e em restrição calórica (Figura 3.3, Painel A), sobretudo entre a 144ª h e a 240ª h, refletindo a existência

de profundas diferenças metabólicas entre as células cultivadas nas duas condições; além disso, podemos verificar que o perfil dessas curvas é sobremaneira influenciado pela ausência do DNA mitocondrial (Figura 3.3, Painel B). Assim, podemos concluir que o metabolismo respiratório é responsável pela acidificação do meio de cultura controle e pela alcalinização do meio de cultura caloricamente restrito em *S. cerevisiae* observadas entre a 144^a h e a 240^a h de cultivo.

3.4. Curvas de exaustão de glicose e de formação e exaustão de etanol, glicerol, acetato, piruvato e succinato em *S. cerevisiae* WT e ρ^0

As curvas de exaustão de glicose e de formação e exaustão de etanol, glicerol, acetato, piruvato e succinato de *S. cerevisiae* WT e ρ^0 fornecem a informação de como as concentrações extracelulares destes metabólitos variam ao longo do seu tempo de vida cronológico, retratando importantes características promovidas não só pela diminuição da disponibilidade inicial de glicose nos meios de cultura caloricamente restritos como também a influência do genoma mitocondrial na dinâmica de geração e consumo destes.

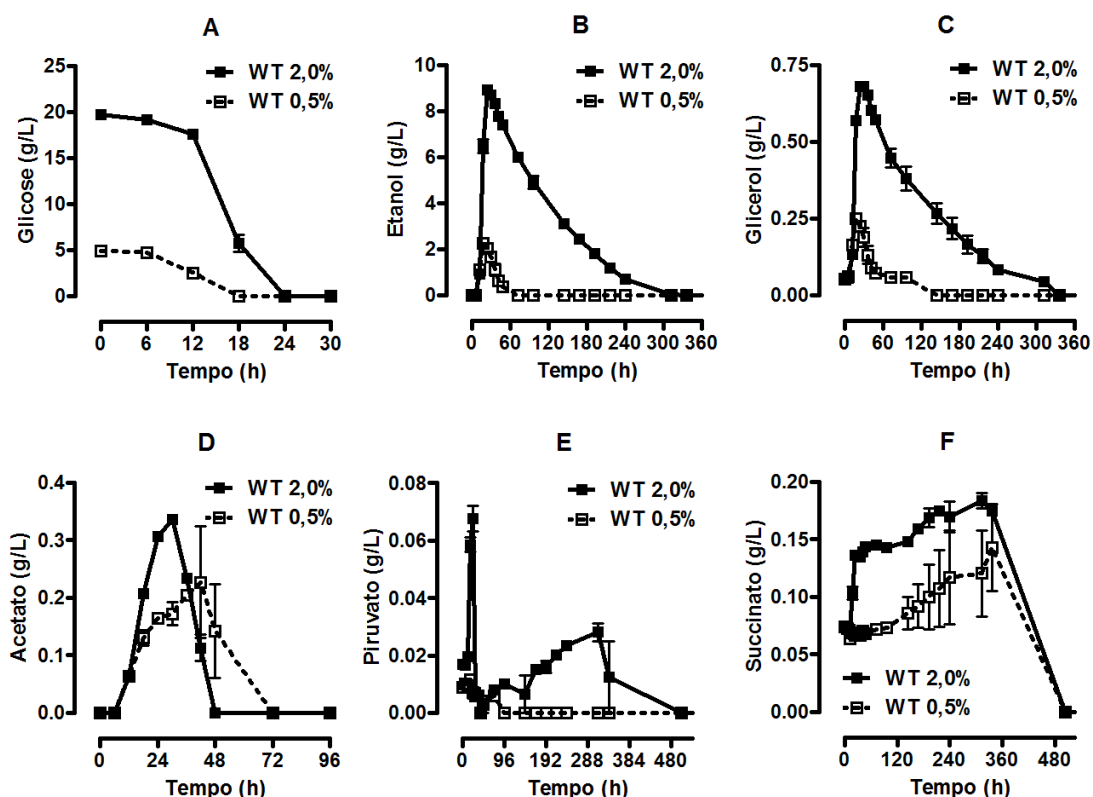


Figura 3.4. Curvas de exaustão de glicose, e de formação e exaustão de etanol, glicerol, acetato, piruvato e succinato ao longo do tempo de vida cronológico de *S. cerevisiae* WT. A determinação das concentrações de glicose (Painel A), etanol (Painel B), glicerol (Painel C), acetato (Painel D), piruvato (Painel E) e succinato (Painel F) ao longo do tempo de vida cronológico de *S. cerevisiae* WT foi realizada conforme descrição em *Materiais e Métodos* (Item 16).

Como esperado, podemos observar que a célula ρ^0 , diferentemente da célula selvagem, não é capaz de consumir substratos que são (i) exclusivamente utilizados de forma aeróbica, tais como

o acetato (Figura 3.5, Painel D) e o succinato (Figura 3.5, Painel F), ou (ii) preferencialmente, tal como o glicerol (Figura 3.5; Painel C). Desta forma, o decaimento progressivo da concentração de etanol – outro substrato metabolizado de forma exclusiva pelo metabolismo aeróbico – nos meios de cultura dos mutantes ρ^0 (Figura 3.5; Painel B) pode ser explicado pela evaporação deste produto ao longo dos 28 dias de cultura.

Outra interessante observação são as semelhantes concentrações máximas de etanol extracelular alcançadas tanto em *S. cerevisiae* WT como no mutante ρ^0 , as quais assumem valores de $8,90 \pm 0,05$ g/L na célula selvagem (em 24 h) e $9,01 \pm 0,05$ g/L no mutante ρ^0 (em 30 h) quando cultivadas em condição controle e $2,25 \pm 0,02$ g/L na célula selvagem (em 18 h) e $2,28 \pm 0,01$ g/L no mutante ρ^0 (em 24 h) quando cultivadas em restrição calórica. Esse fato é consistente com a observação de que não há diferença significativa entre a capacidade de conversão de glicose a etanol entre *S. cerevisiae* WT e ρ^0 (Figura 3.7, Painel B). Além disso, os tempos em que os picos da concentração extracelular de etanol são observados no mutante ρ^0 estão diretamente relacionados com a sua velocidade máxima de consumo de glicose, significativamente diminuída com relação à *S. cerevisiae* WT (Figura 3.6, Painel B).

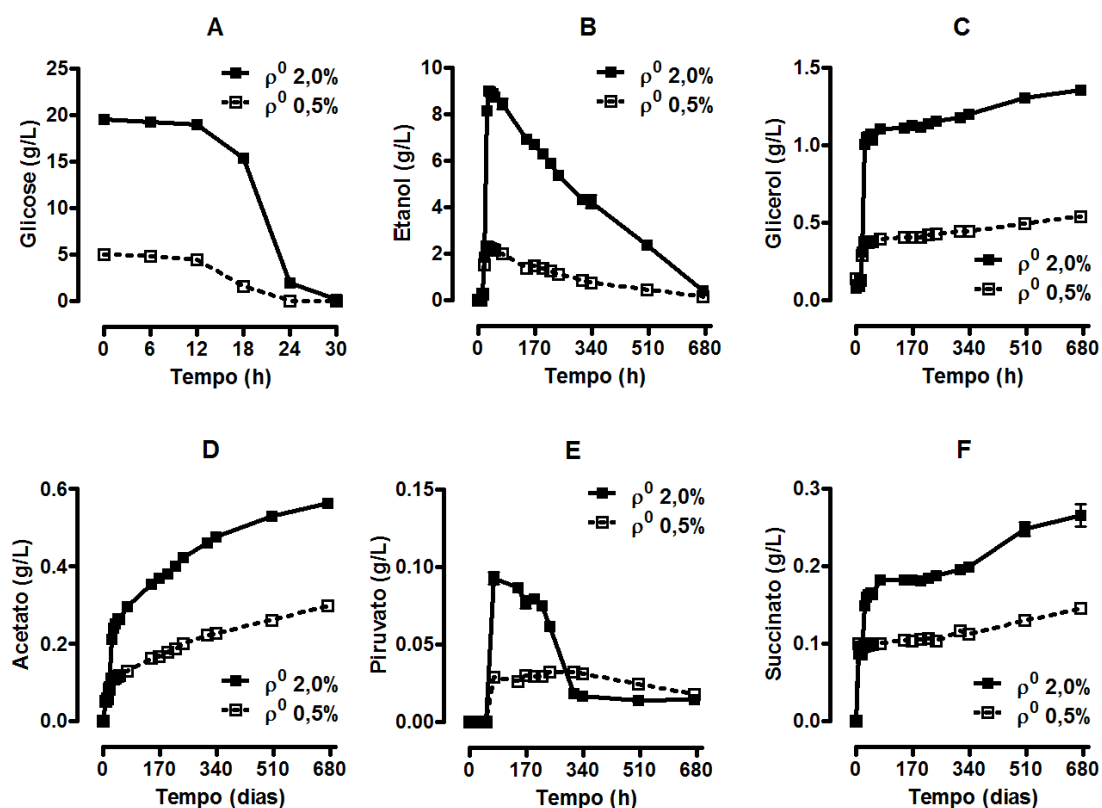


Figura 3.5. Curvas de exaustão de glicose, e de formação e exaustão de etanol, glicerol, acetato, piruvato e succinato ao longo do tempo de vida cronológico de *S. cerevisiae* ρ^0 . A determinação das concentrações de glicose (Painel A), etanol (Painel B), glicerol (Painel C), acetato (Painel D), piruvato (Painel E) e succinato (Painel F) ao longo do tempo de vida cronológico de *S. cerevisiae* ρ^0 foi realizada conforme descrição em *Materiais e Métodos* (Item 16).

3.5. Velocidade específica máxima de crescimento celular em glicose e velocidade específica máxima de consumo de glicose de *S. cerevisiae* WT e ρ^0

Com o objetivo de investigar se a restrição calórica ou a ausência do DNA mitocondrial alteram as taxas de aumento de biomassa e o consumo de glicose em *S. cerevisiae*, determinamos a velocidade específica máxima de crescimento celular em glicose (μ_{Glu}^{\max}) e a velocidade específica máxima de consumo desse substrato (r_{cGlu}^{\max}) em *S. cerevisiae* WT e ρ^0 cultivadas em condição controle e em restrição calórica.

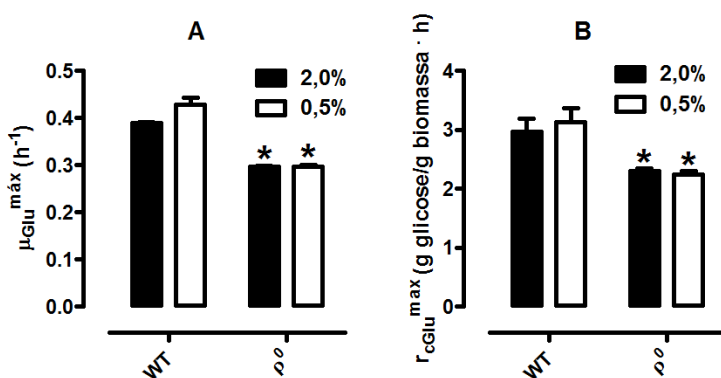


Figura 3.6. Velocidade específica máxima de crescimento celular em glicose e velocidade específica máxima de consumo de glicose em *S. cerevisiae* WT e ρ^0 . Os cálculos para a determinação da velocidade específica máxima de crescimento celular em glicose (μ_{Glu}^{\max} ; Painel A) e da velocidade específica máxima de consumo de glicose (r_{cGlu}^{\max} ; Painel B) de *S. cerevisiae* WT e ρ^0 foram realizados conforme descrição em *Materiais e Métodos* (Itens 20 e 23). Painéis A e B: * $p < 0,05$ vs. WT (teste *t* de Student não-pareado).

Podemos observar que a restrição calórica não altera a μ_{Glu}^{\max} em *S. cerevisiae*, uma vez que não há diferença significativa dos valores deste parâmetro fisiológico nas duas condições de cultivo; entretanto, verificamos que existe uma diminuição significativa da μ_{Glu}^{\max} no mutante ρ^0 em relação à célula selvagem, tanto em condição controle como em restrição calórica (Figura 3.6, Painel A). As diferenças de $23,70 \pm 0,59\%$ existentes entre os valores de da μ_{Glu}^{\max} entre a célula selvagem ($0,389 \pm 0,002 \cdot \text{h}^{-1}$) e o mutante ρ^0 ($0,297 \pm 0,001 \cdot \text{h}^{-1}$) cultivados em condição controle, e de $30,74 \pm 2,44\%$ entre a célula selvagem ($0,429 \pm 0,014 \cdot \text{h}^{-1}$) e o mutante ρ^0 ($0,291 \pm 0,003 \cdot \text{h}^{-1}$) em restrição calórica demonstram, quantitativamente, a parcela de contribuição do metabolismo respiratório para a determinação da μ_{Glu}^{\max} de *S. cerevisiae* nas duas condições de cultivo.

Assim como na determinação da μ_{Glu}^{\max} , verificamos que a ausência do DNA mitocondrial também altera a r_{cGlu}^{\max} de *S. cerevisiae* (Figura 3.6, Painel B). As diferenças de $22,47 \pm 5,96\%$ entre a célula selvagem ($2,96 \pm 0,22 \text{ g glicose/g biomassa} \cdot \text{h}$) e o mutante ρ^0 ($2,30 \pm 0,04 \text{ g glicose/g biomassa} \cdot \text{h}$) cultivados em condição controle, e de $28,23 \pm 5,69\%$ entre a célula selvagem ($3,13 \pm 0,23 \text{ g glicose/g biomassa} \cdot \text{h}$) e o mutante ρ^0 ($2,24 \pm 0,05 \text{ g glicose/g biomassa} \cdot \text{h}$)

cultivados em restrição calórica também demonstram, em termos quantitativos, a parcela de contribuição do metabolismo aeróbico para a determinação da $r_{c\text{Glu}}^{\max}$ em *S. cerevisiae*.

Através dos resultados de μ_{Glu}^{\max} e $r_{c\text{Glu}}^{\max}$ determinamos a relação numérica entre os percentuais de alteração destes dois parâmetros na condição controle e em restrição calórica promovida pela ausência do DNA mitocondrial. Pela Tabela 3.1, podemos perceber que a razão dos percentuais de alteração dos dois parâmetros entre a célula selvagem e o mutante ρ^0 possuem valores numéricos muito próximos de 1,00 ($1,05 \pm 0,28$ na condição controle e $1,08 \pm 0,23$ em restrição calórica). Essa observação demonstra, portanto, que a ausência do DNA mitocondrial afeta igualmente a μ_{Glu}^{\max} e a $r_{c\text{Glu}}^{\max}$ em *S. cerevisiae*.

Tabela 3.1. Relação numérica entre os percentuais de alteração de μ_{Glu}^{\max} e $r_{c\text{Glu}}^{\max}$ promovida pela ausência do DNA mitocondrial na condição controle e em restrição calórica.

	% de alteração mGlu ^{max} (A)	% de alteração r _c Glu ^{max} (B)	A/B
controle	$23,70 \pm 0,59$	$22,47 \pm 5,96$	$1,05 \pm 0,28$
restrição calórica	$30,74 \pm 2,44$	$28,23 \pm 5,69$	$1,08 \pm 0,23$

3.6. Fator de conversão de glicose a células, de glicose a etanol e de glicose a glicerol de *S. cerevisiae* WT e ρ^0

Simplificadamente, a glicose consumida por *S. cerevisiae* pode gerar (i) ATP – o qual, por sua vez, é consumido para a manutenção da viabilidade celular – (ii) biomassa, e também (iii) seus substratos derivados, tais como o etanol e o glicerol (Frick e Wittmann, 2005). Embora o fluxo metabólico da glicose em *S. cerevisiae* seja extremamente complexo, e esse açúcar tenha os seus fluxos determinados com exatidão somente através de experimentos que o utilizem na forma de traçador isotópico – uma vez que dessa maneira é possível determinar a dinâmica do ^{13}C através das vias metabólicas (Grotkjaer *et al.*, 2004; Raghevendran *et al.*, 2004) – essa abordagem simplificada ainda é uma forma de aproximação bastante válida para a determinação do fator de conversão de glicose a produtos. Em nosso caso, determinamos os fatores de conversão de glicose a células ($Y_{X/\text{Glu}}^{\exp}$), a etanol ($Y_{\text{EtOH}/\text{Glu}}^{\exp}$) e a glicerol ($Y_{\text{Gli}/\text{Glu}}^{\exp}$) em *S. cerevisiae* WT e ρ^0 cultivadas em condição controle e em restrição calórica.

Observamos que os mutantes ρ^0 não exibem diminuição da $Y_{X/\text{Glu}}^{\exp}$, tampouco da $Y_{\text{EtOH}/\text{Glu}}^{\exp}$, quando comparados à célula selvagem; além disso, a restrição calórica também não alterou esses dois parâmetros fisiológicos em *S. cerevisiae* (Figura 3.7, Painéis A e B). Desta forma, podemos afirmar, surpreendentemente, que as conversões de glicose a células e a etanol não são influenciadas pelo estado funcional de seu DNA mitocondrial e da condição de cultivo em *S. cerevisiae*; em outras palavras, a capacidade dessa levedura em gerar biomassa e em formar etanol a partir de glicose não depende da integridade do seu genoma mitocondrial e nem é alterada pela

quantidade de glicose disponível no meio de cultura no início do cultivo. A maior biomassa observada na condição controle em relação à observada em restrição calórica (Figura 3.2, Painel B) é justificada, portanto, pelo tempo total que *S. cerevisiae* cultivada em meio YPD contendo 2,0% de glicose é capaz de gerar biomassa exponencialmente (Tabela 2 em *Materiais e Métodos*), já que essa é uma observação diretamente relacionada com a quantidade inicial de glicose disponível do meio de cultura, ainda que o aproveitamento energético das células cultivadas em meio controle seja menor (Item 3.2). Da mesma maneira, a maior quantidade de etanol gerado pelas células em meio controle (Figura 3.4, Painel B) também é explicada pela maior concentração inicial de glicose disponível no meio de cultura controle.

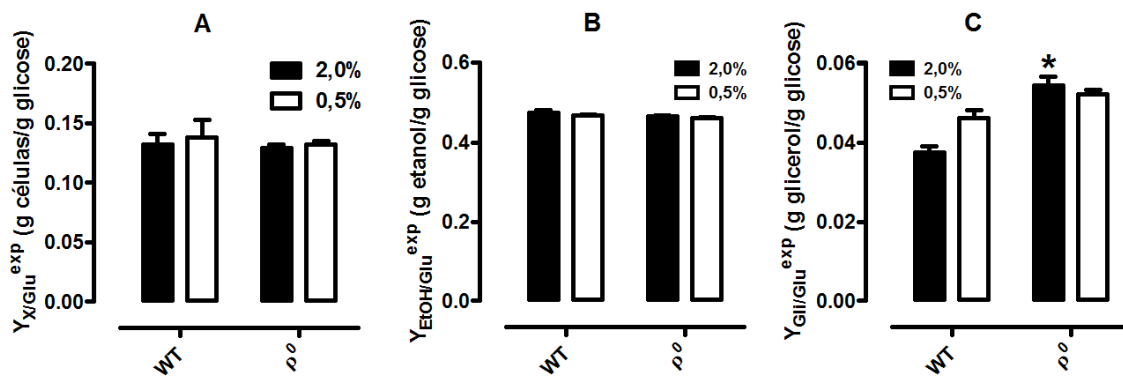


Figura 3.7. Fator de conversão de glicose a células, de glicose a etanol e de glicose a glicerol em *S. cerevisiae* WT e ρ^0 . Os cálculos para a determinação do fator de conversão de glicose a células ($Y_{X/Glu}^{exp}$; Painel A), de glicose a etanol ($Y_{EtOH/Glu}^{exp}$; Painel B) e de glicose a glicerol ($Y_{Gli/Glu}^{exp}$; Painel C) de *S. cerevisiae* WT e ρ^0 foram realizados conforme descrição em *Materiais e Métodos* (Itens 21 e 22). Painel C: * $p < 0,05$ vs. WT (teste *t* de Student não-pareado).

Com relação ao $Y_{Gli/Glu}^{exp}$, observamos uma diferença significativa entre os valores apresentados pelo mutante ρ^0 e a linhagem parental em condição controle de cultivo (Figura 3.7, Painel C). Além disso, há uma tendência observável de esse parâmetro ser também alterado significativamente pela restrição calórica na célula selvagem ($p = 0,07$ para WT 0,5% vs. WT 2,0%, teste *t* de Student não-pareado).

3.7. Velocidade específica máxima de formação de etanol/glicerol; de crescimento celular em etanol/glicerol; de consumo de etanol/glicerol; e fator de conversão de etanol/glicerol a células

Uma vez que o etanol e o glicerol possuem consumos temporalmente paralelos em *S. cerevisiae* (Figura 3.4, Painéis B e C), as velocidades específicas máximas de crescimento celular em etanol e em glicerol não puderam ser calculadas isoladamente. Desta forma, o cálculo da formação, do consumo e do fator de conversão a células desses dois substratos foi realizado em conjunto, ainda que tenhamos determinado uma estimativa da contribuição individual do etanol e do glicerol na velocidade específica máxima de crescimento celular (Item 3.8).

Com o objetivo de investigar se a restrição calórica e a ausência do mtDNA alteram a velocidade específica máxima de formação de etanol/glicerol a partir de glicose ($r_{f\text{EtOH+Gli}^{\max}}$), e se a restrição calórica influencia a velocidade específica de crescimento celular em etanol/glicerol ($\mu_{\text{EtOH+Gli}^{\max}}$), de consumo de etanol/glicerol ($r_{c\text{EtOH+Gli}^{\max}}$) e a conversão destes a células ($Y_{X/\text{EtOH+Gli}^{\exp}}$) em *S. cerevisiae*, realizamos a determinação desses parâmetros fisiológicos.

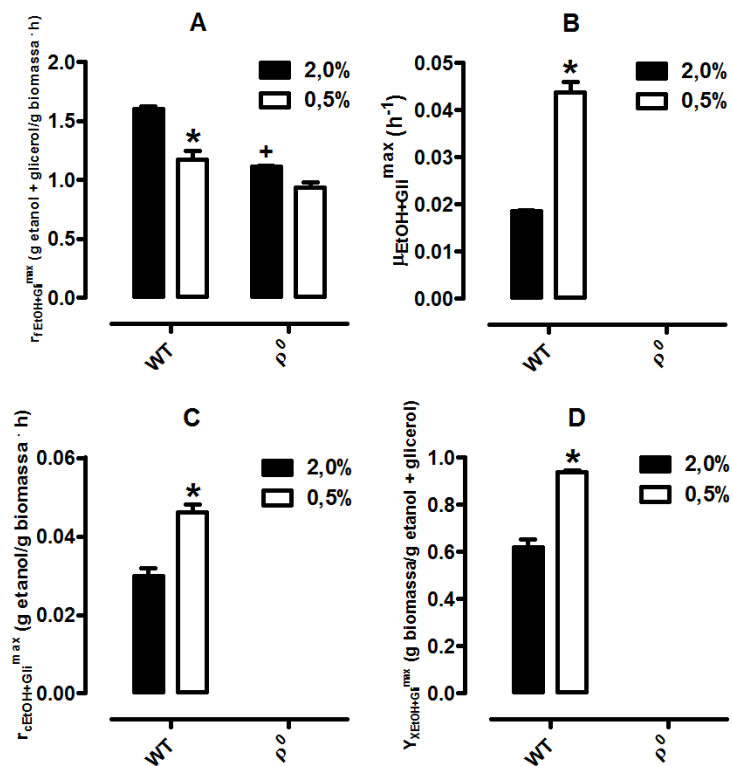


Figura 3.8. Velocidades específicas máximas de formação de etanol, de crescimento celular em etanol, de consumo de etanol e fator de conversão de etanol a células em *S. cerevisiae* WT e ρ^0 . Os cálculos para a determinação da velocidade específica máxima de formação de etanol/glicerol ($r_{f\text{EtOH+Gli}^{\max}}$; Painel A), de crescimento celular em etanol/glicerol ($\mu_{\text{EtOH+Gli}^{\max}}$; Painel B), de consumo de etanol/glicerol ($r_{c\text{EtOH+Gli}^{\max}}$; Painel C) e do fator de conversão de etanol/glicerol a células ($Y_{X/\text{EtOH+Gli}^{\exp}}$; Painel D) foram realizados conforme descrição em *Materiais e Métodos* (Itens 20, 21 e 23) Painel A: * $p < 0,05$ vs. 2,0%; * $p < 0,05$ vs. WT (teste *t* de Student não-pareado). Painel B: * $p < 0,05$ vs. 2,0% (teste *t* de Student não-pareado). Painel C: * $p < 0,05$ vs. 2,0% (teste *t* de Student não-pareado). Painel D: * $p < 0,05$ vs. 2,0% (teste *t* de Student não-pareado).

Podemos observar que a $r_{f\text{EtOH+Gli}^{\max}}$ é diminuída tanto pela restrição calórica como pela ausência do DNA mitocondrial (Figura 3.8, Painel A). Além disso, verificamos que a $\mu_{\text{EtOH+Gli}^{\max}}$ das células caloricamente restritas é maior do que a observada na condição controle (Figura 3.8, Painel B): as últimas exibiram uma $\mu_{\text{EtOH+Gli}^{\max}}$ 136,38 ± 12,54% maior em relação às primeiras. Essa observação é consistente com o aumento significativo da $r_{c\text{EtOH+Gli}^{\max}}$ e do $Y_{X/\text{EtOH+Gli}^{\exp}}$ em *S. cerevisiae* WT caloricamente restrita (Figura 3.8, Painéis C e D).

O fato de a extensão da repressão por glicose ser menor nas células caloricamente restritas não só justifica sua elevada $\mu_{\text{EtOH}^{\max}}$ como também o aumentado período de tempo para que as células cultivadas em condição controle começassem a exibir aumento de biomassa suportado por etanol (Tabela 2 em *Materiais e Métodos*).

Finalmente, uma vez que as células ρ^0 não são capazes de utilizar o etanol e o glicerol como fontes de carbono, o aumento de biomassa suportado por esse substrato nesses mutantes não foi observado (Figura 3.2, Painel C; Figura 3.8, Painel B) e, consequentemente, a $\mu_{\text{EtOH+Gli}^{\max}}$, assim como a $r_{c\text{EtOH+Gli}^{\max}}$ e a $Y_{X/\text{EtOH+Gli}^{\exp}}$ não puderam ser calculados (Figura 3.8, Painéis B, C e D). Essas

observações evidenciam a inabilidade de os mutantes ρ^o utilizarem substratos metabolizados aerobicamente para a manutenção de sua viabilidade celular e para o crescimento celular, estando, portanto, em concordância com a sua menor geração de biomassa (Figura 3.2, Painel D).

3.8. Velocidade específica máxima de crescimento celular em etanol e em glicerol

Como previamente discutido, o etanol e o glicerol possuem consumos temporalmente paralelos em *S. cerevisiae*, (Figura 3.4, Painéis B e C; Item 3.7). Assim, com o objetivo de realizar uma estimativa da velocidade específica máxima de crescimento celular em etanol (μ_{EtOH}^{\max}) em relação à velocidade específica máxima de crescimento celular em glicerol (μ_{Gli}^{\max}), realizamos a transferência de *S. cerevisiae* WT cultivadas em meio YPD a meios YP contendo ou etanol ou glicerol, nas concentrações máximas previamente determinadas (Item 24 em *Materiais e Métodos*), nos tempos em que estas eram atingidas (Figura 3.4, Painel C).

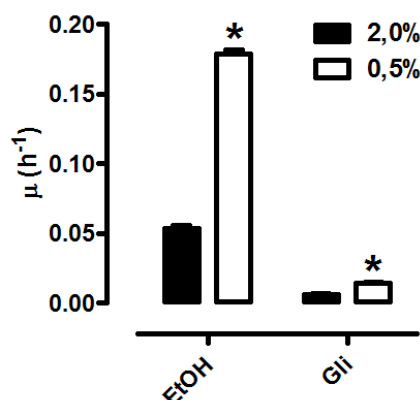


Figura 3.9. Velocidade específica máxima de crescimento celular de *S. cerevisiae* WT em etanol e glicerol. A determinação dos valores de μ_{EtOH}^{\max} e de μ_{Gli}^{\max} foram realizadas segundo descrição em *Materiais e Métodos* (Item 24). * $p < 0,05$ vs. 2,0% (teste *t* de Student não-pareado). EtOH: etanol. Gli: glicerol.

Podemos observar que os valores absolutos da velocidade específica máxima de crescimento celular em etanol aqui determinados são maiores do que os valores absolutos da velocidade específica máxima de crescimento celular em etanol/glicerol previamente verificados (Figura 3.8). Isso pode ser explicado pelo fato de que os meios frescos aqui utilizados não estavam condicionados e, portanto, isentos de modificações tanto químicas quanto físicas que podem diminuir a velocidade específica máxima de crescimento celular de *S. cerevisiae*. Entretanto, pela análise dos valores obtidos, verificamos que, em condição controle, a μ_{EtOH}^{\max} ($0,0535 \pm 0,002 \cdot \text{h}^{-1}$) é $87,85 \pm 7,90\%$ maior do que a μ_{Gli}^{\max} ($0,0065 \pm 0,0005 \cdot \text{h}^{-1}$) e que, em restrição calórica, a μ_{EtOH}^{\max} ($0,179 \pm 0,003 \cdot \text{h}^{-1}$) é $91,89 \pm 3,52\%$ maior do que a μ_{Gli}^{\max} ($0,0145 \pm 0,0005 \cdot \text{h}^{-1}$). Em outras palavras, o glicerol contribui com $12,15 \pm 7,90\%$ e $8,11 \pm 3,52\%$ dos valores dos parâmetros fisiológicos calculados no Item 3.6 em condição controle e em restrição calórica, respectivamente.

3.9. Conclusões

Podemos concluir que a disponibilidade diminuída de glicose nos meios de cultura promove às células em restrição calórica (i) a exibição mais precoce do início do período de máxima respiração celular e também (ii) uma taxa de consumo de oxigênio máxima significativamente maior do que a das células controle, um fenótipo decorrente da mitigação da repressão por glicose nas células caloricamente restritas. Também concluímos que a conversão energética nas células em restrição calórica é maior do que nas células controle, e que a ausência do DNA mitocondrial possui significativa influência na formação máxima de biomassa de *S. cerevisiae*. Além disso, verificamos que o metabolismo respiratório de *S. cerevisiae* é responsável pela presença de uma diferença de mais de 3 unidades de pH extracelular existente entre os cultivos controle e os caloricamente restritos. Também concluímos que as concentrações máximas de etanol e glicerol formadas nas culturas de *S. cerevisiae* são dependentes da condição de cultivo, mas não da funcionalidade do genoma mitocondrial: a velocidade específica máxima de crescimento celular em glicose e a velocidade específica máxima de consumo desse substrato não se mostram dependentes da condição de cultivo, mas sim da presença funcional do DNA mitocondrial, cuja ausência afeta ambos igualmente. Embora a condição de cultivo não tenha alterado a formação (i) de biomassa, (ii) de etanol e (iii) de glicerol a partir de glicose nas células selvagens, ela influenciou a velocidade específica de formação de etanol e glicerol a partir de glicose – sendo maiores nas células cultivadas em condição controle – e também a (i) velocidade específica de crescimento celular em etanol e glicerol, (ii) de formação de etanol e glicerol e (iii) conversão de etanol e glicerol a biomassa – sendo maiores nas células em restrição calórica.

**Seção 4 – Metabolismo de espécies reativas de oxigênio ao longo do tempo de vida cronológico de
*Saccharomyces cerevisiae***

4.1. Espécies reativas de oxigênio no envelhecimento

Como previamente discutido (Item 1.5), as espécies reativas de oxigênio são produtos do metabolismo celular, podendo ser geradas a partir de processos enzimáticos e não-enzimáticos. A larga oxidação de macromoléculas – como, por exemplo, proteínas, lipídeos e DNA – é prevenida pela existência, no ambiente celular, de um balanço fisiológico entre a formação e a remoção dessas espécies reativas, como também anteriormente abordado (Item 1.4). Todavia, em determinadas condições, a geração descompensada das espécies reativas de oxigênio e seus derivados pode induzir danos a macromoléculas causando, via de regra, perda de função que leva à perda da manutenção da homeostase celular (Bevilacqua *et al.*, 2005; Hagopian *et al.*, 2005; Sanz *et al.*, 2005; Gredilla e Barja, 2005; Zheng *et al.*, 2005). De fato, a observação de prejuízos funcionais devido a modificações oxidativas irreversíveis a componentes celulares tem sido utilizada como o alicerce que sustenta a teoria dos radicais livres no envelhecimento, proposta por Denham Harman em meados do século passado (Harman, 1956).

Apesar de ter sofrido alterações ao longo do tempo, essa teoria postula, fundamentalmente, que o envelhecimento é um fenômeno baseado em um único processo comum – o aumento das reações de iniciação de geração dos radicais livres e espécies reativas. Embora a teoria dos radicais livres no envelhecimento ofereça um conjunto de argumentos bastante plausíveis, tais como o aumento do acúmulo de modificações oxidativas que precedem a disfunção celular (Fukagawa, 1999; Sohal *et al.*, 2002; Jacobs, 2003; Choksi *et al.*, 2007; Choksi e Papaconstantinou, 2008), e a relação inversa entre essas modificações e o tempo de vida (Barja e Herrero, 2000; Barja, 2002), uma análise mais cuidadosa da literatura da área não é capaz de fornecer provas irrefutáveis de que a oxidação de biomoléculas é o efeito causal definitivo da perda da homeostase e do envelhecimento celular (Andziak *et al.*, 2006; Buffenstein *et al.*, 2008; Ristow e Schmeisser, 2011; Rodriguez *et al.*, 2011); ao contrário, vários estudos clínicos que preconizaram a administração de antioxidantes não verificaram a promoção de benefícios à saúde humana (Greenberg *et al.*, 1994; Liu *et al.*, 1999; Czernichow *et al.*, 2005; Kataja-Tuomola *et al.*, 2008; Sesso *et al.*, 2008; Katsiki e Manes, 2009). Além disso, outros trabalhos sugerem a associação entre a suplementação de antioxidantes com o aumento de doenças que possuem efeitos adversos sobre a longevidade humana (Omenn *et al.*, 1996; Bjelakovic *et al.*, 2007; Ward *et al.*, 2007).

Conseqüentemente, em conjunto, essas observações não só colocam a teoria dos radicais livres no envelhecimento em xeque como também exigem que a geração e o papel biológico das espécies reativas de oxigênio sejam analisados sob outro ponto de vista. De fato, recentemente, um grande número de trabalhos tem indicado que essas espécies podem atuar como importantes sinalizadores celulares na medida em que a sua formação promoveria, *a posteriori*, maior resistência celular ao estresse oxidativo – um cenário no qual o fenômeno da hormese parece ser a causa direta desse benefício (Kaiser, 2003; Ristow e Zarse, 2010; Ristow e Schmeisser, 2011; Calabreze *et al.*, 2011).

A hormese tem sido descrita como um participante decisivo no envelhecimento, uma vez que *C. elegans* submetidos a diferentes tipos de estresses ambientais exibem um aumento do tempo de vida (Cypser e Johnson, 2002). Além disso, Mesquita e colaboradores recentemente demonstraram que em *S. cerevisiae*, as inativações das catalases peroxissomal e citosólica foram capazes de aumentar o tempo de vida cronológico, enquanto as suas superexpressões levaram à sua diminuição (Mesquita *et al.*, 2010), sugerindo a existência de mecanismos horméticos mediados pelo estado de óxido-redução celular.

Diante de todos esses argumentos, torna-se plausível considerar a hipótese de que modificações oxidativas específicas e delimitadas por um período de tempo possam contribuir, em conjunto com outros fatores – ambientais e/ou genéticos – com a determinação do destino fenotípico celular. Portanto, a quantificação da liberação induzida de peróxido de hidrogênio, bem como a determinação das quantidades de glutationa total, GSH e GSSG, e o teste de tolerância a oxidante exógeno, em diferentes tempos de cultivo, foram realizados para a obtenção de dados que permitam avaliar se o aumento do tempo de vida de *S. cerevisiae* em virtude da restrição calórica é um fenômeno hormético mediado por modificações do estado de óxido-redução celular.

4.2. Liberação de peróxido de hidrogênio induzida por substratos exógenos ao longo do tempo de vida cronológico de *S. cerevisiae* WT

Dada a mudança metabólica promovida pelo consumo da glicose e formação de seus substratos derivados (Seção 3) questionamos se existem diferenças significativas – e se existem, qual o seu padrão de variação – em relação à liberação induzida de espécies reativas de oxigênio entre as células controle e as caloricamente restritas durante seu envelhecimento cronológico. Desta forma, verificamos como se comporta a liberação de peróxido de hidrogênio induzida por substratos exógenos na 16^a h (nos painéis representada como “1 d”), bem como no 7^º, 14^º, 21^º, e 28^º dia de cultivo em *S. cerevisiae* WT.

Observamos que em ambas as condições de suplementação de substratos exógenos – piruvato 0,5 mM (Figura 4.1, Painel A) – ou malato 1 mM, glutamato 1 mM e etanol 2% (Figura 4.2, Painel B) – as taxas de liberação de peróxido de hidrogênio pelos esferoplastos obtidos de células controle na 16^a hora de cultivo sempre são significativamente maiores do que as observadas nas células caloricamente restritas. É notável que a liberação induzida de peróxido de hidrogênio em ambas as situações de cultivo cai de forma significativa da 16^a hora até o 7^º dia de cultivo, assumindo os seus menores níveis absolutos ao longo do tempo. Essa verificação sugere que, direta ou indiretamente, o estado metabólico das células durante a fase logarítmica tardia e a fase estacionária precoce de crescimento (transição observada aproximadamente em 16 h de cultivo, em nossas condições; Figura 3.2, Painel A) – que é distinto do estado metabólico em fase estacionária tardia – está relacionado com a geração celular de oxidantes.

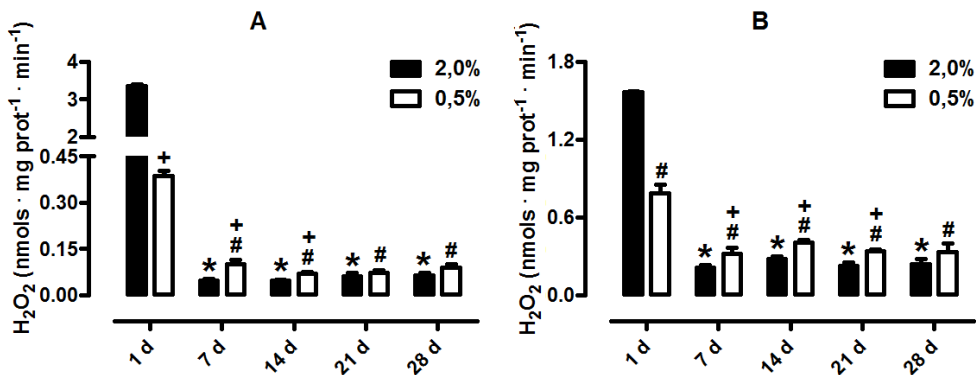


Figura 4.1. Liberação de peróxido de hidrogênio induzida por substratos exógenos ao longo do tempo de vida cronológico de *S. cerevisiae* WT. A determinação da liberação de peróxido de hidrogênio em esferoplastos de *S. cerevisiae* WT (100 µg/mL) induzida por piruvato 0,5 mM (Painel A) e malato 1 mM, glutamato 1 mM e etanol 2% (Painel B) na 16^a h (“1d”) e no 7^º, 14^º, 21^º e 28^º dia foi realizada segundo descrição em *Materiais e Métodos* (Item 9). Uma quantidade de digitonina que variou entre 0,007% e 0,010% foi utilizada para proporcionar o aumento da permeabilidade dos esferoplastos à peroxidase de raiz forte – necessária para a oxidação da sonda fluorescente *Amplex Red* pelo peróxido de hidrogênio – e aos substratos exógenos. Painéis A e B: **p* < 0,05 vs. WT 2,0% 1 d, #*p* < 0,05 vs. WT 0,5% 1 d (one-way ANOVA/Bonferroni); +*p* < 0,05 vs. WT 2,0% (teste *t* de Student não-pareado).

Também é notável que, quando suplementados com piruvato, os esferoplastos obtidos de células caloricamente restritas exibem um aumento significativo na geração induzida de oxidantes no 7^º e no 14^º dia de cultivo (Figura 4.1, Painel A), situação que é também observada no 7^º, 14^º e 21^º dia de cultivo quando esses mesmos esferoplastos são suplementados com malato, glutamato e etanol (Figura 4.1, Painel B).

Finalmente, também verificamos que esferoplastos preparados a partir de células controle, quando suplementados com piruvato, apresentam uma liberação de peróxido de hidrogênio significativamente maior do que os mesmos esferoplastos na presença de malato, glutamato e etanol [3,36 ± 0,03 nmols · mg prot⁻¹ · min⁻¹ (piruvato) vs. 1,57 ± 0,01 nmols · mg prot⁻¹ · min⁻¹ (malato, glutamato e etanol); *p* = 0,0004]. O inverso é observado quando se leva em conta os esferoplastos advindos de células em restrição calórica: a liberação de peróxido de hidrogênio é significativamente maior quando a suplementação é realizada com etanol, malato e glutamato [0,38 ± 0,01 nmols · mg prot⁻¹ · min⁻¹ (piruvato) vs. 0,78 ± 0,06 nmols · mg prot⁻¹ · min⁻¹ (malato, glutamato e etanol); *p* = 0,02].

4.3. Estado de óxido-redução da glutationa ao longo do tempo de vida cronológico de *S. cerevisiae* WT

Como já previamente discutido, a determinação do estado de óxido-redução da glutationa é de grande importância para a verificação de o quão deslocado para a geração de oxidantes ou para a detoxificação destes está o *steady-state* celular (Item 1.4). Assim, determinamos a quantidade de glutationa total, GSH e GSSG, bem como calculamos a razão entre GSSG e GSH na 16^º h (nos painéis representada como “1 d”), e no 7^º, 14^º, 21^º e 28^º dia de cultivo para verificar se os estados fisiológicos de óxido-redução celular desses dois mutantes de *S. cerevisiae* estavam em

concordância com aqueles sugeridos pela liberação de peróxido de hidrogênio induzida por substratos exógenos da mesma forma que anteriormente (Figura 1.3).

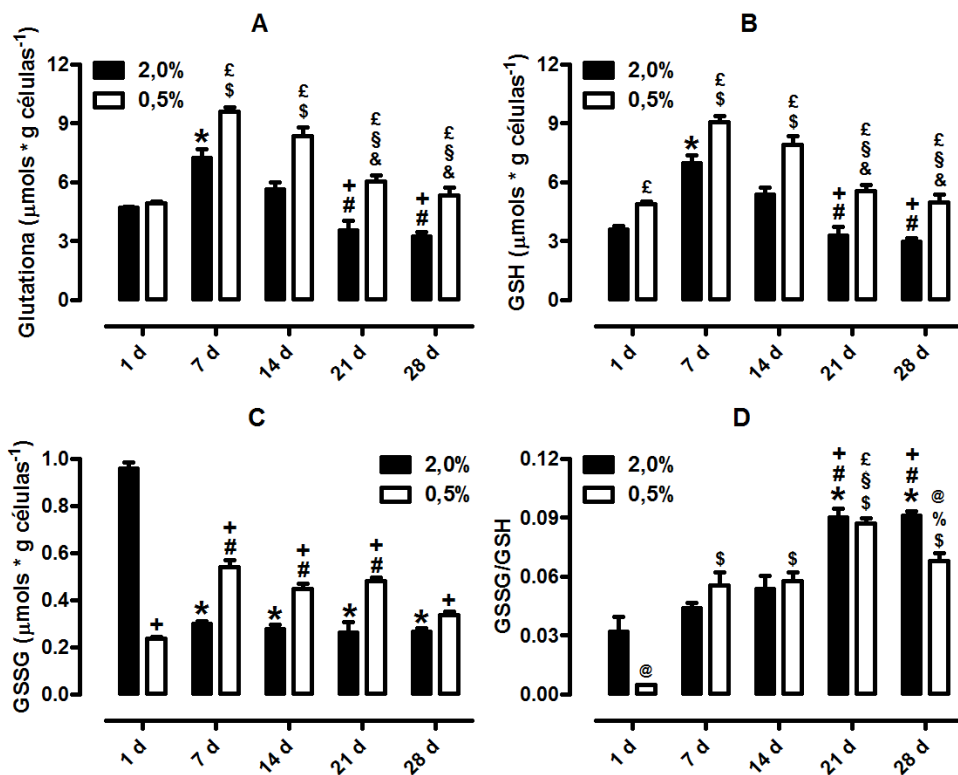


Figura 4.2. Estado de óxido-redução da glutationa ao longo do tempo de vida cronológico de *S. cerevisiae* WT. As quantidades de glutationa total (Painel A), GSH (Painel B), GSSG (Painel C) e a razão GSSG-GSH (D) foram determinadas conforme descrito em *Materiais e Métodos* (Item 10). Painéis A e B: * $p < 0,05$ vs. 2,0% 1 d, # $p < 0,05$ vs. 2,0% 7 d, + $p < 0,05$ vs. 2,0% 14 d, \$ $p < 0,05$ vs. 0,5% 1 d, ^ $p < 0,05$ vs. 0,5% 7 d, & $p < 0,05$ vs. 0,5% 14 d (one-way ANOVA/Bonferroni); £ $p < 0,05$ vs. 2,0% (teste *t* de Student não-pareado). C: * $p < 0,05$ vs. 2,0% 1 d, # $p < 0,05$ vs. 0,5% 1 d (one-way ANOVA/Bonferroni); + $p < 0,05$ vs. 2,0% (teste *t* de Student não-pareado). D: * $p < 0,05$ vs. 2,0% 1 d, # $p < 0,05$ vs. 2,0% 7 d, + $p < 0,05$ vs. 2,0% 14 d, \$ $p < 0,05$ vs. 0,5% 1 d, ^ $p < 0,05$ vs. 0,5% 7 d, £ $p < 0,05$ vs. 0,5% 14 d, % $p < 0,05$ vs. 0,5% 21 d (one-way ANOVA/Bonferroni); @ $p < 0,05$ vs. 2,0% (teste *t* de Student não-pareado).

Verificamos que os dados de liberação de peróxido de hidrogênio induzida por substratos exógenos (Figura 4.1) estão, mais uma vez, coerentemente alinhados com os valores de glutationa total, GSH, GSSG e com a razão entre GSSG e GSH (Figura 4.2). Além disso, observamos que a restrição calórica promove um aumento da síntese celular de glutationa entre o 1º e o 7º dia de cultivo (Painel A), o que sempre é refletido em uma maior disponibilidade de glutationa reduzida para as células cultivadas nessa condição, inclusive na 16ª h de cultivo (Figura 4.1, Painel B). De fato, na 16ª h de cultivo, há um pool significativamente menor de glutationa reduzida nas células controle devido à grande quantidade de glutationa oxidada nesse mesmo ponto (Figura 4.1, Painel C). Embora exista uma maior quantidade de GSSG nas células caloricamente restritas no 7º, 14º e 21º dia de cultivo (Figura 4.1, Painel C), as maiores quantidades de glutationa reduzida nesses mesmos dias (Figura 4.1, Painel B) compensam essa maior oxidação, uma vez que a razão entre GSSG e GSH não é significativamente diferente entre a condição controle e a restrição calórica nesses três dias de cultivo (Figura 4, Painel D). Notadamente, essa razão é significativamente maior

nas células controle no 1º e no 28º dia de cultivo, o que sugere que nesses dias há uma geração de oxidantes que possivelmente não é compensada, ao menos, pelo sistema antioxidante da glutationa peroxidase e pela atividade antioxidante da GSH *per se*.

4.4. Tolerância ao estresse oxidativo ambiental ao longo do tempo de vida cronológico de *S. cerevisiae* WT

Com o objetivo de determinarmos se a capacidade antioxidante das células sugerida pelos resultados da quantificação da glutationa total, GSH, GSSG e do estado de óxido-redução celular indicado pela razão GSSG-GSH seria refletida em sua capacidade de tolerar um determinado estresse oxidativo ambiental, realizamos um teste de tolerância celular a peróxido de hidrogênio exógeno durante o tempo de vida cronológico de *S. cerevisiae*, no qual verificamos a extensão do crescimento dessa levedura em placas de meio sintético completo suplementadas com diferentes concentrações desse oxidante.

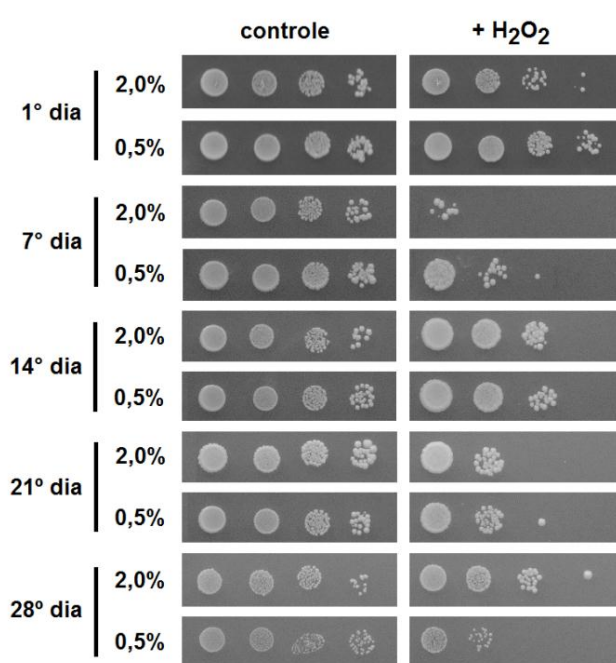


Figura 4.3. Tolerância ao estresse oxidativo ambiental ao longo do tempo de vida cronológico de *S. cerevisiae* WT. A determinação da tolerância a estresse oxidativo ambiental de *S. cerevisiae* WT através da capacidade de crescimento em meio suplementado com peróxido de hidrogênio (H_2O_2) em meio sintético completo foi realizada conforme descrição em *Materiais e Métodos* (Item 25). H_2O_2 1º dia: 1,2 mM; H_2O_2 7º, 14º, 21º e 28º dia: 2,5 mM. A figura ao lado é representativa de, no mínimo, 4 repetições independentes.

Podemos observar que, no 1º e no 7º dia de cultivo, as células caloricamente restritas possuem uma maior tolerância ao estresse ambiental promovido pelo peróxido de hidrogênio. Essa tolerância torna-se igual no 14º dia, permanecendo assim até o 21º. Interessantemente, no 28º dia de cultivo, a tolerância das células controle não só se torna maior do que a as células em restrição calórica, como aparentemente a capacidade absoluta em tolerar o estresse oxidativo ambiental apresenta-se maior do que aquela verificada no 21º dia. Embora essas observações sejam de difícil interpretação quando analisadas somente com os demais dados aqui apresentados, elas indicam

que a capacidade antioxidante de *S. cerevisiae* obedece a uma dinâmica específica, sensível à condição de cultivo, mas cuja regulação ao longo do tempo e efetores ainda necessitam ser determinados.

4.5. Morfologia mitocondrial ao longo do tempo de vida cronológico de *S. cerevisiae* WT

Em dois trabalhos recentemente publicados, Yu e colaboradores demonstraram a existência de uma correlação entre a morfologia mitocondrial e a liberação de espécies reativas de oxigênio em mamíferos (Yu *et al.*, 2006 e 2008). Decidimos, então, realizar a aquisição de imagens de *S. cerevisiae* previamente tratadas com a sonda fluorescente *MitoTracker Green* com o objetivo de verificar (i) a existência de possíveis diferenças morfológicas entre a condição controle de cultivo e a restrição calórica que poderiam ser associadas às taxas de liberação de oxidantes em *S. cerevisiae* e também (ii) como o envelhecimento modula a morfologia mitocondrial dessa levedura.

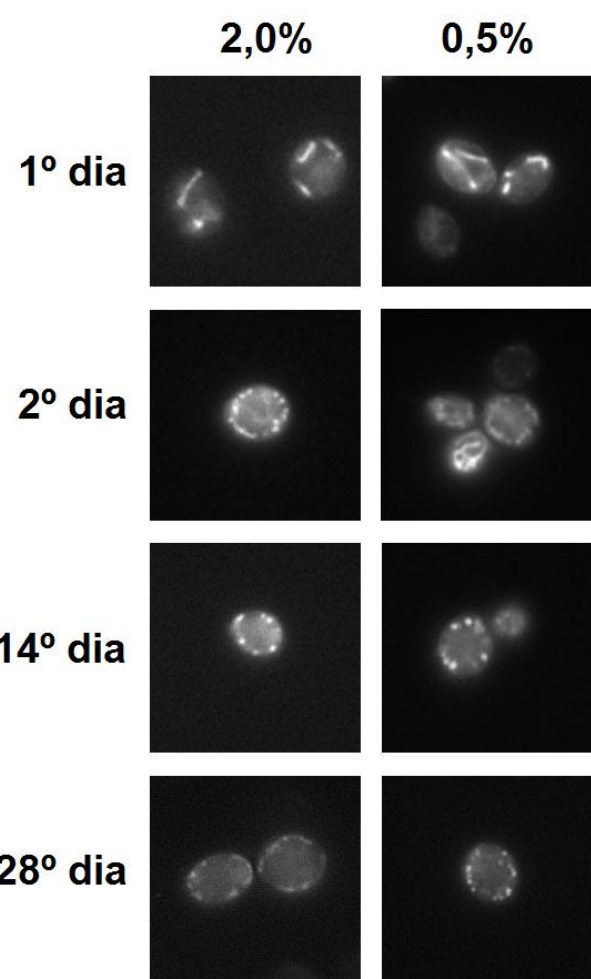


Figura 4.4. Morfologia mitocondrial ao longo do tempo de vida cronológico de *S. cerevisiae* WT. A determinação da morfologia mitocondrial com o uso de *MitoTracker Green* 500 nM na 16^a h (“1º dia”), na 40^a h (“2º dia”) e no 14º e 28º dia de cultivo em *S. cerevisiae* WT foi realizada conforme descrição em *Materiais e métodos* (Item 26) As imagens aqui utilizadas são representativas da análise de uma média de 100 células em, no mínimo, 4 experimentos independentes.

Pela análise da Figura 4.4, podemos observar que na 16^a hora de cultivo (representada na figura como “1º dia”), as mitocôndrias apresentam-se em redes de estrutura alongada, ocupando a periferia da célula em condição controle de cultivo e tanto a periferia como o centro da célula em restrição calórica. Já em restrição calórica, na 40^a h de cultivo (representada na figura como “2º dia”) – momento em que não há mais glicose nos meios de cultura e em que o metabolismo aeróbico é prevalente (Seção 3) – observamos que há duas populações mitocondriais bem distintas: enquanto uma já se mostra altamente fragmentada, outra ainda permanece na forma alongada anteriormente observada na 16^a h de cultivo. Por sua vez, na condição controle, as mitocôndrias de todas as células analisadas já se apresentavam em um grau avançado de fragmentação, embora tanto estas como as células em restrição calórica já estivessem utilizando substratos respiratórios como fonte de carbono (Figura 3.4). Essa diferença pode ser explicada pelo único fator que inicialmente as diferenciou, *i.e.*, a quantidade de glicose disponível no início dos cultivos. De fato, podemos observar que o perfil de metabólitos gerados nas duas condições é bastante distinto entre a condição controle e a restrição calórica (Figura 3.4), assim como o consumo de oxigênio e a liberação de oxidantes (Figuras 3.1 e 4.1), evidenciando a existência de uma correlação entre o estado metabólico celular – e todos os fenótipos secundários a essa condição, tais como respiração celular, liberação mitocondrial de oxidantes e estado de óxido-redução celular (Figuras 3.1, 4.1 e 4.2) – e a morfologia mitocondrial. Finalmente, a partir do 14º dia, as mitocôndrias já aparecem totalmente fragmentadas em ambas as condições, assumindo claramente uma localização celular estritamente periférica.

4.6. Conclusões

Podemos concluir, portanto, que a liberação mitocondrial de peróxido de hidrogênio em *S. cerevisiae* cultivada em condição controle é maior do que aquela apresentada pelas células caloricamente restritas na fase logarítmica tardia de crescimento, porém não na fase estacionária de crescimento. Além disso, a liberação de peróxido de hidrogênio induzida por piruvato – um substrato celular de considerável relevância já que é o produto final da glicólise – foi significativamente maior do que a promovida pela mistura de malato, glutamato e etanol. Essa observação indica que, nessa condição, a Lpd1p da piruvato desidrogenase pode ser a responsável pela elevada liberação de peróxido de hidrogênio – de fato, nosso grupo demonstrou que a Lpd1p é uma importante fonte de espécies reativas de oxigênio também na célula selvagem (Tahara *et al.*, 2007). Além disso, observamos que a quantidade de GSH sempre é maior nas células cultivadas em restrição calórica, e que *S. cerevisiae* cultivada em condição controle não consegue compensar a maior oxidação de GSH no 1º e no 28º dia de cultivo. Curiosamente, a tolerância a peróxido de hidrogênio exógeno por células caloricamente restritas é maior do que a apresentada pelas células controle apenas no primeiro e no sétimo dia de cultivo, não esclarecendo se os possíveis mecanismos horméticos no envelhecimento de *S. cerevisiae* caloricamente restrita são mediados

pelo estado de óxido-redução celular, ou se estes promovem um aumento da tolerância a estresse oxidativo promovido por peróxido de hidrogênio nas células caloricamente restritas. Finalmente, também observamos que na fase logarítmica tardia de crescimento, tanto as mitocôndrias de células caloricamente restritas como as de células controle apresentam-se organizadas em redes, as quais progressivamente vão se fragmentando – embora em uma dinâmica diferente, aparentemente mais lenta na célula caloricamente restrita – e assumindo uma localização estritamente periférica ao longo do tempo de cultivo. As elevadas taxas de liberação de oxidantes na fase logarítmica tardia de crescimento, assim como as relativamente diminuídas durante a fase estacionária, correlacionam-se, portanto, com a morfologia mitocondrial, embora a relação causal entre esses dois parâmetros ainda tenha que ser determinada.

Conclusões finais

- As inativações de *NPT1* e *BNA6* não promovem diminuição do tempo de vida cronológico, tampouco suprimem o aumento do tempo de vida mediado pela restrição calórica em *S. cerevisiae*, porém diminuem o consumo de oxigênio e aumentam a liberação de espécies reativas de oxigênio por intermédio da Lpd1p;
- Inativações de genes que codificam enzimas do ciclo dos ácidos tricarboxílicos, tais como *LPD1*, *ACO1*, *KGD1* e *SDH1* não impedem o aumento do tempo de vida cronológico em virtude da restrição calórica;
- Aco1p, Kgd1p, Lpd1p e Sdh1p alteram a estabilidade do DNA mitocondrial de forma dependente da disponibilidade inicial de glicose nos meios de cultura e do tempo de cultivo: no primeiro dia de cultivo, enquanto as ausências de Aco1p e Kgd1p diminuem a porcentagem de células respiratório-competentes em uma condição em que há uma maior disponibilidade de glicose nos meios de cultura, Lpd1p o faz em restrição calórica. Já no sétimo dia de cultivo, a ausência de Kgd1p aumenta a instabilidade do genoma mitocondrial em ambas as condições, assim como Lpd1p e Sdh1p o fazem em *S. cerevisiae* caloricamente restrita;
- A ausência da funcionalidade do genoma mitocondrial, seja pela ausência deste *per se*, seja pela ausência da atividade de Abf2p, abolem completamente a responsividade de *S. cerevisiae* à restrição calórica;
- A inativação do gene nuclear *CYT1* também suprime o aumento do tempo de vida mediado pela restrição calórica, demonstrando que a integridade da cadeia de transporte de elétrons é um requisito necessário para o aumento do tempo de vida cronológico de *S. cerevisiae* em resposta à restrição calórica;
- A responsividade de *S. cerevisiae* à restrição calórica, exceção feita ao mutante *npt1Δlpd1Δ*, correlaciona-se à capacidade de apresentar crescimento em meio seletivo rico para respiração
- O protocolo de restrição calórica para levedura aumenta o tempo de vida cronológico de *S. cerevisiae* por mitigar o fenômeno da repressão por glicose nessa levedura Crabtree-positiva. O tempo de vida cronológico de *K. lactis*, uma levedura Crabtree-negativa, não é capaz de ser aumentado pela restrição calórica;

- A repressão por glicose promove um *imprinting* em *S. cerevisiae* que não é revertido ao longo do tempo, uma vez que a taxa respiratória máxima dessa levedura cultivada em condição controle é significativamente menor que a dessa levedura cultivada sob restrição calórica;
- A ausência do DNA mitocondrial diminui a velocidade específica máxima de formação de biomassa e a velocidade específica máxima de consumo de glicose, e abole a capacidade de utilização de substratos oxidáveis para a geração de células, resultando em uma quantidade de biomassa diminuída nos mutantes ρ^0 ;
- O fator de conversão de glicose a células e a etanol não é alterado pela condição de cultivo tampouco pela funcionalidade do DNA mitocondrial;
- As células caloricamente restritas apresentam um menor índice de formação de etanol e glicerol (por hora) do que as células cultivadas em condição controle, mas elas são comparativamente mais aptas a consumir esses dois substratos, apresentando maior velocidade específica de crescimento e consequentemente maior formação de biomassa (por hora) promovida por esses dois substratos;
- Em ambas as condições de cultivo, a liberação de espécies reativas de oxigênio na fase logarítmica tardia de crescimento é sempre maior do que na fase estacionária e consideravelmente maior quando da suplementação de piruvato ao invés de malato, glutamato e etanol.
- A liberação de espécies reativas de oxigênio nas células caloricamente restritas na 16^a hora de cultivo é menor do que nas células controle, cenário que é invertido ao longo do restante do tempo de vida cronológico de *S. cerevisiae*;
- A restrição calórica aumenta a quantidade de glutatona total em todos os tempos de cultivo, e a célula cultivada sob condição controle possui um aumento da razão entre GSSG e GSH na 16^a h e no 28^o dia de cultivo;
- Não há correlação entre o estado de óxido-redução da glutatona com a tolerância ao estresse oxidativo ambiental em *S. cerevisiae*;
- As mitocôndrias de *S. cerevisiae*, na 16^a h de cultivo, mostram-se organizadas em uma rede alongada; bem definida; com o passar do tempo, essa rede é fragmentada, gerando mitocôndrias que se localizam na periferia da célula.

Materiais e métodos

1. Linhagem parental e mutantes de *S. cerevisiae*

A linhagem parental de *S. cerevisiae* utilizada foi a BY4741 (MAT α ; *his3Δ1*; *leu2Δ0*; *met15Δ0*; *ura3Δ0*; Brachmann *et al.*, 1998). Os mutantes *npt1Δ*, *bna6Δ*, *lpd1Δ*, *npt1Δlpd1Δ*, *bna6Δlpd1Δ*, *aco1Δ*, *kgd1Δ*, *sdh1Δ*, *abf2Δ*, *cyt1Δ*, e *atp2Δ* também foram utilizados.

2. Linhagem parental de *K. lactis*

A linhagem parental de *K. lactis* utilizada foi a CBS 2359 (Kiers *et al.*, 1998).

3. Meios de cultura, armazenamento e cultura celular

Os meios de cultura utilizados para os procedimentos foram (i) o YPD líquido (peptona 2,0%, extrato de levedura 1,0% e glicose 2,0% ou 0,5%); (ii) o YPD sólido (YPD líquido com glicose 2,0% suplementado com ágar bacteriológico 2,0%); (iii) o YPEG sólido (peptona 2,0%, extrato de levedura 1,0%, etanol 2,0%, glicerol 2,0% e ágar bacteriológico 2,0%); (iv) o SD sólido suplementado (base nitrogenada 0,17%, sulfato de amônio 0,5%, glicose 2,0%, sulfato de adenina 20 mg/L, uracila 20 mg/L, triptofano 20 mg/L, histidina 20 mg/L, arginina 20 mg/L, metionina 20 mg/L, tirosina 20 mg/L, leucina 100 mg/L, isoleucina 30 mg/L, lisina 30 mg/L, fenilalanina 50 mg/L, glutamato 100 mg/L, aspartato 100 mg/L, valina 150 mg/L, treonina 200 mg/L, serina 400 mg/L e ágar bacteriológico 2,0%); e (v) o SGE sólido suplementado (base nitrogenada 0,17%, sulfato de amônio 0,5%, etanol 2,0%, glicerol 2,0%, sulfato de adenina 20 mg/L, uracila 20 mg/L, triptofano 20 mg/L, histidina 20 mg/L, arginina 20 mg/L, metionina 20 mg/L, tirosina 20 mg/L, leucina 100 mg/L, isoleucina 30 mg/L, lisina 30 mg/L, fenilalanina 50 mg/L, glutamato 100 mg/L, aspartato 100 mg/L, valina 150 mg/L, treonina 200 mg/L, serina 400 mg/L e ágar bacteriológico 2,0%), todos esterilizados em vapor úmido a 121 °C, por 20 min. O armazenamento celular foi realizado em meio YPD sólido a 6 °C ou YPD líquido com glicose 2,0% acrescido de 15% de glicerol, a -80 °C. Os cultivos celulares eram realizados assepticamente em erlenmeyers fechados com tampas de estopa envolta em gaze em volumes de meio de cultura que variaram de 50 mL a 80 mL, por até 6 dias (*K. lactis*) ou 28 dias (*S. cerevisiae*), a 30 °C, em incubadora operando sob constante agitação orbital a 200 rpm. As pré-culturas eram realizadas por aproximadamente 18 h e o número de células inoculadas por mL de meio fresco para o início das culturas foi fixado em 1·10⁵.

4. Determinação do tempo de vida cronológico de *S. cerevisiae* e *K. lactis*

A determinação do tempo de vida cronológico de *S. cerevisiae* e *K. lactis* foi realizado através da medida da viabilidade celular verificada pela capacidade de formação de colônias ao longo tempo. Na 16^a h e no 7^º, 14^º, 21^º e 28^º dia de crescimento, um volume de 2 mL de cultura de *S. cerevisiae* era transferida para um tubo côncico de centrífuga estéril, ao qual eram adicionados 3 mL de água ultrapura estéril. A suspensão era então centrifugada por 1 min a 1000 × g, a 25 °C, e o sobrenadante era descartado. Este procedimento de lavagem era repetido e, por fim, as células eram ressuspensas em 2 mL de água ultrapura estéril. A absorbância a 600 nm (Abs₆₀₀) era determinada, e diluições em série a uma Abs₆₀₀ final de 0,2, 0,02, 0,002 e 0,0002 eram realizadas. Um volume de 50 µL da última diluição – o qual continha 100 células – era adicionado às placas de YPD sólido, as quais eram incubadas por 72 h a 30 °C para promover o crescimento celular; após esse período, o número de colônias era então determinado. Os resultados estão indicados nas figuras pelo número absoluto de colônias contadas – eles não foram propositalmente corrigidos para a porcentagem de sobrevivência em cada tempo de determinação a fim de refletir as verdadeiras diferenças no comportamento de cada mutante estudado. Em *K. lactis*, os mesmos procedimentos foram efetuados; entretanto, as determinações de viabilidade celular foram realizadas após 16 h e 2, 3, 4, 5 e 6 dias de crescimento.

5. Obtenção de esferoplastos de *S. cerevisiae*

Os esferoplastos de *S. cerevisiae* foram obtidos por duas maneiras diferentes, variando-se a quantidade de zimoliase utilizada para a preparação, bem como o tempo e a temperatura de incubação para a digestão enzimática.

Para as preparações utilizadas nas Figuras 1.2, 1.3 e 1.5, um volume que variava entre 5 mL e 20 mL de meio de cultura era transferido para um tubo côncico de centrífuga e 20 mL de água ultrapura eram adicionados. A suspensão era então centrifugada por 3 min a 1200 × g, a 25 °C, e o sobrenadante era descartado. O procedimento de lavagem era repetido, e o precipitado celular tinha a sua massa determinada em balança analítica. Conhecendo-se a massa celular da amostra, eram adicionados, por g de células, 3 mL de tampão sorbitol 1,2 M, MgCl₂ 10 mM e Tris-Cl 50 mM (pH = 7,5) contendo ditiotreitol 30 mM. Essa suspensão era então incubada a temperatura ambiente, com moderada agitação orbital (50 rpm), por 15 min, ao final dos quais era novamente centrifugada 3 min a 1200 × g, a 25 °C. O sobrenadante era descartado, e eram adicionados, por g de células, 5 mL do mesmo tampão sorbitol 1,2 M, MgCl₂ 10 mM e Tris-Cl 50 mM (pH = 7,5) contendo 1 mM de ditiotreitol e zimoliase 20 U/mg células. A suspensão resultante era então incubada com moderada agitação orbital (50 rpm), a 37 °C, por 40 min, ao final dos quais aproximadamente 40 mL de tampão sorbitol 1,2 M, MgCl₂ 10 mM e Tris-Cl 50 mM (pH = 7,5)

gelado eram adicionados ao tubo cônico. A suspensão era centrifugada por 1800 x g, por 5 min, a 4 °C. O procedimento de lavagem era novamente realizado, e o precipitado resultante de esferoplastos era ressuspenso em aproximadamente 1 mL de sorbitol 1,2 M, MgCl₂ 10 mM e Tris-Cl 50 mM (pH = 7,5) gelado, sendo reservados em gelo até o momento da sua utilização.

Para as preparações utilizadas na Figura 4.1 foram utilizados os procedimentos anteriormente descritos; porém a quantidade de zimoliase utilizada para a digestão foi aumentada para 60 U/mg células, e a incubação subsequente teve o tempo aumentado para 3 h e a temperatura diminuída para 30 °C.

6. Quantificação de proteína

A quantificação de proteína foi realizada segundo o método de Lowry (Lowry *et al.*, 1951).

7. Determinação da quantidade de digitonina necessária para permeabilização de esferoplastos de *S. cerevisiae*

A digitonina, um glicosídeo esteróide, é capaz de aumentar a permeabilidade de diferentes tipos de células a íons, metabólitos e enzimas (Dubinsky e Cockrell, 1975; Siess e Wieland, 1976; Mackall *et al.*, 1979; Fiskum *et al.*, 1980; Brocks *et al.*, 1980). Este efeito é resultado da ligação da digitonina ao colesterol e outros β-hidroxiesteróides presentes na membrana plasmática. Uma vez que, em eucariotos, a razão molar entre o colesterol e fosfolipídeos é algumas vezes maior na membrana plasmática do que em membranas intracelulares (Coulbeau *et al.*, 1971), o tratamento de células intactas – ou ainda esferoplastos de levedura – com baixas quantidades de digitonina promove a perda da continuidade da membrana plasmática e, consequentemente, o aumento da permeabilidade desta, preservando, porém, a integridade organelar. Esta técnica vem sendo empregada desde o final da década de 70 para a realização de medidas *in situ* da atividade do transporte mitocondrial e retículo endoplasmático em células (Dubinsky e Cockrell, 1975; Fiskum *et al.*, 1980).

Desta forma, a quantidade de digitonina a ser utilizada para a permeabilização dos esferoplastos de *S. cerevisiae* na determinação do consumo de oxigênio e da liberação de peróxido de hidrogênio induzido por substratos exógenos foi determinada através do monitoramento da integridade da membrana mitocondrial, *i.e.*, da verificação da preservação do potencial de membrana mitocondrial após a adição de quantidades conhecidas deste glicosídeo. Nos dois ensaios acima citados, a permeabilização fez-se necessária para que a membrana plasmática exibisse um aumento de permeabilidade aos substratos exógenos e à peroxidase de raiz forte – enzima necessária para a detecção de peróxido de hidrogênio através da sonda fluorescente *Amplex Red*.

(Item 9). Com a utilização de um volume adequado de digitonina 1%, a membrana plasmática tem a sua permeabilidade à safranina O aumentada, que é então acumulada na membrana mitocondrial interna, de forma dependente do potencial de membrana mitocondrial – já que a safranina O possui carga positiva e o interior da mitocôndria é negativamente carregado. Uma vez ligada, a safranina O já não mais fluoresce quando excitada a 495 nm, o que é verificado pelo alcance e sustentação da intensidade de fluorescência do traçado analítico nos menores valores possíveis. Caso a quantidade de digitonina 1% utilizada seja superior àquela necessária para a permeabilização, o traçado analítico mostrará, num primeiro momento, uma diminuição da intensidade de fluorescência da safranina O; porém, essa diminuição será seguida por um aumento da intensidade de fluorescência com o tempo, indicando a perda do potencial de membrana mitocondrial promovida pelo excesso do glicosídeo.

Assim, a integridade da membrana mitocondrial foi avaliada por 10 min com o uso de um espectrofotômetro de fluorescência operando a 495 nm de excitação e 586 nm de emissão, com agitação constante, a 30 °C, em suspensões de esferoplastos (100 µg/mL) em tampão sorbitol 1,2 M, EDTA 1 mM (pH = 7,5) e fosfato de potássio 75 mM (pH = 7,5), contendo etanol 2%, malato 1 mM (pH = 7,5) e glutamato 1 mM (pH = 7,5) como substratos, na presença de safranina O 5 µM. Quantidades conhecidas de uma solução de digitonina 1% foram adicionadas às suspensões de esferoplastos, e os volumes adequados foram utilizados, então, na determinação do consumo de oxigênio e da liberação de peróxido de hidrogênio induzido por substratos exógenos em esferoplastos de *S. cerevisiae*.

8. Determinação do consumo de oxigênio induzido por substratos exógenos em esferoplastos de *S. cerevisiae*

O consumo de oxigênio foi monitorado ao longo do tempo em suspensões de esferoplastos (800 µg/mL) em tampão sorbitol 1,2 M, EDTA 1 mM (pH = 7,5) e fosfato de potássio 75 mM (pH = 7,5) contendo malato 1 mM (pH = 7,5), glutamato 1 mM (pH = 7,5) e etanol 2%, como substratos, com o uso de um eletrodo de Clark interfaciado com computador e operando com agitação contínua, a 30°C.

9. Determinação da liberação de peróxido de hidrogênio induzido por substratos exógenos em esferoplastos de *S. cerevisiae*

A liberação de peróxido de hidrogênio induzida por substratos exógenos em esferoplastos de *S. cerevisiae* foi monitorada por 10 minutos com o uso de um espectrofotômetro de fluorescência operando a 563 nm de excitação e 587 nm de emissão, com agitação constante, a 30

°C, em suspensões de esferoplastos (100 µg/mL) em tampão sorbitol 1,2 M, EDTA 1 mM (pH = 7,5) e fosfato de potássio 75 mM (pH = 7,5) contendo (i) piruvato 0,5 mM (pH = 7,5) ou (ii) malato 1 mM (pH = 7,5), glutamato 1 mM (pH = 7,5) e etanol 2%, como substratos, na presença de peroxidase de raiz forte 0,5 U/mL e de *Amplex Red* 50 µM.

10. Quantificação de glutationa total, oxidada e reduzida em *S. cerevisiae*

A quantificação de glutationa total e GSSG foi realizada segundo Demasi *et al.* (2001), com algumas modificações. Um volume que variou entre 15 mL e 35 mL de meio de cultura foi transferido para um tubo cônico de centrífuga e 15 mL de água ultrapura foram adicionados. A suspensão foi então centrifugada por 3 min a 1200 x g, a 25 °C, e o sobrenadante foi descartado. O precipitado celular foi ressuspenso em 1 mL de água ultrapura e transportado a um microtubo de centrífuga sendo, em seguida, centrifugado a 20000 x g, por 3 min, a 25 °C. O sobrenadante foi retirado com uma micropipeta e o precipitado celular teve a sua massa determinada em balança analítica – em caso de uma massa superior a 200 mg, o excesso era retirado com o auxílio de uma espátula. Assim, a massa celular de aproximadamente 200 mg era então rompida por 15 minutos na presença de 100 mg de *glass beads* e 150 µL de ácido sulfosalicílico 3,5% por duas vezes, com o uso de um homogeneizador tipo vórtex, a 4 °C. Os homogenatos obtidos foram centrifugados a 20000 x g por 5 min, a 4 °C, para a recuperação da solução de ácido sulfosalicílico que continha a glutationa celular total. Em seguida, um volume de 250 mL era separado, tinha o seu pH corrigido para 7 com KOH e era incubado por 1 h com N-etilmaleimida 5 mM. A determinação da glutationa total foi realizada com o sobrenadante final pela sua reação com ácido 5-5'-ditiobis-2-nitrobenzóico 76 mM na presença de glutationa redutase 0,12 U/mL e NADPH 0,27 mM em um espectrofotômetro operando a 412 nm, sob agitação constante, a 30 °C. Os volumes das amostras reservados para a determinação de glutationa oxidada foram analisados sob as mesmas condições. A quantidade de glutationa reduzida foi determinada matematicamente pela diferença entre a glutationa total e a oxidada.

11. Construção dos mutantes *npt1Δlpd1Δ* e *bna6Δlpd1Δ*

Os mutantes *npt1Δlpd1Δ* e *bna6Δlpd1Δ* foram gerados, respectivamente, pelo cruzamento de mutantes com alelos nulos de *NPT1* e *BNA6* com um mutante *LPD1* do tipo de acasalamento oposto. Os diplóides resultantes foram então esporulados. Após análise das tétrades resultantes, os duplos mutantes foram selecionados de tétrades verdadeiras com segregação 2:2 para resistência a geneticina. As mutações simples e duplas foram confirmadas por reação em cadeia da polimerase, utilizando os seguintes primers localizados na região promotora dos respectivos genes: NPT1F 5'-GCCCTGCAAAAGCTTATAAAG; BNA6F 5'-GGTACAAGCTTGGTTACAAAC; LPD1F 5'-

GGCAAGCTTCGATTGTCTCTGTCG, com primer reverso presente no cassete de disruptão *kanMX*: kanB 5'-CTGCAGCGAGGAGCCGTAAT.

12. Isolamento de *S. cerevisiae* ρ⁰

Os mutantes ρ⁰ de *S. cerevisiae* foram obtidos após o cultivo de células selvagens por 20 h em YPD líquido de 2,0%. Então 100 células foram plaqueadas em YPD sólido e após 72 h, esta placa foi replicado em YPEG sólido. Após 48 h de incubação, as colônias respiratório-incompetentes foram então identificadas e isoladas da placa de YPD. O fenótipo ρ⁰ das colônias selecionadas foi confirmado por meio de cruzamentos com linhagens mit de *S. cerevisiae* contendo mutações pontuais nos genes mitocondriais *COX1*, *cob1* e *atp6* (Slonimski e Tzagoloff, 1976). Após a seleção baseada na complementação auxotrófica dos diplóides, não observamos a reversão da incompetência respiratória.

13. Determinação da capacidade de crescimento em meio seletivo rico e sintético para respiração

A capacidade de crescimento em meio seletivo para respiração foi realizada pela verificação do crescimento de *S. cerevisiae* WT, *aco1Δ*, *kgd1Δ*, *lpd1Δ*, *npt1Δlpd1Δ*, *bna6Δlpd1Δ*, *cyt1Δ*, *atp2Δ*, *abf2Δ* e ρ⁰ em meio YPEG sólido (seletivo rico) e SEG suplementado (seletivo sintético). Para tal, 5 µL de suspensões celulares de Abs_{600nm} de valores 1,0; 0,1; 0,01; e 0,001 foram seqüencialmente adicionados em placas contendo YPD, YPEG, SD suplementado e SEG suplementado sólidos, as quais foram incubadas por 7 dias a 30 °C.

14. Determinação da porcentagem de colônias respiratório-competentes em *S. cerevisiae*

A determinação da porcentagem de colônias ρ⁺ foi realizada replicando-se todas as colônias crescidas nas placas de YPD sólido em placas contendo YPEG sólido e se contando o número de colônias formadas também após 48 h de incubação a 30 °C. As colônias originadas em YPD a partir de células que não possuem o DNA mitocondrial íntegro não são capazes de crescer nesse meio seletivo para respiração e foram, portanto, inequivocamente consideradas como colônias do tipo *petite* (ρ⁰). Dessa forma, conseguimos determinar o número e a porcentagem de colônias ρ⁺.

15. Determinação do consumo de oxigênio em células intactas de *S. cerevisiae* WT

A determinação do consumo de oxigênio em células intactas de *S. cerevisiae* WT foi monitorado em alíquotas de 1 mL de cultura através o uso de um eletrodo de Clark interfaciado com computador e operando com agitação contínua, a 30 °C. A absorbância a 600 nm foi determinada para cada amostra, em todos os tempos, para a posterior correção do valor de consumo de oxigênio por biomassa.

16. Separação, análise e quantificação dos metabólitos extracelulares de *S. cerevisiae* WT e ρ^o

A separação dos analitos contidos nos meios de cultura YPD de *S. cerevisiae* WT e ρ^o foi realizada através do uso de uma coluna Bio-Rad Aminex HPX-87H (operando a 60 °C) acoplada a um cromatógrafo de alta eficiência operando com H₂SO₄ 5 mM como fase móvel, a uma vazão de 0,6 mL/min. A análise dos metabólitos extracelulares de *S. cerevisiae* WT e ρ^o foi realizada através do uso de um detector de índice de refração Waters 2414 (operando a 50 °C) e de um detector de absorbância Waters UV/Vis 2489 (operando em 214 nm). A quantificação desses metabólitos foi realizada através da determinação da altura dos picos cromatográficos com o uso do programa Empower 2 Chromatography Data Software (Waters). Alíquotas de 1 mL dos meios YPD 2,0% e 0,5% foram retiradas das culturas de *S. cerevisiae* no tempo inicial (0 h) e na 6^a; 12^a; 18^a; 24^a; 30^a; 36^a; 42^a e 48^a h de cultivo, e também no 3^o; 6^o; 7^o; 8^o; 9^o; 10^o; 14^o; 21^o e 28^o dia de cultivo. Após coletadas, as alíquotas foram filtradas com unidades filtrantes GV Millex com membrana Durapore de poro 0,22 µm para a retirada do conteúdo celular e estocadas a -20 °C até a sua análise. Os analitos estudados foram a glicose, o etanol, o glicerol, o acetato e o succinato (todos detectados pelo detector de índice de refração), além do piruvato (detectado pelo detector de absorbância).

Tabela 1. Tempos de retenção aproximados e canais de detecção dos metabólitos extracelulares de *S. cerevisiae* cultivada em YPD. IR: detector de índice de refração; UV/Vis: detector de absorbância.

Analito	Tempo de retenção (min)	Canal
Glicose	9,39	IR
Piruvato	9,58	UV/Vis
Succinato	12,33	IR
Glicerol	13,81	IR
Acetato	15,76	IR
Etanol	22,29	IR

Os padrões utilizados para a construção das curvas de calibração eram analisados no início, meio e final de todas as baterias de análise cromatográfica, e possuíam glicose 10,0 g/L, etanol e glicerol 5,0 g/L, e piruvato, succinato e acetato 1,0 g/L; ou glicose 5,0 g/L, etanol e glicerol 2,5 g/L, e piruvato, succinato e acetato 0,5 g/L. Os tempos de retenção aproximados de todos os analitos e os canais pelos quais eles são detectados estão listados na Tabela 1.

17. Determinação da curva de crescimento celular e de pH do meio extracelular

As curvas de crescimento celular e de pH extracelular de *S. cerevisiae* WT e ρ^o, cultivadas em condição controle e em restrição calórica, foram construídas com a obtenção dos dados de Abs₆₀₀ e de pH do meio extracelular nos mesmos tempos em que eram realizadas as retiradas de alíquotas para a análise dos metabólitos extracelulares. Exclusivamente para a curva de crescimento, sempre que necessário, eram feitas diluições convenientes para que as leituras analíticas no espectrofotômetro fossem de, no máximo, 0,6.

18. Determinação do fator de conversão de Abs₆₀₀ para biomassa

O cálculo do fator de conversão de Abs₆₀₀ para biomassa fez-se necessário para a determinação dos parâmetros fisiológicos relacionados aos cultivos, e foi realizado segundo Olsson e Nielsen (1997), com algumas modificações. Um volume que variou entre 3 e 20 mL de meio de cultura contendo *S. cerevisiae* foi filtrado por um sistema composto por membrana filtrante Millipore de 0,45 mm, unidade filtrante, kitassato e bomba de vácuo. As membranas filtrantes foram previamente armazenadas em uma estufa de secagem a 85 °C, por 8 h, ao final das quais uma a uma tinham as suas massas aferidas. Após a filtração, as membranas filtrantes eram retiradas da unidade filtrante e armazenadas novamente na estufa de secagem, a 85 °C, por mais 8 h. Após esse período de secagem, tinham suas massas aferidas novamente, e a massa seca de leveduras era determinada pela subtração do valor da massa da membrana filtrante seca da massa da membrana filtrante seca acrescida de leveduras. Após dez repetições deste procedimento, cujo resultado mostrou-se altamente reproduzível, chegamos ao valor de 0,194 mg de massa seca de *S. cerevisiae* BY4741 por mL de meio de cultura para cada unidade de Abs₆₀₀, independentemente da fase de crescimento.

19. Cálculo dos parâmetros fisiológicos associados aos cultivos

Os dados cromatográficos obtidos foram utilizados para a construção de gráficos em função do tempo. As regressões lineares utilizadas para a determinação dos parâmetros fisiológicos foram obtidas com o uso do software OpenOffice.org Calc 3.2.1 (Oracle). O coeficiente de regressão linear mínimo aceito para a análise dos dados foi de 0,9.

20. Determinação da velocidade específica máxima de crescimento em glicose e etanol/glicerol

Para a determinação da velocidade específica máxima de crescimento (μ^{\max} ; em h^{-1}) de *S. cerevisiae*, tanto em glicose (μ_{Glu}^{\max}) como em etanol/glicerol ($\mu_{\text{EtOH+Gli}}^{\max}$), foi gerado, primeiramente, o gráfico do logaritmo natural da concentração celular (Abs_{600} ; ordenada) contra o tempo (abcissa). O μ^{\max} para cada substrato corresponde ao coeficiente angular da regressão linear obtida com os pontos pertencentes ao trecho linear da curva de crescimento em logaritmo natural; esse trecho linear corresponde à fase exponencial de crescimento celular promovida pelo consumo de cada um desses substratos (Doran, 1995).

Os intervalos de tempo utilizados para o cálculo da μ_{Glu}^{\max} e da $\mu_{\text{EtOH+Gli}}^{\max}$ foram determinados pela curva de Abs_{600} , e encontram-se na tabela abaixo, assim como o intervalo de tempo decorrido para o início da metabolização do etanol após a exaustão total da glicose.

Tabela 2. Intervalos de tempo utilizados para o cálculo da μ_{Glu}^{\max} e da μ_{EtOH}^{\max} e intervalo de tempo decorrido para o início da metabolização do etanol após a exaustão total da glicose em *S. cerevisiae*. Δt : intervalo de tempo.

	Δt para m_{Glu}^{\max} (h)	Δt para m_{EtOH}^{\max} (h)	Δt entre m_{Glu}^{\max} e m_{EtOH}^{\max} (h)
WT 2,0%	0 a 18	30 a 48	12
WT 0,5%	0 a 12	18 a 42	6
ρ^o 2,0%	0 a 24	-	-
ρ^o 0,5%	0 a 18	-	-

As determinações da velocidade específica máxima de crescimento em etanol e glicerol foram realizadas em conjunto, como um só índice, uma vez que os consumos desses dois substratos é temporalmente paralelo.

21. Determinação do fator de conversão de substrato a biomassa

Para o cálculo do fator de conversão de substrato a biomassa, ou rendimento celular ($Y_{X/S}^{\exp}$, em g células/g substrato), tanto para glicose ($Y_{X/\text{Glu}}^{\exp}$ em g células/g glicose) como para etanol/glicerol ($Y_{X/\text{EtOH+Gli}}^{\exp}$ em g células/g etanol), foi primeiramente necessário transformar os valores de Abs_{600} em biomassa. O coeficiente angular da regressão linear obtida no gráfico da concentração celular (em g células/L; ordenada) em função da concentração de substrato (g glicose/L ou g etanol+glicerol/L; abcissa) corresponde ao fator de conversão dos substratos a biomassa. Os intervalos de tempo da curva de biomassa utilizados para esses cálculos correspondem exatamente àqueles encontrados na Tabela 2.

22. Determinação do fator de conversão de substrato a produto

Para a determinação do fator de conversão de substrato a produto ($Y_{P/S}$; em g produto/g substrato), ou rendimento em produto, foi primeiramente gerado um gráfico da concentração do produto (g produto/L; ordenada) em função da concentração de substrato (g substrato/L). O coeficiente angular da regressão linear obtida corresponde ao $Y_{P/S}$; assim, os fatores de conversão de glicose a etanol ($Y_{EtOH/Glu}^{exp}$) e de glicose a glicerol ($Y_{Gli/Glu}^{exp}$) puderam ser obtidos. Os intervalos de tempo utilizados para a determinação desses parâmetros foram aqueles em que, necessariamente, eram observados, de forma concomitante, o consumo de glicose e a geração dos produtos. Outros fatores de conversão, como o de conversão de glicose a acetato, a piruvato e a succinato não puderam ser calculados uma vez que estes foram somente detectados após a total exaustão da glicose dos meios de cultura.

23. Determinação da velocidade específica máxima de consumo de substrato e de geração de produto

A velocidade específica máxima de consumo de substrato (r_c^{\max} ; em g substrato/g célula·h) e a velocidade específica máxima de geração do produto (r_f^{\max}) foram calculadas pelas equações 1 e 2, respectivamente. A velocidade específica máxima de consumo de glicose (r_{cGlu}^{\max} ; em g glicose/g células · h); de etanol e glicerol ($r_{cEtOH+Gli}^{\max}$; em g etanol e glicerol/g células · h); e a velocidade específica máxima de formação de etanol (r_{fEtOH}^{\max} ; em g etanol/g células · h); de glicerol (r_{fGli}^{\max} ; em g glicerol/g células · h) foram assim determinadas.

$$r_c^{\max} = m^{\max}/Y_{X/S}^{exp} \quad [1]$$

$$r_f^{\max} = (m^{\max}/Y_{X/S}) * Y_{P/S}^{exp} \quad [2]$$

24. Estimativa da velocidade específica de crescimento em etanol e glicerol

A estimativa da velocidade específica máxima de crescimento celular em etanol (μ_{EtOH}^{\max}) e da velocidade específica máxima de crescimento celular em glicerol (μ_{Gli}^{\max}), foi realizada a partir da transferência de *S. cerevisiae* WT cultivadas em meio YPD 2,0% e 0,5% a meios YP contendo ou etanol ou glicerol, nas concentrações máximas determinadas [etanol: 8,90 g/L (2,0%) e 2,25 g/L (0,5%); glicerol: 0,68 g/L (2,0%) e 0,25 g/L (0,5%)], nos tempos em que estas eram atingidas [etanol: 24 h (2,0%) e 18 h (0,5%); glicerol: 30 h (2,0%) e 18 h (0,5%)]. Os cultivos tiveram as suas Abs₆₀₀ registradas até a 48^a hora de cultivo.

25. Determinação da tolerância a estresse oxidativo ambiental

A determinação da tolerância celular de *S. cerevisiae* WT a estresse oxidativo ambiental foi verificada através da capacidade de crescimento em meio SD suplementado sólido com concentrações variadas de peróxido de hidrogênio após 3 dias de incubação a 30 °C. As diluições realizadas e o volume de células adicionado às placas foram os mesmos descritos no Item 13.

26. Determinação da morfologia mitocondrial

A determinação da morfologia mitocondrial de *S. cerevisiae* WT foi realizada através da análise de células previamente incubadas com sonda fluorescente utilizando um microscópio de fluorescência. Para tal, 1.10^7 células ressuspensas em seu próprio meio de cultura foram incubadas na presença de MitoTracker Green 500 nM por 45 minutos. A microscopia foi realizada em um microscópio invertido Nikon TE300 operando com filtro para proteína verde fluorescente. As imagens foram capturadas com uma câmera Roper HQ CoolSnap. Os tempos de exposição variaram de 0,5 a 2 segundos. As imagens obtidas foram processadas e analisadas com os softwares Metamorph 7.1 (Universal Imaging) e ImageJ (<http://rsb.info.nih.gov/ij/>).

27. Geração de gráficos e análise estatística

A geração dos gráficos e a realização da análise estatística foram feitas através do programa GraphPad Prism 5.00 (GraphPad Software, Inc.). Os resultados são expressos em média \pm erro médio.

Bibliografia

- Andziak, B., O'Connor, T.P., Qi, W., DeWaal, E.M., Pierce, A., Chaudhuri, A.R., Van Remmen, H., Buffenstein R. (2006) High oxidative damage levels in the longest-living rodent, the naked mole-rat. *Aging Cell* **5**: 463-741.
- Artal-Sanz, M., Tavernarakis, N. (2008). Mechanisms of aging and energy metabolism in *Caenorhabditis elegans*. *IUBMB Life* **60**: 315-322.
- Balaban, R.S., Nemoto, S., Finkel, T. Mitochondria, oxidants, and aging. (2005) *Cell* **120**: 483-495.
- Barea, F., Bonatto, D. (2009) Aging defined by a chronologic-replicative protein network in *Saccharomyces cerevisiae*: an interactome analysis. *Mech. Ageing Dev.* **130**: 444-460.
- Barhoumi, R., Bowen, J.A., Stein, L.S., Echols, J., Burghardt, R.C. (1993) Concurrent analysis of intracellular glutathione content and gap junctional intercellular communication. *Cytometry* **14**: 747-756.
- Barja, G. (2002). Rate of generation of oxidative stress-related damage and animal longevity. *Free Radic. Biol. Med.* **33**: 1167-1172.
- Barja, G., Herrero, A. (2000). Oxidative damage to mitochondrial DNA is inversely related to maximum life span in the heart and brain of mammals. *FASEB J.* **14**: 312-318.
- Barros, M.H., Bandy, B., Tahara, E.B., Kowaltowski, A.J. (2004) Higher respiratory activity decreases mitochondrial reactive oxygen release and increases life span in *Saccharomyces cerevisiae*. *J. Biol. Chem.* **279**: 49883-49888.
- Barros, M.H., da Cunha, F.M., Oliveira, G.A., Tahara, E.B., Kowaltowski, A.J. (2010). Yeast as a model to study mitochondrial mechanisms in ageing. *Mech. Ageing Dev.* **131**: 494-502.
- Basso, T.O., Dario, M.G., Tonso, A., Stambuk, B.U., Gombert, A.K. (2010) Insufficient uracil supply in fully aerobic chemostat cultures of *Saccharomyces cerevisiae* leads to respiro-fermentative metabolism and double nutrient-limitation. *Biotechnol. Lett.* **32**: 973-977.
- Beckman, K.B., Ames, B.N. (1998) The free radical theory of aging matures. *Physiol. Rev.* **78**: 547-581.

Bevilacqua, L., Ramsey, J. J., Hagopian, K., Weindruch, R., Harper, M. E. (2005) Long-term caloric restriction increases UCP3 content but decreases proton leak and reactive oxygen species production in rat skeletal muscle mitochondria. *Am. J. Physiol.* **289**: 429-438.

Bitterman, K.J., Medvedik, O., Sinclair, D.A. (2003). Longevity regulation in *Saccharomyces cerevisiae*: linking metabolism, genome stability, and heterochromatin. *Microbiol. Mol. Biol. Rev.* **67**: 376-399.

Bjelakovic, G., Nikolova, D., Gluud, L.L., Simonetti, R.G., Gluud, C. (2007) Mortality in randomized trials of antioxidant supplements for primary and secondary prevention: Systematic review and meta-analysis. *JAMA* **297**: 842-857.

Blander, G., Guarente, L. (2004) The Sir2 family of protein deacetylases. *Annu Rev Biochem.* **73**:417-35.

Brachmann, C.B., Davies, A., Cost, G.J., Caputo, E., Li, J., Hieter, P., Boeke, J.D. (1998) Designer deletion strains derived from *Saccharomyces cerevisiae* S288C: a useful set of strains and plasmids for PCR-mediated gene disruption and other applications. *Yeast* **14**: 115-132.

Brachmann, C.B., Sherman, J.M., Devine, S.E., Cameron, E.E., Pillus, L., Boeke, J.D. (1995) The *SIR2* gene family, conserved from bacteria to humans, functions in silencing, cell cycle progression, and chromosome stability. *Genes Dev.* **9**: 2888–2902

Brewer, L.R., Friddle, R., Noy, A., Baldwin, E., Martin, S.S., Corzett, M., Balhorn, R., Baskin, R.J. (2003) Packaging of single DNA molecules by the yeast mitochondrial protein Abf2p. *Biophys. J.* **85**: 2519-2524.

Brocks, D.G., Siess, E.A., Wieland, O.H. Validity of the digitonin method for metabolite compartmentation in isolated hepatocytes. *Biochem J.* **188**: 207-212.

Bryk , M., Banerjee, M., Murphy, M., Knudsen, K.E., Garfinkel, D.J, Curcio M.J. (1997) Transcriptional silencing of Ty1 elements in the RDN1 locus of yeast. *Genes Dev.* **11**: 255–269.

Buffenstein, R., Edrey, Y.H., Yang, T., Mele, J. (2008) The oxidative stress theory of aging: embattled or invincible? Insights from non-traditional model organisms. *Age* **30**: 99-109.

Calabrese, V., Cornelius, C., Cuzzocrea, S., Iavicoli, I., Rizzarelli, E., Calabrese, E.J. (2011) Hormesis, cellular stress response and vitagenes as critical determinants in aging and longevity. *Mol Aspects Med.* [no prelo].

Chapman, K.B., Solomon, S.D., Boeke, J.D. (1992) *SDH1*, the gene encoding the succinate dehydrogenase flavoprotein subunit from *Saccharomyces cerevisiae*. *Gene* **118**: 131-136.

Chen, X.J., Wang, X., Kaufman, B.A., Butow, R.A. (2005). Aconitase couples metabolic regulation to mitochondrial DNA maintenance. *Science* **307**: 714-717.

Chen, Y.B., Yang, C.P., Li, R.X., Zeng, R., Zhou, J.Q. (2005) Def1p is involved in telomere maintenance in budding yeast. *J Biol Chem.* **280**: 24784-24791.

Choksi, K.B., Nuss, J.E., Boylston, W.H., Rabek, J.P., Papaconstantinou, J. (2007) Age-related increases in oxidatively damaged proteins of mouse kidney mitochondrial electron transport chain complexes. *Free Radic. Biol. Med.* **43**: 1423-1438.

Choksi, K.B., Papaconstantinou, J. (2008) Age-related alterations in oxidatively damaged proteins of mouse heart mitochondrial electron transport chain complexes. *Free Radic. Biol. Med.* **44**: 1795-805.

Colbeau, A., Nachbaur, J., Vignais, P.M. Enzymic characterization and lipid composition of rat liver subcellular membranes. *Biochim Biophys Acta* **249**: 462-492.

Cypser, J., Johnson, T.E. (2001) Hormesis extends the correlation between stress resistance and life span in long-lived mutants of *Caenorhabditis elegans*. *Hum. Exp. Toxicol.* **20**: 295-296.

Czernichow, S., Bertrais, S., Blacher, J., Galan, P., Briancon, S., Favier, A., Safar, M., Hercberg, S. (2005) Effect of supplementation with antioxidants upon long-term risk of hypertension in the SU.VI.MAX study: association with plasma antioxidant levels. *J. Hypertens.* **23**: 2013-2018.

Davies, M.J., Fu, S., Dean, R.T. (1995) Protein hydroperoxides can give rise to reactive free radicals. *Biochem. J.* **305**: 643-649.

De Deken, R.H. (1996) The Crabtree effect: a regulatory system in yeast. *J Gen Microbiol.* **44**: 149-56.

- Demasi, M., Shringarpure, R., Davies, K.J. (2001) Glutathiolation of the proteasome is enhanced by proteolytic inhibitors. *Arch. Biochem. Biophys.* **389**: 254-263.
- DeRisi, J.L., Iyer, V.R., Brown, P.O. (1997). Exploring the metabolic and genetic control of gene expression on a genomic scale. *Science* **278**: 680-686.
- Diffley, J.F., Stillman, B. (1991). A close relative of the nuclear, chromosomal high-mobility group protein HMG1 in yeast mitochondria. *Proc. Natl. Acad. Sci. USA* **88**: 7864-7868.
- Diffley, J.F., Stillman, B. (1992). DNA binding properties of an HMG1-related protein from yeast mitochondria. *J. Biol. Chem.* **267**: 3368-3374.
- D'mello, N.P., Childress, A.M., Franklin, D.S., Kale, S.P., Pinswasdi, C., Jazwinski, S.M. (1994) Cloning and characterization of *LAG1*, a longevity-assurance gene in yeast. *J Biol Chem.* **269**: 15451-15459.
- Doran, P. M. (1995) *Bioprocess Engineering Principles*. London: Academic Press.
- Douce. R, Bourguignon, J., Neuburger, M., Rébeillé, F. (2001) The glycine decarboxylase system: a fascinating complex. *Trends. Plant Sci.* **6**: 167-176.
- Dubinsky WP, Cockrell RS (1975) Ca²⁺ transport across plasma and mitochondrial membranes of isolated hepatocytes. *FEBS Lett.* **59**: 39-43.
- Fabrizio, P., Li, L., Longo, V.D. (2005). Analysis of gene expression profile in yeast aging chronologically. *Mech. Ageing Dev.* **126**: 11-16.
- Fabrizio, P., Longo, V.D. (2003). The chronological life span of *Saccharomyces cerevisiae*. *Aging Cell* **2**: 73-81.
- Fabrizio, P., Pozza , F., Pletcher, S.D., Gendron, C.M., Longo, V.D. (2001) Regulation of longevity and stress resistance by Sch9 in yeast. *Science* **292**: 288-290.
- Falkenberg, M., Larsson, N.G., Gustafsson, C.M. (2007). DNA replication and transcription in mammalian mitochondria. *Annu. Rev. Biochem.* **76**: 679-699.
- Ferguson, L.R., von Borstel, R.C. (1992). Induction of the cytoplasmic 'petite' mutation by chemical and physical agents in *Saccharomyces cerevisiae*. *Mutat. Res.* **265**: 103-148.

Fiechter, A., Fuhrmann, G.F., Käppeli, O. (1981) Regulation of glucose metabolism in growing yeast cells. *Adv. Microb. Physiol.* **22**: 123-183.

Fiskum, G., Craig, S.W., Decker, G.L., Lehninger, A.L. (1980) The cytoskeleton of digitonin-treated rat hepatocytes. *Proc. Natl. Acad. Sci. USA.* **77**: 3430-3434.

Fontana, L., Partridge, L., Longo, V.D. (2010). Extending healthy life span--from yeast to humans. *Science* **328**: 321-326.

Foury, F., Roganti, T., Lecrenier, N., Purnelle, B. (1998). The complete sequence of the mitochondrial genome of *Saccharomyces cerevisiae*. *FEBS Lett.* **440**: 325-331.

Foyer , C.H., Mullineaux, P.M. (1998) The presence of dehydroascorbate and dehydroascorbate reductase in plant tissues. *FEBS Lett.* **425**:528-529.

Frick O, Wittmann C. (2005) Characterization of the metabolic shift between oxidative and fermentative growth in *Saccharomyces cerevisiae* by comparative ¹³C flux analysis. *Microb Cell Fact.* **4**: 30.

Fukagawa, N.K., Li, M., Liang, P., Russell, J.C., Sobel, B.E., Absher, P.M. (1999) Aging and high concentrations of glucose potentiate injury to mitochondrial DNA. *Free Radic. Biol. Med.* **27**: 1437-1443.

Gangloff, S.P., Marguet, D., Lauquin, G.J. (1990). Molecular cloning of the yeast mitochondrial aconitase gene (ACO1) and evidence of a synergistic regulation of expression by glucose plus glutamate. *Mol. Cell Biol.* **10**: 3551-3561.

Golden, T.R., Hinerfeld, D.A., Melov, S. (2002) Oxidative stress and aging: beyond correlation. *Aging Cell* **1**: 117-123.

Gottlieb, S., Esposito, R.E. (1989) A new role for a yeast transcriptional silencer gene, *SIR2*, in regulation of recombination in ribosomal DNA. *Cell*, **56**: 771-776

Gottschling, D.E., Aparicio, O.M., Billington, B.L., Zakian, V.A. (1990) Position effect at *S. cerevisiae* telomeres: reversible repression of Pol II transcription. *Cell* **63**: 751-762.

Grant, C.M. (2001) Role of the glutathione/glutaredoxin and thioredoxin systems in yeast growth and response to stress conditions. *Mol. Microbiol.* **39**: 533-541.

Gredilla, R., Barja, G. (2005) Minireview: the role of oxidative stress in relation to caloric restriction and longevity. *Endocrinology* **146**: 3713-3717.

Greenberg, E.R., Baron, J.A., Tosteson, T.D., Freeman, D.H. Jr, Beck, G.J., Bond, J.H., Colacchio, T.A., Coller, J.A., Frankl, H.D., Haile, R.W., Mandel, J.S., Nierenberg, D.W., Rothstein, R., Snover, D.C., Stevens, M.M., Summers, R.W., van Stolk, R.U. (1994) A clinical trial of antioxidant vitamins to prevent colorectal adenoma. *N. Engl. J. Med.* **331**: 141-147.

Grotewiel, M.S., Martin, I., Bhandari, P., Cook-Wiens, E., (2005). Functional senescence in *Drosophila melanogaster*. *Ageing Res. Rev.* **4**: 372-397.

Grotkjaer, T., Akesson, M., Christensen, B., Gombert, A.K., Nielsen, J. (2004) Impact of transamination reactions and protein turnover on labeling dynamics in (13)C-labeling experiments. *Biotechnol Bioeng.* **86**: 209-216.

Guarente, L., Picard, F. (2005) Calorie restriction--the SIR2 connection. *Cell* **120**: 473-482.

Hagopian, K., Harper, M.E., Ram, J.J., Humble, S.J., Weindruch, R., Ramsey, J.J. (2005) Long-term calorie restriction reduces proton leak and hydrogen peroxide production in liver mitochondria. *Am. J. Physiol. Endocrinol. Metab.* **288**: 674-684.

Harman, D. (1956) Aging: a theory based on free radical and radiation chemistry. *J. Gerontol.* **11**: 298-300.

Harman, D. (2001) Aging: overview. *Ann. N. Y. Acad. Sci.* **928**: 1-21.

Hobbs, A.E., Srinivasan, M., McCaffery, J.M., Jensen, R.E. (2001) Mmm1p, a mitochondrial outer membrane protein, is connected to mitochondrial DNA (mtDNA) nucleoids and required for mtDNA stability. *J Cell Biol.* **152**: 401-410.

Hoopes, L.L., Budd, M., Choe, W., Weitao, T., Campbell, J.L. (2002) Mutations in DNA replication genes reduce yeast life span. *Mol. Cell. Biol.* **12**: 4136-4146.

Hursting, S. D., Lavigne, J. A., Berrigan, D., Perkins, S. N., Barrett, J. C. (2003) Calorie restriction, aging, and cancer prevention: mechanisms of action and applicability to humans. *Annu. Rev. Med.* **54**: 131-152.

Jacobs, H.T. (2003) The mitochondrial theory of aging: dead or alive? *Aging Cell* **2**: 11-17.

Jayaraman, J., Cotman, C., Mahler, H.R., Sharp, C.W. (1966) Biochemical correlates of respiratory deficiency. VII. Glucose repression. *Arch. Biochem. Biophys.* **116**: 224–251.

Jazwinski, S.M. (1996) Longevity, genes, and aging. *Science* **273**: 54-59.

Jazwinski, S.M. (2002). Growing old: metabolic control and yeast aging. *Annu. Rev. Microbiol.* **56**: 769-792.

Jazwinski, S.M. (2004). Yeast replicative life span--the mitochondrial connection. *FEMS Yeast Res.* **5**: 119-125.

Jazwinski, S.M. (2001) New clues to old yeast. *Mech. Ageing Dev.* **122**: 865-882.

Jensen, P.K. (1996) Antimycin-insensitive oxidation of succinate and reduced nicotinamide-adenine dinucleotide in electron-transport particles. I. pH dependency and hydrogen peroxide formation. *Biochim. Biophys. Acta.* **122**: 157-166.

Jiang, J.C., Jaruga, E., Repnevskaya, M.V., Jazwinski, S.M. (2000). An intervention resembling caloric restriction prolongs life span and retards aging in yeast. *FASEB J.* **14**: 2135-2147.

Kaeberlein, M., Hu, D., Kerr, E.O., Tsuchiya, M., Westman, E.A., Dang, N., Fields, S., Kennedy, B.K. (2005). Increased life span due to calorie restriction in respiratory-deficient yeast. *PloS Genet.* **1**: e69.

Kaeberlein, M., McVey, M., Guarente, L. (1999) The SIR2/3/4 complex and *SIR2* alone promote longevity in *Saccharomyces cerevisiae* by two different mechanisms. *Genes Dev.* **13**: 2570-2580.

Kaeberlein, M., McVey, M., Guarente, L. (2000) Using yeast to discover the fountain of youth. *Sci. Aging Knowledge Environ.* **1**: pe1.

Kaeberlein, M., Powers, R.W. (2007) Sir2 and calorie restriction in yeast: a skeptical perspective. *Ageing Res. Rev.* **6**: 128–140.

Kaiser, J. (2003) Hormesis. Sipping from a poisoned chalice. *Science* **302**: 376-379.

Kataja-Tuomola, M., Sundell, J.R., Mannisto, S., Virtanen, M.J., Kontto, J., Albanes, D., Virtamo, J. (2008) Effect of alpha-tocopherol and beta-carotene supplementation on the incidence of type 2 diabetes. *Diabetologia* **51**: 47-53.

Katsiki, N., Manes, C. (2009) Is there a role for supplemented antioxidants in the prevention of atherosclerosis? *Clin. Nutr.* **28**: 3-9.

Kaufman, B.A., Kolesar, J.E., Perlman, P.S., Butow, R.A. (2003). A function for the mitochondrial chaperonin Hsp60 in the structure and transmission of mitochondrial DNA nucleoids in *Saccharomyces cerevisiae*. *J. Cell Biol.* **163**: 457-461.

Kennedy, B.K., Austriaco, N.R. and Guarente, L. (1994) Daughter cells of *Saccharomyces cerevisiae* from old mothers display a reduced life span. *J. Cell Biol.* **127**: 1985–1993.

Kennedy, B.K., Guarente, L. (1996) Genetic analysis of aging in *Saccharomyces cerevisiae*. *Trends Genet.* **12**: 355-359.

Kenyon, C. (2001). A conserved regulatory system for aging. *Cell* **105**: 165-168.

Kiers, J., Zeeman, A.M., Luttk, M., Thiele, C., Castrillo, J.I., Steensma, H.Y., van Dijken, J.P., Pronk, J.T. (1998) Regulation of alcoholic fermentation in batch and chemostat cultures of *Kluyveromyces lactis* CBS 2359. *Yeast* **14**: 459-469.

Kim, S., Benguria, A., Lai, C.Y., Jazwinski, S.M. (1999) Modulation of life-span by histone deacetylase genes in *Saccharomyces cerevisiae*. *Mol. Biol. Cell.* **10**: 3125–3136.

Kirkwood, T.B. (2002). Evolution of ageing. *Mech. Ageing Dev.* **123**: 737-745.

Kowaltowski, A.J., de Souza-Pinto, N.C., Castilho, R.F., Vercesi, A.E. (2009) Mitochondria and reactive oxygen species. *Free Radic. Biol. Med.* **47**: 333-343.

Kucej, M., Butow, R.A. (2007) Evolutionary tinkering with mitochondrial nucleoids. *Trends Cell Biol.* **12**: 586-592

Kucej, M., Kucejova, B., Subramanian, R., Chen, X.J., Butow, R.A. (2008). Mitochondrial nucleoids undergo remodeling in response to metabolic cues. *J. Cell Sci.* **121**: 1861-1868.

Lambeth, J.D. (2004) NOX enzymes and the biology of reactive oxygen. *Nat. Rev. Immunol.* **4**: 181-189.

Landry, J., Sutton, A., Tafrov, S.T., Heller, R.C., Stebbins, J., Pillus, L., Sternglanz, R. (2000) The silencing protein *SIR2* and its homologs are NAD-dependent protein deacetylases. *Proc. Natl. Acad. Sci. USA* **97**: 5807-5811.

Lee, I., Li, Zhihua, Marcotte E.M. (2007) An Improved, Bias-Reduced Probabilistic Functional Gene Network of Baker's Yeast, *Saccharomyces cerevisiae*. *PLoS ONE* **10**: e988.

Lin, S.J., Defossez, P.A., Guarente, L. (2000). Requirement of NAD and *SIR2* for life-span extension by calorie restriction in *Saccharomyces cerevisiae*. *Science* **289**: 2126-2128.

Lin, S.J., Kaeberlein, M., Andalis, A.A., Sturtz, L.A., Defossez, P.A., Culotta, V.C., Fink, G.R., Guarente, L. (2002). Calorie restriction extends *Saccharomyces cerevisiae* lifespan by increasing respiration. *Nature* **418**: 344-348.

Linnane, A.W., Haslam, J.M., Lukins, H.B., Nagley, P. (1972). The biogenesis of mitochondria in microorganisms. *Annu. Rev. Microbiol.* **26**: 163-198.

Linnane, A.W., Marzuki, S., Ozawa, T., Tanaka, M. (1989). Mitochondrial DNA mutations as an important contributor to ageing and degenerative diseases. *Lancet* **25**: 642-645.

Liu, S., Ajani, U., Chae, C., Hennekens, C., Buring, J.E., Manson, J.E. (1999) Long-term beta-carotene supplementation and risk of type 2 diabetes mellitus: a randomized controlled trial. *JAMA* **282**: 1073-1075.

Lowry, O.H., Rosenbrough, N.J., Farr, A.L., Randall, R.J. (1951) Protein measurement with the Folin phenol reagent. *J. Biol. Chem.* **193**: 265-275.

Mackall, J., Meredith, M., Lane, M.D. A mild procedure for the rapid release of cytoplasmic enzymes from cultured animal cells. *Anal. Biochem.* **95**: 270-274.

MacLean, M., Harris, N., Piper, P.W. (2001). Chronological lifespan of stationary phase yeast cells; a model for investigating the factors that might influence the ageing of postmitotic tissues in higher organisms. *Yeast* **18**: 499-509.

McCay, C.M., Cromwell, M.F., Maynard, L.A. (1935) The effect of retarded growth upon the length of life span and upon the body size. *J. Nutr.* **10**: 63-79.

Meeusen, S., Tieu, Q., Wong, E., Weiss, E., Schieltz, D., Yates, J.R., Nunnari, J. (1999) Mgm101p is a novel component of the mitochondrial nucleoid that binds DNA and is required for the repair of oxidatively damaged mitochondrial DNA. *J. Cell Biol.* **145**: 291-304.

Mesquita, A., Weinberger, M., Silva, A., Sampaio-Marques, B., Almeida, B., Leão, C., Costa, V., Rodrigues, F., Burhans, W.C., Ludovico, P. (2010) Caloric restriction or catalase inactivation extends yeast chronological lifespan by inducing H₂O₂ and superoxide dismutase activity. *Proc. Natl. Acad. Sci. USA* **107**: 15123-15128.

Miller, A.A., Drummond, G.R., Sobey, C.G. (2006). Reactive oxygen species in the cerebral circulation: are they all bad? *Antioxid. Redox Signal.* **8**: 1113-1120.

Minois, M., Frajnt, M., Wilsonm, C., Vaupel, J.W. (2005) Advances in measuring lifespan in the yeast *Saccharomyces cerevisiae*. *Proc. Natl. Acad. Sci. USA* **102**: 402-426.

Miyakawa, I., Aoi, H., Sando, N., Kuroiwa, T. (1984) Fluorescence microscopic studies of mitochondrial nucleoids during meiosis and sporulation in the yeast, *Saccharomyces cerevisiae*. *J. Cell Sci.* **66**: 21-38.

Miyakawa, I., Fumoto, S., Kuroiwa, T., Sando, N. (1995) Characterization of DNA-binding proteins involved in the assembly of mitochondrial nucleoids in the yeast *Saccharomyces cerevisiae*. *Plant Cell Physiol.* **36**: 1179-1188.

Miyakawa, I., Sando, N., Kawano, S., Nakamura, S., Kuroiwa, T. (1987) Isolation of morphologically intact mitochondrial nucleoids from the yeast, *Saccharomyces cerevisiae*. *J. Cell Sci.* **88**: 431-439.

Monod, J. (1949) The Growth of Bacterial Cultures. *Ann. Rev. Microbiol.* **3**: 371-394.

Mortimer, R.K., Johnston, J.R. (1959) Life span of individual yeast cells. *Nature* **183**: 1751-1752.

Müller, I., Zimmermann, M., Becker, D., Flömer, M. (1980). Calendar life span versus budding life span of *Saccharomyces cerevisiae*. *Mech. Ageing Dev.* **12**: 47-52.

Newman, S.M., Zelenaya-Troitskaya, O., Perlman, P.S., Butow, R.A. (1996). Analysis of mitochondrial DNA nucleoids in wild-type and a mutant strain of *Saccharomyces cerevisiae* that lacks the mitochondrial HMG box protein Abf2p. *Nucleic Acids Res.* **24**: 386-393.

Nosek, J., Tomaska, L., Bolotin, Fukuhara, M., Miyakawa, I. (2006) Mitochondrial chromosome structure: an insight from analysis of complete yeast genomes. *FEMS Yeast Res.* **6**: 356-370.

Omenn, G.S., Goodman, G.E., Thornquist, M.D., Balmes, J., Cullin, M.R., Glass A. (1996) Risk factors for lung cancer and for intervention effects in CARET, the Beta-Carotene and Retinol Efficacy Trial. *J. Natl. Cancer Inst.* **334**: 1150-1155.

Panzo, C., Nawara, M., Suski, C., Kucharczyka, R., Skoneczny, M., Becam, A.M., Rytka, J., Herbert, C.J. (2002) Aerobic and anaerobic NAD⁺ metabolism in *Saccharomyces cerevisiae*. *FEBS Lett.* **517**: 97-102.

Pathak, S.K., Bhattacharyya, A., Pathak, S., Basak, C., Mandal, D., Kundu, M., Basu, J. (2004) Toll-like receptor 2 and mitogen- and stress-activated kinase 1 are effectors of *Mycobacterium avium*-induced cyclooxygenase-2 expression in macrophages. *J. Biol. Chem.* **279**: 55127-55136.

Piper, P.W. (2006). Long-lived yeast as a model for ageing research. *Yeast* **23**: 215-226.

Polakis, E.S., Bartley, W. (1965) Changes in the enzyme activities of *Saccharomyces cerevisiae* during aerobic growth on different carbon sources. *Biochem. J.* **97**: 284-297.

Pompella, A., Visvikis, A., Paolicchi, A., De Tata, V., Casini, A.F. (2003) The changing faces of glutathione, a cellular protagonist. *Biochem. Pharmacol.* **66**: 1499-1503.

Post, S.G., Binstock, R.H. (2004) *The Fountain of Youth: Culture, Scientific, and Ethical Perspectives on a Biomedical Goal*. Oxford: University Press.

Pronk, J.T., Yde Steensma, H., Van Dijken, J.P. (1996) Pyruvate metabolism in *Saccharomyces cerevisiae*. *Yeast* **12**: 1607-1633.

Raghavendran, V., Gombert, A.K., Christensen, B., Kotter, P., Nielsen, J. (2004) Phenotypic characterization of glucose repression mutants of *Saccharomyces cerevisiae* using experiments with ¹³C-labelled glucose. *Yeast* **21**: 769-779.

Repetto, B., Tzagoloff, A. (1989). Structure and regulation of *KGD1*, the structural gene for yeast alpha-ketoglutarate dehydrogenase. *Mol. Cell. Biol.* **9**: 2695-2705.

Reverter-Branchat, G., Cabisco, E., Tamarit, J., Ros, J. (2004). Oxidative damage to specific proteins in replicative and chronological-aged *Saccharomyces cerevisiae*: common targets and prevention by calorie restriction. *J. Biol. Chem.* **279**: 31983-31989.

Rickwood, D., Chambers, J.A., Barat, M. (1981) Isolation and preliminary characterisation of DNA protein complexes from the mitochondria of *Saccharomyces cerevisiae*. *Exp. Cell. Res.* **133**: 1-13.

Ristow, M., Schmeisser, S. (2011) Extending life span by increasing oxidative stress. *Free Radic. Biol. Med.* **51**: 327-336.

Ristow, M., Zarse, K. (2010) How increased oxidative stress promotes longevity and metabolic health: The concept of mitochondrial hormesis (mitohormesis). *Exp. Gerontol.* **45**: 410-418.

Rodriguez, K.A., Wywial, E., Perez, V.I., Lambert, A.J., Edrey, Y.H., Lewis, K.N., Grimes, K., Lindsey, M.L., Brand M.D., Buffenstein, R. (2011) Walking the Oxidative Stress Tightrope: A Perspective from the Naked Mole-Rat, the Longest Living Rodent. *Curr. Pharm. Des.* [no prelo]

Rolland, F., Winderickx, J., Thevelein, J.M. (2002) Glucose-sensing and -signalling mechanisms in yeast. *FEMS Yeast Res.* **2**: 183-201.

Roth, G. S., Ingram, D. K., Lane, M. A. (1999) Caloric restriction in primates and relevance to humans. *J. Am. Geriatr. Soc.* **47**: 896-903.

Roy, D.J., Dawes, I.W. (1987) Cloning and characterization of the gene encoding lipoamide dehydrogenase in *Saccharomyces cerevisiae*. *J. Gen. Microbiol.* **133**: 925-933.

Saffi, J., Feldmann, H., Winnacker, E.L., Henriques, J.A. (2001) Interaction of the yeast Ps05/Rad16 and Sgs1 proteins: influences on DNA repair and aging. *Mutat. Res.* **486**: 195-206.

Saltzgaber-Muller, J., Kunapuli, S.P., Douglas, M.G. (1983) Nuclear genes coding the yeast mitochondrial adenosine triphosphatase complex. Isolation of *ATP2* coding the F1-ATPase beta subunit. *J. Biol. Chem.* **258**: 11465-11470.

Samokhvalov, V., Ignatov, V., Kondrashova, M. (2004). Inhibition of Krebs cycle and activation of glyoxylate cycle in the course of chronological aging of *Saccharomyces cerevisiae*. Compensatory role of succinate oxidation. *Biochimie* **86**: 39-46.

Sanz, A., Caro, P., Ibanez, J., Gomez, J., Gredilla, R., Barja, G. (2005) Dietary restriction at old age lowers mitochondrial oxygen radical production and leak at complex I and oxidative DNA damage in rat brain. *J. Bioenerg. Biomembr.* **37**: 83-90.

Schrader, M., Fahimi, H.D. (2006) Peroxisomes and oxidative stress. *Biochim Biophys Acta.* **1763**: 1755-1766.

Sesso, H.D., Buring, J.E., Christen, W.G., Kurth, T., Belanger, C., MacFadyen, J., Bubes, V., Manson, J.E., Glynn, R.J., Gaziano, J.M. (2008) Vitamins E and C in the prevention of cardiovascular disease in men: the Physicians' Health Study II randomized controlled trial. *JAMA* **300**: 2123-2133.

Sickmann, A., Reinders, J., Wagner, Y., Joppich, C., Zahedi, R., Meyer, H.E., Schonfisch, B., Perschil, I., Chacinska, A., Guiard, B., Rehling, P., Pfanner, N., Meisinger, C. (2003) The proteome of *Saccharomyces cerevisiae* mitochondria. *Proc. Natl. Acad. Sci. USA* **100**: 13207-13212.

Sidhu, A., Beattie, D.S. (1983). Kinetics of assembly of complex III into the yeast mitochondrial membrane. Evidence for a precursor to the iron-sulfur protein. *J. Biol. Chem.* **258**: 10649-10656.

Siess, E.A., Wieland, O.H. (1976) Phosphorylation state of cytosolic and mitochondrial adenine nucleotides and of pyruvate dehydrogenase in isolated rat liver cells. *Biochem J.* **156**: 91-102.

Sinclair, D., Mills, K., Guarente, L. (1998). Aging in *Saccharomyces cerevisiae*. *Annu. Rev. Microbiol.* **52**: 533-560.

Sinclair, D.A., Guarente, L. (1997) Extrachromosomal rDNA circles--a cause of aging in yeast. *Cell.* **91**: 1033-1042.

Slonimski, P.P., Tzagoloff, A. (1976). Localization in yeast mitochondrial DNA of mutations expressed in a deficiency of cytochrome oxidase and/or coenzyme QH₂-cytochrome c reductase. *Eur. J. Biochem.* **61**: 27-41.

Smith, D.L. Jr, McClure, J.M., Matecic, M., Smith, J.S. (2007). Calorie restriction extends the chronological lifespan of *Saccharomyces cerevisiae* independently of the Sirtuins. *Aging Cell* **6**: 649-662.

Smith, J.S., Boeke, J.D. (1997) An unusual form of transcriptional silencing in yeast ribosomal DNA. *Genes Dev.* **11**: 241–254.

Sohal, R.S. (2002) Role of oxidative stress and protein oxidation in the aging process. *Free Radic. Biol. Med.* **33**: 37-44.

Sohal, R.S., Mockett, R.J., Orr, W.C. (2002) Mechanisms of aging: an appraisal of the oxidative stress hypothesis. *Free Radic. Biol. Med.* **33**: 575-586.

Starkov, A.A., Fiskum, G., Chinopoulos, C., Lorenzo, B.J., Browne, S.E., Patel, M.S., Beal, M.F. (2004) Mitochondrial alpha-ketoglutarate dehydrogenase complex generates reactive oxygen species. *J. Neurosci.* **24**: 7779-7788.

Stephanopoulos, G.N., Aristidou, A.A., Nielsen, J. (1998) *Metabolic engineering principles and methodologies*. London: Academic Press.

Sun, J., Kale, S.P., Childress, A.M., Pinswasdi, C., Jazwinski, S.M. (1994) Divergent roles of *RAS1* and *RAS2* in yeast longevity. *J. Biol. Chem.* **269**: 18638–18645.

Tretter, L., Adam-Vizi, V. (2004) Generation of reactive oxygen species in the reaction catalyzed by alpha-ketoglutarate dehydrogenase. *J. Neurosci.* **24**, 7771-7778.

Turrens, J.F. (2003) Mitochondrial formation of reactive oxygen species. *J. Physiol.* **552**: 335-344.

Tzagoloff, A. (1982) *Mitochondria*, New York: Plenum Press.

Viña, J., Borrás, C., Miquel, J. (2007) Theories of ageing. *IUBMB Life* **59**: 249-254.

Walford, R.L., Harris, S.B., Weindruch, R. (1987) Dietary restriction and aging: historical phases, mechanisms and current directions. *J. Nutr.* **117**: 1650-1654.

Ward, N.C., Wu, J.H., Clarke, M.W., Puddey, I.B., Burke, V., Croft, K.D., Hodgson, J.M. (2007) The effect of vitamin E on blood pressure in individuals with type 2 diabetes: A randomized, double-blind, placebo-controlled trial. *J. Hypertens.* **25**: 227-234.

Weindruch, R., Walford, R.L., (1988). *The retardation of aging and disease by dietary restriction*. CC Thomas, Springfield, IL.

Yotsuyanagi, Y. (1962) Study of yeast mitochondria. I. Variations in mitochondrial ultrastructure during the aerobic growth cycle. *J. Ultrastruct. Res.* **7**: 121–140.

Yu, T., Robotham, J.L., Yoon, Y. (2006) Increased production of reactive oxygen species in hyperglycemic conditions requires dynamic change of mitochondrial morphology. *Proc. Natl. Acad. Sci. USA* **103**: 2653-2658.

Yu, T., Sheu, S.S., Robotham, J.L., Yoon, Y. (2008) Mitochondrial fission mediates high glucose-induced cell death through elevated production of reactive oxygen species. *Cardiovasc. Res.* **79**: 341-351.

Zelenaya-Troitskaya, O., Perlman, P.S., Butow, R.A. (1995). An enzyme in yeast mitochondria that catalyzes a step in branched-chain amino acid biosynthesis also functions in mitochondrial DNA stability. *EMBO J.* **14**: 3268-3276.

Zheng, J., Mutcherson, R. 2nd, Helfand, S.L. (2005) Calorie restriction delays lipid oxidative damage in *Drosophila melanogaster*. *Aging Cell* **4**: 209-216.

Higher Respiratory Activity Decreases Mitochondrial Reactive Oxygen Release and Increases Life Span in *Saccharomyces cerevisiae**

Received for publication, August 4, 2004, and in revised form, September 8, 2004
Published, JBC Papers in Press, September 21, 2004, DOI 10.1074/jbc.M408918200

Mario H. Barros[‡], Brian Bandy[§], Erich B. Tahara[¶], and Alicia J. Kowaltowski^{||}

From the [‡]Departamento de Genética, Instituto de Biociências de Botucatu, Universidade Estadual Paulista, Botucatu, São Paulo 18618–000, Brazil, [§]College of Pharmacy and Nutrition, University of Saskatchewan, Saskatoon, Saskatchewan S7N 5C9, Canada, and the [¶]Departamento de Bioquímica, Instituto de Química, Universidade de São Paulo, São Paulo, 05508–900, Brazil

Increased replicative longevity in *Saccharomyces cerevisiae* because of calorie restriction has been linked to enhanced mitochondrial respiratory activity. Here we have further investigated how mitochondrial respiration affects yeast life span. We found that calorie restriction by growth in low glucose increased respiration but decreased mitochondrial reactive oxygen species production relative to oxygen consumption. Calorie restriction also enhanced chronological life span. The beneficial effects of calorie restriction on mitochondrial respiration, reactive oxygen species release, and replicative and chronological life span could be mimicked by uncoupling agents such as dinitrophenol. Conversely, chronological life span decreased in cells treated with antimycin (which strongly increases mitochondrial reactive oxygen species generation) or in yeast mutants null for mitochondrial superoxide dismutase (which removes superoxide radicals) and for RTG2 (which participates in retrograde feedback signaling between mitochondria and the nucleus). These results suggest that yeast aging is linked to changes in mitochondrial metabolism and oxidative stress and that mild mitochondrial uncoupling can increase both chronological and replicative life span.

The only intervention known to increase average and maximum life span in mammals is caloric restriction (CR),¹ a reduction of 25–60% in calorie intake without essential nutrient deficiency. This diet not only extends life span but also delays many unwanted effects of aging and age-related pathologies. CR is highly effective in a wide range of organisms, increasing life span by up to 50% in some species (reviewed in Refs. 1–3). Unfortunately, the mechanisms through which it results in increased life span are still controversial (see Ref. 4 for a critical review).

A leading hypothesis on the mechanism through which CR

prevents aging is that this process decreases reactive oxygen species (ROS) generation and, hence, the oxidation of cellular components (5–8). Indeed, aging is usually accompanied by oxidative damage of DNA, proteins, and lipids (9, 10). CR promotes a metabolic shift resulting in more efficient electron transport in the mitochondrial respiratory chain (1, 5). Faster and more efficient electron transport may lead to lower production of ROS by mitochondria, one of the major intracellular ROS sources. This occurs because of reduced leakage of electrons from the respiratory chain and/or lower oxygen concentrations in the mitochondrial microenvironment (11, 12). Indeed, artificially increasing mitochondrial respiration using uncouplers such as 2,4-dinitrophenol (DNP) strongly prevents mitochondrial ROS release (11). Furthermore, CR decreases ROS release/O₂ consumed in isolated mammalian mitochondria (13), possibly because of enhanced expression of mitochondrial uncoupling proteins (14, 15). Despite this evidence supporting a correlation between ROS-induced damage and aging, a clear cause-effect relationship has been hard to establish, and conflicting results are often presented in the literature (see Ref. 4 for a critical review).

Saccharomyces cerevisiae has been used as a model system to study mechanisms of life span modulation. Two types of life span may be measured in *S. cerevisiae*: chronological and replicative (10, 16–18). Chronological life span is measured in the stationary growth phase, in which reproduction rates are low. Under these conditions, cells gradually senesce in a manner that may be related to ROS removal capacity (19, 20). However, factors influencing chronological longevity (or aging in non-dividing cells) are expected to be different from those influencing replicative life span, which is defined by the number of generations a yeast cell produces when in logarithmic growth phase (16). Possible shared pathways and differences in these forms of aging have not been thoroughly explored to date, and it is unclear which form of life span relates best to longevity in multicellular organisms.

Relicative life span has been more extensively studied in yeast, and a hypothesis relating CR and changes in life span to altered gene expression has been developed using this model. Guarante and co-workers (21) have shown that replicative life span extension in *S. cerevisiae* can be achieved by decreasing the culture media substrate content, a condition mimicking CR. Yeast replicative life span extension promoted by CR depends on the activity of the *SIR2* gene. *SIR2* codes for a histone deacetylase and prevents the formation of extrachromosomal rDNA circles (ERCs), which accumulate during replicative aging (16, 22). Because Sir2p activity depends on nicotinamide adenine dinucleotide as a substrate, the effect of CR in yeast

* This work was supported by Fundação de Amparo à Pesquisa do Estado de São Paulo, Conselho Nacional de Desenvolvimento Científico e Tecnológico, and the Natural Sciences and Engineering Research Council. The costs of publication of this article were defrayed in part by the payment of page charges. This article must therefore be hereby marked “advertisement” in accordance with 18 U.S.C. Section 1734 solely to indicate this fact.

† To whom correspondence should be addressed: Av. Prof. Lineu Prestes, 748, 05508–900, Cidade Universitária, São Paulo, SP, Brazil. Fax: 55-11-3815-5579; E-mail: alicia@iq.usp.br.

¹ The abbreviations used are: CR, caloric restriction; DNP, 2,4-dinitrophenol; ERC, extrachromosomal rDNA circle; ROS, reactive oxygen species; SOD, superoxide dismutase; YPD, yeast extract/peptone/dextrose medium.

may be related to an increase in the NAD⁺/NADH ratios in restricted cells due to higher respiratory rates (23, 24). Lower glucose levels increase respiration, shifting the preferred fermentation pathway toward oxidative phosphorylation (reviewed in Ref. 4).

Guarente and co-workers (23) found that CR in yeast did not enhance the resistance of these cells to exogenous oxidants, such as paraquat or H₂O₂, or alter the expression of antioxidant enzymes, a finding presented as an indication for the lack of a ROS effect in replicative aging. However, oxidative stress is the result of an imbalance between ROS removal and ROS formation, which was not measured under their conditions. Furthermore, these authors detected increased respiratory rates in CR yeast (23), which may alter mitochondrial ROS release rates, as discussed above. It is thus important to reconsider a possible participation of changes in mitochondrial ROS release levels in the replicative life span effects of CR.

Other aspects that warrant investigation are the comparison of replicative and chronological aging and the effects of factors known to influence replicative life span on chronological life span. CR and *SIR2* have been extensively shown to enhance replicative life span by decreasing ERCs, but their effects on chronological life span have not, to our knowledge, been determined to date. Retrograde feedback between nucleus and mitochondria also plays a role in replicative life span by decreasing ERCs, as indicated by the fact that deletion of *RTG2*, a gene that plays a central role in relaying retrograde response signals, decreases replicative life span (25). However, the effect of *RTG2* on chronological life span is also unknown.

To analyze further the role of mitochondrial activity in yeast longevity, we measured the effects of CR on mitochondrial respiration and ROS release. We also tested the effects of well established regulators of mitochondrial ROS release and genes involved in the regulation of replicative aging on chronological life span, using a recently developed fluorescence technique. Finally, we uncovered links between respiration, ROS release, and aging in yeast by demonstrating that CR and mitochondrial uncoupling can affect both chronological and replicative life span.

EXPERIMENTAL PROCEDURES

Yeast Strains and Media—*S. cerevisiae* W303–1A cells (R. Rothstein, Columbia University, New York, NY) were used in most experiments. EUROFAN BYT4741 wild type strain and strains harboring null mutations of *SIR2*, *SOD2*, and *RTG2*, named here Δ*SIR2*, Δ*SOD2*, and Δ*RTG2*, respectively, were used in Fig. 2, C and D. Cells were cultured at 30 °C with continuous shaking in standard YPD medium (26) containing 0.5 or 2% glucose.

Mitochondrial Isolation—Mitochondria were prepared from yeast strain W303–1A cultures grown in YPD to early stationary phase by the method of Faye *et al.* (27), except for the use of zymolyase 20,000 units/g (ICN) instead of glusulase to convert cells to spheroplasts. Mitochondria isolated in this manner present intact inner membranes and respiratory complexes (28).

Oxygen Consumption—O₂ consumption was followed at 30 °C in isolated mitochondrial suspensions incubated in 0.6 M sorbitol, 20 mM Tris-HCl (pH 7.5), and 0.5 mM EDTA in the presence of 2% ethanol, 0.5 mM malate, and 0.5 mM glutamate, using a computer-interfaced Clark electrode operating in an air-tight chamber with continuous stirring.

Hydrogen Peroxide (H₂O₂) Release—H₂O₂ production was measured as described elsewhere (28) by measuring the oxidation of 50 μM AmplexTM Red (Molecular Probes[®]) in the presence of 1.0 units/ml horseradish peroxidase (Sigma). The incubation media contained 0.6 M sorbitol, 20 mM Tris-HCl (pH 7.5), and 0.5 mM EDTA, using 2% ethanol, 0.5 mM malate, and 0.5 mM glutamate as substrates. The rate of AmplexTM oxidation was recorded at 30 °C using a Hitachi F-4500 fluorescence spectrophotometer equipped with continuous stirring, operating at excitation and emission wavelengths of 563 and 587 nm, respectively.

Yeast Chronological Life Span—Yeast were cultured with continuous shaking for 4 days at 30 °C. Viability was assessed in the stationary phase using the fluorescent FUN[®] 1 (Molecular Probes) probe. This method provides faster and more reliable results than colony counts

(29). Culture quantities were determined by measuring the absorbance at 600 nm. ~2 × 10⁸ cells were added to 1 ml of reaction buffer consisting of 5 μM FUN[®] 1, 2% glucose, and 10 mM HEPES, pH 7.5. FUN[®] 1 determines yeast metabolic activity through fluorimetric analysis. Only metabolically active cells can convert the bright green fluorescent probe into an intravacuolar orange-red compound in a manner independent of fermentation or respiratory metabolism (29). The fluorescent conversion was detected using a Hitachi F-4500 fluorescence spectrophotometer with 470 nm excitation and 535 and 580 nm emission wavelengths. Data are expressed as the difference in 580 and 535 nm emissions over time, in arbitrary fluorescence units.

Yeast Replicative Life Span—Replicative life span measures the number of generations a yeast cell is capable of generating by budding (30) and was determined as described previously (31). Briefly, 1 μl of cells grown logarithmically overnight in liquid YPD or YPD supplemented with 10 nM DNP was plated on YPD and YPD + 10 nM DNP plates. A group of unbudded cells was separated from the rest by micromanipulation (TDM400TM micromanipulator and Nikon Eclipse E400 microscope) and allowed to produce buds. Fifty of these buds were removed and used as the starting mother cell population. The number of daughter cells (generations) for each mother cell was counted by following cell division and separating daughter cells. Cells were grown at 30 °C during the day and at 8 °C overnight. Each experiment involved ~50 mother cells and was carried out three times independently. There was no significant variability among the independent repetitions. Statistical significance of life span differences was determined using a Mann-Whitney Rank sum test.

RESULTS

ROS Release and O₂ Consumption in CR and Control *S. cerevisiae* Mitochondria—Because CR increases mitochondrial respiratory rates (23), we examined the possibility that CR alters ROS production in isolated yeast mitochondria. To do so, we measured the release of H₂O₂, a membrane-permeable ROS, in suspensions of mitochondria isolated from *S. cerevisiae* grown in YPD containing 2 or 0.5% glucose, a condition previously shown to extend replicative life span (21). Interestingly, although oxygen consumption rates tended to be larger in CR mitochondria (Fig. 1A), the release of H₂O₂ was not directly proportional to the oxygen consumption rates measured (panel B). In fact, H₂O₂ release/O₂ consumption ratios in yeasts grown in 2% glucose were significantly higher than those of CR mitochondria (panel C), indicating that CR alters the quantity of H₂O₂ generated per O₂ consumed. As a result, despite the fact that yeasts grown in 0.5% glucose display O₂ consumption rates larger than those observed in 2% glucose (23), their total mitochondrial ROS release may be lower. Indeed, the uncoupler carbonyl cyanide 3-chlorophenylhydrazone, which artificially enhances respiration, decreased H₂O₂ production in *S. cerevisiae* mitochondria by 27% (panel D), as observed previously in animal tissues (11, 12). DNP (5 μM), a structurally unrelated uncoupler, also lowered H₂O₂ release by 25–30% (results not shown), whereas antimycin A, a respiratory inhibitor, strongly enhanced H₂O₂ release (panel D).

Respiration and ROS in Yeast Chronological Life Span—Yeast CR has been shown to increase replicative life span (21), but its effects on chronological life span have not been determined to date. To measure chronological life span, we grew cells in stationary phase and marked them with the fluorescent FUN[®] 1 probe, which is gradually metabolized in aerobic or anaerobic live cells, leading to a fluorescence peak at 580 nm when excited at 470 nm. Metabolically inactive cells do not process the probe and fluoresce at 535 nm. Thus, the difference in 580 and 535 nm fluorescence is proportional to the live/dead cell contents (29).

We observed that cells cultured under CR conditions (0.5% glucose) in stationary phase present a larger proportion of live cells than yeast grown in 2% glucose (Fig. 2A), indicating that CR also increases chronological life span. To verify the effects of respiration and ROS release on chronological life span, we used DNP as a mild uncoupler (to avoid cell death due to excessive

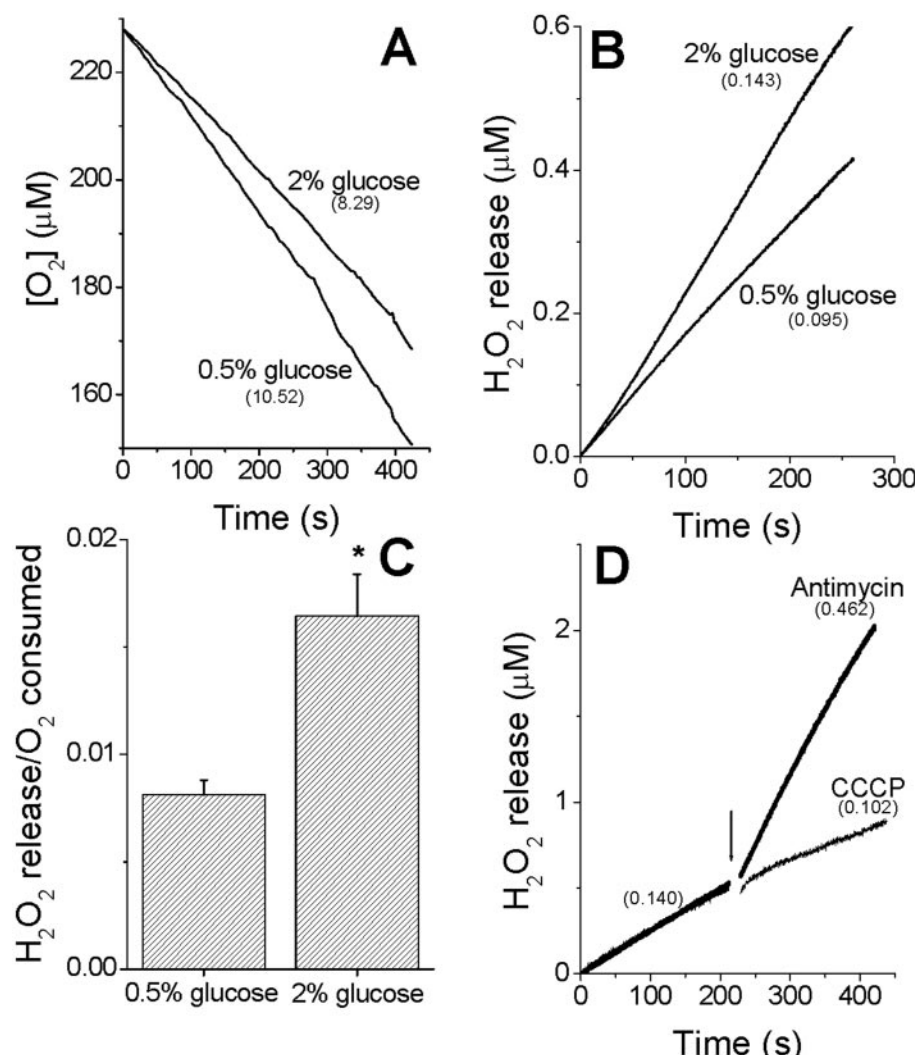


FIG. 1. CR and uncoupling decrease mitochondrial H₂O₂ release/O₂ consumed. Mitochondria were isolated from W303–1A *S. cerevisiae* grown in the presence of 2 or 0.5% glucose as described under “Experimental Procedures.” Respiratory rates (*A*) and H₂O₂ release rates (*B*) were measured in parallel. The average \pm S.E. H₂O₂ detected/O₂ consumed of three separate experiments, such as those in panels *A* and *B*, is depicted in panel *C* (*, $p < 0.01$ relative to 0.5% glucose, pairwise Tukey test). *D*, H₂O₂ release from mitochondria isolated from cells grown in 2% glucose was measured, and 0.5 μM carbonyl cyanide 3-chlorophenylhydrazone or 0.5 μg/ml antimycin A was added where indicated. Numbers in parentheses indicate O₂ consumption and H₂O₂ release rates in μM/min. *A*, *B*, and *D*, representative experiments of at least three similar repetitions.

H⁺ transport) and antimycin A to block respiration (Fig. 2*B*). We found that low doses of DNP (1–10 nM) significantly increase 2% glucose live cell contents, a result indicative of enhanced survival. This effect was not observed in cells grown in 0.5% glucose (results not shown). Higher DNP doses (100 nM, not shown, to 1 mM, Fig. 2*B*) did not affect or slightly decreased stationary phase viability relative to control cells, probably because of perturbed energy metabolism. On the other hand, the respiratory inhibitor antimycin A consistently and strongly increased dead cell contents at every concentration tested (Fig. 2*B* and results not shown). These results are in agreement with the hypothesis that ROS affect yeast viability during the stationary phase (20).

Confirming the idea that mitochondrial ROS determine chronological life span, the null mutant of mitochondrial superoxide dismutase (ΔSOD2), which is incapable of dismutating intra-mitochondrial superoxide radicals to H₂O₂, showed decreased chronological life span relative to its wild type strain BYT4741 (Fig. 2*C*). A *rtg2* mutant, which has been previously shown to present decreased replicative life span (25) due to defective retrograde (mitochondria-nuclear) signaling, also presented decreased chronological life span (Fig. 2*C*). This result indicates

more parallels between chronological and replicative life span in yeast.

However, aspects affecting chronological and replicative life span were not identical. Although the BYT4741 strain also presented increased chronological life span in response to CR, deletion of *SIR2*, which is essential for the beneficial effects of CR in replicative life span (22, 23), did not strongly decrease the effects of CR on chronological life span (Fig. 2*D*).

Mild Uncoupling and Replicative Life Span—Because we found that mild uncoupling reproduces the effects of CR on mitochondrial respiration, H₂O₂ release, and chronological life span, we tested its effect on replicative life span. In three independent experiments involving 50 yeast mother cells each, we found that 10 nM DNP led to a small but reproducible and statistically significant increase of ~15% in replicative life span (see Fig. 3 for a representative experiment). Thus, mild uncoupling mimics CR and increases both chronological and replicative life span.

DISCUSSION

The role of mitochondrial metabolism, respiration, and ROS in life span and the beneficial effects of CR have been the focus

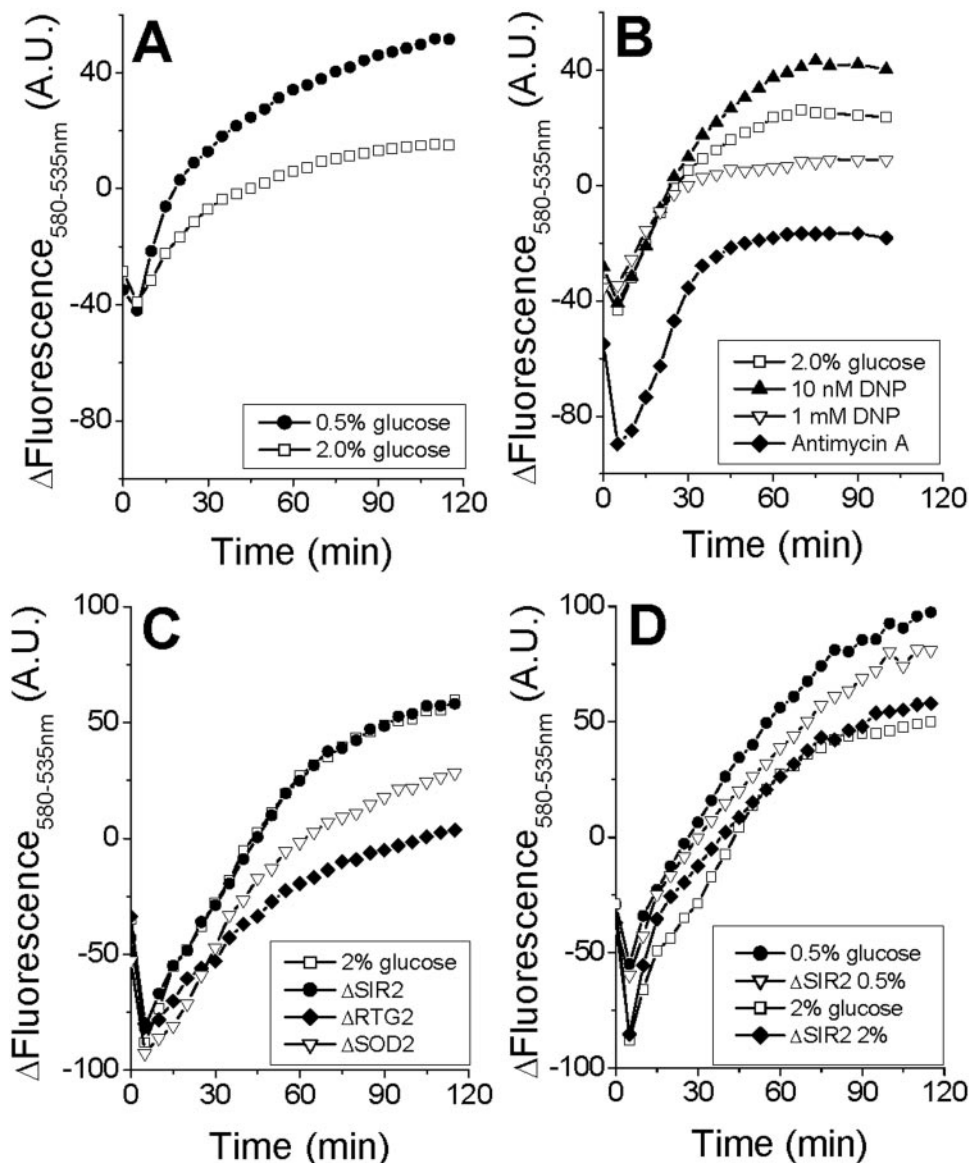


FIG. 2. CR and mild uncoupling enhance chronological life span. The difference between metabolized red-orange FUN® 1 fluorescence (living cells) and bright green fluorescence (dead cells) was measured every 5 min and plotted over time until stable levels were obtained (see “Experimental Procedures”). The initial decrease in values occurs because of FUN® 1 incorporation by the cells, whereas fluorescence differences after stabilization are proportional to live cell counts. *A* and *B*, the fluorescence of W303-1A cells grown for 4 days in 2% glucose (*B*, all traces) or 0.5% glucose, as shown, in the presence of DNP (at the concentrations shown) or 0.1 µg/ml antimycin A where indicated. *C* and *D*, BYT4741 wild type or null mutants of *SIR2*, *SOD2*, and *RTG2* cells were grown for 4 days in 2% (*C*, all traces) or 0.5% glucose as shown. The results presented are representative experiments of at least three similar repetitions.

of many studies. Although most research using animals has found an inverse correlation between levels of mitochondrial ROS and life span (reviewed in Refs. 5–8), a causative effect of ROS-promoted oxidation in limiting life span has been hard to establish because of the inconsistent and/or nonexistent effects of antioxidants (4, 32).

Further questions involving the role of ROS in life span have been uncovered by studies using *S. cerevisiae* as a model for aging and longevity (30). These studies, which focused on replicative life span, show that CR does not enhance the expression of redox-related genes or resistance against oxidative stress (23). Although the authors suggest this evidence excludes a role for ROS in the replicative life span-extending effects of CR, they demonstrate that mitochondrial metabolism and respiration play a role in this process. By intensifying respiration, CR increases intracellular NAD⁺/NADH ratios and the activity of Sir2p, which prevents the accumulation of ERCS and loss of replicative ability in the logarithmic growth stage (24) (see Fig.

4). Recently, the mammalian *SIR2* orthologue, *Sirt1*, has been shown to be up-regulated as a result of CR (33).

In this study, we have attempted to establish a more integrative link between mitochondrial metabolism, ROS, and both chronological and replicative life span. We began by measuring ROS release levels in mitochondria from yeasts grown under control and CR conditions and found that CR significantly decreases ROS release/O₂ consumed (Fig. 1). This finding suggests that even though CR yeast do not present more antioxidant defenses or increased resistance against exogenous oxidants (23), their redox balance is improved by lower levels of mitochondrial ROS release. The effects of CR on ROS release could be mimicked by artificially increasing respiration with uncouplers, whereas respiratory inhibition strongly enhanced ROS release, indicating the CR effect occurs as a result of respiratory stimulation. Yeast growth in 2% glucose represses the synthesis of electron transport chain components (23, 34). As a result, electrons may accumulate at intermediate levels of

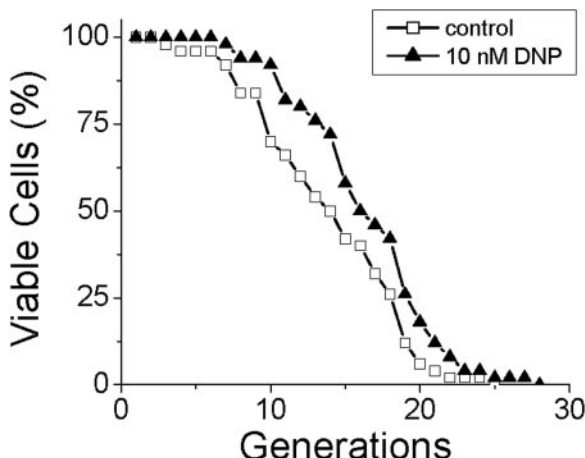


FIG. 3. Mild uncoupling enhances replicative life span. W303-1A cells were incubated overnight in the presence or absence (control cells) of 10 nM DNP and then plated on YPD medium containing 10 nM DNP or with no further additions (*control*). Mother cells were separated by micromanipulation, and the number of generations was counted in each group. The generation average of three experiments for control cells was 13.6 ± 0.20 and 15.6 ± 0.26 for cells treated with 10 nM DNP. The differences in the median values between the two groups are greater than would be expected by chance ($p = 0.016$, Mann-Whitney Rank sum test). The experiment shown is representative of three similar repetitions.

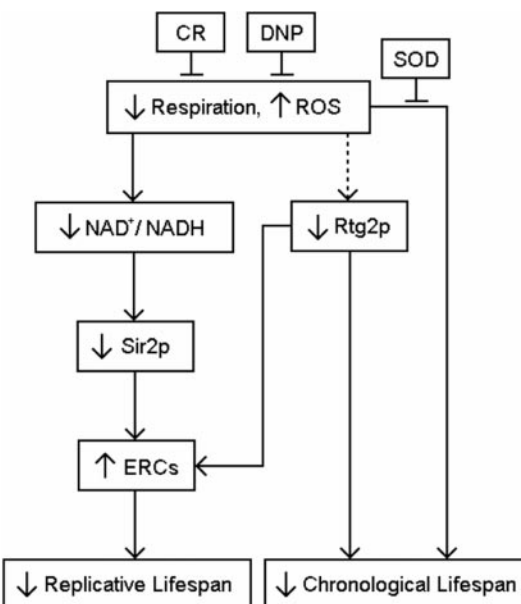


FIG. 4. Schematic representation of the proposed role of mitochondria in yeast life span. Decreased respiratory rates increase NAD⁺/NADH ratios, leading to a lower Sir2p activity and ERC accumulation, which limits replicative life span. In addition, lower respiratory rates increase ROS production, which diminishes chronological life span, in a manner prevented by superoxide dismutase (SOD). Rtg2p deletion decreases chronological life span and increases ERC accumulation leading to reduced replicative life span. CR and mild uncoupling promoted by DNP increase respiration and limit mitochondrial ROS release, enhancing both chronological and replicative life span.

the respiratory chain, favoring electron leakage and ROS formation. In CR yeast, glucose repression of mitochondrial respiration is reduced, stimulating electron transport and preventing ROS formation. In this manner, the effects of CR are similar to those of mild uncoupling that decreases mitochondrial ROS by enhancing respiration and preventing the accumulation of electrons at early steps of the transport chain where they can reduce oxygen monoelectronically, generating superoxide radical anions (11, 12).

To verify whether mild uncoupling was the cause of the beneficial effects of CR, we measured the effects of low concentrations of the uncoupler DNP on life span in *S. cerevisiae*. We initially studied chronological life span, which has been the focus of fewer studies in the area. We found that CR increases chronological life span in two yeast strains (W303-1A and BY4741), indicating that chronological and replicative life spans share some common pathways (Fig. 2). Furthermore, the effects of CR could be mimicked by low doses of DNP, whereas respiratory inhibition decreased cell viability under these conditions, suggesting the CR effect is related to changes in respiration and ROS release promoted by this treatment. Because the deletion of mitochondrial superoxide dismutase also decreased cell viability, it seems chronological life span is limited by mitochondrial ROS production, as suggested previously (17, 20).

Further support for a role of mitochondrial metabolism in the determination of chronological life span was obtained by the finding that *ΔRTG2*, a mutant strain deficient in retrograde signaling, also displays reduced chronological life span. The deletion of this gene has previously been shown to affect replicative life span (25), bringing further support for the existence of some common pathways in these processes (see Fig. 4). However, there are clear differences between the two mechanisms of aging in yeast. The null *sir2* mutant, which still responds to the effects of CR on chronological life span (Fig. 3), represses the effect of CR on replicative life span (23). This result indicates chronological life span is not limited by ERC accumulation, as expected in a non-dividing cell. Further support for this notion was provided by the finding that a null mutant of *PNC1*, which affects NAD⁺/NADH levels and ERC accumulation (35), displayed an increase in chronological life span similar to that observed in wild type cells when incubated under CR conditions (results not shown).

Because mild uncoupling with DNP promoted the same respiratory, ROS, and chronological life span effects as CR, we tested its effects on replicative life span. The finding that DNP leads to an ~15% increase in replicative life span indicates that mild uncoupling efficiently mimics CR (which increases replicative life span by ~24% (21)) and improves life span in both dividing cells and those in stationary phase.

Based on our results, we propose a model which relates the effects of mitochondrial respiration and ROS release with chronological and replicative life span (Fig. 4). The finding that mild uncoupling, like CR, enhances both forms of life span suggests this may be a viable intervention to prevent aging in more complex organisms. Indeed, CR has been shown to promote a decrease in protonmotive force and ROS release in rats (36). Furthermore, individual mice with longer life spans have larger respiratory rates and proton leaks (37), supporting the idea that CR causes mild uncoupling that is responsible for the prevention of aging. Although the use of DNP as an uncoupler has many unwanted toxic effects, mammals contain naturally occurring pathways that lead to mild uncoupling, such as mitochondrial ATP-sensitive K⁺ channels (38) and uncoupling proteins (39, 40). These pathways, when activated, decrease H₂O₂ release/O₂ consumption ratios and could prove useful in further studies designed to establish a link between mild uncoupling and longevity.

Acknowledgments—We thank Camille C. da Silva and Edson A. Gomes for excellent technical assistance and Prof. Sandro R. Valentin (Universidade Estadual Paulista, Araraquara, São Paulo) for the kind donation of yeast strains.

REFERENCES

1. Weindruch, R., Walford, R. L., Fligiel, S., and Guthrie, D. (1986) *J. Nutr.* **116**, 641–654
2. Masoro, E. J. (2000) *Exp. Gerontol.* **35**, 299–305
3. Barger, J. L., Walford, R. L., and Weindruch, R. (2003) *Exp. Gerontol.* **38**, 1343–1351
4. Koubova, J., and Guarente, L. (2003) *Genes Dev.* **17**, 313–321
5. Sohal, R. S., and Weindruch, R. (1996) *Science* **273**, 59–63
6. Merry, B. J. (2004) *Aging Cell* **3**, 7–12
7. Sohal, R. S. (2002) *Free Radic. Biol. Med.* **33**, 37–44
8. Barja, G. (2002) *Ageing Res. Rev.* **1**, 397–411
9. Fraga, C. G., Shigenaga, M. K., Park, J. W., Degan, P., and Ames, B. N. (1990) *Proc. Natl. Acad. Sci. U. S. A.* **87**, 4533–4537
10. Reverter-Branchat, G., Cabiscol, E., Tamarit, J., and Ros, J. (2004) *J. Biol. Chem.* **279**, 31983–31989
11. Korshunov, S. S., Skulachev, V. P., and Starkov, A. A. (1997) *FEBS Lett.* **416**, 15–18
12. Starkov, A. A. (1997) *Biosci. Rep.* **17**, 273–279
13. Gredilla, R., Barja, G., and Lopez-Torres, M. (2001) *J. Bioenerg. Biomembr.* **33**, 279–287
14. Merry, B. J. (2002) *Int. J. Biochem. Cell Biol.* **34**, 1340–1354
15. Bevilacqua, L., Ramsey, J. J., Hagopian, K., Weindruch, R., and Harper, M. E. (2004) *Am. J. Physiol.* **286**, E852–E861
16. Sinclair, D. A., and Guarente, L. (1997) *Cell* **26**, 1033–1042
17. Harris, N., Costa, V., MacLean, M., Mollapour, M., Moradas-Ferreira, P., and Piper, P. W. (2003) *Free Radic. Biol. Med.* **34**, 1599–1606
18. Fabrizio, P., and Longo, V. D. (2003) *Aging Cell* **2**, 73–81
19. Longo, V. D., Gralla, E. B., and Valentine, J. S. (1996) *J. Biol. Chem.* **271**, 12275–12280
20. Longo, V. D., Liou, L. L., Valentine, J. S., and Gralla, E. B. (1999) *Arch. Biochem. Biophys.* **365**, 131–142
21. Lin, S. J., Defossez, P. A., and Guarente, L. (2000) *Science* **289**, 2126–2128
22. Kaeberlein, M., McVey, M., and Guarente, L. (1999) *Genes Dev.* **13**, 2570–2580
23. Lin, S. J., Kaeberlein, M., Andalis, A. A., Sturtz, L. A., Defossez, P. A., Culotta, V. C., Fink, G. R., and Guarente, L. (2002) *Nature* **418**, 344–348
24. Lin, S. J., Ford, E., Haigis, M., Liszt, G., and Guarente, L. (2004) *Genes Dev.* **18**, 12–16
25. Borghouts, C., Benguria, A., Wawryn, J., and Jazwinski, S. M. (2004) *Genetics* **166**, 765–777
26. Myers, A. M., Pape, L. K., and Tzagoloff, A. (1985) *EMBO J.* **4**, 2087–2092
27. Faye, G., Kujawa, C., and Fukuhara, H. (1974) *J. Mol. Biol.* **88**, 185–203
28. Barros, M. H., Netto, L. E. S., and Kowaltowski, A. J. (2003) *Free Radic. Biol. Med.* **35**, 179–188
29. Millard, P. J., Roth, B. L., Thi, H. P., Yue, S. T., and Haugland, R. P. (1997) *Appl. Environ. Microbiol.* **63**, 2897–2905
30. Sinclair, D., Mills, K., and Guarente, L. (1998) *Annu. Rev. Microbiol.* **52**, 533–560
31. Kennedy, B. K., Austriaco, N. R., Jr., and Guarente, L. (1994) *J. Cell Biol.* **127**, 1985–1993
32. Barja, G. (2004) *Biol. Rev. Camb. Philos. Soc.* **79**, 235–251
33. Picard, F., Kurtev, M., Chung, N., Topark-Ngarm, A., Senawong, T., Machado De Oliveira, R., Leid, M., McBurney, M. W., and Guarente, L. (2004) *Nature* **429**, 771–776
34. Schuller, H. J. (2003) *Curr. Genet.* **43**, 139–160
35. Anderson, R. M., Bitterman, K. J., Wood, J. G., Medvedik, O., and Sinclair, D. A. (2003) *Nature* **423**, 181–185
36. Lambert, A. J., and Merry, B. J. (2004) *Am. J. Physiol.* **286**, R71–R79
37. Speakman, J. R., Talbot, D. A., Selman, C., Snart, S., McLaren, J. S., Redman, P., Krol, E., Jackson, D. M., Johnson, M. S., and Brand, M. D. (2004) *Aging Cell* **3**, 87–95
38. Ferranti, R., da Silva, M. M., and Kowaltowski, A. J. (2003) *FEBS Lett.* **536**, 51–55
39. Negre-Salvayre, A., Hirtz, C., Carrera, G., Cazenave, R., Troly, M., Salvayre, R., Penicaud, L., and Casteilla, L. (1997) *FASEB J.* **11**, 809–815
40. Talbot, D. A., Lambert, A. J., and Brand, M. D. (2004) *FEBS Lett.* **556**, 111–115

Dihydrolipoyl dehydrogenase as a source of reactive oxygen species inhibited by caloric restriction and involved in *Saccharomyces cerevisiae* aging

Erich B. Tahara,* Mario H. Barros,^{†,‡} Graciele A. Oliveira,* Luis E. S. Netto,[§] and Alicia J. Kowaltowski*,¹

*Departamento de Bioquímica, Instituto de Química, Universidade de São Paulo, São Paulo, SP, Brazil; [†]Departamento de Genética, Instituto de Biociências, Universidade Estadual Paulista, Botucatu, SP, Brazil; [‡]Departamento de Microbiologia, Instituto de Ciências Biomédicas, Universidade de São Paulo, São Paulo, SP, Brazil; and [§]Departamento de Biologia, Instituto de Biociências, Universidade de São Paulo, São Paulo, SP, Brazil

ABSTRACT Replicative life span in *Saccharomyces cerevisiae* is increased by glucose (Glc) limitation [calorie restriction (CR)] and by augmented NAD⁺. Increased survival promoted by CR was attributed previously to the NAD⁺-dependent histone deacetylase activity of sirtuin family protein Sir2p but not to changes in redox state. Here we show that strains defective in NAD⁺ synthesis and salvage pathways (*pnc1Δ*, *npt1Δ*, and *bna6Δ*) exhibit decreased oxygen consumption and increased mitochondrial H₂O₂ release, reversed over time by CR. These null mutant strains also present decreased chronological longevity in a manner rescued by CR. Furthermore, we observed that changes in mitochondrial H₂O₂ release alter cellular redox state, as attested by measurements of total, oxidized, and reduced glutathione. Surprisingly, our results indicate that matrix-soluble dihydrolipoyl-dehydrogenases are an important source of CR-preventable mitochondrial reactive oxygen species (ROS). Indeed, deletion of the *LPD1* gene prevented oxidative stress in *npt1Δ* and *bna6Δ* mutants. Furthermore, pyruvate and α-ketoglutarate, substrates for dihydrolipoyl dehydrogenase-containing enzymes, promoted pronounced reactive oxygen release in permeabilized wild-type mitochondria. Altogether, these results substantiate the concept that mitochondrial ROS can be limited by caloric restriction and play an important role in *S. cerevisiae* senescence. Furthermore, these findings uncover dihydrolipoyl dehydrogenase as an important and novel source of ROS leading to life span limitation.—Tahara, E. B., Barros, M. H., Oliveira, G. A., Netto, L. E. S., Kowaltowski, A. J. Dihydrolipoyl dehydrogenase as a source of reactive oxygen species inhibited by caloric restriction and involved in *Saccharomyces cerevisiae* aging. *FASEB J.* 21, 274–283 (2007)

Key Words: free radicals • yeast • senescence • α-ketoglutarate dehydrogenase

MCCAY ET AL. (1) ORIGINALLY OBSERVED that rodents submitted to low-calorie diets [calorie restriction (CR)]

had increased life spans compared to animals fed *ad libitum*. Their results were later reproduced in a wide range of multicellular organisms, including rotifers, arachnids, worms, fish, mice, rats, and primates (for reviews, see refs. 2, 3). Although increases in life span through CR certainly occur due to multiple alterations in metabolic regulation and gene expression, a common finding is that the generation of free radicals and other ROS by mitochondria from CR animals is decreased (4–6). Concomitantly, many groups have found that increases in levels of oxidative stress markers during aging are prevented by CR (7, 8). These findings support the idea that CR prevents mitochondrial ROS formation and the accumulation of oxidative cellular modifications that lead to cell damage during aging.

Mitochondria are the main source of ROS in most cells due to multiple one-electron transfer reactions. Within the electron transport chain, a small quantity of the electrons transported is sidetracked to oxygen at intermediate points such as Complexes I and III, generating superoxide radical anions, which are transformed into mitochondrial H₂O₂ and other ROS (9–13). In addition to the electron transport chain, recent work has indicated that ROS may also be generated by matrix-soluble enzymes such as pyruvate and α-ketoglutarate dehydrogenases (14, 15). Each mitochondrial ROS source responds differently to substrates, changes in energy metabolism, and O₂ tensions (10). As a result, mitochondrial ROS generation varies widely with metabolic conditions and the effects of CR on redox state are still not fully understood (4, 11).

Saccharomyces cerevisiae has been used as a model to study the effects of CR, with the advantage of exhibiting short life spans and allowing simplified metabolic and

¹ Correspondence: Lineu Prestes, 748, Departamento de Bioquímica, Instituto de Química, Universidade de São Paulo, SP, 05508–900, Brazil. E-mail: alicia@iq.usp.br
doi: 10.1096/fj.06-6686com

genetic manipulation. Two forms of aging are typically measured in *S. cerevisiae*: replicative and chronological (16–18). Replicative life span measures the number of generations produced by a single mother cell. This measurement is the most common form of life span determination in yeast (19–21). On the other hand, chronological life span measures cell survival during the stationary growth phase, in which budding rates are low (18). The correlation between these forms of yeast life span and aging in multicellular animals has yet to be determined, but it has been suggested that chronological life span may resemble survival in nondividing cells, while replicative life span mimics aging in dividing tissues (18).

Most studies in yeast have focused on genes that regulate replicative life span such as *SIR2*, which causes increased life span when overexpressed and decreased longevity when deleted (see ref. 22 for review). *SIR2* encodes Sir2p, a highly conserved NAD⁺-dependent histone deacetylase involved in telomeric and rDNA silencing (19, 23), repressing the generation of toxic extrachromosomal ribosomal DNA circles (21). Lin *et al.* (20) and Jiang *et al.* (24) demonstrated that CR, promoted by decreasing the concentration of Glc or amino acids in growth media, extends *S. cerevisiae* replicative longevity, in a Sir2p-sensitive manner. Enhanced respiratory rates promoted by CR (21) result in higher NAD⁺/NADH ratios (25), which may activate Sir2p and augment replicative life span. On the other hand, Anderson *et al.* (26) have proposed that CR also up-regulates Pnc1p, an enzyme in the NAD⁺ salvage pathway, reducing nicotinamide levels and consequently increasing Sir2p activity (22). Independently of the proposed mechanism, it seems clear that NAD metabolism plays a central role in the control of replicative life span by CR.

In addition to increasing replicative life span, we found that CR-promoted respiratory increments in yeast enhance chronological longevity in a manner independent of Sir2p (27). Indeed, artificial increments in respiratory rates using mitochondrial uncouplers improve both replicative and chronological life span (27). Furthermore, survival in the stationary phase is decreased when cellular antioxidants such as superoxide dismutase (SOD) are absent (27–29), suggesting links between CR, mitochondrial respiratory rates, redox balance, and chronological longevity similar to those observed in multicellular animals. Unfortunately, further mechanisms regulating chronological longevity remain to be uncovered, since studies involving this form of life span are fewer than those relating to replicative longevity. However, the finding that CR and changes in respiratory rates lead to increments in both replicative and chronological life span indicates that mitochondrial metabolism is a central regulatory point for both forms of aging in yeast (30).

Here, we further investigate the link between respiration and yeast life span, focusing on redox balance. We found that CR enhances O₂ consumption and concomitantly prevents mitochondrial ROS formation

and glutathione oxidation. Indeed, a strong inverse correlation between respiratory rates and ROS release was observed. We also found that decreased NAD⁺ synthesis inhibits respiration, enhances mitochondrial ROS release, and decreases chronological life span. Surprisingly, our results suggest that the main CR-sensitive ROS source was not the electron transport chain but matrix dihydrolipoyl dehydrogenases. This finding implicates a new mitochondrial ROS source in cellular life span limitation.

MATERIALS AND METHODS

Culture media and yeast strains

Yeast were cultured with continuous shaking at 220 rpm, 30°C, in liquid YPD (1% yeast extract, 2% peptone, and 2.0% or 0.5% Glc). Cells were inoculated (10⁵/ml) and grown for 16 or 64 h to reach early and late stationary growth phases, respectively, as confirmed by growth curves (results not shown). Under these conditions, Glc levels in the culture media were undetectable by HPLC analysis after 24 h for both 2.0 and 0.5% Glc cultures. Strains used were wild-type BY4741 and BY4742 and single null mutants of BY4741: *sir2Δ*, *pnc1Δ*, *npt1Δ*, *bna6Δ*, and *lpd1Δ* obtained from the EUROFAN collection (<http://web.uni-frankfurt.de/fb15/mikro/euroscarf/index.html>). Double mutants *bna6Δlpd1Δ* and *npt1Δlpd1Δ* were, respectively, generated by crossing null allele mutants of *BNA6* and *NPT1* with a *LPD1* mutant of opposite mating type. The resultant diploids were sporulated. After tetrad analysis, the double mutants were selected from true tetrads with 2:2 segregation for geneticin resistance. Single and double mutations were confirmed by polymerase chain reaction (PCR) using the following primers located in the promoter region of the respective gene: *BNA6F* 5'-GGTACAAGCTTGGTTACAAAC, *NPT1F* 5'-GCCCTGAAAAGCTTATAAAG, *LPD1F* 5'-GGCAAGCTTC-GATTGTCTCTGTCG, with the reversed primer present in the *kanMX* disruption cassette: *kanB* 5'-CTGCAGCGAGGAGCCG-TAAT.

Spheroplast generation

S. cerevisiae spheroplasts were obtained through yeast cell wall digestion (31) for 45 min at 37°C with 20 U zymolyase/g cells in 1.2 M sorbitol, 10 mM MgCl₂, and 50 mM Tris, pH 7.5, after 15 min pretreatment with 30 mM dithiotreitol at room temperature. The resultant spheroplasts were washed twice with 1.2 M sorbitol, 10 mM MgCl₂, and 50 mM Tris, pH 7.5, at 4°C and resuspended to a final concentration of 5 mg protein/ml in 75 mM phosphate buffer, pH 7.5 (KOH), with 1.2 M sorbitol and 1 mM EDTA. Protein was quantified using the Lowry method.

Mitochondrial isolation and permeabilization

Mitochondria from yeast strains grown in 2% Glc YPD were isolated as described elsewhere (27). One-hundred micrograms of the resulting mitochondria were incubated at room temperature in 2 ml reaction media (0.6 M sorbitol, 32.5 mM phosphate, 10 mM Tris, and 1 mM EDTA, pH 7.5, KOH) supplemented with 5 µg alamethicin for permeabilization. Samples were then washed and resuspended in the media described in Fig. 1.

O₂ consumption assay

O₂ consumption was monitored over time using a computer-interfaced Clark electrode operating at 30°C with continuous stirring. Spheroplasts were suspended at 800 µg/ml in 75 mM phosphate, 1.2 M sorbitol, and 1 mM EDTA, pH 7.5 (KOH) in the presence of 2% ethanol and 1 mM buffered malate/glutamate. Digitonin (0.004–0.006%) was added as necessary to promote plasma membrane permeabilization, maintaining mitochondrial integrity (31).

H₂O₂ production assay

H₂O₂ production was monitored by following resorufin fluorescence (27) in 100 µg/ml spheroplasts suspended in 75 mM phosphate, 1.2 M sorbitol, 1 mM EDTA, 50 µM Amplex Red, 0.5 U/ml horseradish peroxidase (HRP), 2% ethanol, and 1 mM malate/glutamate, pH 7.5 (KOH), using a Hitachi F-4500 fluorescence spectrophotometer operating at 563 nm excitation and 587 nm emission, with continuous stirring, at 30°C. Digitonin (0.002–0.003%) was added as necessary to promote spheroplast permeabilization (31). Permeabilized mitochondria were assayed at 50 µg/ml in media described in Results, supplemented with Amplex Red and HRP.

Glutathione assays

Oxidized glutathione (GSSG), reduced glutathione (GSH), and total glutathione were determined in the late stationary phase using a DTNB colorimetric assay, as described by Monteiro et al. (32). Values are expressed as glutathione content per gram cells.

Resistance to H₂O₂

Yeasts were cultured in YPD containing 2.0 or 0.5% Glc for 16 h. Culture quantities were determined by measuring the absorbance at 600 nm. Cells were then plated on solid minimum media (0.67% yeast nitrogen based media supplemented with amino acids and 2.0% Glc) in the presence or absence of H₂O₂. Spots were compared and photographed after 36–40 h growth at 30°C.

Chronological life span determinations

Chronological life span can be defined as the measure of survival in the stationary phase (18). Survival was measured in two distinct manners: metabolic integrity determinations or the ability to metabolize the FUN 1 probe (Molecular Probes, 33), and reproductive integrity or the ability to form colonies when plated in solid media.

FUN 1 determinations were performed as described by Barros et al. (27). This probe marks metabolically active vs. inactive cells, which fluoresce at 580 and 535 nm, respectively, when excited at 470 nm; 2 · 10⁸ cells were added to 1.5 ml of reaction buffer consisting of 5 µM FUN 1, 2.0% Glc, and 10 mM HEPES, pH 7.5 (NaOH). Fluorescence differences were monitored until stable using a Hitachi F-4500 fluorescence spectrophotometer. FUN 1 metabolism occurs both in aerobic and nonaerobic cells (33) and has been previously shown to correlate with colony-forming ability (34). It should be noted that FUN 1 fluorescence changes allow for qualitative, not quantitative, metabolic activity determinations.

Reproductive survival was quantitatively measured by plating 100 stationary phase cells (as determined by absorbance at 600 nm after being washed in distilled water) in individual

solid YPD plates. Colonies were counted in each plate after 36 h growth at 30°C.

Statistical analysis

Data are averages ± SE of at least three repetitions using distinct preparations or representative results of at least three similar repetitions. Statistical analysis and comparisons were performed using unpaired Student's t tests conducted by GraphPad Prism software.

RESULTS

CR decreases ROS release from mitochondria

Lin et al. (21) demonstrated that increments in cellular oxygen consumption are necessary for replicative life span extension promoted by CR in yeast. In support for this finding, we observed that artificially enhancing mitochondrial respiration improves both replicative and chronological longevity (27). To study the respiratory effects of CR and directly relate them to possible changes in mitochondrial ROS release, we measured O₂ consumption and H₂O₂ generation in mitochondria within permeabilized *S. cerevisiae* spheroplasts, both in early (16 h) and late (64 h) stationary growth phases. In the early stationary phase (Fig. 1A), mitochondria within cells grown in 0.5% Glc (CR, empty bars) exhibit significantly higher respiratory rates when compared to 2.0% Glc (control, full bars), a result that confirms measurements conducted in intact cells (21) and isolated mitochondria (27). High Glc levels are well known to inhibit respiration in *S. cerevisiae* through Glc repression (35), which may account for the changes in respiratory rates observed in the early stationary growth phase. Interestingly, although Glc levels were undetectable after 24 h under both culture conditions (results not shown), O₂ consumption by mitochondria grown under control conditions decreased significantly when cells reached the late stationary phase, while CR cells maintained high O₂ consumption over time.

Parallel H₂O₂ release measurements indicated that cells grown in 2.0% Glc maintained similar H₂O₂ release rates over 3 days growth, whereas lower levels of H₂O₂ (Fig. 1B) and H₂O₂/O₂ (Fig. 1C) were detected in CR cells after a similar interval. These results indicate that the cumulative release of ROS from CR mitochondria over 64 h in culture is lower than that of control cells.

Defective NAD⁺ synthesis or salvage results in CR-sensitive decrease in O₂ consumption

CR increases NAD⁺/NADH ratios, a determinant effect in yeast replicative longevity linked to changes in O₂ consumption (20, 21, 25). To verify the importance of NAD⁺/NADH in mitochondrial respiratory and redox metabolism, we tested strains with altered NAD⁺ synthesis. *PNC1* encodes a nicotinamidase for the NAD⁺ salvage pathway that, when absent, decreases intracellular

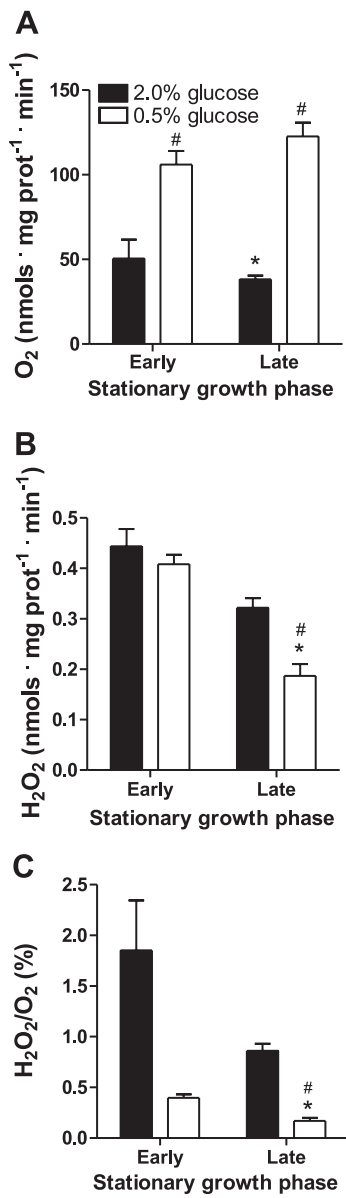


Figure 1. CR enhances O₂ consumption (A) and prevents H₂O₂ release (B, C). O₂ consumption and H₂O₂ release by spheroplasts prepared from WT cells grown under control (2.0% Glc, full bars) or CR (0.5% Glc, empty bars) conditions were measured in parallel, in early and late stationary growth phases, as described in Materials and Methods. *P < 0.05 vs. early stationary phase; #P < 0.05 vs. 2.0% Glc.

lular NAD⁺ and, consequently, replicative life span (26). *NPT1* encodes nicotinate phosphoribosyl transferase, necessary for *de novo* NAD⁺ synthesis from nicotinate. Deletions of this gene also promote reduced intracellular NAD levels in *S. cerevisiae* and prevent life span extension mediated by CR (20, 26, 36). We found that *npt1* Δ and *pnc1* Δ strains in the early stationary phase presented diminished respiratory rates relative to WT strains grown in 2.0% Glc (Fig. 2A, full bars). Confirming that this decreased respiration is related to the lack of NAD⁺ synthesis, similar results were observed in cells devoid of Bna6p, an enzyme responsible for NAD⁺ synthesis from tryptophan-derived quinolinic

acid (36). On the other hand, *sir2* mutants behaved similarly to WT strains, indicating that the respiratory effect is related to defects in NAD⁺ synthesis and salvage but not use.

In the late stationary phase (Fig. 2B), respiratory rates of *pnc1* Δ , *npt1* Δ , and *bna6* Δ cells were more similar to WT strains than in the early phase, although still significantly lower in *npt1* Δ and *bna6* Δ strains. Interestingly, oxygen consumption by *pnc1* Δ , *npt1* Δ , and *bna6* Δ cells was considerably increased by CR (empty bars), resulting in complete respiratory rate recovery in the late stationary phase. Presumably, the alternative NAD⁺-generating pathway is up-regulated over time, in a manner stimulated by CR.

ROS release and O₂ consumption are inversely correlated

In all cells and growth conditions studied, lower O₂ consumption promoted by lack of NAD or high Glc growth conditions was accompanied by higher H₂O₂ release (Fig. 2C–F). Indeed, a strong inverse correlation between respiratory rates and H₂O₂ release was observed in early (Fig. 2G, $r^2=0.73$, $P=0.02$) and late stationary phase cells (Fig. 2H, $r^2=0.79$, $P<0.001$). In the early stationary phase (Fig. 2E,G), WT and *sir2* Δ cells grown in 0.5% Glc had the lowest H₂O₂/O₂ relationships. WT and *sir2* Δ cells grown in 2.0% Glc and *pnc1* Δ , *npt1* Δ , and *bna6* Δ cells grown in 0.5% Glc formed an intermediate group. Finally, *pnc1* Δ , *npt1* Δ , and *bna6* Δ cells grown in 2.0% Glc presented the highest H₂O₂/O₂ relationships. In the late stationary phase (Fig. 2F,H), a clear separation between CR and control growth conditions was observed, demonstrating that CR cells present very significant increments in respiration concomitantly to decreased ROS formation. As a result, cumulative ROS formation is lowest in CR cells with no lack of NAD, intermediate in control cells with unaffected NAD⁺ synthesis or CR cells with defective NAD⁺ synthesis/salvage, and highest in cells with defective NAD⁺ synthesis/salvage incubated in 2.0% Glc.

CR prevents cellular oxidative stress

Further evidence supporting the concept that CR and respiratory increments prevent oxidative stress was provided by glutathione measurements. We found that CR decreased oxidized glutathione (GSSG) levels (Fig. 3A) and improved GSSG/GSH ratios (Fig. 3C) in all strains. *npt1* Δ and *bna6* Δ cells presented significantly higher amounts of GSSG and total glutathione levels (Fig. 3B), a result typical of chronic oxidative stress, which stimulates glutathione synthesis (37). Thus, increased mitochondrial H₂O₂ release levels measured in Fig. 2 correlate closely with changes in intracellular redox potential.

The ability to grow in the presence of exogenously added H₂O₂, a reflection of levels of major peroxide-removing systems, was also tested for the different cell

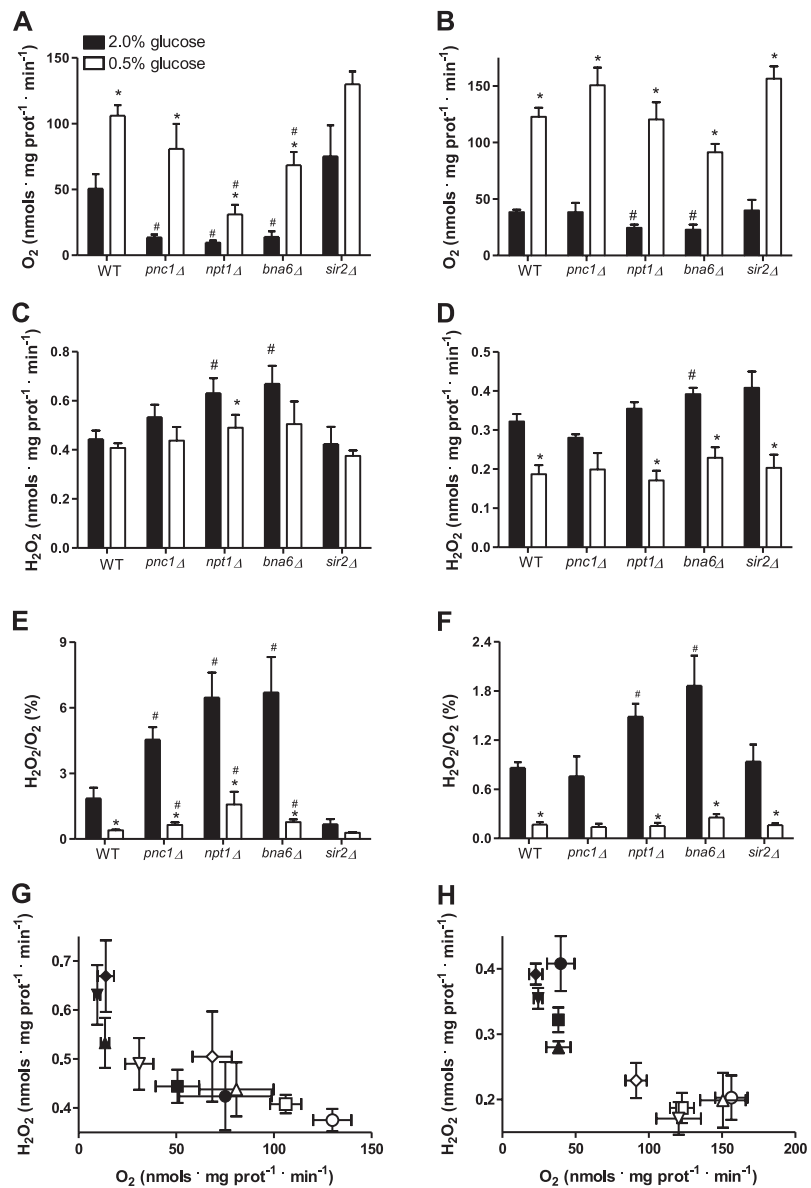


Figure 2. O_2 consumption (A, B, E, F) and H_2O_2 release (C–F) are inversely correlated (G, H). O_2 consumption and H_2O_2 release by spheroplasts prepared from WT (■), *sir2Δ* (●), *pnc1Δ* (▲), *npt1Δ* (▼), and *bna6Δ* (◆) cells grown under control (full bars/symbols) or CR (empty bars/symbols) conditions were measured in parallel, in early (A, C, E, G) and late stationary (B, D, F, H) growth phases, as described in Materials and Methods. * $P < 0.05$ vs. 2.0% Glc; # $P < 0.05$ vs. WT.

types and growth conditions (Fig. 4). CR did not significantly alter the ability to grow in media supplemented with H_2O_2 , a result supported by the finding that CR does not alter the expression of antioxidants in WT cells (21). The *npt1Δ* cells, but not the other mutants tested, presented a marked decrease in resistance to 0.6 mM exogenous H_2O_2 . Even at higher H_2O_2 concentrations (0.9 mM), all other cell types and growth conditions presented similar sensitivity, indicating that other mutations and CR do not change cellular resistance to H_2O_2 .

CR improves chronological longevity

To verify if the changes in ROS release observed over time in the mutants tested affect life span, we measured chronological life span in WT (Fig. 5) vs. *npt1Δ* cells grown in 2.0 vs. 0.5% Glc. *npt1Δ* cells were chosen due

to their known limitation in replicative life span (20), high H_2O_2 release rates, high exogenous H_2O_2 sensitivity, increased GSSG, and efficient response to CR. In Fig. 5, metabolic integrity in the late stationary phase was qualitatively measured using the FUN 1 probe (27), which is metabolized over time in live cells to a product fluorescent at 580 nm (33). We found that *npt1* deletion limited FUN 1 metabolism in a manner partially reversed by CR. This indicates that oxidative stress in *npt1Δ* strains and the beneficial effects of CR on ROS release observed previously (Fig. 2) are reflected as decreased and improved metabolic integrity, respectively. In addition to measurements using FUN 1, we also determined the ability to resume cellular division once cells are removed from stationary phase growth conditions (Fig. 5B), a quantitative measurement of replicative integrity. The number of colonies generated by *npt1Δ* strains was lower than WT, in a manner

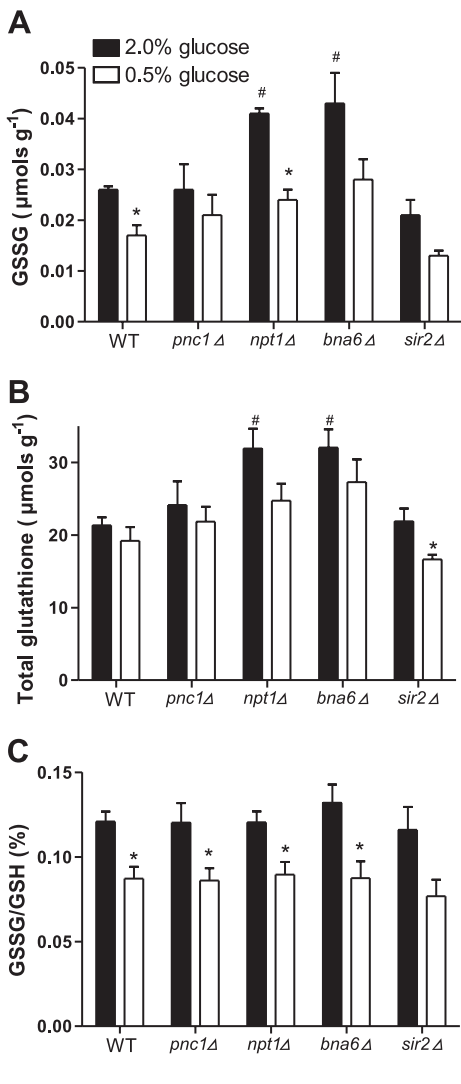


Figure 3. CR and enhanced respiration prevent cellular glutathione oxidation. Total (B), oxidized (GSSG; A) and reduced (GSH; C) glutathione per gram cell weight were measured as described in Materials and Methods section in late stationary phase WT or mutant strains grown under control (full bars) or CR (empty bars) conditions. *P < 0.05 vs. 2.0% Glc; #P < 0.05 vs. WT.

rescued by CR. Similar results, both using FUN 1 and colony counts, were observed with *bna6*Δ cells (results not shown). Thus, we found that decreased chronological life span correlates with lower respiratory rates and higher H₂O₂ release in these strains.

Matrix-soluble dehydrogenases are an important source of CR-sensitive ROS release

Our data demonstrate that mitochondrial respiration and NAD⁺ levels are critical for chronological longevity, in addition to their already known effects on replicative longevity (25). Our data also show that respiration and NAD⁺ content strongly affect redox balance. However, the increased mitochondrial H₂O₂ production exhibited by *bna6*Δ, *pnc1*Δ, and *npt1*Δ strains is probably not a result of enhanced electron

leakage from the mitochondrial electron transport chain, since levels and turnover of NADH (which provides these electrons) are lower. This observation suggests that electron leakage occurring upstream of the respiratory chain contributes toward CR-sensitive mitochondrial ROS production.

Recent work using mammalian tissue (14, 15) demonstrated that matrix-soluble dihydrolipoyl-containing dehydrogenases (pyruvate and, mainly, α-ketoglutarate dehydrogenase) can also generate ROS, in a manner stimulated by low NAD⁺ availability. To investigate if these dehydrogenases were the source of ROS under our conditions, we measured O₂ consumption and H₂O₂ release in a strain harboring a null allele of *lpd1*, which does not display dihydrolipoyl dehydrogenase activity (38). As expected, *lpd1*Δ mitochondria present low O₂ consumption rates (9.82 ± 0.54 O₂ mg protein⁻¹·min⁻¹, in the early stationary growth phase), comparable to *npt1*Δ and *bna6*Δ mutants (see Fig. 2A). However, low respiratory rates in these mutants are not accompanied by increased H₂O₂ release relative to WT strains (Fig. 6). Furthermore, we generated *lpd1*Δ*npt1*Δ and *lpd1*Δ*bna6*Δ double mutants and verified that the *lpd1* null allele is epistatic over *bna6* and *npt1* null alleles, reverting increments in H₂O₂ release observed in the single deletions (Fig. 6). This indicates that ROS release enhanced by lack of NAD synthesis occurs primarily at the level of dihydrolipoyl-containing dehydrogenases.

To investigate if dihydrolipoyl dehydrogenases were also important ROS sources in WT cells, we compared ROS release rates in WT mitochondria using different substrates. In intact mitochondria, the limited matrix space allows products of enzymatic reactions to accumulate and act as substrates for other enzymes, so individual contributions of each reaction toward ROS

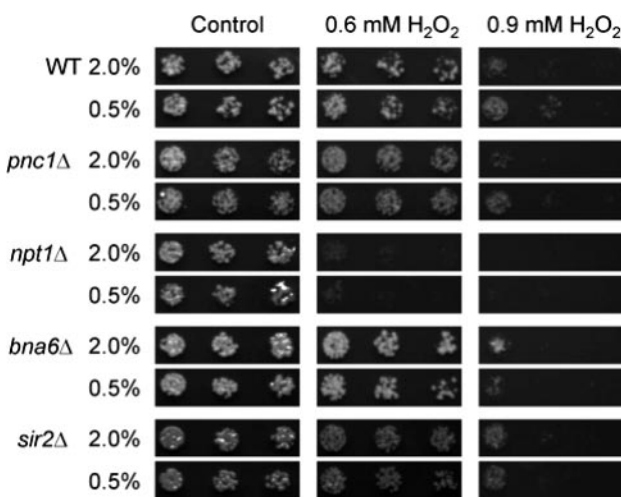


Figure 4. *npt1* deletion results in reduced resistance to exogenous H₂O₂. WT and mutant strains were grown in 2.0 or 0.5% Glc-containing liquid media. After 16 h, $2 \cdot 10^6$, $4 \cdot 10^5$, and $8 \cdot 10^4$ cells were plated sequentially (from left to right) on solid minimum media in the presence or absence of 0.6 or 0.9 mM H₂O₂, as shown. Plate growth was photographed after 36–40 h growth at 30°C.

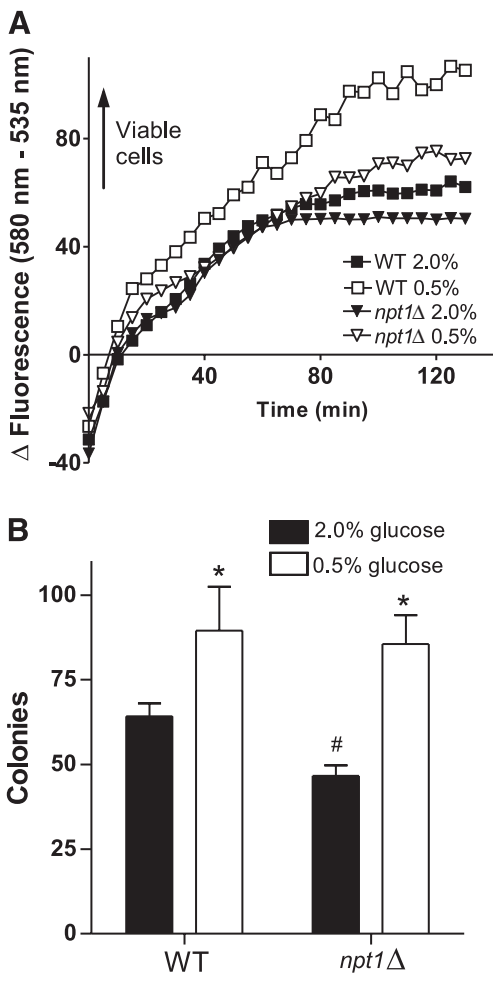


Figure 5. CR-sensitive decrease in chronological life span in *npt1Δ* cells. Cell viability after 4 days in culture in 2.0% (full symbols/bars) or 0.5% Glc (empty symbols/bars) was assessed in WT (■) and *npt1Δ* (▼) cells, using the FUN 1 probe to measure metabolic integrity (A) or by measuring colony-forming ability (B), as described in Materials and Methods. **P* < 0.05 vs. 2.0% Glc; #*P* < 0.05 vs. WT.

generation cannot be determined. To circumvent this situation, we measured ROS release in mitochondria in which membranes were permeabilized by the pore-forming compound alamethicin, which allows for free substrate passage, but does not release mitochondrial matrix enzymes (14). The use of different substrates under these conditions allows for the comparison of ROS release rates by individual mitochondrial sources, since the products of enzymatic reactions are largely diluted.

We found (Fig. 7) that the addition of α -ketoglutarate and pyruvate (substrates for dihydrolipoyl dehydrogenase-containing enzymes) but not malate to WT permeabilized mitochondria resulted in substantial ROS formation. In *lpd1Δ* cells, no H_2O_2 release was measured after the addition of these substrates, indicating that the release was, indeed, dependent on the activity of Lpd1p. Succinate was added to compare ROS formation by these matrix-soluble dehydrogenases with respiratory chain ROS release, since NADH cannot be

added due to interference with all horseradish peroxidase-based measurements. In mammals, succinate leads to large quantities of ROS formation in most tissues, since it can feed electrons to coenzyme Q in Complex III and (by reverse electron transport) to Complex I, where superoxide formation occurs (10). Surprisingly, under our conditions electron leakage promoted by succinate at the respiratory chain was substantial but still slightly lower than that observed with α -ketoglutarate. These results confirm that although the electron transport chain generates ROS, ROS generated by dihydrolipoyl dehydrogenase-containing enzymes α -ketoglutarate and pyruvate dehydrogenase are the main source of these species in WT cells.

DISCUSSION

Aging studies in *S. cerevisiae* have uncovered a complex control system for replicative life span involving suppression by Sir2p family proteins of toxic ribosomal DNA circle accumulation in dividing cells (for review, see 22). CR alters replicative life span by regulating Sir2p activity in a manner dependent on fluctuations in $NAD^+/NADH$ levels promoted by changes in respiratory rates (20, 21, 25).

However, Sir2p family proteins are not the only determinants of *S. cerevisiae* life span. Some groups (23, 39) have found that CR increases replicative life span even in *sir2Δ* cells. Furthermore, although *S. cerevisiae* CR enhances both replicative and chronological longevity, *sir2* mutations do not decrease chronological life span (27, 40). Interestingly, chronological life span, but apparently not replicative, is limited by mitochondrial oxidative stress (27–29, 34).

In animals, there is ample evidence that ROS participate in aging processes, including enhanced levels of oxidative markers with age and in short-lived animals,

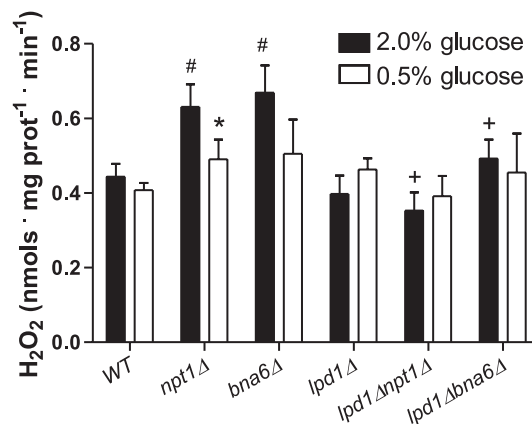


Figure 6. H_2O_2 release changes are dependent on dihydrolipoyl dehydrogenase. H_2O_2 release by spheroplasts prepared from WT or mutant strains grown under control (full bars) or CR (empty bars) conditions were measured in parallel, in early stationary growth phase, as described in Materials and Methods. **P* < 0.05 vs. 2.0% Glc; #*P* < 0.05 vs. WT; +*P* < 0.05 vs. *npt1Δ* or *bna6Δ*.

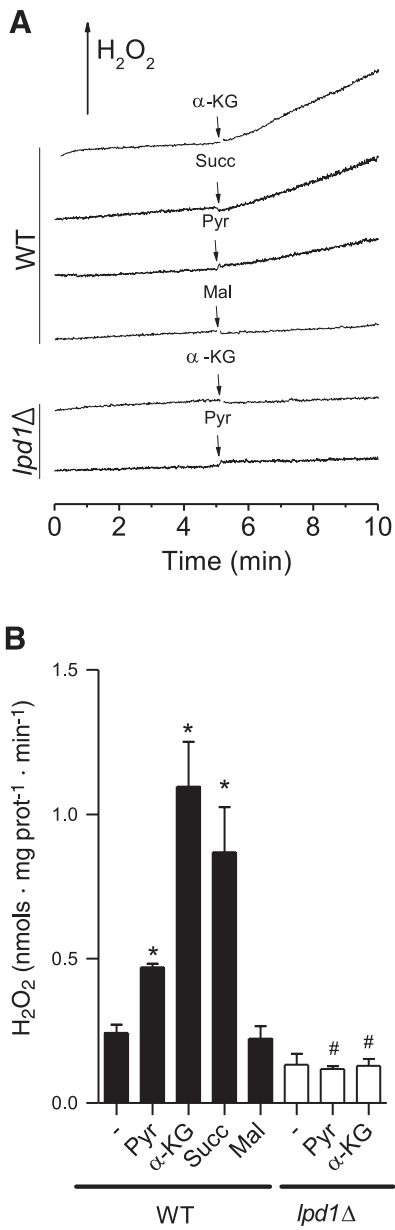


Figure 7. Pyruvate and α -ketoglutarate dehydrogenases are significant sources of mitochondrial ROS. WT (full bars) or $lpd1\Delta$ (empty bars) alamethicin-permeabilized mitochondria (50 μ g/ml) were added to 30°C, pH 7.5 (KOH), reaction media containing 0.6 M sorbitol, 32.5 mM phosphate, 10 mM Tris, 1 mM EDTA, and 100 μ M coenzyme A (CoA). H_2O_2 release was measured as described in Materials and Methods. Pyruvate (Pyr), α -ketoglutarate (α -KG), succinate (Succ), and malate (Mal) were added where indicated, at 5 mM. A depicts typical traces, and B shows average H_2O_2 release rates. * $P < 0.01$ vs. no added substrates; # $P < 0.001$ vs. WT.

inverse correlations between levels of mitochondrial ROS release and life span and involvement of oxidative stress in many age-associated diseases (for reviews, see refs. 4, 12, 13, 41–43). Furthermore, CR in animals prevents mitochondrial ROS release and oxidative stress markers accumulated with aging (for reviews, see ref. 4, 12, 13). Considering the complexity of the aging process, it is not surprising that it is regulated by multiple factors both in simpler model organisms such

as yeast and in multicellular animals. Other factors proposed to mediate aging are metabolic rates, telomere loss, loss of DNA repair and genome stability, and aggregated protein accumulation (for review, see ref 44). Most likely, all these factors play a role in aging, acting in concert. The genetic, metabolic, and oxidative processes involved in *S. cerevisiae* aging support the use of this model, since it bears a closer resemblance to multifactor aging processes in animals.

We have previously demonstrated using *S. cerevisiae* that the link between the beneficial effects of CR in chronological and replicative aging is the increase in respiratory rates that results from Glc limitation. Indeed, artificially increasing respiration by using a proton ionophore enhances both replicative and chronological life span (27). Here, we investigate the effects of respiratory rates on mitochondrial and cellular redox state and uncover the mechanisms through which ROS metabolism is altered under conditions that change yeast longevity.

We found that respiratory rates of a variety of yeast strains grown in distinct Glc concentrations are inversely correlated with the release of mitochondrial H_2O_2 , a relatively stable and membrane-permeable ROS (Fig. 2). Supporting the idea that increased mitochondrial H_2O_2 release is reflective of cellular oxidative imbalance *in vivo*, GSSG and total glutathione contents increase in cell types and growth conditions in which mitochondrial ROS release is highest (Fig. 3). These findings are in line with measurements of protein carbonylation in *S. cerevisiae* indicating that this form of oxidative damage is prevented by CR (45). In addition, we found that cellular oxidative stress promoted by lack of CR and/or defects in NAD⁺ synthesis resulted in limited chronological longevity (Fig. 5). This result further supports the idea that yeast chronological longevity is limited by mitochondrially generated ROS.

The strong correlation between O₂ consumption and H₂O₂ release measurements (Fig. 2) suggests they are related in a cause/effect manner. Indeed, there is ample evidence in the literature that ROS generation in mitochondria from animals and plants is prevented by increasing O₂ consumption (for reviews, see refs. 10, 46–48). Previously, two main reasons for reduced mitochondrial ROS generation promoted by enhanced electron transport have been presented: 1) enhanced O₂ consumption creates a lower oxygen tension micro-environment, preventing the donation of electrons from complexes I and/or III to oxygen that leads to superoxide radical formation; or 2) enhanced electron transport results in lower life times of the reduced forms of respiratory complexes that can generate superoxide anions (48, 49). However, neither of these explanations seems plausible in the case of enhanced ROS release observed in *npt1Δ*, *bna6Δ* and *pnc1Δ* cells, since the levels of total and reduced NAD are lower, feeding a smaller quantity of electrons into the respiratory chain (see Fig. 8). As a result, we focused our attention on sites upstream of NAD⁺ reduction which could generate ROS.

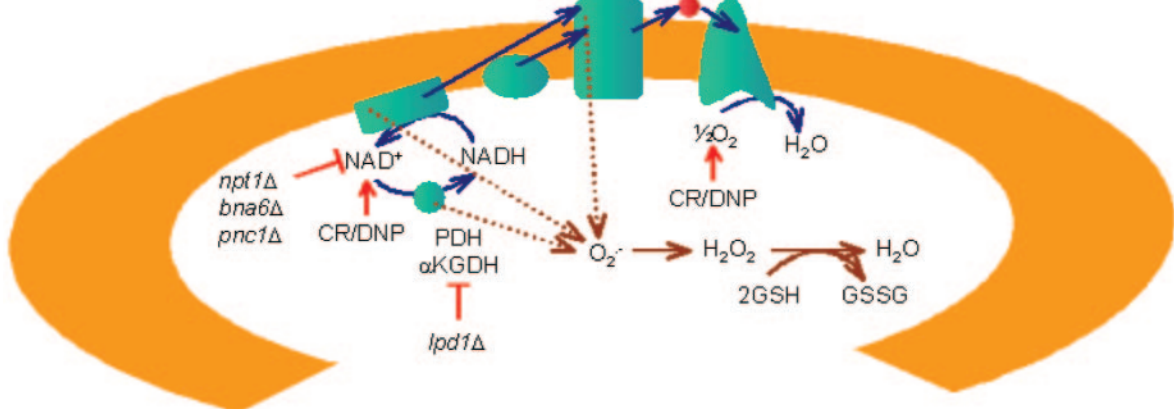


Figure 8. Proposed control of mitochondrial ROS generation in CR. Electron leakage leading to superoxide radical ($O_2^{-\cdot}$) and hydrogen peroxide (H_2O_2) generation can originate from the respiratory chain or pyruvate (PDH) and α -ketoglutarate (α -KGDH) dehydrogenases. This generation is prevented by increments in electron transport promoted by CR or uncouplers such as dinitrophenol (DNP). ROS generation by PDH and α -KGDH is enhanced by low respiratory rates (leading to decreased NAD^+ /NADH ratios) and mutations in NAD^+ synthesis and rescue pathways (*NPT1*, *BNA6*, and *PNC1*). The absence of dihydrolipoyl dehydrogenase (*lpd1*) prevents ROS release by these enzymes. ROS accumulation leads to oxidation of mitochondrial and cytosolic glutathione ($GSH \rightarrow GSSG$), and limits life span.

Recent studies by the groups of Beal and Adam-Vizi (14, 15) suggest that dihydrolipoyl dehydrogenase-containing enzymes, in particular α -ketoglutarate dehydrogenase, are major sources of mitochondrial ROS in mammals. Indeed, these groups found that superoxide radical generation by these enzymes is augmented by the lack of NAD^+ or by high NADH/ NAD^+ ratios. The product of the mammalian *Dld* gene, which encodes the E3 subunit of α -ketoglutarate dehydrogenase, was identified as the probable source of ROS generated by this enzyme using heterozygous knockout mice. This concept is consistent with the finding that flavoenzymes are ROS sources (50). Within these enzymes, the absence of NAD^+ keeps lipoamide dehydrogenase in the reduced state because the cellular environment is reductant. Consequently, there is an increased probability of lipoamide dehydrogenase reactions with oxygen, generating ROS.

We found support for the idea that dihydrolipoyl dehydrogenase generates ROS by testing strains that do not express Lpd1p, the E3 subunit of α -ketoglutarate and pyruvate dehydrogenase in yeast (38). *LPD1* deletion completely reversed the increased ROS release levels found in *npt1Δ* and *bna6Δ* cells (Fig. 6). Furthermore, in experiments comparing ROS release rates induced by different substrates in alamethicin-permeabilized mitochondria (Fig. 7), we found substantial ROS formation promoted by pyruvate and very pronounced ROS formation induced by α -ketoglutarate. These results unequivocally indicate that dihydrolipoyl dehydrogenase-containing enzymes pyruvate and α -ketoglutarate dehydrogenase are very important mitochondrial ROS sources. Interestingly, ROS formation by these enzymes is strongly controlled by NADH/ NAD^+ levels (18, 19) and will thus decrease when higher respiratory rates are present, such as under CR growth conditions (25).

It is important to stress that our study does not rule

out the existence of other mitochondrial ROS sources such as NADH dehydrogenases and respiratory complex III (see Fig. 8). Indeed, succinate is capable of generating significant amounts of ROS in permeabilized mitochondria. However, ROS release levels in the presence of α -ketoglutarate and pyruvate are, together, larger than those induced by succinate (Fig. 7). This finding, and evidence that ROS release by this enzyme in *npt1Δ* and *bna6Δ* cells can limit life span, highlight the importance of dihydrolipoyl dehydrogenase within redox metabolism and emphasize the necessity of additional research concerning the causes and effects of mitochondrial ROS generation. ■

The authors thank Camille C. Caldeira da Silva, Simone V. Alves, and Edson A. Gomes for excellent technical assistance; Gustavo M. da Silva and Gisele Monteiro for help with glutathione measurements; Cassius V. Stevani for the use of equipment; and Roger F. Castilho for stimulating discussions. This work is supported by grants from Fundação de Amparo à Pesquisa do Estado de São Paulo (FAPESP), The John Simon Guggenheim Memorial Foundation, and Conselho Nacional de Pesquisa e Tecnologia (CNPq), as part of the Instituto do Milênio Redoxoma. E. B. Tahara and G. A. Oliveira are supported by CNPq and FAPESP fellowships, respectively.

REFERENCES

- McCay, C. M., Cromwell, M. F., and Maynard, L. A. (1935) The effect of retarded growth upon the length of life span and upon the ultimate body size. *J. Nutr.* **10**, 63–79
- Walford, R. L., Harris, S. B., and Weindruch, R. (1987) Dietary restriction and aging: historical phases, mechanisms and current directions. *J. Nutr.* **117**, 1650–1654
- Hursting, S. D., Lavigne, J. A., Berrigan, D., Perkins, S. N., and Barrett, J. C. (2003) Calorie restriction, aging, and cancer prevention: mechanisms of action and applicability to humans. *Annu. Rev. Med.* **54**, 131–152
- Sohal, R. S., and Weindruch, R. (1996) Oxidative stress, caloric restriction, and aging. *Science* **273**, 59–63

5. Lambert, A. J., and Merry, B. J. (2004) Effect of caloric restriction on mitochondrial reactive oxygen species production and bioenergetics: reversal by insulin. *Am. J. Physiol.* **286**, R71–79
6. Sanz, A., Caro, P., Ibanez, J., Gomez, J., Gredilla, R., and Barja, G. (2005) Dietary restriction at old age lowers mitochondrial oxygen radical production and leak at complex I and oxidative DNA damage in rat brain. *J. Bioenerg. Biomembr.* **37**, 83–90
7. Radak, Z., Asano, K., Fu, Y., Nakamura, A., Nakamoto, H., Ohno, H., and Goto, S. (1998) The effect of high altitude and caloric restriction on reactive carbonyl derivatives and activity of glutamine synthetase in rat brain. *Life Sci.* **62**, 1317–1322
8. Gredilla, R., Sanz, A., Lopez-Torres, M., and Barja, G. (2001) Caloric restriction decreases mitochondrial free radical generation at complex I and lowers oxidative damage to mitochondrial DNA in the rat heart. *FASEB J.* **15**, 1589–1591
9. Kowaltowski, A. J., and Vercesi, A. E. (1999) Mitochondrial damage induced by conditions of oxidative stress. *Free Radic. Biol. Med.* **26**, 463–471
10. Turrens, J. F. (2003) Mitochondrial formation of reactive oxygen species. *J. Physiol.* **552**, 335–344
11. Merry, B. J. (2004) Oxidative stress and mitochondrial function with aging—the effects of calorie restriction. *Aging Cell* **3**, 7–12
12. Barja, G. (2004) Free radicals and aging. *Trends Neurosci.* **27**, 595–600
13. Balaban, R. S., Nemoto, S., and Finkel, T. (2005) Mitochondria, oxidants, and aging. *Cell* **120**, 483–495
14. Starkov, A. A., Fiskum, G., Chinopoulos, C., Lorenzo, B. J., Browne, S. E., Patel, M. S., and Beal, M. F. (2004) Mitochondrial alpha-ketoglutarate dehydrogenase complex generates reactive oxygen species. *J. Neurosci.* **24**, 7779–7788
15. Tretter, L., and Adam-Vizi, V. (2004) Generation of reactive oxygen species in the reaction catalyzed by alpha-ketoglutarate dehydrogenase. *J. Neurosci.* **24**, 7771–7778
16. Mortimer, R. K., and Johnston, J. R. (1959) Life span of individual yeast cells. *Nature* **183**, 1751–1752
17. Sinclair, D. A., and Guarente, L. (1997) Extrachromosomal rDNA circles—a cause of aging in yeast. *Cell* **91**, 1033–1042
18. Fabrizio, P., and Longo, V. D. (2003) The chronological life span of *Saccharomyces cerevisiae*. *Aging Cell* **2**, 73–81
19. Kim, S., Benguria, A., Lai, C. Y., and Jazwinski, S. M. (1999) Modulation of life-span by histone deacetylase genes in *Saccharomyces cerevisiae*. *Mol. Biol. Cell* **10**, 3125–3136
20. Lin, S. J., Defossez, P. A., and Guarente, L. (2000) Requirement of NAD and SIR2 for life-span extension by calorie restriction in *Saccharomyces cerevisiae*. *Science* **289**, 2126–2128
21. Lin, S. J., Kaeberlein, M., Andalis, A. A., Sturtz, L. A., Defossez, P. A., Culotta, V. C., Fink, G. R., and Guarente, L. (2002) Calorie restriction extends *Saccharomyces cerevisiae* lifespan by increasing respiration. *Nature* **418**, 344–348
22. Guarente, L., and Picard, F. (2005) Calorie restriction—the SIR2 connection. *Cell* **120**, 473–482
23. Kaeberlein, M., Kirkland, K. T., Fields, S., and Kennedy, B. K. (2004) Sir2-independent life span extension by calorie restriction in yeast. *PLoS Biol.* **2**, E296
24. Jiang, J. C., Jaruga, E., Repnevskaya, M. V., and Jazwinski, S. M. (2000) An intervention resembling caloric restriction prolongs life span and retards aging in yeast. *FASEB J.* **14**, 2135–2137
25. Lin, S. J., Ford, E., Haigis, M., Liszt, G., and Guarente, L. (2004) Calorie restriction extends yeast life span by lowering the level of NADH. *Genes Dev.* **18**, 12–16
26. Anderson, R. M., Bitterman, K. J., Wood, J. G., Medvedik, O., and Sinclair, D. A. (2003) Nicotinamide and PNC1 govern lifespan extension by calorie restriction in *Saccharomyces cerevisiae*. *Nature* **423**, 181–185
27. Barros, M. H., Bandy, B., Tahara, E. B., and Kowaltowski, A. J. (2004) Higher respiratory activity decreases mitochondrial reactive oxygen release and increases life span in *Saccharomyces cerevisiae*. *J. Biol. Chem.* **279**, 49883–49888
28. Harris, N., Costa, V., MacLean, M., Mollapour, M., Moradas-Ferreira, P., and Piper, P. W. (2003) MnSOD overexpression extends the yeast chronological (G(0)) life span but acts independently of Sir2p histone deacetylase to shorten the replicative life span of dividing cells. *Free Radic. Biol. Med.* **34**, 1599–1606
29. Longo, V. D., Gralla, E. B., and Valentine, J. S. (1996) Superoxide dismutase activity is essential for stationary phase survival in *Saccharomyces cerevisiae*. Mitochondrial production of toxic oxygen species *in vivo*. *J. Biol. Chem.* **271**, 12275–12280
30. Jazwinski, S. M. (2005) Yeast longevity and aging—the mitochondrial connection. *Mech. Ageing Dev.* **126**, 243–248
31. Kowaltowski, A. J., Vercesi, A. E., Rhee, S. G., and Netto, L. E. S. (2000) Catalases and thioredoxin peroxidase protect *Saccharomyces cerevisiae* against Ca^{2+} -induced mitochondrial membrane permeabilization and cell death. *FEBS Lett.* **473**, 177–182
32. Monteiro, G., Kowaltowski, A. J., Barros, M. H., and Netto, L. E. S. (2004) Glutathione and thioredoxin peroxidases mediate susceptibility of yeast mitochondria to Ca^{2+} -induced damage. *Arch. Biochem. Biophys.* **425**, 14–24
33. Millard, P. J., Roth, B. L., Thi, H. P., Yue, S. T., and Haugland, R. P. (1997) Development of the FUN-1 family of fluorescent probes for vacuole labeling and viability testing of yeasts. *Appl. Environ. Microbiol.* **63**, 2897–2905
34. Fabrizio, P., Liou, L. L., Moy, V. N., Diaspro, A., Valentine, J. S., Gralla, E. B., and Longo, V. D. (2003) SOD2 functions downstream of Sch9 to extend longevity in yeast. *Genetics* **163**, 35–46
35. Carlson, M. (1999) Glucose repression in yeast. *Curr. Opin. Microbiol.* **2**, 202–207
36. Panizzo, C., Nawara, M., Suski, C., Kucharczyka, R., Skoneczny, M., Becam, A. M., Rytka, J., Herbert, C. J. (2002) Aerobic and anaerobic NAD^+ metabolism in *Saccharomyces cerevisiae*. *FEBS Lett.* **517**, 97–102
37. Grant, C. M. (2001) Role of the glutathione/glutaredoxin and thioredoxin systems in yeast growth and response to stress conditions. *Mol. Microbiol.* **39**, 533–541
38. Dickinson, J. R., Roy, D. J., and Dawes, I. W. (1986) A mutation affecting lipoamide dehydrogenase, pyruvate dehydrogenase and 2-oxoglutarate dehydrogenase activities in *Saccharomyces cerevisiae*. *Mol. Gen. Genet.* **204**, 103–107
39. Jiang, J. C., Wawryn, J., Shantha Kumara, H. M., and Jazwinski, S. M. (2002) Distinct roles of processes modulated by histone deacetylases Rpd3p, Hda1p, and Sir2p in life extension by caloric restriction in yeast. *Exp. Gerontol.* **37**, 1023–1030
40. Fabrizio, P., Gattazzo, C., Battistella, L., Wei, M., Cheng, C., McGrew, K., and Longo, V. D. (2005) Sir2 blocks extreme life-span extension. *Cell* **123**, 655–667
41. Harman, D. (2003) The free radical theory of aging. *Antioxid. Redox Signal.* **5**, 557–561
42. Stadtman, E. R. (2004) Role of oxidant species in aging. *Curr. Med. Chem.* **11**, 1105–1112
43. Skulachev, V. P. (2004) Mitochondria, reactive oxygen species and longevity: some lessons from the Barja group. *Aging Cell* **3**, 17–19
44. Kirkwood, T. B. (2005) Understanding the odd science of aging. *Cell* **120**, 437–447
45. Reverter-Branchat, G., Cabiscol, E., Tamarit, J., and Ros, J. (2004) Oxidative damage to specific proteins in replicative and chronological-aged *Saccharomyces cerevisiae*: common targets and prevention by caloric restriction. *J. Biol. Chem.* **279**, 31983–31989
46. Brand, M. D., and Esteves, T. C. (2005) Physiological functions of the mitochondrial uncoupling proteins UCP2 and UCP3. *Cell Metab.* **2**, 85–93
47. Brookes, P. S. (2005) Mitochondrial H^+ leak and ROS generation: an odd couple. *Free Radic. Biol. Med.* **38**, 12–23
48. Skulachev, V. P. (1997) Membrane-linked systems preventing superoxide formation. *Biosci. Rep.* **17**, 347–366
49. Starkov, A. A. (1997) “Mild” uncoupling of mitochondria. *Biosci. Rep.* **17**, 273–279
50. Imlay, J. A. (2003) Pathways of oxidative damage. *Ann. Rev. Microbiol.* **57**, 395–418

Received for publication June 21, 2006.
Accepted for publication July 31, 2006.

Increased aerobic metabolism is essential for the beneficial effects of caloric restriction on yeast life span

Graciele A. Oliveira · Erich B. Tahara ·
Andreas K. Gombert · Mario H. Barros ·
Alicia J. Kowaltowski

Received: 25 March 2008 / Accepted: 16 July 2008 / Published online: 15 August 2008
© Springer Science + Business Media, LLC 2008

Abstract Calorie restriction is a dietary regimen capable of extending life span in a variety of multicellular organisms. A yeast model of calorie restriction has been developed in which limiting the concentration of glucose in the growth media of *Saccharomyces cerevisiae* leads to enhanced replicative and chronological longevity. Since *S. cerevisiae* are Crabtree-positive cells that present repression of aerobic catabolism when grown in high glucose concentrations, we investigated if this phenomenon participates in life span regulation in yeast. *S. cerevisiae* only exhibited an increase in chronological life span when incubated in limited concentrations of glucose. Limitation of galactose, raffinose or glycerol plus ethanol as substrates did not enhance life span. Furthermore, in *Kluyveromyces lactis*, a Crabtree-negative yeast, glucose limitation did not promote an enhancement of respiratory capacity nor a decrease in reactive oxygen species formation, as is characteristic of conditions of caloric restriction in *S. cerevisiae*. In addition,

K. lactis did not present an increase in longevity when incubated in lower glucose concentrations. Altogether, our results indicate that release from repression of aerobic catabolism is essential for the beneficial effects of glucose limitation in the yeast calorie restriction model. Potential parallels between these changes in yeast and hormonal regulation of respiratory rates in animals are discussed.

Keywords Calorie restriction · Crabtree effect · Free radicals · Aging · Respiration

Introduction

Calorie restriction, or the reduction of caloric intake without lack of essential nutrients, is a dietary regimen capable of extending life span in a variety of laboratory animals ranging from *C. elegans* to mice and, probably, primates. The effects of this diet are widespread, and involve physiological, metabolic, hormonal, gene expression and morphological changes. It is not yet clear which of these observed changes are directly related to decreased incidence of age-related pathologies and increased life span (Weindruch and Walford 1988; Partridge and Gems 2002).

Yeast models of calorie restriction have been developed in order to study the results of this diet in a less complex organism. In *Saccharomyces cerevisiae*, growth in rich media with lower glucose concentrations significantly increases both replicative and chronological longevity (Jiang et al. 2000; Lin et al. 2000). Interestingly, the beneficial effects of glucose restriction in yeast are related to increases in respiratory rates that occur when glucose levels in the media are lower (Lin et al. 2002; Barros et al. 2004). These enhanced respiratory rates elevate intracellular

G. A. Oliveira and E. B. Tahara contributed equally to this work.

G. A. Oliveira · E. B. Tahara · A. J. Kowaltowski (✉)
Departamento de Bioquímica, Instituto de Química,
Universidade de São Paulo,
Cidade Universitária, Lineu Prestes, 748,
São Paulo, São Paulo 05508-900, Brazil
e-mail: alicia@iq.usp.br

A. K. Gombert
Departamento de Engenharia Química,
Escola Politécnica, Universidade de São Paulo,
São Paulo, Brazil

M. H. Barros
Departamento de Microbiologia, Instituto de Ciências
Biomédicas, Universidade de São Paulo,
São Paulo, Brazil

NAD^+ levels, which may be involved in the regulation of life span by modulating the activity of Sir2 family proteins (Lin and Guarente 2003) and reducing mitochondrial reactive oxygen species release (Tahara et al. 2007).

S. cerevisiae are Crabtree-positive cells, yeast in which fermentation is the preferred metabolic pathway and aerobic metabolism is inhibited, despite the presence of oxygen, when glucose levels are high (De Dekken 1966). Taking this into account, we questioned whether repression of aerobic catabolism was necessary for the efficacy of the yeast caloric restriction model. In order to investigate this possibility, we compared chronological life spans of *S. cerevisiae* in the presence of different substrates metabolized by the glycolytic pathway which lead to different levels of respiratory repression. We also compared the effects of glucose limitation in *S. cerevisiae* and glucose limitation in *Kluyveromyces lactis*, a Crabtree-negative yeast (Breunig et al. 2000).

Experimental procedures

1. *S. cerevisiae* and *K. lactis*: BY4741 *S. cerevisiae* (Brachmann et al. 1998) and CBS 2359 *K. lactis* were used for all experiments.
2. Culture media: Culture media used for all experiments were liquid yeast extract (1%) and peptone (2%) plus 0.2–3.0% glucose, galactose, raffinose or glycerol plus ethanol, as indicated.
3. Chronological life span determinations: Chronological life span was determined by colony forming ability and metabolic integrity, or the ability to accumulate calcein. *Colony-forming ability*: 100 cells from *S. cerevisiae* or *K. lactis* in late stationary phase (96 h) cultured in liquid media (1% yeast extract, 2% peptone and 0.2–3.0% glucose, 0.2–3.0% galactose, 0.2–3.0% raffinose or 0.2–3.0% glycerol plus 0.2–3.0% ethanol, as indicated) were plated in 2% solid YPD media (1% yeast extract, 2% peptone, 2% glucose and 2% bacteriological agar). After ~36 h of growth at 30 °C, the number of colonies formed was counted (Tahara et al. 2007). *Metabolic integrity*: Yeast in late stationary phase were centrifuged at 1,000×g for 5 min at 30 °C and washed twice using ultrapure water. Cells were resuspended (2×10^6) in 1 mL of 0.6 M sorbitol, 32.5 mM K-phosphate, 10 mM Tris–Cl and 1 mM EDTA (pH 7.5) and were incubated with 1 µg/mL calcein-AM for 20 min. Cytometry parameters used were: FS=17.6 (gain=5.0); SS=243 (gain=50.0); FL1=752 (gain=2.0); discriminant value=20.0.
4. Spheroplast generation: Spheroplasts were obtained through yeast cell wall digestion with 20 U zymolyase/g of cells, for ~45 min at 37 °C, under mild shaking, in

1.2 M sorbitol, 10 mM MgCl₂ and 50 mM Tris, pH 7.5. Spheroplasts were resuspended in 75 mM K-phosphate buffer with 1.2 M sorbitol and 1 mM EDTA, pH 7.5, to a final concentration of 10 mg protein/mL (Tahara et al. 2007). Protein concentrations were determined using the Lowry method.

5. Cytochrome absorption spectra: Respiratory chain cytochrome spectra were assayed with mitochondria prepared by the method of Faye et al. (1974), except that zymolyase 20T instead of glusulase was used for the conversion of cells to spheroplasts. Mitochondria were extracted at a final protein concentration of 4 mg/mL with 1% deoxycholate to solubilize all cytochromes (Tzagoloff et al. 1975). Difference spectra of sodium dithionite-reduced versus potassium ferricyanide-oxidized extracts were recorded at room temperature.
6. NADH-cytochrome c reductase activity: NADH oxidation and cytochrome c reduction were estimated as described previously (Tzagoloff et al. 1975). Briefly, 20 µg of mitochondrial proteins, previously permeabilized with 0.1% of potassium deoxycholate, were incubated in 10 mM potassium-phosphate buffer, pH 7.5, containing 0.1 mM KCN and 0.08% cytochrome c. The rate of cytochrome c reduction was measured at 550 nm, at room temperature, after the addition of 1 mM NADH.
7. O₂ consumption: O₂ consumption was monitored over time in 800 µg/mL spheroplast suspensions in the presence of 2% ethanol and 1 mM malate/glutamate as substrates, using a computer-interfaced Clark-type electrode operating with continuous stirring, at 30 °C. Spheroplasts were permeabilized using 0.004–0.006% digitonin, as described by Tahara et al. 2007.
8. H₂O₂ production: H₂O₂ release from mitochondria was monitored for 10 min in 100 µg/mL spheroplast suspensions in the presence of 50 µM Amplex Red, 0.5 U/mL horse radish peroxidase, 2% ethanol and 1 mM malate/glutamate, using a fluorescence spectrophotometer operating at 563 nm excitation and 587 nm emission, with continuous stirring, at 30 °C. Spheroplasts were permeabilized using 0.002–0.003% digitonin, as described by Tahara et al. (2007). Measurements were calibrated by adding known quantities of H₂O₂, as described previously (Ferranti et al. 2003).

Results

Decreasing the concentration of glucose in the culture media results in an enhancement of replicative (Jiang et al. 2000; Lin et al. 2000) and chronological (Barros et al. 2004; Tahara et al. 2007; Smith et al. 2007) life span in *S.*

cerevisiae. Indeed, we found that *S. cerevisiae* cultured until the late stationary growth phase in media containing lower glucose concentrations (0.2–0.5%) generated significantly more colonies (representing more viable cells) than those cultured in higher glucose concentrations (1–3%, Fig. 1, upper left Panel). This higher generation of colonies in the late stationary phase represents an extended chronological life span (Tahara et al. 2007; Smith et al. 2007). In order to verify if this effect was dependent on the significant repression of aerobic catabolism promoted by growth in high concentrations of glucose, we compared glucose restriction to the effect of restricting galactose, raffinose, and glycerol plus ethanol.

Galactose is metabolized by the Leloir pathway to produce glucose 6 phosphate, which is then degraded by the glycolytic pathway. Although metabolism of this sugar leads to some degree of respiratory inhibition, the effect is significantly smaller than that observed with glucose (Gancedo 1998; Rodríguez and Gancedo 1999). Raffinose is a trisaccharide composed of galactose, fructose, and glucose, which also promotes less significant changes in aerobic catabolism than glucose, due to the lower concentrations of free glucose produced (Gancedo 1998). Interestingly, no beneficial effect of limiting galactose or raffinose was seen on *S. cerevisiae* chronological life span (Fig. 1). Furthermore,

limitation of glycerol plus ethanol, which are non-fermentable substrates, also did not enhance chronological life span, suggesting that repression of aerobic catabolism is essential for the beneficial effects of the yeast caloric restriction model. Indeed, limiting raffinose and glycerol/ethanol decreased cell survival.

In order to ascertain that high glucose concentrations were not exclusively decreasing replication and colony-forming ability, we also determined chronological life span by measuring cellular metabolic integrity, or the ability of the cells to accumulate fluorescent calcein when incubated with calcein-AM. Flow cytometry fluorescence histograms (Fig. 2) demonstrate that restriction of glucose, and to a lesser extent galactose, but not raffinose or glycerol plus ethanol, lead to significantly improved cell integrity, as indicated by peaks at higher fluorescence levels.

We have previously shown that a beneficial effect associated with glucose restriction leading to extended chronological life span is the prevention of oxidative stress. While antioxidant levels are largely unchanged (Lin et al. 2002), glucose restriction limits mitochondrial reactive oxygen species generation in mitochondria (Barros et al. 2004; Tahara et al. 2007). In order to compare the redox effects of fermentative versus respiratory substrates (promoting maximal and minimal respiratory repression, respectively), we

Fig. 1 Glucose, but not galactose, raffinose or glycerol/ethanol restriction increases chronological life span (colony-forming ability) in *S. cerevisiae*. One hundred late stationary cells cultured using glucose, galactose, raffinose or glycerol plus ethanol (as indicated) as substrates were plated in solid 2% YPD. Colonies were counted after 36 h of growth at 30 °C. * $p<0.05$ versus 3.0%

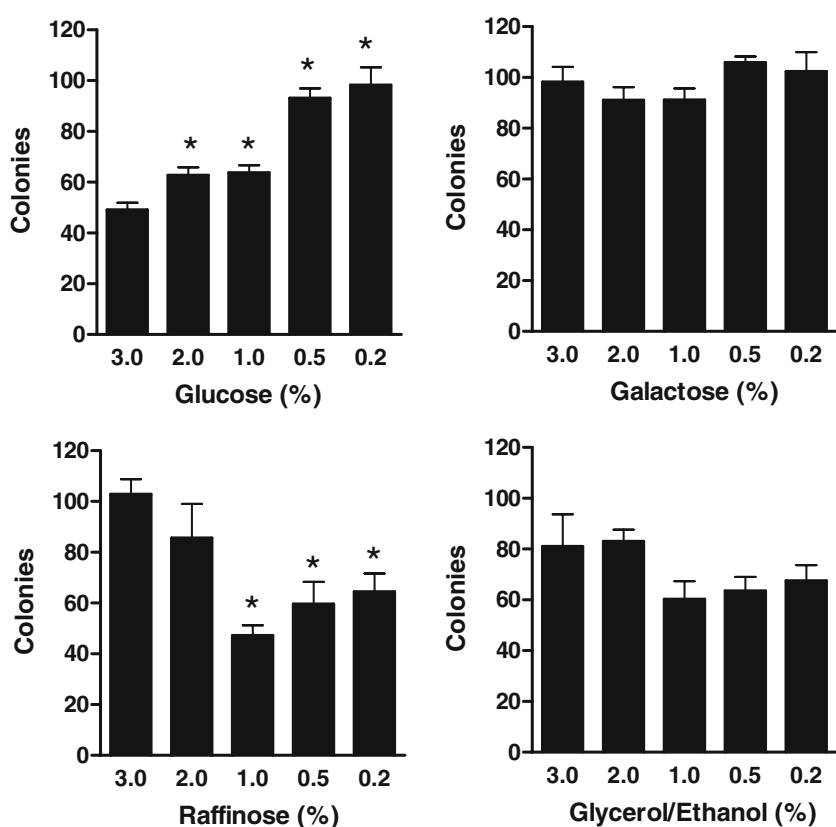
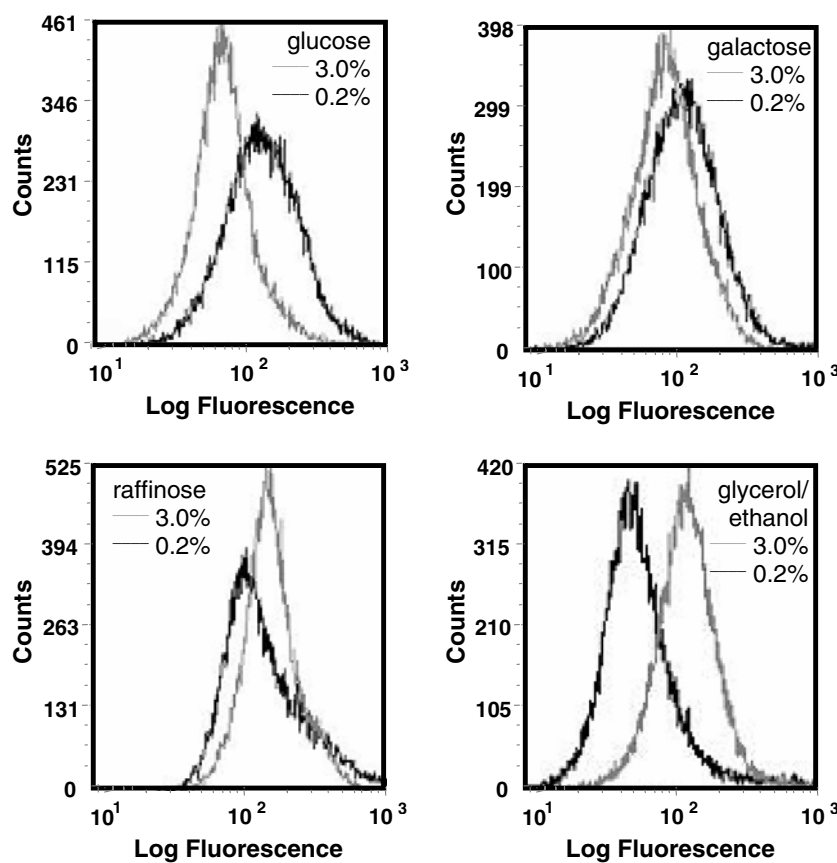


Fig. 2 Glucose, but not galactose, raffinose or glycerol/ethanol restriction increases chronological life span (metabolic integrity) in *S. cerevisiae*. Calcein retention of late stationary cells cultured in 0.2% (black lines) or 3.0% (grey lines) glucose, galactose, raffinose or glycerol plus ethanol was measured as described in “Experimental procedures”



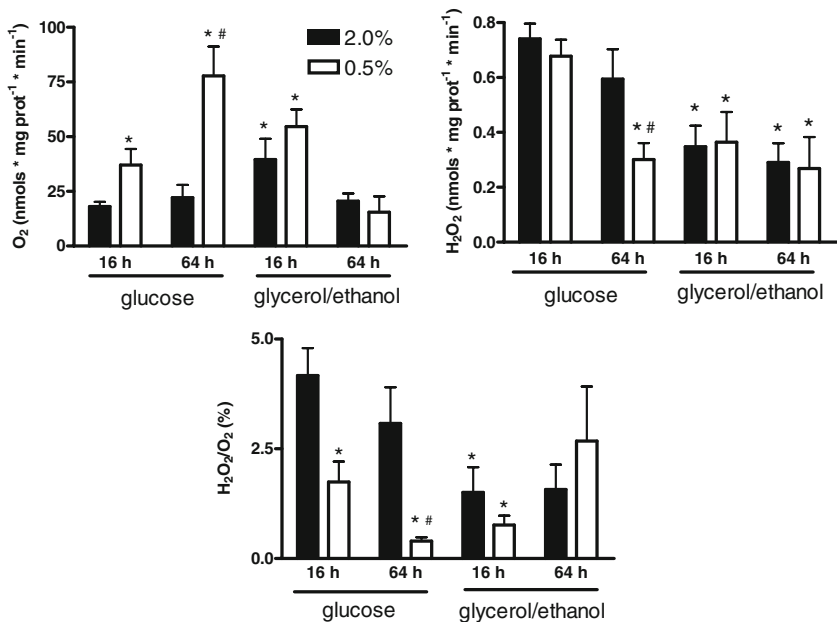
measured oxygen consumption and the release of H_2O_2 (a membrane-permeable reactive oxygen species) in digitonin-permeabilized spheroplasts (Tahara et al. 2007) from *S. cerevisiae* grown in 2.0% or 0.5% glucose or ethanol/glycerol

(Fig. 3). As expected, we found that yeasts grown in 2.0% glucose present lower respiratory rates than those grown in ethanol/glycerol. In addition, glycerol/ethanol-grown cells presented lower levels of both absolute (H_2O_2) and relative

Fig. 3 Glucose restriction or glycerol/ethanol decrease H_2O_2 release in *S. cerevisiae*.

Spheroplasts obtained from early and late stationary phase yeast were incubated in 1.2 M sorbitol, 1 mM EDTA, 75 mM phosphate, 2% ethanol, 1 mM malate and 1 mM glutamate, pH 7.5 (KOH). Plasma membrane permeabilization was obtained using digitonin (0.002–0.006%), and O_2 consumption and H_2O_2 release rates were measured as described in “Experimental procedures”.

* $p<0.05$ versus 2.0% glucose;
$p<0.05$ versus 16 h



($\text{H}_2\text{O}_2/\text{O}_2$) mitochondrial H_2O_2 production. Taken together, the results presented to this point strongly suggest that enhanced chronological life span and prevention of oxidative stress in yeasts grown in limited glucose are due to the loss of repression of aerobic catabolism promoted by high glucose growth conditions.

If loss of repression of aerobic catabolism is indeed necessary for the beneficial effects of calorie restriction in yeast, these effects should only be observed in Crabtree-positive yeasts. We thus investigated if a Crabtree-negative yeast, *K. lactis*, responded to glucose restriction similarly to *S. cerevisiae*. As expected, restriction of glucose in *S. cerevisiae* cultures leads to a clear increment in respiratory cytochromes content (Fig. 4, black lines), both in early and late stationary growth phases. On the other hand, *K. lactis* mitochondrial respiratory cytochromes did not show any

significant increment when cells were cultured under glucose restricted conditions. Consistently, the respiratory activity of *K. lactis*, reflected here as NADH-cytochrome c reductase activity, did not change when the two growth conditions were compared. This enzymatic activity is strongly stimulated in *S. cerevisiae* mitochondria isolated from cells cultured under glucose restriction (open bars), at both 16 and 64 h.

We then determined the functional effects of these respiratory capacity changes by measuring oxygen consumption and release of H_2O_2 in digitonin-permeabilized spheroplasts of these yeasts (Tahara et al. 2007). Figure 5 shows that *S. cerevisiae* grown in low glucose exhibit significantly higher respiratory rates after 16 and 64 h in culture, despite the fact that glucose was undetectable after only 16 h (Tahara et al. 2007). As discussed previously,

Fig. 4 Glucose limitation increases cytochrome contents and NADH-cytochrome c reductase activity in *S. cerevisiae*, but not *K. lactis*. Cytochrome spectra (upper panels) and NADH-cytochrome c reductase activity (lower panels) were measured as described in “Experimental procedures” in *S. cerevisiae* or *K. lactis* cultured for 16 or 64 h, as shown. Letters above the spectra indicate the absorption peaks of specific cytochromes. * $p<0.05$ versus 2.0% glucose

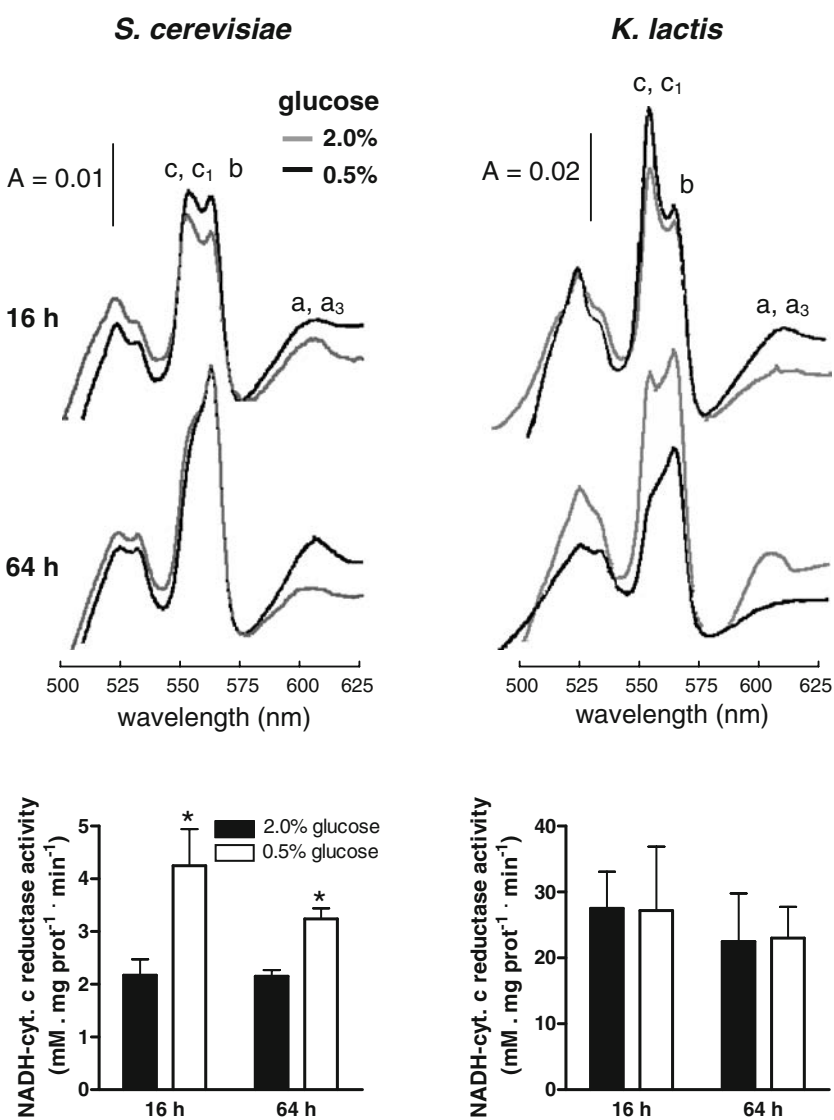
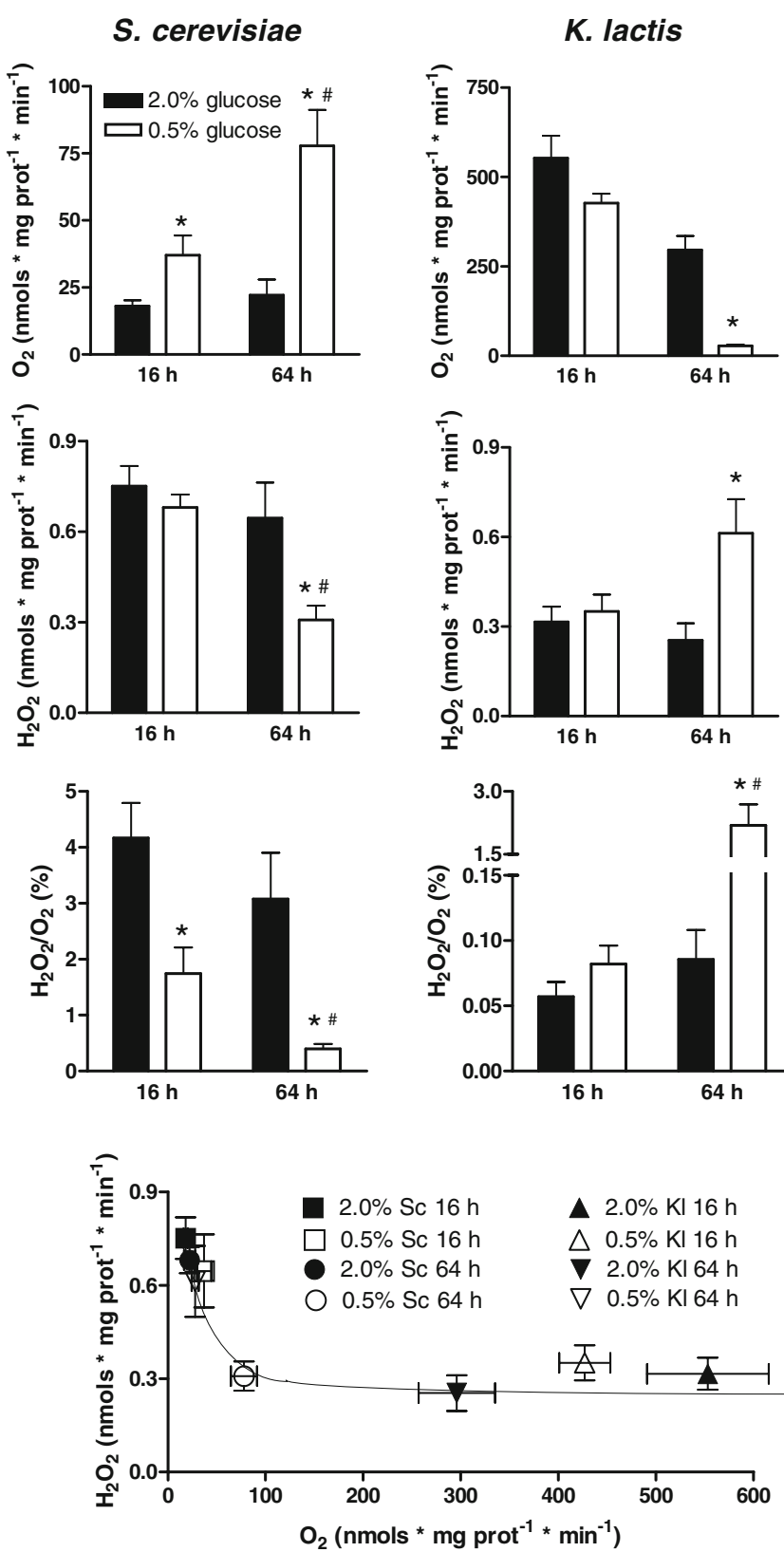


Fig. 5 Calorie restriction decreases H_2O_2 release in *S. cerevisiae*, but not *K. lactis*. Spheroplasts obtained from early and late stationary phase yeast were incubated in 1.2 M sorbitol, 1 mM EDTA, 75 mM phosphate, 2% ethanol, 1 mM malate and 1 mM glutamate, pH 7.5 (KOH). Plasma membrane permeabilization was obtained using digitonin (0.002–0.006%), and O_2 consumption and H_2O_2 release rates were measured as described in “Experimental procedures”.

* $p<0.05$ versus 2.0% glucose;
$p<0.05$ versus 16 h



higher respiratory rates in *S. cerevisiae* are accompanied by a decrease in both absolute (H_2O_2) and relative (H_2O_2/O_2) mitochondrial H_2O_2 production, most noticeably after 64 hours in culture. However, in *K. lactis* the results were strikingly different. Respiratory rates were not enhanced by low glucose concentrations, and, instead, showed marked inhibition after longer culture times, accompanied by an increment in H_2O_2 release rates. These results clearly indicate that the beneficial effects of caloric restriction on *S. cerevisiae* redox state do not occur in the Crabtree-negative *K. lactis*.

Interestingly, respiratory rates and H_2O_2 release presented a strong inverse correlation in both cell types, regardless of culture phases (Fig. 5, lower panel). This suggests that respiratory rates are a major determinant of yeast oxidant generation. Since we have previously shown that redox state limits chronological longevity in *S. cerevisiae* (Barros et al. 2004; Tahara et al. 2007), our results support the notion that enhancement of aerobic metabolism is an important step in chronological life span extension promoted by glucose limitation.

In this sense, we investigated next if *K. lactis* responded to glucose restriction with enhanced chronological longevity. We found that *K. lactis* does not present an increase in life span, as measured by colony-forming ability or calcein retention (Fig. 6), when incubated in decreasing concentrations of glucose. In *K. lactis*, no colony formation and low calcein retention were observed at the late stationary growth phase in media containing low glucose levels, despite the finding that cell replication occurred normally, as indicated by cell growth in the

logarithmic phase (results not shown). Thus, *K. lactis* clearly does not present an increase in chronological life span under conditions of low glucose that favor life span extension in *S. cerevisiae*.

Discussion

Calorie restriction by limiting glucose concentrations in the growth media has been widely shown to extend life span in *S. cerevisiae*. Most studies in this sense have been conducted measuring replicative life span, which consists in determining the number of generations a mother cell produces after removal from the growth media (Sinclair et al. 1998). Under these conditions, a variety of differing experiments (although not all, see Kaeberlein et al. 2005) suggest that the beneficial effects of glucose restriction are mediated by changes from fermentative to aerobic metabolism. These experiments include studies indicating that deletion or inhibition of respiratory chain components decreases life span and the response to glucose restriction (Lin et al. 2002), while activation of mitochondrial respiration by overexpressing Hap4 (Lin et al. 2002) or treatment with mitochondrial uncoupling agents (Barros et al. 2004) extends replicative life span.

We have previously shown that *S. cerevisiae* chronological life span, or the survival of cells in stationary phase (Fabrizio and Longo 2003), is intimately related to respiratory rates and mitochondrial levels of reactive oxygen species (Barros et al. 2004; Tahara et al. 2007). Interventions such as glucose limitation and mitochondrial uncoupling, which increase respiratory rates, decrease H_2O_2 release and augment chronological life span. Altogether, these results strongly suggest that enhanced life span in the yeast caloric restriction model depends on a phenomenon typical of *S. cerevisiae* and yeasts specifically adapted for fermentation: repression of aerobic catabolism upon incubation in the presence of high glucose concentrations.

This hypothesis is directly tested in this manuscript. Initially, we verified if limiting other carbohydrates as growth substrates promoted the same beneficial effects as glucose in *S. cerevisiae*, and found, using two distinct techniques to measure cell survival in the stationary phase, that improved chronological longevity was exclusive to the limitation of glucose (Figs. 1 and 2). Our results are in agreement with those of Smith et al. (2007), who did not see an increment in *S. cerevisiae* replicative capacity after long cultures in substrates other than glucose. In addition to life span extension, we show that *S. cerevisiae* cultured in the presence of lower glucose levels present a decrease in mitochondrial reactive oxygen species release associated with higher respiratory rates. On the other hand, cultures using respiratory substrates glycerol/ethanol present low

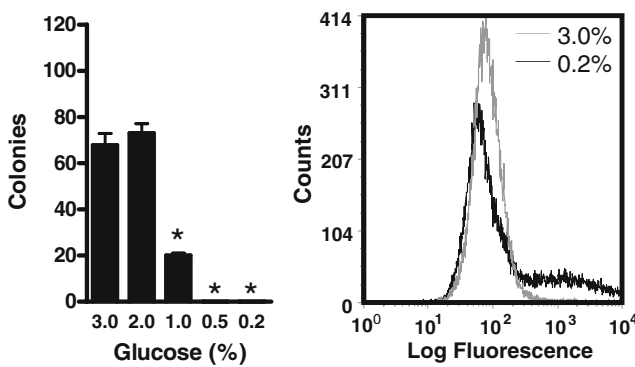


Fig. 6 *K. lactis* does not display enhanced chronological life span with glucose restriction. In the leftmost panel, colony-forming ability was measured by plating 100 late stationary cells cultured in 0.2–3.0% liquid glucose on solid media. Colonies were counted after 36 h of growth at 30°C. * $p<0.05$ versus 3.0% glucose. In the rightmost panel, metabolic integrity was determined by measuring calcein retention in cells cultured in 0.2% (black lines) or 3.0% (grey lines) glucose, as described in “Experimental procedures”

reactive oxygen release independently of the concentration of the substrate in the culture media (Fig. 3).

We also found that a model Crabtree-negative yeast, *K. lactis*, exhibited no beneficial decreases in reactive oxygen release (Fig. 5) or increments in life span (Fig. 6) when incubated in low glucose concentrations. Thus, our results using either alternative substrates or Crabtree-negative yeasts establish that repression of aerobic catabolism is the cause of lower life spans observed in high glucose cultures of *S. cerevisiae*.

It could be argued that the dependence on repression of aerobic catabolism for the effectiveness of the calorie restriction model in yeast underplays its importance as a model system to study this diet, since no such phenomenon is observed in animals. However, repression of respiration in *S. cerevisiae* resembles effects found in response to hormone signaling regulated by diet in more complex organisms. For example, calorie restriction in rats leads to enhanced mitochondrial respiratory rates, decreased proton-motive force and prevention of reactive oxygen species production, in a manner reversed by treatment with insulin (Lambert and Merry 2004). Indeed, many animal models including Klotho and dwarf mice (Bartke et al. 2001; Kurosu et al. 2005) suggest a close link between reduced insulin secretion levels, metabolic efficiency, respiratory rates and enhanced life span. In this sense, the *S. cerevisiae* model of caloric restriction holds many parallels with the mammalian effects of this dietary regimen.

Acknowledgements The authors thank Camille C. da Silva, Adriana Y. Matsukuma and Edson A. Gomes for excellent technical assistance, Professor Luis E. S. Netto for experimental suggestions and Professor Robert Ivan Schumacher for help with flow cytometry measurements. This work is supported by grants from the Fundação de Amparo à Pesquisa do Estado de São Paulo (FAPESP), John Simon Guggenheim Memorial Foundation, Conselho Nacional de Desenvolvimento Científico e Tecnológico (CNPq) and Instituto do Milênio Redoxoma. GAO and EBT are students supported by FAPESP.

References

- Barros MH, Bandy B, Tahara EB, Kowaltowski AJ (2004) J Biol Chem 279:49883–49888
- Bartke A, Brown-Borg H, Mattison J, Kinney B, Hauck S, Wright C (2001) Exp Gerontol 36:21–28
- Brachmann CB, Davies A, Cost GJ, Caputo E, Li J, Hieter P, Boeke JD (1998) Yeast 14:115–132
- Breunig KD, Bolotin-Fukuhara M, Bianchi MM, Bourgarel D, Falcone C, Ferrero II, Frontali L, Goffrini P, Krijger JJ, Mazzoni C, Milkowski C, Steensma HY, Wesolowski-Louvel M, Zeeman AM (2000) Enzyme Microb Technol 26:771–780
- De Deken RH (1966) J Gen Microbiol 44:149–156
- Fabrizio P, Longo VD (2003) Aging Cell 2:73–81
- Faye G, Kujawa C, Fukuhara H (1974) J Mol Biol 88:185–203
- Ferranti R, da Silva MM, Kowaltowski AJ (2003) FEBS Lett 536:51–55
- Gancedo JM (1998) Microbiol Mol Biol Rev 62:334–361
- Jiang JC, Jaruga E, Repnevskaya MV, Jazwinski SM (2000) FASEB J 14:2135–2137
- Kaeberlein M, Hu D, Kerr EO, Tsuchiya M, Westman EA, Dang N, Fields S, Kennedy BK (2005) PLoS Genet 1:e69
- Kurosu H, Yamamoto M, Clark JD, Pastor JV, Nandi A, Gurnani P, McGuinness OP, Chikuda H, Yamaguchi M, Kawaguchi H, Shimomura I, Takayama Y, Herz J, Kahn CR, Rosenblatt KP, Kuro-o M (2005) Science 309:1829–1833
- Lambert AJ, Merry BJ (2004) Am J Physiol Regul Integr Comp Physiol 286:R71–R79
- Lin SJ, Guarente L (2003) Curr Opin Cell Biol 15:241–246
- Lin SJ, Defossez PA, Guarente L (2000) Science 289:2126–2128
- Lin SJ, Kaeberlein M, Andalis AA, Sturtz LA, Defossez PA, Culotta VC, Fink GR, Guarente L (2002) Nature 418:344–348
- Partridge L, Gems D (2002) Nature Rev Genet 3:165–175
- Rodríguez C, Gancedo JM (1999) Mol Cell Biol Res Commun 1:52–58
- Sinclair D, Mills K, Guarente L (1998) Ann Rev Microbiol 52:533–560
- Smith DL, McClure JM, Matecic M, Smith JS (2007) Aging Cell 6:649–662
- Tahara EB, Barros MH, Oliveira GA, Netto LE, Kowaltowski AJ (2007) FASEB J 21:274–283
- Tzagoloff A, Akai A, Needleman RB (1975) J Biol Chem 250:8228–8235
- Weindruch R, Walford RL (1988) The retardation of aging and disease by dietary restriction. Charles C. Thomas, Springfield, IL



Original Contribution

Tissue-, substrate-, and site-specific characteristics of mitochondrial reactive oxygen species generation

Erich B. Tahara, Felipe D.T. Navarete, Alicia J. Kowaltowski*

Departamento de Bioquímica, Instituto de Química, Universidade de São Paulo, São Paulo, SP 05508-900, Brazil

ARTICLE INFO

Article history:

Received 11 November 2008

Revised 29 January 2009

Accepted 5 February 2009

Available online 23 February 2009

Keywords:

Mitochondria

Free radical

Respiration

Oxidative stress

Hydrogen peroxide

Superoxide radical

ABSTRACT

Reactive oxygen species are a by-product of mitochondrial oxidative phosphorylation, derived from a small quantity of superoxide radicals generated during electron transport. We conducted a comprehensive and quantitative study of oxygen consumption, inner membrane potentials, and H_2O_2 release in mitochondria isolated from rat brain, heart, kidney, liver, and skeletal muscle, using various respiratory substrates (α -ketoglutarate, glutamate, succinate, glycerol phosphate, and palmitoyl carnitine). The locations and properties of reactive oxygen species formation were determined using oxidative phosphorylation and the respiratory chain modulators oligomycin, rotenone, myxothiazol, and antimycin A and the uncoupler CCCP. We found that in mitochondria isolated from most tissues incubated under physiologically relevant conditions, reactive oxygen release accounts for 0.1–0.2% of O_2 consumed. Our findings support an important participation of flavoenzymes and complex III and a substantial role for reverse electron transport to complex I as reactive oxygen species sources. Our results also indicate that succinate is an important substrate for isolated mitochondrial reactive oxygen production in brain, heart, kidney, and skeletal muscle, whereas fatty acids generate significant quantities of oxidants in kidney and liver. Finally, we found that increasing respiratory rates is an effective way to prevent mitochondrial oxidant release under many, but not all, conditions. Altogether, our data uncover and quantify many tissue-, substrate-, and site-specific characteristics of mitochondrial ROS release.

© 2009 Elsevier Inc. All rights reserved.

Mitochondria are the central executioners of energy metabolism, in charge of the vast majority of ATP synthesis driven by the catabolism of carbohydrates, proteins, and lipids. As a result, these organelles are responsible for a large number of oxidation-reduction reactions, carried out in a step-wise fashion to maximize energy conservation. The final result of these reactions is the reduction of oxygen to water in four one-electron steps. These oxidation-reduction reactions are coupled to ATP synthesis by the mitochondrial proton electrochemical potential gradient [1].

About 40 years ago, clear evidence was presented that a side effect of ATP synthesis through oxidative phosphorylation in mitochondria is the generation of reactive oxygen species (ROS). Although hampered by less sensitive methods than those available today, these early studies were surprisingly detailed and pertinent [2–11], demonstrating that the primary ROS produced in mitochondria is the superoxide radical anion (O_2^-), owing to the monoelectronic reduc-

tion of O_2 , whereas the main ROS released from mitochondria is membrane-permeable hydrogen peroxide (H_2O_2), produced by dismutation catalyzed by superoxide dismutase (SOD) [2,7,9,12]. These early studies also indicated that electron transport complexes I and III (see Scheme 1) were important sources of mitochondrial ROS and established that conditions associated with higher respiration, such as enhanced oxidative phosphorylation or use of uncouplers, generally decreased this release [4,5,8,10,11]. Finally, evidence was presented indicating that different substrates lead to distinct rates of ROS formation [3,4].

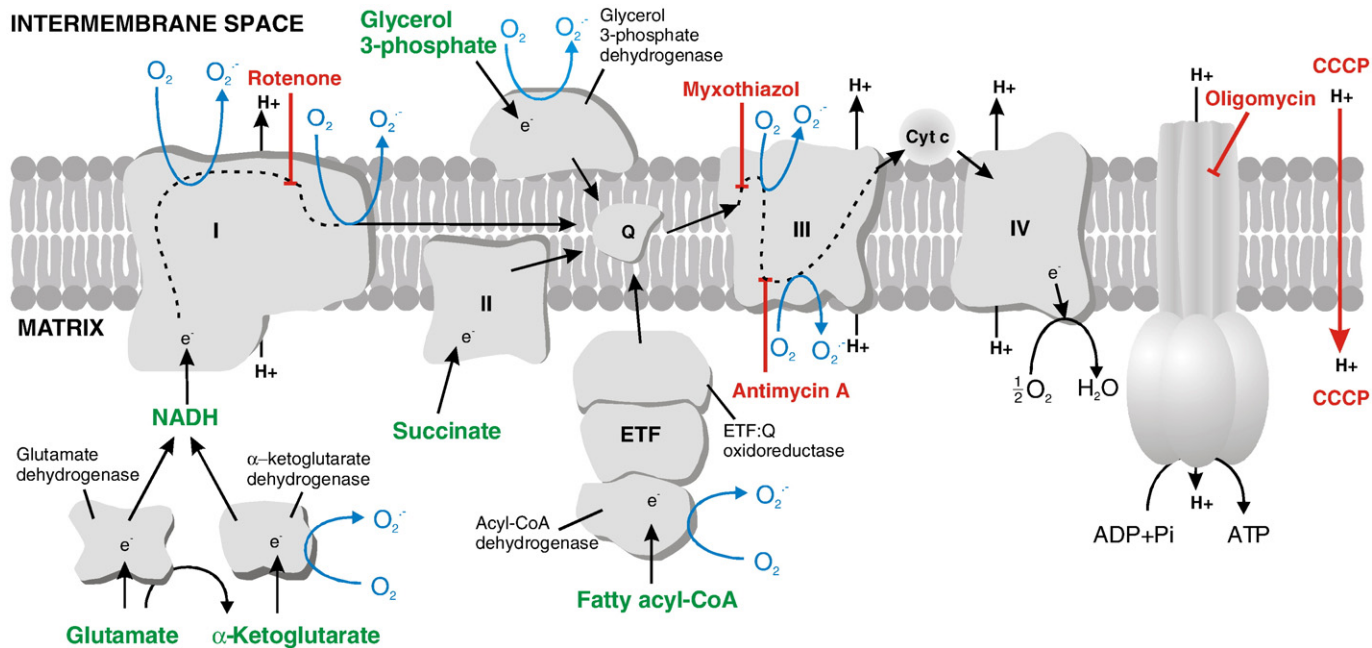
More recent studies added to the understanding of the characteristics of mitochondrial ROS release by pinpointing sites and mechanisms within mitochondrial respiratory complexes I and III that lead to superoxide radical formation [11,13–15]. ROS release from complex I was shown to occur through both forward electron transfer, involving electrons originating from NADH, and reverse electron transfer, involving electrons derived from succinate [15,16]. Experimental support was also presented for the involvement of other mitochondrial enzymes, in particular flavoenzymes such as α -ketoglutarate dehydrogenase and glycerol phosphate dehydrogenase, as important sources of ROS [17–21].

The importance of mitochondrial ROS is clearly illustrated by studies indicating that mitochondrial SOD-knockout animals do not

Abbreviations: α KG, α -ketoglutarate; AA, antimycin A; BSA, bovine serum albumin; CCCP, carbonyl cyanide *m*-chlorophenylhydrazone; ETF, electron-transferring flavoprotein; glut, glutamate; glyc, glycerol phosphate; ΔV , mitochondrial inner membrane potential; myx, myxothiazol; palm, palmitoyl carnitine; ROS, reactive oxygen species; rot, rotenone; succ, succinate; SOD, superoxide dismutase; O_2^- , superoxide radical anion.

* Corresponding author. Fax: +55 11 38155579.

E-mail address: alicia@iq.usp.br (A.J. Kowaltowski).



Scheme 1. Mitochondrial substrate metabolism, respiratory chain organization, electron leakage sites, and effects of respiratory modulators.

survive unless treated with a SOD mimetic [22]. Furthermore, decreasing ROS generation by uncoupling mitochondria or targeting catalase to this organelle increases longevity in healthy animals [23,24]. Indeed, there is an inverse correlation between life span in specific species and the rate of ROS release [25], strongly supporting a role for mitochondrial ROS as one of the factors limiting life span [25,26]. ROS release from these organelles is a relevant process in many pathological situations and participates in cell damage and death associated with conditions such as heart attack, changes in oxygen tension, diabetes, cancer, and neurodegeneration (for a comprehensive review, see [27]). In addition to acting as damaging molecules, moderate amounts of mitochondrial ROS can act as signaling intermediates activating protective pathways such as those involved in ischemic preconditioning [28,29]. ROS formation by mitochondria may also participate in physiological redox regulation, by activating mild mitochondrial uncoupling pathways that, in turn, decrease ROS release [30,31].

Despite the gain in knowledge regarding the mechanisms of generation, functions, and consequences of mitochondrial ROS, there is still uncertainty in the literature regarding specific characteristics of this release. Points to be clarified or detailed include the quantity of ROS formed, which sites of this formation are most relevant under selected conditions, tissue-specific characteristics, and how substrates and respiratory states affect ROS formation. In this sense, significant differences observed in the literature may be explained by differences in experimental conditions and organelle isolation processes [16,32–34]. To provide a comprehensive side-by-side study of ROS formation in different tissues, we measured inner membrane potentials ($\Delta\Psi$), O₂ consumption, and H₂O₂ release in mitochondria from rat brain, heart, kidney, liver, and skeletal muscle. ROS release was quantified in various respiratory states, using distinct substrates and respiratory modulators. Our findings indicate many tissue-, substrate-, and site-specific characteristics of mitochondrial ROS formation.

Experimental procedures

Materials

Chemicals were purchased at analytical purity grade or better, mostly from Sigma-Aldrich. Safranin O, horseradish peroxidase (type

I), and palmitoyl carnitine stock solutions were prepared in deionized water, while Amplex Red (Invitrogen), rotenone, myxothiazol, antimycin A, and CCCP stock solutions were prepared in dimethyl sulfoxide. ADP, α-ketoglutarate, glutamate, succinate, and glycerol phosphate solutions were prepared in deionized water and buffered to pH 7.2 using KOH. All stock solutions were kept frozen until just before use.

Mitochondrial isolation

Experiments were approved by the local *Comitê de Ética em Cuidados e Uso Animal* and follow NIH guidelines. Adult, 3-month-old, male Sprague-Dawley rats bred and lodged at the *Biotério de Produção e Experimentação da Faculdade de Ciências Farmacêuticas e Instituto de Química* were used. Methodology was selected for each tissue to yield the best purity and respiratory control ratios at 37°C (see Table 1). All preparations were performed over ice.

Liver mitochondria

Liver mitochondria [35] were isolated from fasted rats. The organ was minced finely and washed with 4°C isolation buffer [250 mM sucrose, 10 mM Hepes, 1 mM EGTA (pH 7.2, KOH)] and homogenized with a 40-ml tissue grinder. The suspension was centrifuged at 600 g

Table 1
Respiratory rates and respiratory control ratios

	State 3	State 4	RCR
Brain	100.2 ± 27.6	19.2 ± 3.9	5.06 ± 0.41
Heart	147.8 ± 17.0	14.7 ± 2.7	10.49 ± 0.57
Kidney	202.3 ± 27.2	44.1 ± 8.2	5.01 ± 0.40
Liver	105.7 ± 29.7	22.7 ± 1.6	4.65 ± 1.30
Muscle	108.0 ± 17.2	24.7 ± 7.7	5.77 ± 1.01

Mitochondria (0.50 mg protein/ml) were incubated in experimental buffer (see Experimental procedures) at 37°C. Succinate (1 mM) was used as respiratory substrate for kidney and liver, 1 mM glutamate for heart and skeletal muscle, and 1 mM malate plus 1 mM glutamate for brain. ADP (1 mM) was added to induce State 3 respiratory rates (shown in nmol O₂ mg⁻¹ min⁻¹). A subsequent addition of oligomycin (at quantities indicated in Table 2) was used to determine State 4 rates. Respiratory control ratios (RCR) were calculated by dividing State 3 by State 4.

Table 2

Quantities of mitochondrial modulators used

Tissue	Modulator				
	Oligomycin (μ g)	Rotenone (nmol)	Myxothiazol (nmol)	Antimycin A (μ g)	CCCP (nmol)
Brain	6.25	1.00	1.50	0.40	0.30
Heart	5.00	4.00	2.00	0.30	0.80
Kidney	5.00	8.00	1.50	0.20	0.80
Liver	1.00	0.80	0.40	0.15	0.40
Muscle	1.00	0.50	1.00	0.75	0.50

Mitochondria (0.50 mg protein) were incubated in 1 ml of medium as described for Table 1. Minimal quantities of respiratory modulators necessary to obtain maximal respiratory changes per mg protein were measured using 1 mM succinate as a substrate for mitochondria from heart, kidney, and liver, except for rotenone titrations, for which 1 mM malate plus 1 mM glutamate was used. Brain mitochondria were energized with 1 mM malate plus 1 mM glutamate, and skeletal muscle mitochondria were energized with 1 mM α -ketoglutarate for all titrations. Antimycin A, myxothiazol, rotenone, and oligomycin were added to mitochondria in the presence of 1 mM ADP to induce State 3 respiration. CCCP was added to State 4 mitochondria treated with oligomycin at the quantity determined for each tissue.

for 5 min. The resulting supernatant was centrifuged at 12,000 g for 10 min. The pellet was washed and the final mitochondrial pellet was resuspended in a minimal volume of isolation buffer.

Kidney mitochondria

Kidney mitochondria were isolated using the same protocol as for liver, from nonfasted rats, using a 15-ml tissue grinder.

Heart mitochondria

Heart mitochondria [36] were isolated in 300 mM sucrose, 10 mM Hepes, 2 mM EGTA (pH 7.2, KOH), at 4°C. The tissue was minced in the presence of 0.5 mg of type I protease (bovine pancreas) to release mitochondria from within muscle fibers and later washed in the same buffer in the presence of 1 mg/ml BSA. The suspension was homogenized in a 40-ml tissue grinder and centrifuged at 800 g for 5 min. The resulting supernatant was centrifuged at 9500 g for 10 min. The mitochondrial pellet was washed and the final pellet was resuspended in a minimal volume of isolation buffer.

Brain mitochondria

Brain mitochondria were isolated as described by Andreyev and Fiskum [37]. This preparation uses digitonin to release mitochondria from synaptosomes and results in a mixture of synaptosomal and nonsynaptosomal mitochondria, with no detectable lactate dehydrogenase activity [37–40]. It should be noted that, because digitonin interacts with cholesterol, which is not abundant in mitochondria, it

does not alter mitochondrial membrane integrity at the concentrations used [41]. Rat brains were finely minced and washed with 125 mM sucrose, 250 mM mannitol, 10 mM Hepes, 10 mM EGTA, 0.01% BSA (pH 7.2, KOH), at 4°C. Protease (0.5 mg) was added and the preparation was transferred to a 15-ml tissue grinder and homogenized. The homogenate was centrifuged at 2000 g for 3 min. The supernatant was transferred to a clean tube and centrifuged at 12,000 g for 8 min. The pellet was treated with 20 μ l of 10% digitonin and centrifuged at 12,000 g for 8 min. The resulting mitochondrial pellet was resuspended in a minimal volume of isolation buffer devoid of EGTA.

Skeletal muscle mitochondria

Skeletal muscle mitochondria were isolated from rat hind limbs as described in [42], with some modifications. Hind-limb muscles were dissected in iced 10 mM Na⁺-EDTA-supplemented PBS to remove fatty and connective tissues and then washed and finely minced in 300 mM sucrose, 50 mM Hepes, 10 mM Tris, 1 mM EGTA, and 0.2% BSA (pH 7.2, HCl), at 4°C. The tissue was processed for 2 s with a Polytron homogenizer and then transferred to a mechanized potter and homogenized. The suspension was centrifuged at 850 g for 3 min, and the supernatant was centrifuged again at 10,000 g for 5 min. The pellet was resuspended and centrifuged at 7000 g for 3 min. The final mitochondrial pellet was resuspended in a minimal volume of isolation buffer.

The quality of the preparations was assessed by conducting measurements of respiratory control ratios (State 3/State 4, Table 1). It should be noted that State 4 respiratory rates calculated in the presence of added ADP plus oligomycin such as those shown in Table 1 are lower than those measured in mitochondria incubated with oligomycin alone (as in other data in this article) because ADP and ATP synthesized by mitochondria inhibit naturally occurring mild uncoupling pathways such as uncoupling proteins and the ATP-sensitive K⁺ channel [30,31,43,44]. All preparations were kept over ice and used within 4 h. Protein quantification was conducted using the Lowry method [45].

Mitochondrial H₂O₂ release

Mitochondrial H₂O₂ release was measured in 0.125 or 0.25 mg protein/ml mitochondrial suspensions in experimental buffer [125 mM sucrose and 65 mM KCl (or 150 KCl for brain), 10 mM Hepes, 2 mM inorganic phosphate, 2 mM MgCl₂, and 0.01% bovine serum albumin (or 0.1% for brain), adjusted to pH 7.2 with KOH], at 37°C, with continuous stirring. Amplex Red (25 μ M) oxidation was

Table 3Tissue and substrate-specific mitochondrial O₂ consumption rates and $\Delta\Psi$

Tissue	Substrate				
	α -Ketoglutarate	Glutamate	Succinate	Glycerol phosphate	Palmitoyl carnitine
Brain					
O ₂ (nmol mg ⁻¹ min ⁻¹)	19.2 ± 3.3	23.3 ± 2.4	60.7 ± 8.3	11.1 ± 0.1	12.4 ± 2.8
$\Delta\Psi$ (mV)	194.7 ± 16.1	192.5 ± 14.3	198.5 ± 15.7	180.1 ± 24.1	144.1 ± 12.0
Heart					
O ₂ (nmol mg ⁻¹ min ⁻¹)	26.8 ± 4.7	32.1 ± 4.5	61.3 ± 6.6	19.0 ± 1.5	29.9 ± 1.4
$\Delta\Psi$ (mV)	148.2 ± 13.4	157.4 ± 10.8	164.3 ± 8.7	146.3 ± 14.3	134.2 ± 15.6
Kidney					
O ₂ (nmol mg ⁻¹ min ⁻¹)	29.4 ± 3.3	23.9 ± 2.4	84.8 ± 8.9	22.6 ± 1.6	48.0 ± 2.0
$\Delta\Psi$ (mV)	146.3 ± 3.3	147.1 ± 4.4	182.5 ± 5.9	147.1 ± 3.1	120.9 ± 19.6
Liver					
O ₂ (nmol mg ⁻¹ min ⁻¹)	22.2 ± 2.0	28.8 ± 2.3	39.9 ± 4.4	16.4 ± 2.6	17.6 ± 2.4
$\Delta\Psi$ (mV)	124.2 ± 5.3	117.8 ± 9.4	186.8 ± 18.5	153.1 ± 16.2	65.4 ± 16.3
Muscle					
O ₂ (nmol mg ⁻¹ min ⁻¹)	34.5 ± 6.6	24.7 ± 7.7	36.4 ± 3.4	18.5 ± 1.3	24.0 ± 3.9
$\Delta\Psi$ (mV)	171.8 ± 4.7	166.9 ± 4.6	189.1 ± 2.4	184.8 ± 5.2	126.9 ± 8.9

O₂ consumption rates and $\Delta\Psi$ were measured as described under Experimental Procedures in the medium used in experiments shown in Table 1, supplemented with oligomycin, at quantities described in Table 2, to induce State 4 respiration. Substrates used were α -ketoglutarate, glutamate, succinate, and glycerol phosphate (1 mM each) or palmitoyl carnitine (50 μ M), as indicated.

followed in the presence of 0.5 U/ml horseradish peroxidase and using α -ketoglutarate, glutamate, succinate, glycerol phosphate (1 mM of each), or palmitoyl carnitine (50 μ M) as substrate. In most experiments (excluding those conducted in State 3), oligomycin was present at the concentrations shown in Table 2. Amplex Red is oxidized in the presence of extramitochondrial horseradish peroxidase bound to H_2O_2 , generating resorufin, which can be detected fluorimetrically using a fluorescence spectrophotometer operating at 563 nm of excitation and 587 nm of emission. This technique displays good signal/noise ratios and little artifactual interference and has recently been widely accepted by researchers in the area [13,19,31,46–48]. Indeed, controls conducted in the absence of mitochondria or in the absence of peroxidase indicate that nonspecific probe oxidation is negligible (<1% of the increment observed in the presence of mitochondria and peroxidase). In addition, fluorescence increments are largely suppressed (>90%) in the presence of added catalase, indicating the response is mostly due to H_2O_2 formation. Furthermore, responses were not influenced by the addition of any of the substrates or respiratory inhibitors used in this study (results not shown). Calibration was conducted by adding H_2O_2 at known concentrations ($A_{240} = 43.6 \text{ M}^{-1} \text{ cm}^{-1}$).

Mitochondrial O_2 consumption

Mitochondrial O_2 consumption was monitored in 0.25 or 0.5 mg mitochondrial protein/ml suspension under the same conditions as H_2O_2 release measurements using a computer-interfaced Clark-type electrode operating with continuous stirring at 37°C.

Mitochondrial inner membrane potential measurements

Mitochondrial $\Delta\Psi$ was estimated through fluorescence changes of 5 μ M safranin O at excitation and emission wavelengths of 485 and

586 nm, respectively, at 37°C and with continuous stirring, as described in Ref. [49]. Incubation conditions were the same as for H_2O_2 release measurements. Data obtained were calibrated using a K^+ gradient [49,50]. The $\Delta\Psi$ value obtained for each K^+ concentration was determined using the Nernst equation, assuming intramitochondrial $[K^+]$ to be 150 mM [49], and plotted against measured fluorescence values to generate a calibration curve for each tissue. It should be noted that errors in the estimated concentrations of intramitochondrial K^+ do not substantially alter calculated $\Delta\Psi$ values [50,51].

Statistical analysis

Data are represented as averages \pm SEM of 3–18 repetitions using distinct preparations. Multiple comparisons were performed using one-way ANOVA followed by Tukey multiple comparison test against all data sets for Figs. 1 and 2 or Dunnett's multiple comparison test against the control column for Figs. 3–7. Pair comparisons between H_2O_2/O_2 release rates in control and CCCP-treated mitochondria in Figs. 3–7 were conducted using Student's *t* test. All comparisons were performed using GraphPad Prism software.

Results

Titration of electron transport chain and oxidative phosphorylation modulators

Because our aim was to conduct a systematic analysis of mitochondrial ROS release, special care was taken with specific methodological aspects, to avoid results lacking technical precision. The quality of isolated mitochondrial preparations was assessed by conducting respiratory control ratio measurements in all tissues to ensure that highly coupled preparations were obtained (Table 1).

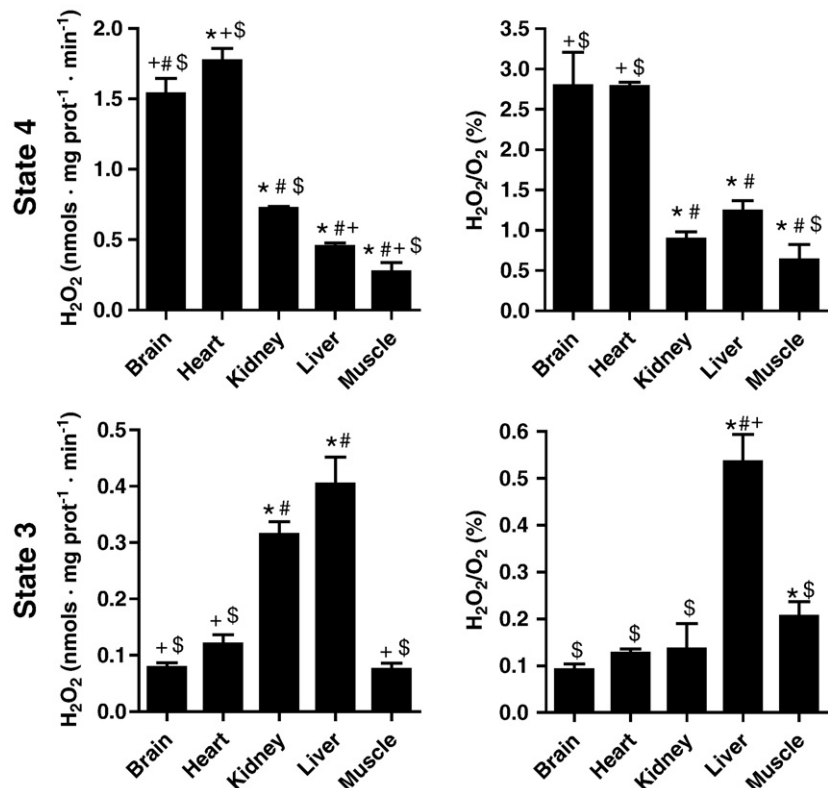


Fig. 1. Tissue- and state-dependent H_2O_2 release. Measurements of H_2O_2 release and O_2 consumption were performed in succinate-energized mitochondria as described under Experimental procedures under conditions described in Table 1, in the presence of oligomycin (in quantities determined in Table 2, State 4) or 1 mM ADP (State 3). * p <0.05 vs brain; $+p$ <0.05 vs heart; $#p$ <0.05 vs kidney, $$p$ <0.05 vs liver.

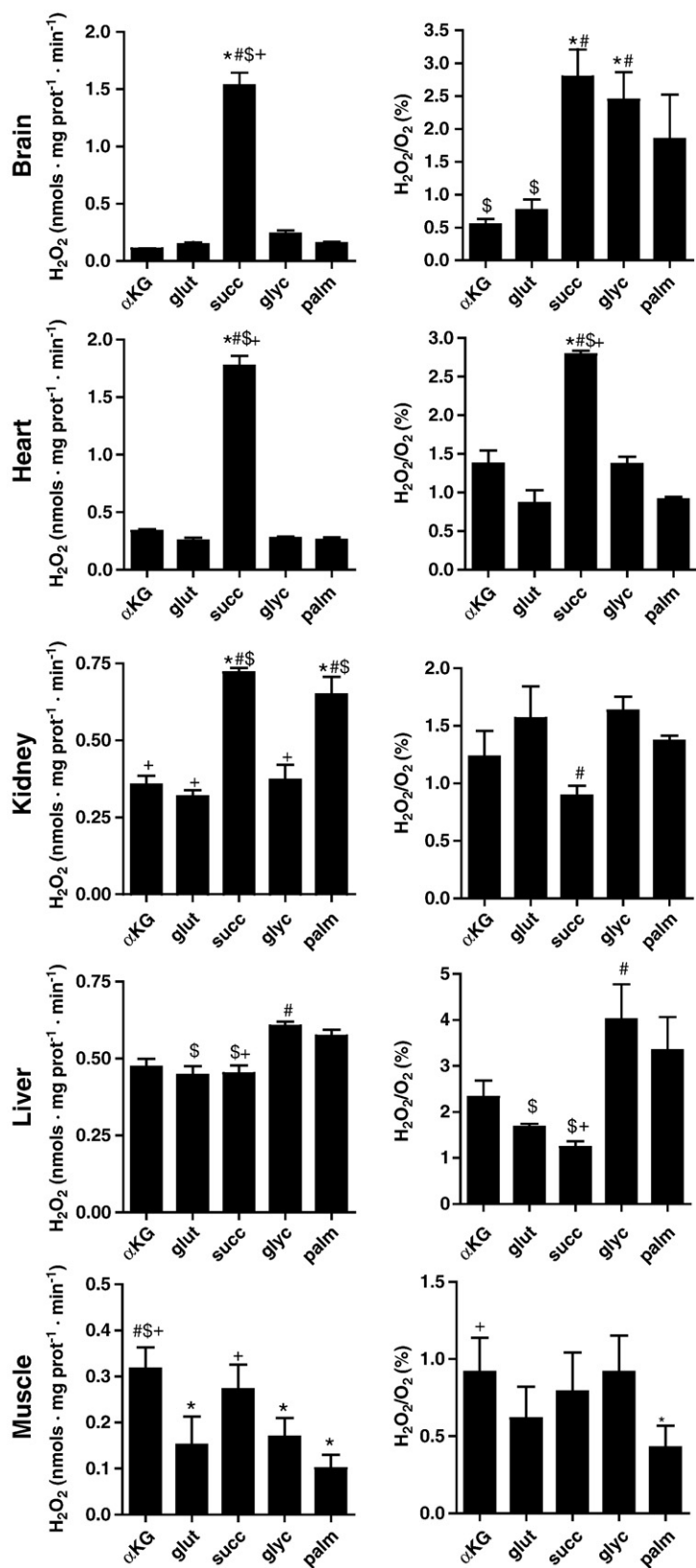


Fig. 2. Substrate-dependent H_2O_2 release. Measurements of H_2O_2 release and O_2 consumption were performed as described under Experimental procedures under conditions described in Table 1 using α -ketoglutarate (αKG), glutamate (glut), succinate (succ), glycerol phosphate (glyc), or palmitoyl carnitine (palm) as substrate. * $p<0.05$ vs αKG ; # $p<0.05$ vs glut; \$ $p<0.05$ vs glyc; + $p<0.05$ vs palm.

Furthermore, the use of appropriate concentrations of respiratory chain modulators was considered vital, because excessive quantities of these modulators promote nonspecific effects. Thus, we performed

electron transport chain and oxidative phosphorylation modulator titration to use the minimal effective quantities of these compounds during experiments (Table 2).

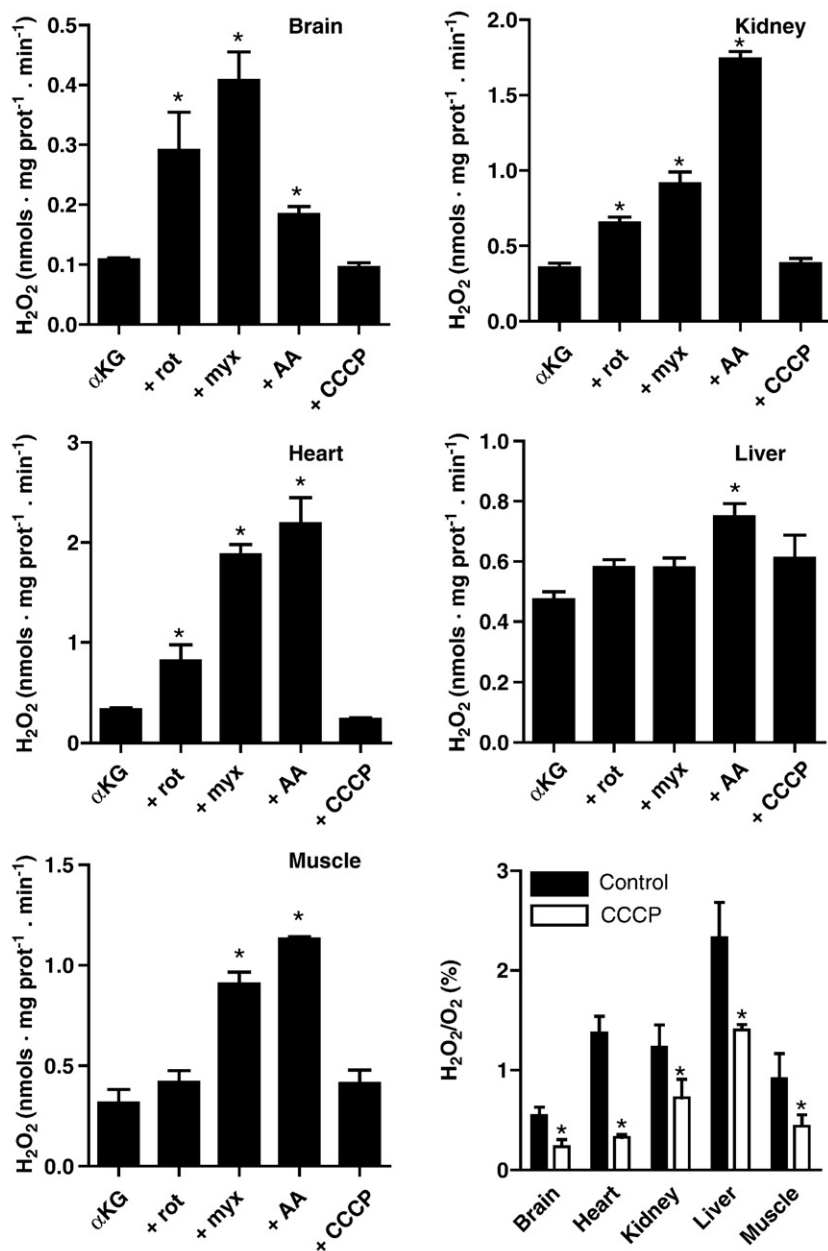


Fig. 3. α -Ketoglutarate-induced H_2O_2 release. Measurements of H_2O_2 release and O_2 consumption were performed as described under Experimental procedures under conditions described in Table 1, using α -ketoglutarate as a substrate in the presence of rotenone (rot), myxothiazol (myx), antimycin A (AA), or carbonyl cyanide *m*-chlorophenylhydrazone (CCCP), as shown, in quantities depicted in Table 2. * $p < 0.05$ vs αKG .

The respiratory inhibitors antimycin A, myxothiazol, and rotenone, as well as ATP synthase inhibitor oligomycin (see Scheme 1), were titrated to mitochondria in which respiration was stimulated by ADP (Respiratory State 3). The uncoupler CCCP was added to mitochondria in which ATP synthesis was inhibited by oligomycin (Respiratory State 4). Oxygen consumption traces were followed (results not shown), and the minimal quantity of each modulator capable of promoting the maximal respiratory alteration was established for each tissue (Table 2). Interestingly, quantities of respiratory modulators necessary varied substantially between the tissues tested. Notably, liver required smaller quantities of protein-targeted modulators, probably because these mitochondria contain a relatively larger proportion of proteins unrelated to electron transport and oxidative phosphorylation [52,53], owing to intense amino acid metabolism and carbohydrate synthesis activity in this tissue.

O_2 consumption and $\Delta\Psi$

Mitochondrial ROS release has been strongly associated with changes in O_2 consumption rates and $\Delta\Psi$ [23,44,54]. Oxygen consumption rates establish the turnover of electrons and redox state of electron transport chain components, which determine the ability to generate O_2^- at different respiratory chain sites. $\Delta\Psi$ determines the energy barrier for electron transport and is thus also intimately related to both respiratory rates and the formation of mitochondrial ROS. We quantified (Table 3) O_2 consumption and $\Delta\Psi$ in State 4 mitochondria from brain, heart, kidney, liver, and skeletal muscle in the presence of α -ketoglutarate, a citric acid cycle intermediate that primarily generates NADH (leading to reduction of mitochondrial complex I); the amino acid glutamate (which generates NADH and α -ketoglutarate); the citric acid intermediate succinate (which donates electrons to FAD-containing complex II of

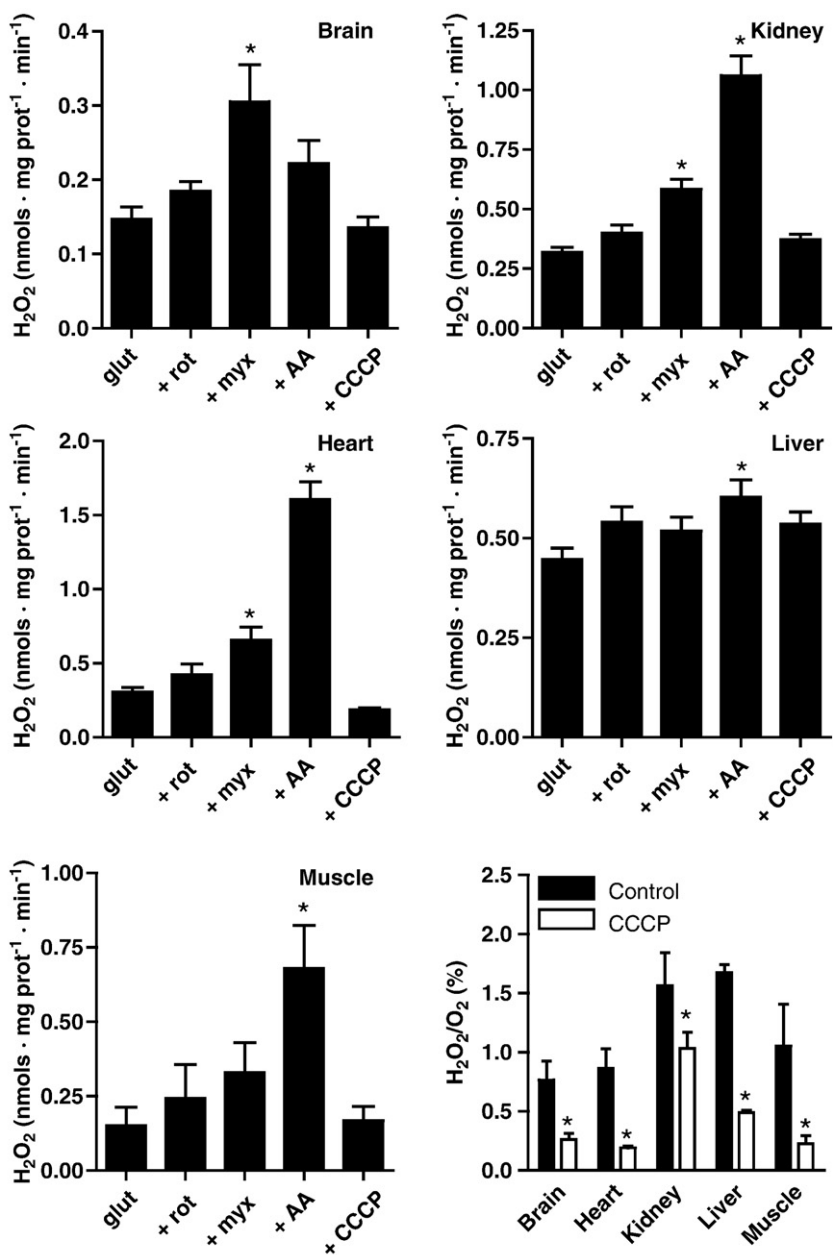


Fig. 4. Glutamate-induced H₂O₂ release. Measurements of H₂O₂ release and O₂ consumption were performed as described under Experimental procedures under conditions described in Table 1, using glutamate as a substrate in the presence of rot, myx, AA, or CCCP, as shown, in quantities depicted in Table 2. *p<0.05 vs glut.

the electron transport chain); glycerol phosphate (which reduces mitochondrial coenzyme Q via the flavoenzyme glycerol phosphate dehydrogenase); and the activated fatty acid palmitoyl carnitine (which primarily reduces coenzyme Q via the electron-transferring flavoprotein) (see Scheme 1). In preliminary experiments, pyruvate was also used as a NADH-linked substrate; however, respiratory rates obtained by the use of this substrate in isolation in many tissues were lower than necessary for adequate oxidative phosphorylation (results not shown).

We found that the highest ΔΨ was obtained in most tissues using succinate as a substrate, although associated O₂ consumption rates were understandably faster than those observed using the NADH-linked substrates α-ketoglutarate and glutamate, which allow proton pumping also at the level of complex I. Palmitoyl carnitine generated the lowest ΔΨs, possibly because free fatty acids are effective mitochondrial uncouplers and may be present in minimal quantities

in our substrate stock [55,56]. Indeed, care was taken in this study to use concentrations of this substrate that supported oxygen consumption and the formation of ΔΨ but did not promote overt mitochondrial uncoupling. Brain mitochondria do not utilize fatty acids as substrates, which may justify the poor respiratory rates observed with palmitate in this tissue. The use of palmitoyl CoA in the presence of added carnitine did not present any experimental differences relative to the use of palmitoyl carnitine (results not shown). Liver and heart mitochondria presented the lowest ΔΨ formation with most substrates, whereas kidney mitochondria presented the highest O₂ consumption rates, as has been described previously [43].

Altogether, O₂ consumption and ΔΨ measurements determined tissue- and substrate-specific characteristics, which correlate with changes in mitochondrial ROS release described in the following experiments.

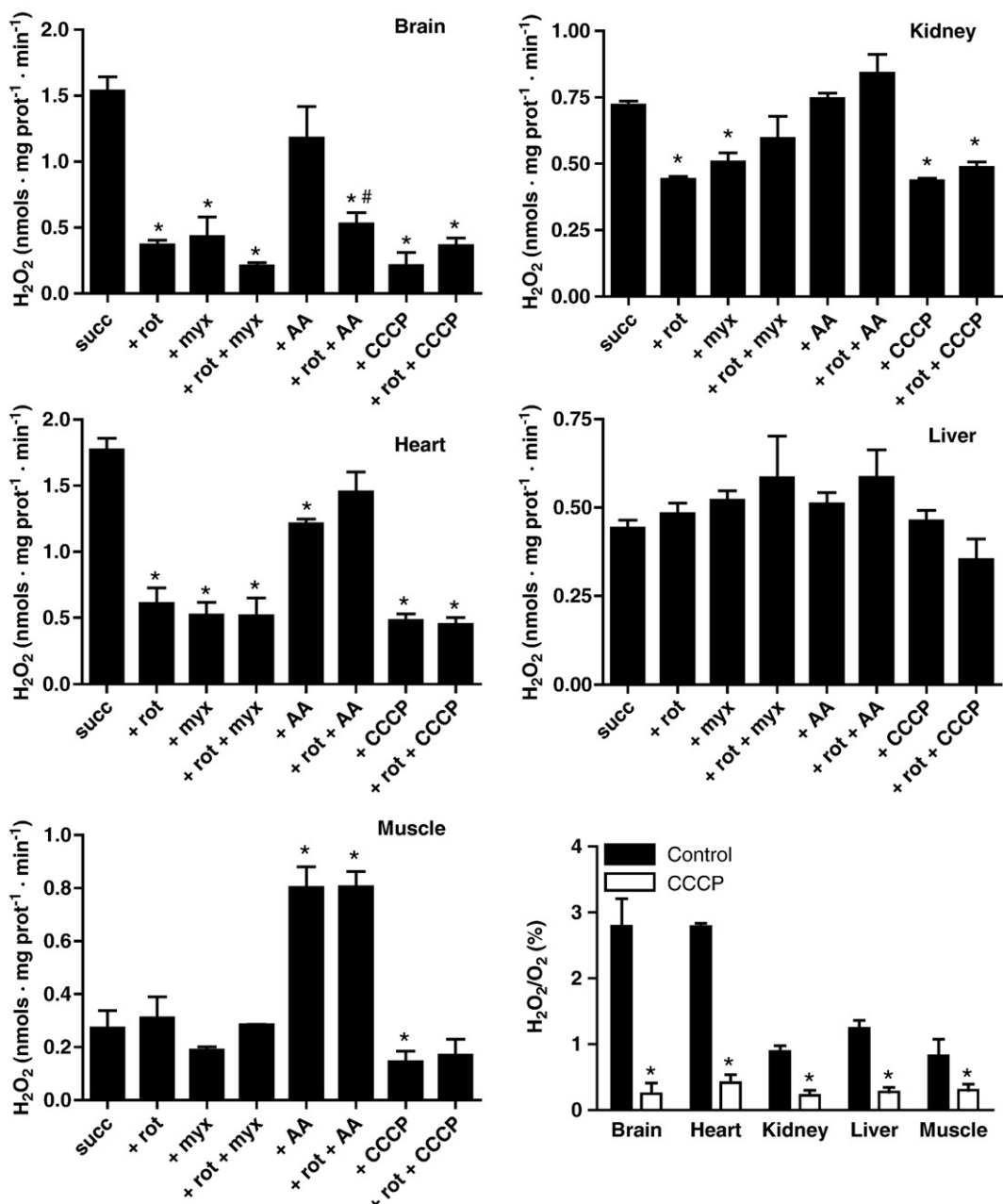


Fig. 5. Succinate-induced H_2O_2 release. Measurements of H_2O_2 release and O_2 consumption were performed as described under Experimental procedures under conditions described in Table 1, using succinate as a substrate in the presence of rot, myx, AA, or CCCP, as shown, in quantities depicted in Table 2. * $p<0.05$ vs succ; # $p<0.05$ vs +AA.

Mitochondrial H_2O_2 release—effect of respiratory states

Fig. 1 compares absolute (H_2O_2) and relative ($\text{H}_2\text{O}_2/\text{O}_2$) ROS release from mitochondria isolated from the various tissues respiring on succinate. The highest absolute H_2O_2 release rates observed were in the range of $1.5 \text{ nmol mg protein}^{-1} \text{ min}^{-1}$ in State 4 from brain and heart, corresponding to almost 3% of oxygen consumption under these conditions. These high rates of ROS release are probably, however, rarely observed in vivo, because ROS release varies strongly with the respiratory state. In State 3, H_2O_2 release was under $0.2 \text{ nmol mg protein}^{-1} \text{ min}^{-1}$ in brain, heart, and skeletal muscle and under $0.5 \text{ nmol mg protein}^{-1} \text{ min}^{-1}$ in kidney and liver. Interestingly, kidney and liver present both lower ROS production rates in State 4 and a smaller decrease in these rates when in State 3. $\text{H}_2\text{O}_2/\text{O}_2$ ratios

in Respiratory State 3 were on the order of 0.1–0.2% for brain, heart, kidney, and skeletal muscle and 0.5% for liver. Because even small decreases in $\Delta\Psi$ associated with oxidative phosphorylation strongly prevent ROS release [44,54], physiological in vivo levels of oxidant production are probably more closely related to those observed in isolated mitochondria in State 3.

Interestingly, ROS generation rates varied very significantly with the tissue studied. Absolute and relative H_2O_2 release rates in kidney and liver are about half of those observed in brain and heart in State 4, but are at least twice as high in these tissues in State 3. Skeletal muscle mitochondria present low ROS release rates in both State 4 and State 3 compared to other tissues. This indicates that the dynamics of ROS release in different tissues presents particularities that warrant further side-by-side comparisons.

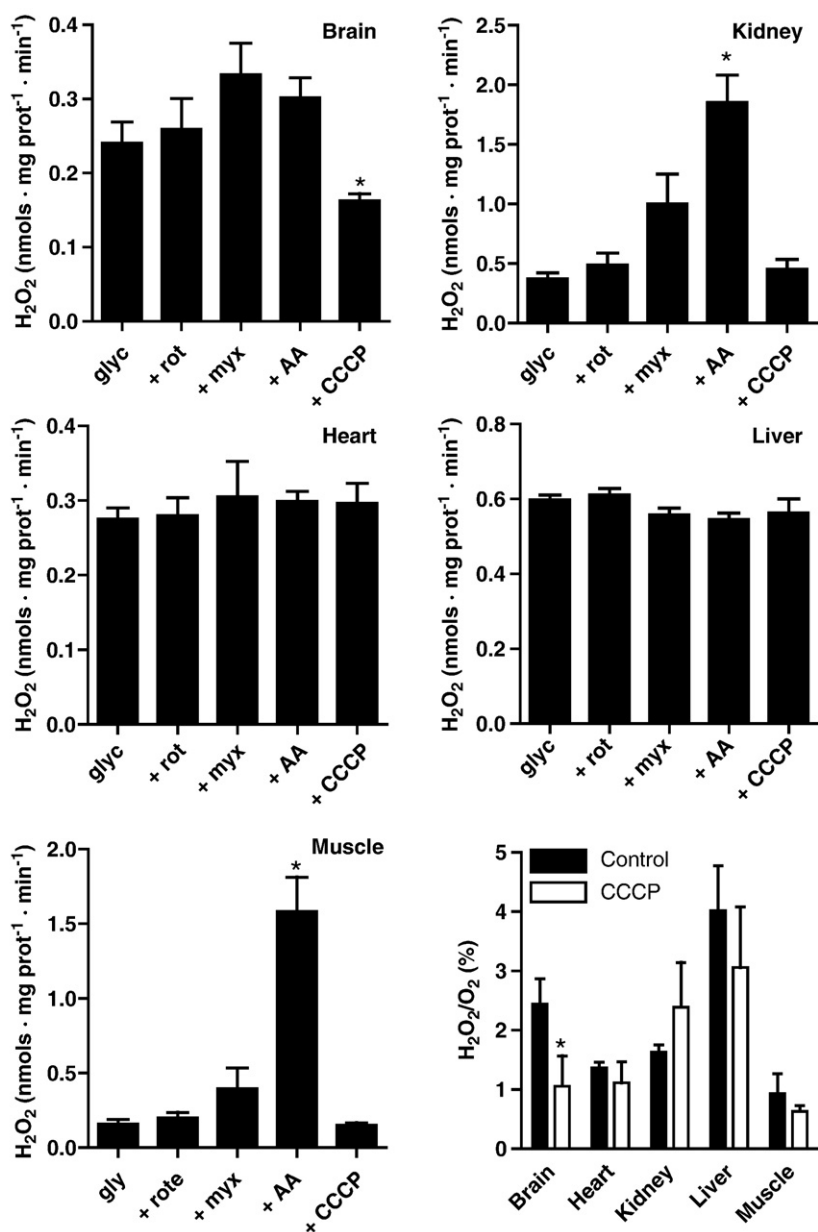


Fig. 6. Glycerol phosphate-induced H₂O₂ release. Measurements of H₂O₂ release and O₂ consumption were performed as described under Experimental Procedures under conditions described in Table 1, using glycerol phosphate as a substrate in the presence of rot, myx, AA, or CCCP, as shown, in quantities depicted in Table 2. *p<0.05 vs glyc.

Mitochondrial H₂O₂ release supported by different substrates

Fig. 2 compares the effects of the various substrates on State 4 ROS release in the tissues assessed. Succinate was the substrate that generally promoted the most significant ROS release rates. In brain and heart, H₂O₂ release supported by succinate was between 5 and 15 times higher than that observed using other substrates. H₂O₂/O₂ ratios in heart and brain respiring on succinate were above 2.0%, whereas those observed in the presence of NADH-linked substrates α-ketoglutarate and glutamate were in the range of 0.5–1.0%. In kidney, succinate promoted high absolute H₂O₂ release, although H₂O₂/O₂ was in the range of 1.0%, owing to the fast respiratory rates in this tissue (Table 3; [43]). Interestingly, succinate did not support ROS release rates higher than those observed with NADH-linked substrates in liver [57], and H₂O₂/O₂ ratios with this substrate were lower than with any other substrate tested, despite robust O₂ consumption (Table 3; [43]). Furthermore, in liver, absolute H₂O₂ release rates generated with NADH-linked substrates were higher than those observed in all

other tissues (note differences in scales). In skeletal muscle, the absolute ROS release rates were highest with α-ketoglutarate and succinate, although relative release was similar for most substrates.

Glycerol phosphate and palmitate are often suggested to be important mitochondrial ROS sources [34,58,59]. Surprisingly, however, we found that these substrates did not promote substantial absolute H₂O₂ release in brain, heart, or skeletal muscle, although H₂O₂/O₂ was high for these substrates in brain. Palmitate promoted substantial H₂O₂ generation in kidney mitochondria, and both palmitate and glycerol phosphate promoted increased H₂O₂ release in liver relative to other substrates studied. These findings are in line with proteomic studies demonstrating that liver mitochondria present higher fatty acid oxidation capacity relative to other tissues [52,53]. Interestingly, palmitate generated the lowest H₂O₂ release rates in skeletal muscle relative to other substrates.

Because succinate, glycerol phosphate, and palmitate primarily reduce FAD, but generate different ROS release patterns, our results, as well as those of others conducted in mouse tissue [33], indicate that

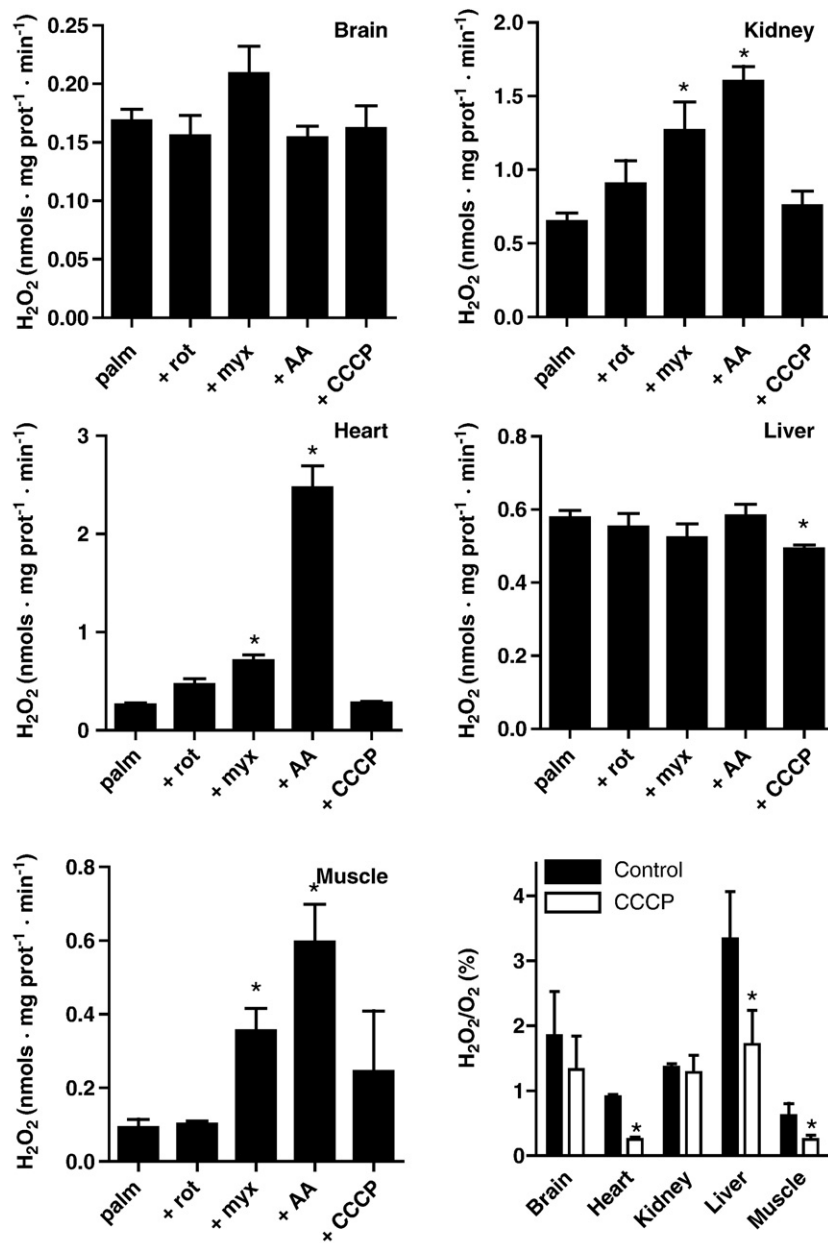


Fig. 7. Palmitoyl carnitine-induced H₂O₂ release. Measurements of H₂O₂ release and O₂ consumption were performed as described under Experimental Procedures under conditions described in Table 1, using glutamate as a substrate in the presence of rot, myx, AA, or CCCP, as shown, in quantities depicted in Table 2. *p<0.05 vs palm.

the tissue-specific generation of mitochondrial oxidants has substrate-specific characteristics that cannot be attributed only to the entry point of electrons into the respiratory chain.

Effects of respiratory inhibition and ΔΨ decreases on mitochondrial H₂O₂ release

Figs. 3 and 4 show the effects of the respiratory inhibitors (see Scheme 1) rotenone (which inhibits complex I), myxothiazol (which inhibits semiquinone formation in complex III), and antimycin A (which promotes semiquinone accumulation in complex III), in addition to the uncoupler CCCP, on mitochondrial ROS generation supported by NADH-linked substrates α-ketoglutarate and glutamate in different tissues. Both substrates promoted similar ROS release patterns. In general, we found that this release was stimulated by the inhibition of electron transport, which leads to more reduced states of complexes I and III, the primary sources of electron leakage at the

respiratory chain [16,34]. The fact that inhibition of complex III led to higher H₂O₂ release rates than inhibition of complex I suggests that ROS formation supported by NADH-linked substrates occurs both upstream and downstream of the inhibitory site of rotenone within complex I. One important site downstream of rotenone inhibition is the semiquinone radical formed during the Q cycle in complex III, which is accumulated upon the addition of antimycin A (see Scheme 1; [16,32]). This site of electron leakage is clearly important in heart, kidney, and skeletal muscle mitochondria, as indicated by the very strong stimulation of ROS formation promoted by antimycin A.

Respiratory enhancement and ΔΨ elimination promoted by the uncoupler CCCP decreased H₂O₂/O₂ ratios in all tissues tested, supporting the notion that mitochondrial uncoupling may preclude oxidant release [44,54,60]. However, absolute H₂O₂ release rates supported by α-ketoglutarate and glutamate were decreased by CCCP only in heart and were even slightly increased in liver. This demonstrates that, despite the prevention of electron leakage by

decreasing $\Delta\Psi$, at very fast respiratory rates promoted by complete mitochondrial uncoupling, total ROS generated may remain unchanged when NADH-linked substrates are used.

Fig. 5 shows the effects of respiratory inhibition and uncoupling on succinate-supported H_2O_2 release. Superoxide radical formation in succinate-energized mitochondria can occur through two mechanisms: electron leakage at complex III or at complex I due to reverse electron transport from succinate dehydrogenase to complex I via coenzyme Q [13,14,16]. Reverse electron transport is stimulated by high $\Delta\Psi$ and a highly reduced complex III and coenzyme Q pool [15,16]. Rotenone, which does not inhibit succinate-supported respiration, inhibits ROS release due to reverse electron transfer [13,15,16]. Indeed, succinate-supported H_2O_2 formation in brain, heart, and kidney was strongly prevented by rotenone, indicating this is a major source of ROS in succinate-energized mitochondria from these tissues. CCCP prevented H_2O_2 release to the same level as rotenone in these tissues, suggesting that the presence of high $\Delta\Psi$ is important for ROS release due to reverse electron transfer. Indeed, CCCP very significantly decreased H_2O_2 and H_2O_2/O_2 in brain and heart, tissues in which this substrate leads to high levels of ROS generation. Liver and skeletal muscle mitochondria did not display a significant decrease in ROS release in the presence of rotenone, suggesting reverse electron transfer is not significant in these tissues. In fact, prior studies have indicated that skeletal muscle mitochondria display reverse electron transfer in a manner strongly dependent on mitochondrial ΔpH [61], which is low under our experimental conditions owing to the addition of physiologically relevant phosphate concentrations.

Myxothiazol, which averts the formation of semiquinone radicals in complex III, also prevented succinate-supported H_2O_2 release in brain, kidney, and heart, probably owing to the decrease in $\Delta\Psi$ associated with respiratory inhibition. On the other hand, antimycin A increases semiquinone radical levels in complex III and can increase ROS formation by this complex [11,13,33,62]. Indeed, in kidney, heart, and skeletal muscle, antimycin A led to ROS release levels higher than those observed with other respiratory inhibitors and that were not significantly prevented by rotenone. In brain, antimycin A also maintained high levels of H_2O_2 release, but this effect was reversed by rotenone, indicating that this release may be attributable to reverse electron flow. Antimycin A can increase reverse electron transfer by fully reducing the Q pool [15].

Liver mitochondria presented a very different pattern of succinate-supported H_2O_2 release. In addition to presenting H_2O_2 release rates similar to those observed with NADH-linked substrates, absolute H_2O_2 production was not significantly altered by any of the respiratory chain modulators tested, although H_2O_2/O_2 ratios were decreased by CCCP. The lack of an effect of rotenone on ROS release in liver mitochondria respiring on succinate indicates that reverse electron transfer is not an important ROS source in this tissue, despite the finding that this tissue displays similar expression of succinate dehydrogenase and complex I [52,53].

Fig. 6 shows the effects of respiratory modulators on H_2O_2 release supported by glycerol phosphate. In general, this substrate in isolation leads to poor respiratory rates (**Table 3**), and absolute H_2O_2 release supported by glycerol phosphate was not substantial in brain, heart, kidney, or skeletal muscle (although H_2O_2/O_2 ratios were relatively high). On the other hand, glycerol phosphate led to high absolute and very high relative H_2O_2 release rates in liver. ROS release supported by glycerol phosphate was not related to reverse electron transfer from glycerol phosphate dehydrogenase to complex I, because rotenone did not inhibit H_2O_2 formation in any tissue. This may be because the glycerol/dihydroxyacetone pair presents a higher oxidation-reduction potential than succinate/fumarate [63]. Alternatively, the organization of respiratory complexes within the mitochondrial inner membrane may create functionally separate pools of coenzyme Q [64], preventing reverse electron transfer from glycerol phosphate,

At least in kidney and skeletal muscle, ROS release in the presence of glycerol phosphate seems to involve complex III, because it is strongly enhanced by antimycin A. In liver, decreased $\Delta\Psi$ promoted by complex III inhibitors or CCCP slightly prevented H_2O_2 release. Interestingly, uncoupling did not affect H_2O_2/O_2 ratios supported by glycerol phosphate in any tissue except brain. This indicates that uncoupling is not an effective mechanism to control ROS generation supported by glycerol phosphate in most tissues [18,65].

Fig. 7 shows the effects of respiratory modulators on palmitate-supported ROS formation. Palmitate primarily generates $FADH_2$ through the activity of mitochondrial acyl-CoA dehydrogenase. Electrons are then transported to the electron transferring flavoprotein (ETF) and reduce coenzyme Q through the activity of ETF: ubiquinone oxidoreductase (**Scheme 1**). Although electrons from palmitate enter the electron transport chain through coenzyme Q, we found that reverse electron transfer is not an important source of palmitate-supported ROS formation, as indicated by the lack of inhibitory effect of rotenone in any tissue (**Fig. 7**). Indeed, rotenone increased H_2O_2 release in heart, possibly owing to accumulation of electrons within complex I from NAD reduced in subsequent steps of palmitate oxidation. Complex III is an important source of ROS formation promoted by palmitate in kidney, heart, and skeletal muscle, as indicated by the strong enhancement of H_2O_2 release promoted by antimycin A. Brain mitochondria do not oxidize fatty acids *in vivo* and presented low respiratory rates and H_2O_2 release in the presence of this substrate. Liver mitochondria displayed high absolute and relative rates of H_2O_2 release in the presence of palmitate, which could be decreased by uncoupling with CCCP.

Discussion

Mitochondria are the major intracellular ROS source in most cell types. These ROS are continuously generated as a by-product of oxidative phosphorylation and have a substantial impact on redox balance. Indeed, enhanced levels of mitochondrial ROS release have been observed and linked to cellular degeneration in several diseases and pathological states and may also act as signaling molecules [26,27]. In addition, ROS derived from mitochondria may lead to oxidative damage of biomolecules that promote some of the characteristics of aging [25–27]. Despite the knowledge that mitochondrial ROS contribute toward degenerative processes under many pathological states, most studies have shown that antioxidant supplementation presents poor (or no) beneficial results [66,67], probably because removing all ROS species from different cellular microenvironments after their formation is an uphill task. Thus, the most effective form of preventing damage associated with mitochondrially generated ROS is to decrease the formation of these species [23,66]. In this sense, a detailed understanding of the processes determining mitochondrial ROS formation, as addressed in this article, is necessary.

The experimental tools currently available allow for measurements of H_2O_2 release from isolated mitochondria, in parallel with other parameters of mitochondrial functionality such oxygen consumption and $\Delta\Psi$, as conducted in this study. Although highly useful owing to their precision, their quantitative nature, and the ability to precisely manipulate experimental conditions, studies using isolated mitochondria have caveats that should be taken into consideration before considering how these reflect *in vivo* mitochondrial ROS release. The first significant difference between studies using isolated mitochondria and *in vivo* conditions is oxygen tension, which is significantly lower in tissues than in mitochondrial suspensions [27,68,69]. A second caveat of isolated mitochondrial experiments is the lack of cellularly originated respiratory modulators and reactants with mitochondrial ROS such as nitric oxide [70,71]. Finally, we must stress that our studies measure H_2O_2 released by mitochondria, and not its production. As a result, differing levels of antioxidants in the

mitochondrial preparations [52,53,57] may influence the levels of ROS measured.

ROS produced by mitochondria originate mostly from O_2^- generated by monoelectronic reduction of O_2 . Cytochrome c oxidase (complex IV), which is responsible for the four-step one-electron reduction of O_2 to H_2O , is highly adapted for this function, and to date no measurable O_2^- release has been detected from this enzyme [21,72]. Cytochrome c is also not a documented ROS source and is, in fact, believed to be an important intracellular antioxidant capable of oxidizing superoxide radicals back to O_2 , as well as removing H_2O_2 [73].

Mitochondrial complex III has been extensively associated with the formation of O_2^- [3,5,7,11,13,32–34,46,74,75]. The formation of ROS by this complex is attributed to the access of molecular oxygen to semiquinone radicals formed during redox cycling within the enzyme. This access occurs primarily at the Qp site, which faces the mitochondrial intermembrane space [1,16,34,46]. Myxothiazol—which prevents the formation of semiquinone radicals—decreases this generation, whereas antimycin A—which enhances semiquinone accumulation at the Qp site—increases ROS formation at the level of complex III. This release is enhanced by antimycin A and decreased by center P inhibitors such as myxothiazol. Alternatively, it has been recently proposed that ROS produced by complex III are stimulated by a partially oxidized Q pool promoted, for example, by partially inhibiting succinate dehydrogenase activity with malonate [13].

In our studies, we found many conditions under which H_2O_2 release was very substantially enhanced by antimycin A, including the use of NADH-linked substrates in heart, kidney, liver, and skeletal muscle (Figs. 3 and 4), glycerol phosphate in kidney and skeletal muscle (Fig. 6), and palmitate in heart, kidney, and skeletal muscle (Fig. 7). As a result, we confirm previous reports that complex III is an important site for ROS formation, with a particular relevance in kidney and skeletal muscle mitochondria. It should be noted that we also found that myxothiazol enhanced ROS release in some circumstances. This enhancement may be related to the maintenance of more reduced electron transport components before complex III and increases in NADH levels [14], as further discussed below. Alternatively, it may be due to the change in redox state of the Q pool within complex III leading to a partially reduced Q pool [13], although this is unlikely because the dose of myxothiazol used promoted total respiratory inhibition (results not shown).

Complex I is the other electron transport chain component most often credited with ROS formation [1,5,10,14,15,27,33,34,52,76]. Electron leakage leading to superoxide radical anion formation at complex I can occur through two mechanisms: forward and reverse electron transfer. Forward transfer involves electrons originating from NADH, which may generate O_2^- at different sites within complex I. The FMN group, low-potential iron-sulfur centers, and Q binding site are often suggested to be sites in which this electron leakage can occur [14]. Rotenone blocks Q binding and maximizes FMN and iron-sulfur center reduction. Indeed, rotenone increases H_2O_2 release promoted by oxidation of the NADH-generating substrates glutamate and α -ketoglutarate (Figs. 3 and 4), confirming that sites upstream of its inhibitory action are important for ROS formation.

Interestingly, myxothiazol also promoted increments in H_2O_2 release supported by NADH-linked substrates, often more substantial than rotenone (Figs. 3 and 4). Myxothiazol is a complex III inhibitor that at higher concentrations can also inhibit Q binding at complex I [14]. Because we titrated the minimal doses necessary of these modulators, myxothiazol effects are expected to be predominantly an inhibition of complex III under our conditions, avoiding semiquinone reduction and ROS formation at this level, although partial complex I inhibitions cannot be excluded. The enhanced levels of ROS production observed with this inhibitor suggest substantial electron leakage

upstream of its inhibitory site in complex III, probably at the Q binding site in complex I, because the effects were more pronounced than those observed with rotenone. Altogether, our results support previous work suggesting that two distinct electron leakage sites exist within complex I, one upstream of the rotenone inhibitory site and another within the Q binding site, probably involving semiquinone radicals [14] (see Scheme 1).

Reverse electron transfer occurs when electrons derived from succinate are transported via complex II to coenzyme Q and then to complex I, where electron leakage generating O_2^- occurs. This form of ROS formation takes place when $\Delta\Psi$ is high or electron transport upstream of complex II is blocked, thermodynamically allowing reverse electron transfer [15,16]. We found that the use of succinate as a substrate generated very significant amounts of H_2O_2 in many of the tissues studied (Fig. 2) [57]. Indeed, H_2O_2 release rates supported by succinate were more than 10 times higher in brain and close to 5 times higher in heart compared to those observed with other substrates. Relative H_2O_2 release rates with succinate in State 4 mitochondria from heart and brain reached almost 2% of oxygen consumed (Figs. 2, upper right, and 5, lower right), indicating very substantial ROS formation. Interestingly, succinate did not lead to higher levels of H_2O_2 release in liver and was the substrate that led to the lowest H_2O_2/O_2 ratio in this tissue (Fig. 2, lower right). Indeed, reverse electron transfer is not an important ROS source in liver, as indicated by the lack of effect of rotenone on succinate-supported H_2O_2 release (Fig. 5). This may be due to differences in liver NAD(P) redox state and higher levels of endogenous substrates relative to other tissues [77]. Reverse electron transfer was also not an important ROS source in skeletal muscle, as indicated by a lack of effect of rotenone on H_2O_2 release, although ROS release rates with succinate were substantial. The lack of reverse electron transfer in muscle may be attributed to low ΔpH due to the presence of physiologically relevant phosphate concentrations in the experimental medium. Reverse electron transfer in skeletal muscle is strongly stimulated by ΔpH [61].

In heart, brain, and kidney, ROS release supported by succinate was strongly prevented by rotenone (Fig. 5), indicating that it occurs owing to reverse electron transfer even in the presence of millimolar phosphate concentrations. ROS release promoted by succinate remained high in the presence of antimycin A, but not myxothiazol (Fig. 5). This result, in addition to the effect of rotenone, indicates that electron leakage in the presence of succinate can be substantial at the level of complex III when semiquinone radicals accumulate owing to the inhibitory action of antimycin A. Indeed, antimycin A-stimulated H_2O_2 release in kidney, heart, and skeletal muscle was not prevented by rotenone, indicating it occurs primarily in complex III. The inhibitory effect of myxothiazol on ROS release suggests that, despite the presence of a reduced Q pool, reverse electron transfer is strongly related to $\Delta\Psi$. Indeed, absolute and relative H_2O_2 release promoted by succinate was prevented by the uncoupler CCCP. Altogether, our results confirm prior suggestions [15,16] that reverse electron transfer is a very important source of mitochondrial ROS in brain and heart and demonstrate its importance in kidney. In previous work in heart and brain, we have found that reverse electron transfer is substantial also under conditions of “dual electron entry,” in which both NAD- and FAD-linked substrates are present [78] (H.T.F. Facundo and A.J. Kowaltowski, unpublished results).

Succinate dehydrogenase itself, as a flavoenzyme [79], could be a ROS source during succinate-supported respiration. However, our data showing strong inhibition of H_2O_2 release by rotenone suggest this enzyme is not the main ROS source under these conditions. Indeed, succinate dehydrogenase may be structurally arranged to avoid ROS formation by the intrinsic FAD [80]. However, other flavoenzymes may be accountable for H_2O_2 release in mitochondria. For example, dihydrolipoyl dehydrogenase within α -ketoglutarate

dehydrogenase is a well-established ROS source [19–21] and may account for the largely enhanced levels of H₂O₂ release observed upon rotenone treatment in α-ketoglutarate- but not glutamate-supported respiration (compare Figs. 3 and 4). Indeed, ROS release by this enzyme is largely stimulated by NADH accumulation [19–21]. Acyl-CoA dehydrogenase or the electron transferring flavoprotein may be responsible for the large levels of H₂O₂ generated by kidney mitochondria in the presence of palmitate (Fig. 2). H₂O₂ release under these conditions cannot be ascribed to reverse electron flux or leakage within complex III because it is not decreased by rotenone and is enhanced by both myxothiazol and antimycin A (Fig. 7). Glycerol phosphate dehydrogenase and acyl-CoA dehydrogenase also seem to play an important role in ROS generation in the liver, a tissue in which substrates for these enzymes lead to substantial formation (Fig. 2), despite low respiratory rates and ΔΨ (Table 3). Indeed, use of glycerol phosphate as a substrate led to high H₂O₂/O₂ ratios in most tissues (Figs. 2 and 6). H₂O₂ release promoted by glycerol phosphate may increase in other tissues, such as brain, when higher levels of Ca²⁺ ions are present [81]. Other flavoenzymes that may contribute toward mitochondrial ROS generation are monoamine oxidases [82] and dihydroorotate dehydrogenase [17,83].

Interestingly, our results uncover substantial differences between tissues with respect to substrate changes in H₂O₂ release levels. In particular, we would like to stress differences observed in relation to glycerol phosphate and palmitoyl carnitine. Some prior studies suggest that fatty acids such as palmitate generate higher amounts of mitochondrial ROS [34,59]. However, in our studies, we found the increment in H₂O₂ release promoted by palmitate versus NADH-linked substrates to be minimal in brain and absent in heart and skeletal muscle. On the other hand, we saw high H₂O₂ release promoted by palmitate in kidney and palmitate and glycerol phosphate in liver. We are unaware of prior studies measuring ROS release in kidney respiring on fatty acids, although our results with glycerol phosphate and succinate in this tissue obtained from rat agree with previous studies conducted using isolated mouse kidney mitochondria [33].

Because our H₂O₂ detection experiments were calibrated and O₂ consumption was measured in parallel, we can establish quantitative isolated mitochondrial ROS release rates. We find that the highest H₂O₂ release rates are in the 1–2 nmol mg protein⁻¹ min⁻¹ range, observed in State 4 mitochondria from brain and heart energized with succinate, reaching almost 3.0% of oxygen consumption (Figs. 1, 2, and 5). A similar H₂O₂/O₂ ratio is also observed using glycerol phosphate or palmitate in liver (Figs. 2, 6 and 7). However, it is not realistic to believe these rates are achieved *in vivo*, because some extent of oxidative phosphorylation occurs in most cells, and ROS release rates decrease substantially with subtle increments in respiratory rates [44,54], as well as being influenced by lower oxygen tensions in tissues *in vivo* [69]. Indeed, H₂O₂/O₂ ratios in phosphorylating (Fig. 1) or uncoupled (Fig. 5) mitochondria from brain, heart, kidney, or skeletal muscle respiring on succinate are under 0.2%. Because this substrate promotes the upper limit of ROS generation in most tissues, our results indicate that in these tissues physiological O₂[−] generation probably accounts for significantly less than 0.2% of oxygen consumption *in vivo*. Following this reasoning, we estimate physiological H₂O₂ release rates *in vivo* are in the 0.1 nmol mg mitochondrial protein⁻¹ min⁻¹ range, or less, in heart, brain, and skeletal muscle, whereas kidney, which displays higher O₂ consumption rates, presents rates in the range of 0.3 nmol mg mitochondrial protein⁻¹ min⁻¹. Liver mitochondria present a very different pattern, however, because H₂O₂ release rates are not strongly altered by oxidative phosphorylation (Fig. 1) or uncoupling (Figs. 3–7). Thus, H₂O₂ release rates in this tissue *in vivo* are probably in the range of 0.4 nmol mg mitochondrial protein⁻¹ min⁻¹ and may account for as much as 2.0% of oxygen consumption using fatty acids as substrates.

Conclusions

Our studies provide a side-by-side comparison of absolute and relative mitochondrial ROS release rates in various tissues respiring on a range of substrates. We confirmed previous findings and uncovered many novel tissue-, substrate-, and site-specific characteristics of this release. Altogether, the results collected indicate that:

- Complexes I and III, in addition to flavoenzymes, are important sites of ROS formation in mitochondria.
- Reverse electron transfer from succinate dehydrogenase to complex I leads to very substantial levels of ROS formation, in particular in brain and heart.
- Use of palmitate as a substrate generates significant ROS release in kidney and liver.
- Increased respiratory rates promoted by oxidative phosphorylation or uncoupling significantly prevent ROS formation in brain, heart, and, to a lesser extent, kidney and skeletal muscle.
- Absolute ROS formation in liver is not substantially prevented by oxidative phosphorylation or uncoupling, except when supported by fatty acids.
- ROS formation probably accounts for less than 0.2% of oxygen consumption in brain, heart, kidney, and skeletal muscle mitochondria *in vivo*, but could comprise up to 2.0% of liver oxygen consumption.

Acknowledgments

The authors thank Professor Roger F. Castilho for expert critical reading of the manuscript and Edson A. Gomes and Camille C. Caldeira da Silva Ortiz for exceptional technical assistance. We are indebted to Dr. Luciane C. Alberici for help in isolating skeletal muscle mitochondria and to Professor Anibal E. Vercesi for equipment use. This work was supported by grants from the Fundação de Amparo à Pesquisa do Estado de São Paulo (FAPESP), the John Simon Guggenheim Memorial Foundation and Conselho Nacional de Pesquisa e Tecnologia (CNPq), and the Instituto Nacional de Ciência e Tecnologia de Processos Redox em Biomedicina (Redoxoma). E.B.T. and F.D.T.N. are students supported by FAPESP fellowships.

References

- [1] Nicholls, D.; Ferguson, S. Bioenergetics 3. Academic Press, San Diego; 2001.
- [2] Boveris, A.; Cadena, E. Mitochondrial production of superoxide anions and its relationship to the antimycin insensitive respiration. *FEBS Lett.* **54**:311–314; 1975.
- [3] Boveris, A.; Chance, B. The mitochondrial generation of hydrogen peroxide: general properties and effect of hyperbaric oxygen. *Biochem. J.* **134**:707–716; 1973.
- [4] Boveris, A.; Oshino, N.; Chance, B. The cellular production of hydrogen peroxide. *Biochem. J.* **128**:617–630; 1972.
- [5] Cadena, E.; Boveris, A.; Ragan, C. I.; Stoppani, A. O. Production of superoxide radicals and hydrogen peroxide by NADH-ubiquinone reductase and ubiquinol-cytochrome c reductase from beef-heart mitochondria. *Arch. Biochem. Biophys.* **180**:248–257; 1977.
- [6] Hinkle, P. C.; Butow, R. A.; Racker, E.; Chance, B. Partial resolution of the enzymes catalyzing oxidative phosphorylation: reverse electron transfer in the flavin-cytochrome beta region of the respiratory chain of beef heart submitochondrial particles. *J. Biol. Chem.* **242**:5169–5173; 1967.
- [7] Loschen, G.; Azzi, A. On the formation of hydrogen peroxide and oxygen radicals in heart mitochondria. *Recent Adv. Stud. Cardiac Struct. Metab.* **7**:3–12; 1975.
- [8] Loschen, G.; Azzi, A.; Flohé, L. Mitochondrial H₂O₂ formation: relationship with energy conservation. *FEBS Lett.* **33**:84–87; 1973.
- [9] Loschen, G.; Azzi, A.; Richter, C.; Flohé, L. Superoxide radicals as precursors of mitochondrial hydrogen peroxide. *FEBS Lett.* **42**:68–72; 1974.
- [10] Turrens, J. F.; Boveris, A. Generation of superoxide anion by the NADH dehydrogenase of bovine heart mitochondria. *Biochem. J.* **191**:421–427; 1980.
- [11] Turrens, J. F.; Alexandre, A.; Lehninger, A. L. Ubisemiquinone is the electron donor for superoxide formation by complex III of heart mitochondria. *Arch. Biochem. Biophys.* **237**:408–414; 1985.
- [12] Weisiger, R. A.; Fridovich, I. Mitochondrial superoxide simutase: site of synthesis and intramitochondrial localization. *J. Biol. Chem.* **248**:4793–4796; 1973.
- [13] Dröse, S.; Brandt, U. The mechanism of mitochondrial superoxide production by the cytochrome bc1 complex. *J. Biol. Chem.* **283**:21649–21654; 2008.
- [14] Lambert, A. J.; Brand, M. D. Inhibitors of the quinone-binding site allow rapid superoxide production from mitochondrial NADH:ubiquinone oxidoreductase (complex I). *J. Biol. Chem.* **279**:39414–39420; 2004.

- [15] Liu, Y.; Fiskum, G.; Schubert, D. Generation of reactive oxygen species by the mitochondrial electron transport chain. *J. Neurochem.* **80**:780–787; 2002.
- [16] Turrens, J. F. Mitochondrial formation of reactive oxygen species. *J. Physiol. (London)* **552**:335–344; 2003.
- [17] Lenaz, G. The mitochondrial production of reactive oxygen species: mechanisms and implications in human pathology. *IUBMB Life* **52**:159–164; 2001.
- [18] Miwa, S.; Brand, M. D. Mitochondrial matrix reactive oxygen species production is very sensitive to mild uncoupling. *Biochem. Soc. Trans.* **31**:1300–1301; 2003.
- [19] Starkov, A. A.; Fiskum, G.; Chinopoulos, C.; Lorenzo, B. J.; Browne, S. E.; Patel, M. S.; Beal, M. F. Mitochondrial alpha-ketoglutarate dehydrogenase complex generates reactive oxygen species. *J. Neurosci.* **24**:7779–7788; 2004.
- [20] Tahara, E. B.; Barros, M. H.; Oliveira, G. A.; Netto, L. E. S.; Kowaltowski, A. J. Dihydrolipoyl dehydrogenase as a source of reactive oxygen species inhibited by caloric restriction and involved in *Saccharomyces cerevisiae* aging. *FASEB J.* **21**: 274–283; 2007.
- [21] Tretter, L.; Adam-Vizi, V. Generation of reactive oxygen species in the reaction catalyzed by alpha-ketoglutarate dehydrogenase. *J. Neurosci.* **24**:7771–7778; 2004.
- [22] Melov, S.; Doctrow, S. R.; Schneider, J. A.; Haberson, J.; Patel, M.; Coskun, P. E.; Huffman, K.; Wallace, D. C.; Malfroy, B. Lifespan extension and rescue of spongiform encephalopathy in superoxide dismutase 2 nullizygous mice treated with superoxide dismutase-catalase mimetics. *J. Neurosci.* **21**:8348–8353; 2001.
- [23] Caldeira da Silva, C. C.; Cerqueira, F. M.; Barbosa, L. F.; Medeiros, M. H. G.; Kowaltowski, A. J. Mild mitochondrial uncoupling in mice affects energy metabolism, redox balance and longevity. *Aging Cell* **7**:552–560; 2008.
- [24] Schriner, S. E.; Linford, N. J.; Martin, G. M.; Treuting, P.; Ogburn, C. E.; Emond, M.; Coskun, P. E.; Ladiges, W.; Wolf, N.; Van Remmen, H.; Wallace, D. C.; Rabinovitch, P. S. Extension of murine life span by overexpression of catalase targeted to mitochondria. *Science* **308**:1909–1911; 2005.
- [25] Sohal, R. S.; Weindruch, R. Oxidative stress, caloric restriction, and aging. *Science* **273**:59–63; 1996.
- [26] Balaban, R. S.; Nemoto, S.; Finkel, T. Mitochondria, oxidants, and aging. *Cell* **120**: 483–495; 2005.
- [27] Dröge, W. Free radicals in the physiological control of cell function. *Physiol. Rev.* **82**:47–95; 2002.
- [28] Facundo, H. T. F.; Carreira, R. S.; de Paula, J. G.; Santos, C. C. X.; Ferranti, R.; Laurindo, F. R. M.; Kowaltowski, A. J. Ischemic preconditioning requires increases in reactive oxygen release independent of mitochondrial K⁺ channel activity. *Free Radic. Biol. Med.* **40**:469–479; 2006.
- [29] Vanden Hoek, T. L.; Becker, L. B.; Shao, Z.; Li, C.; Schumacker, P. T. Reactive oxygen species released from mitochondria during brief hypoxia induce preconditioning in cardiomyocytes. *J. Biol. Chem.* **273**:18092–18098; 1998.
- [30] Echtar, K. S.; Roussel, D.; St-Pierre, J.; Jekabsons, M. B.; Cadena, S.; Stuart, J. A.; Harper, J. A.; Roebuck, S. J.; Morrison, A.; Pickering, S.; Clapham, J. C.; Brand, M. D. Superoxide activates mitochondrial uncoupling proteins. *Nature* **415**:96–99; 2002.
- [31] Facundo, H. T. F.; de Paula, J. G.; Kowaltowski, A. J. Mitochondrial ATP-sensitive K⁺ channels are redox-sensitive pathways that control reactive oxygen species production. *Free Radic. Biol. Med.* **42**:1039–1048; 2007.
- [32] Kowaltowski, A. J.; Vercesi, A. E. Mitochondrial damage induced by conditions of oxidative stress. *Free Radic. Biol. Med.* **26**:463–471; 1999.
- [33] Kwong, L. K.; Sohal, R. S. Substrate and site specificity of hydrogen peroxide generation in mouse mitochondria. *Arch. Biochem. Biophys.* **350**:118–126; 1998.
- [34] St-Pierre, J.; Buckingham, J. A.; Roebuck, S. J.; Brand, M. D. Topology of superoxide production from different sites in the mitochondrial electron transport chain. *J. Biol. Chem.* **277**:44784–44790; 2002.
- [35] Oliveira, G. A.; Kowaltowski, A. J. Phosphate increases mitochondrial reactive oxygen species release. *Free Radic. Res.* **38**:1113–1118; 2004.
- [36] Facundo, H. T. F.; de Paula, J. G.; Kowaltowski, A. J. Mitochondrial ATP-sensitive K⁺ channels prevent oxidative stress, permeability transition and cell death. *J. Bioenerg. Biomembr.* **37**:75–82; 2005.
- [37] Andreyev, A.; Fiskum, G. Calcium induced release of mitochondrial cytochrome c by different mechanisms selective for brain versus liver. *Cell Death Differ.* **6**: 825–832; 1999.
- [38] Andreyev, A. Y.; Fahy, B.; Fiskum, G. Cytochrome c release from brain mitochondria is independent of the mitochondrial permeability transition. *FEBS Lett.* **439**: 373–376; 1998.
- [39] Brown, M. R.; Sullivan, P. G.; Geddes, J. W. Synaptic mitochondria are more susceptible to Ca²⁺ overload than nonsynaptic mitochondria. *J. Biol. Chem.* **281**: 11658–11668; 2006.
- [40] Rosenthal, R. E.; Hamud, F.; Fiskum, G.; Varghese, P. J.; Sharpe, S. Cerebral ischemia and reperfusion: prevention of brain mitochondrial injury by lidoflazine. *J. Cereb. Blood Flow Metab.* **7**:752–758; 1987.
- [41] Fiskum, G.; Kowaltowski, A. J.; Andreyev, A. Y.; Kushnareva, Y. E.; Starkov, A. A. Apoptosis-related activities measured with isolated mitochondria and digitonin-permeabilized cells. *Methods Enzymol.* **322**:222–234; 2000.
- [42] Jarmuszkiewicz, W.; Navet, R.; Alberici, L. C.; Douette, P.; Sluse-Goffart, C. M.; Sluse, F. E.; Vercesi, A. E. Redox state of endogenous coenzyme Q modulates the inhibition of linoleic acid-induced uncoupling by guanosine triphosphate in isolated skeletal muscle mitochondria. *J. Bioenerg. Biomembr.* **36**:493–502; 2004.
- [43] Cancherini, D. V.; Trabuco, L. G.; Reboucas, N. A.; Kowaltowski, A. J. ATP-sensitive K⁺ channels in renal mitochondria. *Am. J. Physiol., Renal Physiol.* **285**:F1291–1296; 2003.
- [44] Skulachev, V. P. Uncoupling: new approaches to an old problem of bioenergetics. *Biochim. Biophys. Acta* **1363**:100–124; 1998.
- [45] Lowry, O. H.; Rosenbrough, N. J.; Farr, A. L.; Randall, R. J. Protein measurement with the Folin phenol reagent. *J. Biol. Chem.* **193**:265–275; 1951.
- [46] Muller, F. L.; Liu, Y.; Van Remmen, H. Complex III releases superoxide to both sides of the inner mitochondrial membrane. *J. Biol. Chem.* **279**:49064–49073; 2004.
- [47] Tompkins, A. J.; Burwell, L. S.; Digerness, S. B.; Zaragoza, C.; Holman, W. L.; Brookes, P. S. Mitochondrial dysfunction in cardiac ischemia-reperfusion injury: ROS from complex I, without inhibition. *Biochim. Biophys. Acta* **1762**:223–231; 2006.
- [48] Zhou, M.; Diwu, Z.; Panchuk-Voloshina, N.; Haugland, R. P. A stable nonfluorescent derivative of resorufin for the fluorometric determination of trace hydrogen peroxide: applications in detecting the activity of phagocyte NADPH oxidase and other oxidases. *Anal. Biochem.* **253**:162–168; 1997.
- [49] Kowaltowski, A. J.; Cocco, R. G.; Campos, C. B.; Fiskum, G. Effect of Bcl-2 overexpression on mitochondrial structure and function. *J. Biol. Chem.* **277**: 42802–42807; 2002.
- [50] Akerman, K. E.; Wikström, M. K. Safranine as a probe of the mitochondrial membrane potential. *FEBS Lett.* **68**:191–197; 1976.
- [51] Vercesi, A. E.; Bernardes, C. F.; Hoffmann, M. E.; Gadelha, F. R.; Docampo, R. Digitonin permeabilization does not affect mitochondrial function and allows the determination of the mitochondrial membrane potential of *Trypanosoma cruzi* in situ. *J. Biol. Chem.* **266**:14431–14434; 1991.
- [52] Johnson, D. T.; Harris, R. A.; French, S.; Blair, P. V.; You, J.; Bemis, K. G.; Wang, M.; Balaban, R. S. Tissue heterogeneity of the mammalian mitochondrial proteome. *Am. J. Physiol. Cell Physiol.* **292**:C689–697; 2007.
- [53] Johnson, D. T.; Harris, R. A.; Blair, P. V.; Balaban, R. S. Functional consequences of mitochondrial proteome heterogeneity. *Am. J. Physiol., Cell Physiol.* **292**:C698–707; 2007.
- [54] Korshunov, S. S.; Skulachev, V. P.; Starkov, A. A. High protonic potential actuates a mechanism of production of reactive oxygen species in mitochondria. *FEBS Lett.* **416**:15–18; 1997.
- [55] Rottenberg, H.; Hashimoto, K. Fatty acid uncoupling of oxidative phosphorylation in rat liver mitochondria. *Biochemistry* **25**:1747–1755; 1986.
- [56] Wojtczak, L.; Schönfeld, P. Effect of fatty acids on energy coupling processes in mitochondria. *Biochim. Biophys. Acta* **1183**:41–57; 1993.
- [57] Santiago, A. P. S. A.; Chaves, E. A.; Oliveira, M. F.; Galina, A. Reactive oxygen species generation is modulated by mitochondrial kinases: correlation with mitochondrial antioxidant peroxidases in rat tissues. *Biochimia* **90**:1566–1577; 2008.
- [58] Duval, C.; Cámera, Y.; Hondares, E.; Sibille, B.; Villarroya, F. Overexpression of mitochondrial uncoupling protein-3 does not decrease production of the reactive oxygen species, elevated by palmitate in skeletal muscle cells. *FEBS Lett.* **581**: 955–961; 2007.
- [59] Lambertucci, R. H.; Hirabara, S. M.; Silveira, L. D. R.; Levada-Pires, A. C.; Curi, R.; Pithon-Curi, T. C. Palmitate increases superoxide production through mitochondrial electron transport chain and NADPH oxidase activity in skeletal muscle cells. *J. Cell. Physiol.* **216**:796–804; 2008.
- [60] Brookes, P. S.; Yoon, Y.; Robotham, J. L.; Anders, M. W.; Sheu, S. Calcium, ATP, and ROS: a mitochondrial love-hate triangle. *Am. J. Physiol., Cell Physiol.* **287**: C817–833; 2004.
- [61] Lambert, A. J.; Brand, M. D. Superoxide production by NADH:ubiquinone oxidoreductase (complex I) depends on the pH gradient across the mitochondrial inner membrane. *Biochem. J.* **382**:511–517; 2004.
- [62] Cadena, E.; Boeris, A. Enhancement of hydrogen peroxide formation by protophores and ionophores in antimycin-supplemented mitochondria. *Biochem. J.* **188**:31–37; 1980.
- [63] Alberti, R. A. Standard apparent reduction potentials of biochemical half reactions and thermodynamic data on the species involved. *Biophys. Chem.* **111**:115–122; 2004.
- [64] Lenaz, G. A critical appraisal of the mitochondrial coenzyme Q pool. *FEBS Lett.* **509**: 151–155; 2001.
- [65] Tretter, L.; Takacs, K.; Hegedus, V.; Adam-Vizi, V. Characteristics of alpha-glycerophosphate-evoked H₂O₂ generation in brain mitochondria. *J. Neurochem.* **100**:650–663; 2007.
- [66] Sanz, A.; Pamplona, R.; Barja, G. Is the mitochondrial free radical theory of aging intact? *Antioxid. Redox Signal.* **8**:582–599; 2006.
- [67] Willcox, B. J.; Curb, J. D.; Rodriguez, B. L. Antioxidants in cardiovascular health and disease: key lessons from epidemiologic studies. *Am. J. Cardiol.* **101**:75D–86D; 2008.
- [68] Bunn, H. F.; Poyton, R. O. Oxygen sensing and molecular adaptation to hypoxia. *Physiol. Rev.* **76**:839–885; 1996.
- [69] Gnaiger, E.; Kuznetsov, A. V. Mitochondrial respiration at low levels of oxygen and cytochrome c. *Biochem. Soc. Trans.* **30**:252–258; 2002.
- [70] Brown, G. C. Nitric oxide and mitochondrial respiration. *Biochim. Biophys. Acta* **1411**:351–369; 1999.
- [71] Radi, R. Nitric oxide, oxidants, and protein tyrosine nitration. *Proc. Natl. Acad. Sci. U.S.A.* **101**:4003–4008; 2004.
- [72] Halliwell, B.; Gutteridge, J. Free Radicals in Biology and Medicine. Oxford University Press, London; 2003.
- [73] Pereverzev, M. O.; Vygodina, T. V.; Konstantinov, A. A.; Skulachev, V. P. Cytochrome c, an ideal antioxidant. *Biochem. Soc. Trans.* **31**:1312–1315; 2003.
- [74] Boeris, A.; Cadena, E.; Stoppani, A. O. Role of ubiquinone in the mitochondrial generation of hydrogen peroxide. *Biochem. J.* **156**:435–444; 1976.
- [75] Han, D.; Williams, E.; Cadena, E. Mitochondrial respiratory chain-dependent generation of superoxide anion and its release into the intermembrane space. *Biochem. J.* **353**:411–416; 2001.
- [76] Grivennikova, V. G.; Vinogradov, A. D. Generation of superoxide by the mitochondrial complex I. *Biochim. Biophys. Acta* **1757**:553–561; 2006.
- [77] Coelho, J. L.; Vercesi, A. E. Retention of Ca²⁺ by rat liver and rat heart mitochondria: effect of phosphate, Mg²⁺, and NAD(P) redox state. *Arch. Biochem. Biophys.* **204**:141–147; 1980.

- [78] Fornazari, M.; de Paula, J. G.; Castilho, R. F.; Kowaltowski, A. J. Redox properties of the adenosine triphosphate-sensitive K^+ channel in brain mitochondria. *J. Neurosci. Res.* **86**:1548–1556; 2008.
- [79] Imlay, J. A. Pathways of oxidative damage. *Annu. Rev. Microbiol.* **57**:395–418; 2003.
- [80] Yankovskaya, V.; Horsefield, R.; Törnroth, S.; Luna-Chavez, C.; Miyoshi, H.; Léger, C.; Byrne, B.; Cecchini, G.; Iwata, S. Architecture of succinate dehydrogenase and reactive oxygen species generation. *Science* **299**:700–704; 2003.
- [81] Tretter, L.; Takacs, K.; Kövér, K.; Adam-Vizi, V. Stimulation of H_2O_2 generation by calcium in brain mitochondria respiring on alpha-glycerophosphate. *J. Neurosci. Res.* **85**:3471–3479; 2007.
- [82] Hauptmann, N.; Grimsby, J.; Shih, J. C.; Cadena, E. The metabolism of tyramine by monoamine oxidase A/B causes oxidative damage to mitochondrial DNA. *Arch. Biochem. Biophys.* **335**:295–304; 1996.
- [83] Forman, J. H.; Kennedy, J. Superoxide production and electron transport in mitochondrial oxidation of dihydroorotic acid. *J. Biol. Chem.* **250**:4322–4326; 1975.



cis-4-decenoic acid provokes mitochondrial bioenergetic dysfunction in rat brain

Patrícia Fernanda Schuck ^{a,d}, Gustavo da Costa Ferreira ^a, Erich Birelli Tahara ^b, Fábio Klamt ^a, Alicia Juliana Kowaltowski ^b, Moacir Wajner ^{a,c,*}

^a Departamento de Bioquímica, Instituto de Ciências Básicas da Saúde, Universidade Federal do Rio Grande do Sul, Porto Alegre, RS, Brazil

^b Departamento de Bioquímica, Instituto de Química, Universidade de São Paulo, São Paulo, SP, Brazil

^c Serviço de Genética Médica, Hospital de Clínicas de Porto Alegre, RS, Brazil

^d Laboratório de Fisiopatologia Experimental, Programa de Pós-Graduação em Ciências da Saúde, Unidade Acadêmica de Ciências da Saúde, Universidade do Extremo Sul Catarinense, Criciúma, SC, Brazil

ARTICLE INFO

Article history:

Received 12 April 2010

Accepted 25 May 2010

Keywords:

MCAD deficiency

Mitochondria

Oxidative phosphorylation

cis-4-decenoic acid

ABSTRACT

Aims: In the present work we investigated the *in vitro* effect of *cis*-4-decenoic acid, the pathognomonic metabolite of medium-chain acyl-CoA dehydrogenase deficiency, on various parameters of bioenergetic homeostasis in rat brain mitochondria.

Main methods: Respiratory parameters determined by oxygen consumption were evaluated, as well as membrane potential, NAD(P)H content, swelling and cytochrome *c* release in mitochondrial preparations from rat brain, using glutamate plus malate or succinate as substrates. The activities of citric acid cycle enzymes were also assessed.

Key findings: *cis*-4-decenoic acid markedly increased state 4 respiration, whereas state 3 respiration and the respiratory control ratio were decreased. The ADP/O ratio, the mitochondrial membrane potential, the matrix NAD(P)H levels and aconitase activity were also diminished by *cis*-4-decenoic acid. These data indicate that this fatty acid acts as an uncoupler of oxidative phosphorylation and as a metabolic inhibitor. *cis*-4-decenoic acid also provoked a marked mitochondrial swelling when either KCl or sucrose was used in the incubation medium and also induced cytochrome *c* release from mitochondria, suggesting a non-selective permeabilization of the inner mitochondrial membrane.

Significance: It is therefore presumed that impairment of mitochondrial homeostasis provoked by *cis*-4-decenoic acid may be involved in the brain dysfunction observed in medium-chain acyl-CoA dehydrogenase deficient patients.

© 2010 Elsevier Inc. All rights reserved.

Introduction

Individuals affected by medium-chain acyl-CoA dehydrogenase (MCAD; E.C. 1.3.99.3) deficiency (MCADD), the most common inherited defect of fatty acid oxidation, present severe episodes of hypoketotic hypoglycemia and encephalopathy with seizures, lethargy that may lead to coma and sudden death (Onkenhout et al. 1995; Rinaldo et al. 1998; Roe and Ding 2001). During crises, which are generally precipitated by prolonged fasting or infection, the levels of the accumulating metabolites are dramatically increased (Derk et al. 2006; Mayell et al. 2007). *cis*-4-decenoic acid (cDA) accumulates in the tissue and body fluids of patients affected by MCADD and is considered the pathognomonic metabolite of this disease. Clinical management relies on the administration of high glucose and L-carnitine amounts during the acute episodes, as well as fat restriction

and L-carnitine supplementation after recovery (Coates 1994; Roe and Ding 2001).

In spite of the high prevalence of this disorder in the general population, which is as frequent as phenylketonuria, little is known about the pathomechanisms responsible for the neurologic symptoms in MCADD. Hypoglycemia may acutely affect the central nervous system. However, the encephalopathic crises often occur in the absence of low blood glucose levels, implying that the accumulating compounds are potentially neurotoxic. In this context, there are a few studies describing deleterious effects of cDA, as well as of octanoic acid (OA) and decanoic acid (DA), which also accumulate in this disorder. Thus, it was previously demonstrated that OA, DA and cDA impair energy metabolism by inhibiting the activities of the respiratory chain, mitochondrial creatine kinase and Na⁺,K⁺-ATPase in cerebral cortex of rats *in vitro* (de Assis et al. 2003, 2006; Reis de Assis et al. 2004; Schuck et al. 2009a), with cDA eliciting the most pronounced effects. In addition, cDA was recently shown to provoke lipid and protein oxidative damages, as well as to reduce the antioxidant defenses at micromolar doses in brain of young rats *in vitro* (Schuck et al. 2007). Considering that *trans,trans*-2,4-decadienal,

* Corresponding author. Departamento de Bioquímica, Universidade Federal do Rio Grande do Sul, Rua Ramiro Barcelos, 2600, Anexo, CEP 90035-003, Porto Alegre, RS, Brazil. Tel.: +55 51 33085571; fax: +55 51 33085540.

E-mail address: mwajner@ufrgs.br (M. Wajner).

a compound structurally similar to cDA, markedly impairs mitochondrial energy homeostasis promoting non-selective inner mitochondrial membrane permeabilization (Sigolo et al. 2008), in the present work we investigated the *in vitro* effects of cDA on various mitochondrial respiratory parameters determined by oxygen consumption, including states 3 and 4 of mitochondrial respiration, the respiratory control ratio (RCR) and the ADP/O ratio in rat brain mitochondrial preparations. Citric acid cycle enzyme activities, mitochondrial membrane potential ($\Delta\Psi_m$), NAD(P)H content, mitochondrial swelling and cytochrome *c* release were also measured in the presence of cDA.

Material and methods

Materials

Chemicals were purchased from Sigma (St. Louis, MO, USA), except for *cis*-4-decenoic acid (cDA) which was prepared by Dr. Ernesto Brunet, Madrid, Spain with 99% purity. cDA was prepared on the day of the experiments in the incubation medium used for each technique and the pH was adjusted to 7.4. cDA was first dissolved in methanol, then diluted in 0.9% NaCl and finally supplemented to the incubation medium containing specific buffers for each technique. The concentrations of methanol in the incubation medium were always less than 1% and those of cDA ranged from 0.1 to 1.0 mM. Concentrations of methanol up to 1% did not interfere with the assays.

Animals

A total of 28 thirty-day-old Wistar rats obtained from our breeding colony were used. The animals were housed five to a cage with food and water available *ad libitum* and were maintained on a normal 12 h light/dark cycle (lights on at 7:00 AM). This study was performed in accordance with the "Principles of Laboratory Animal Care" (NIH publication no. 80-23, revised 1996) and the "Guidelines for the Use of Animals in Neuroscience Research" by the Society for Neuroscience, and also with the approval of the Ethics Committees for Animal Research of the Universidade Federal do Rio Grande do Sul and of the Universidade de São Paulo.

Preparation of mitochondrial fractions

Mitochondria were isolated from the forebrain of 30-day-old rats as described by Rosenthal et al. (1987). Animals were sacrificed by decapitation; brain was rapidly removed and put into ice-cold 10 mM HEPES buffer, pH 7.2, containing 225 mM mannitol, 75 mM sucrose, 1 mM EGTA and 1 mg mL⁻¹ bovine serum albumin (BSA; free fatty acid). The cerebellum, pons, medulla and olfactory bulbs were removed and the remaining material was used as the forebrain. The forebrain was cut into small pieces using surgical scissors, extensively washed and then manually homogenized in a Dounce homogenizer using both a loose-fitting and a tight-fitting pestle. The homogenate was centrifuged for 3 min at 2000×g. After centrifugation, the supernatant was again centrifuged for 8 min at 12,000×g. The pellet was resuspended in 20 mL of isolation buffer containing 10 µL of 10% digitonin and re-centrifuged for 8 min at 12,000×g. The supernatant was discarded and the final pellet was gently washed and resuspended in isolation buffer devoid of EGTA, at an approximate protein concentration of 25–35 mg mL⁻¹. This preparation contains a mixture of synaptosomal and non-synaptosomal mitochondria similar to the general brain composition. All experiments were performed in freshly prepared mitochondria.

We always carried out parallel experiments with various blanks (controls) in the presence or absence of cDA and also with or without brain preparations in the reaction medium in order to detect any

interference (artifacts) of this fatty acid on the techniques utilized to measure the mitochondrial parameters.

Respiratory parameters determined through mitochondrial oxygen consumption

Oxygen consumption rate was measured polarographically using a Clark-type electrode in a thermostatically controlled (37 °C) and magnetically stirred incubation chamber using glutamate plus malate (2.5 mM each) or succinate (5 mM) plus rotenone (2 µg/mL) as substrates. cDA (0.1–1.0 mM) was added to the reaction medium at the beginning of the assay. Purified mitochondrial preparations (0.50 mg protein mL⁻¹) incubated in a buffer containing 0.3 M sucrose, 5 mM MOPS, 5 mM potassium phosphate, 1 mM EGTA and 1 mg mL⁻¹ BSA were used in the assays. State 3 mitochondrial respiration was measured after addition of 1 mM ADP to the incubation medium. State 4 mitochondrial respiration was measured after the addition of 1 µg mL⁻¹ oligomycin A to the medium. The respiratory control ratio (RCR; state 3/state 4) was then calculated. States 3 and 4 were expressed as nmol O₂ consumed min⁻¹ mg of protein⁻¹. The ADP/O ratio was estimated according to Estabrook (1967), using 100 µM ADP in the incubation medium. Only mitochondrial preparations with RCR higher than 4 were used in the experiments.

Spectrophotometric analyses of the activities of citric acid cycle enzymes

The activities of the citric acid cycle (CAC) enzymes were determined using enriched mitochondrial fractions from the cerebrum. *cis*-4-decenoic acid was supplemented to the medium containing mitochondria and submitted to a pre-incubation at 37 °C for 30 min after which the enzyme activities were measured. Citrate synthase activity was measured according to Srere (1969), by determining DTNB reduction at $\lambda = 412$ nm. The activity of aconitase was measured according to Morrison (1954), following the reduction of NADP⁺. The activities of isocitrate dehydrogenase (Plaut 1969), the α -ketoglutarate dehydrogenase complex (Lai and Cooper 1986; Tretter and Adam-Vizi 2004) and malate dehydrogenase (Kitto 1969) were determined by NAD⁺ reduction. The activity of succinate dehydrogenase was determined as described by Fischer et al. (1985) by assessing 2,6-dichlorophenolindophenol reduction. Fumarase activity was measured according to O'Hare and Doonan (1985), by determining the increase of absorbance of fumarate at $\lambda = 250$ nm. NADP⁺ and NAD⁺ reductions were determined at wavelengths of excitation and emission of 340 and 466 nm, respectively. The activities of the citric acid cycle enzymes were calculated as nmol min⁻¹ mg protein⁻¹, mmol min⁻¹ mg protein⁻¹ or µmol min⁻¹ mg protein⁻¹.

Determination of mitochondrial inner membrane potentials ($\Delta\Psi_m$)

Mitochondrial inner membrane potentials ($\Delta\Psi_m$) were measured according to Akerman and Wikström (1976) and Kowaltowski et al. (2002) using mitochondria (0.50 mg protein mL⁻¹) supported by 2.5 mM glutamate plus 2.5 mM malate or 5 mM succinate as substrates, in an incubation medium containing 125 mM KCl, 5 mM MgCl₂, 0.1 mM EGTA, 0.1 mg mL⁻¹ BSA, 5 mM HEPES, 2 mM KH₂PO₄, 1 µg mL⁻¹ oligomycin A, pH 7.3. The fluorescence of 5 µM cationic dye safranin O at an excitation wavelength of 495 nm and emission wavelength of 586 nm on a Hitachi F-4500 spectrofluorometer was followed during 5 min. Data were expressed as fluorescence arbitrary units (FAU).

Determination of NAD(P)H

Matrix mitochondrial NAD(P)H autofluorescence was measured at 37 °C using 366 nm excitation and 450 nm emission wavelengths on a

Hitachi F-4500 spectrophotometer using mitochondrial preparations ($0.5 \text{ mg protein mL}^{-1}$) in an incubation medium containing 125 mM KCl , 5 mM MgCl_2 , 0.1 mM EGTA , 0.1 mg mL^{-1} BSA, 5 mM HEPES , $2 \text{ mM KH}_2\text{PO}_4$, pH 7.3, using 2.5 mM malate plus 2.5 mM glutamate as substrates. Data were expressed as nmol NAD(P)H mg of protein $^{-1}$.

Determination of mitochondrial swelling

Mitochondrial swelling was assessed following light scattering changes on a temperature-controlled Hitachi F-4500 spectrophotometer with magnetic stirring operating at excitation and emission of 520 nm using mitochondrial preparations ($0.50 \text{ mg protein mL}^{-1}$) in an incubation medium containing 125 mM KCl , 5 mM MgCl_2 , 0.1 mM EGTA , 0.1 mg mL^{-1} BSA, 5 mM HEPES , $2 \text{ mM KH}_2\text{PO}_4$, pH 7.3 and using 5 mM succinate as substrate. Some experiments were carried out in the presence of 250 mM sucrose in the incubation medium. Data were expressed as fluorescence arbitrary units (FAU).

Cytochrome c immunocontent measurement

After the mitochondrial swelling experiments, the medium was centrifuged at $12,000 \times g$ for 10 min in order to sediment the mitochondria. Thirty micrograms of mitochondrial protein was

subjected to sodium dodecyl sulfate-polyacrylamide gel electrophoresis and transferred to nitrocellulose membranes for determination of cytochrome *c* release. After blocking with 5% non-fat dry milk to prevent non-specific binding to the membrane of the detecting system, membranes were incubated with mouse monoclonal anti-cytochrome *c* antibody (1:1,000) (BD Biosciences, CA, USA), followed by horseradish peroxidase-conjugated secondary antibody (1:10,000) (Dakocytomation, USA). Bands were visualized by chemiluminescence using the ECL kit from NEN (Boston, MA, USA). Quantification was performed with ImageJ 1.36b (National Institute of Health, USA) software.

Protein determination

Protein was measured by the method of Lowry et al. (1951) using bovine serum albumin as standard.

Statistical analysis

Results are presented as mean \pm standard deviation. Assays were performed in duplicate and the mean was used for statistical analysis. Data were analyzed using one-way analysis of variance (ANOVA) followed by the post-hoc Duncan multiple range test when *F* was

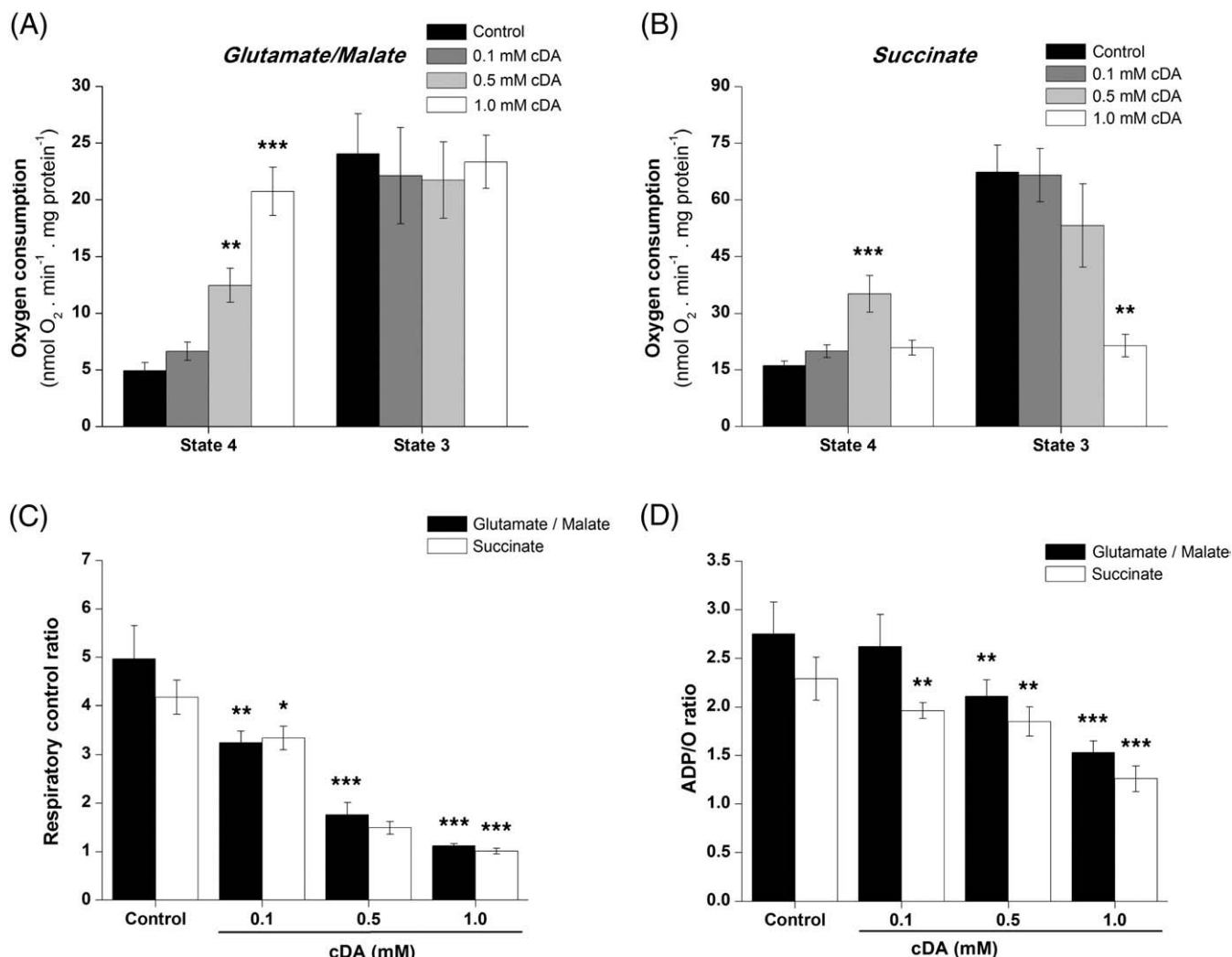


Fig. 1. Effect of cDA on oxygen consumption in ADP-stimulated (state 3) and non-ADP-stimulated (state 4) mitochondria supported by glutamate/malate (A) or succinate (B), on respiratory control ratio (RCR) (C) and on ADP/O ratio (D). After the addition of mitochondrial preparation ($0.5 \text{ mg protein mL}^{-1}$), different concentrations of cDA (0.1–1.0 mM) were supplemented to the incubation medium. Values are means \pm standard deviation for four to five independent experiments. States 3 and 4 of mitochondrial respiration are expressed as nmol O₂ min $^{-1}$ mg of protein $^{-1}$. * $P<0.05$, ** $P<0.01$, *** $P<0.001$ compared to controls (Duncan multiple range test).

significant. Only significant F values are shown in the text. Differences between groups were rated significant at $P < 0.05$. All analyses were carried out using the Statistical Package for the Social Sciences (SPSS) software in a PC compatible computer.

Results

cis-4-decenoic acid alters mitochondrial respiration in the presence or absence of exogenously added ADP

We first verified that rat brain mitochondria incubated under our conditions were well functioning, as indicated by the higher respiratory rates observed in the presence of ADP (state 3) relatively to those obtained after the addition of the ADP synthase inhibitor oligomycin A (state 4) (Figs. 1 and 2). We can also see in the figure that cDA significantly increased oxygen consumption rate in state 4 respiration (up to 419%) regardless of the substrate used [glutamate/malate: $F(3,15) = 25.2$; $P < 0.001$; succinate: $F(3,15) = 8.69$; $P < 0.01$]

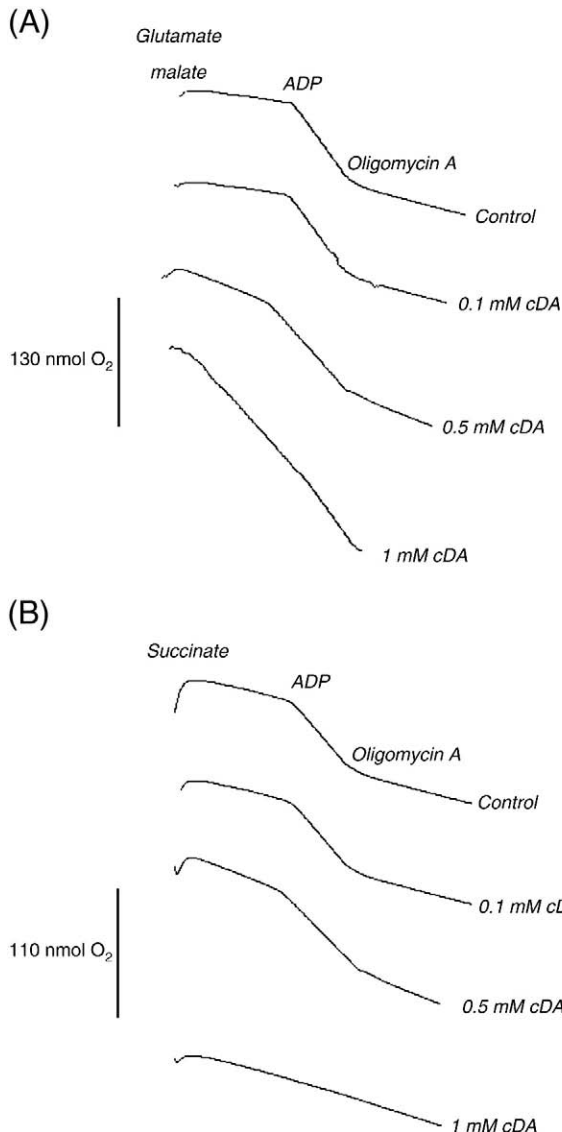


Fig. 2. Representative traces showing the effects of cDA on oxygen consumption in mitochondria supported by glutamate/malate (A) or succinate (B). Mitochondrial preparation ($0.5 \text{ mg protein mL}^{-1}$) and different concentrations of cDA ($0.1\text{--}1.0 \text{ mM}$) were supplemented to the incubation medium at the beginning of the assay. 1 mM ADP and $1 \mu\text{g mL}^{-1}$ oligomycin A were added as indicated. Vertical lines represent oxygen consumption. Traces are representative of four to five independent experiments and are expressed as $\text{nmol O}_2 \text{ min}^{-1} \text{ mg of protein}^{-1}$.

and reduced state 3 respiration (up to 68%) only when succinate was used as substrate [$F(3,15) = 7.80$; $P < 0.01$]. Interestingly, 1 mM cDA reduced oxygen consumption in state 4 respiring mitochondria with succinate as substrate as compared to 0.5 mM cDA . It was also observed that cDA significantly reduced the ADP/O ratio [glutamate/malate: $F(3,15) = 18.8$; $P < 0.001$; succinate: $F(3,15) = 30.1$; $P < 0.001$] and the respiratory control ratio (RCR) [glutamate/malate: $F(3,15) = 19.5$; $P < 0.001$; succinate: $F(3,15) = 45.1$; $P < 0.001$] regardless of the substrate, suggesting that this compound may behave as an uncoupler of the oxidative phosphorylation.

We further evaluated the effect of cDA on citric acid cycle enzyme activities in mitochondrial preparations and observed that this fatty acid significantly inhibited aconitase activity (up to 50%) (control: $698 \pm 111 \mu\text{M NADPH min}^{-1} \text{ mg protein}^{-1}$; 1 mM cDA : $379 \pm 143 \mu\text{M NADPH min}^{-1} \text{ mg protein}^{-1}$; $t(3) = 9.64$; $P < 0.01$), without affecting the other enzyme activities (data not shown).

Reduction of mitochondrial membrane potential by cis-4-decenoic acid

In order to better characterize the uncoupling effect of cDA on oxidative phosphorylation, mitochondrial membrane potentials ($\Delta\Psi_m$) were measured using the fluorescent probe safranin O (Fig. 3). We observed that cDA markedly decreased $\Delta\Psi_m$ with glutamate plus malate (Panel A) or succinate (Panel B) as substrates in

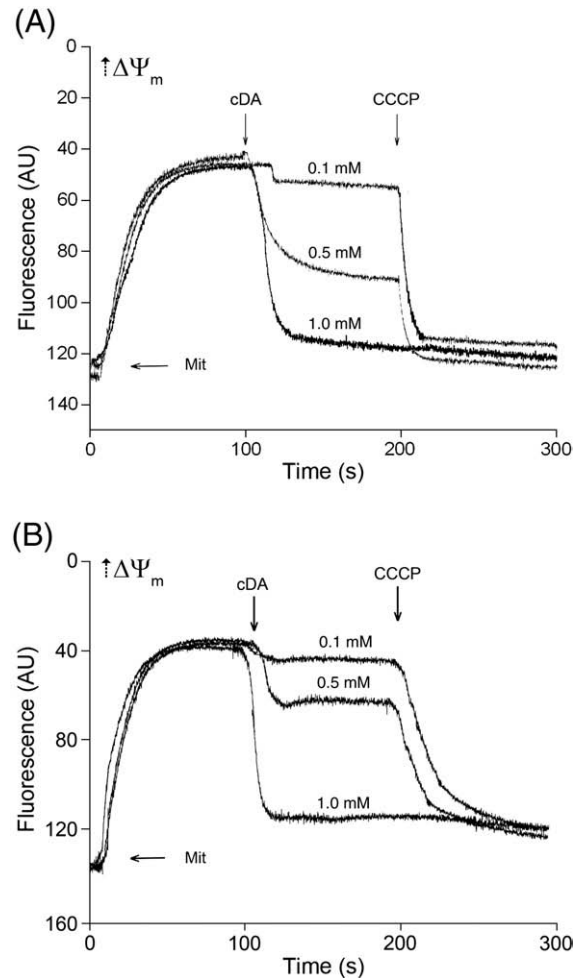


Fig. 3. Effect of cDA on mitochondrial membrane potential using glutamate/malate (A) or succinate (B) as substrates. cDA (1.0 mM) was added to the medium containing the mitochondrial preparation ($0.5 \text{ mg protein mL}^{-1}$) at the beginning of the assay and CCCP ($1 \mu\text{M}$) was added at the end of the measurements. Traces are representative of four independent experiments and were expressed as fluorescence arbitrary units (FAU).

a dose-response manner. Furthermore, the addition of the classical protonophore CCCP was unable to change the $\Delta\Psi_m$ decrease induced by 1 mM cDA, suggesting that maximal uncoupling was already achieved. These data indicate a relevant uncoupling effect of this compound.

The adenine nucleotide translocator is not involved in cis-4-decenoic acid-uncoupler effect

We then assessed oxygen consumption in the presence of 1 μM atracyloside (ATC), an inhibitor of adenine nucleotide translocator (ANT), in order to search for the mechanism through which cDA uncouples mitochondria. We observed that cDA-induced increase of oxygen consumption was not prevented by ATC [$F(3,15)=27.3$; $P<0.001$] (Fig. 4), ruling out a selective mitochondrial membrane permeabilization via ANT in the cDA-elicted uncoupling effect.

NAD(P)H pool is reduced by cis-4-decenoic acid

We then assayed the mitochondrial NAD(P)H content, since uncouplers of the oxidative phosphorylation generally reduce the mitochondrial matrix NAD(P)H pool. cDA provoked a marked decrease in NAD(P)H fluorescence (Fig. 5) with glutamate plus malate (Panel A) or succinate (Panel B) as substrates. Similar results were obtained when CCCP was added to the incubation medium (data not shown). Furthermore, the supplementation of rotenone to the medium, only partially reestablished the reduced equivalent pool in the presence of cDA, indicating that NAD(P)H pool was partially lost from the matrix when cDA was present in the incubation medium.

cis-4-decenoic acid causes mitochondrial swelling

Mitochondrial swelling was also evaluated in the presence of cDA. We verified that cDA provoked a marked mitochondrial swelling (Fig. 6A). Similar results were obtained when mitochondria were incubated in sucrose-based medium, instead of KCl (Fig. 6B). Furthermore, the addition of cyclosporin A did not prevent the cDA-elicted mitochondrial swelling (data not shown), excluding a role for the classical mitochondrial permeability transition (MPTP) in this effect.

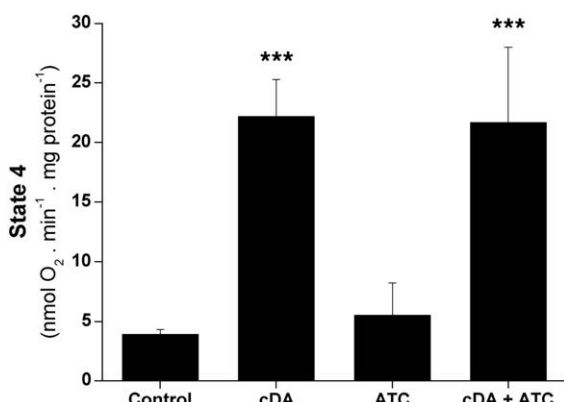


Fig. 4. Effect of cDA on oxygen consumption in glutamate/malate-supported mitochondria respiring in state 4. cDA (1.0 mM) was added to the medium containing the mitochondrial preparation (0.5 mg protein mL^{-1}) in the presence or absence of 1 μM atracyloside (ATC) at the beginning of the assay. Values are means \pm standard deviation for four independent experiments and state 4 of mitochondrial respiration is expressed as $\text{nmol O}_2 \text{ min}^{-1} \text{ mg of protein}^{-1}$. *** $P<0.001$ compared to controls (Duncan multiple range test).

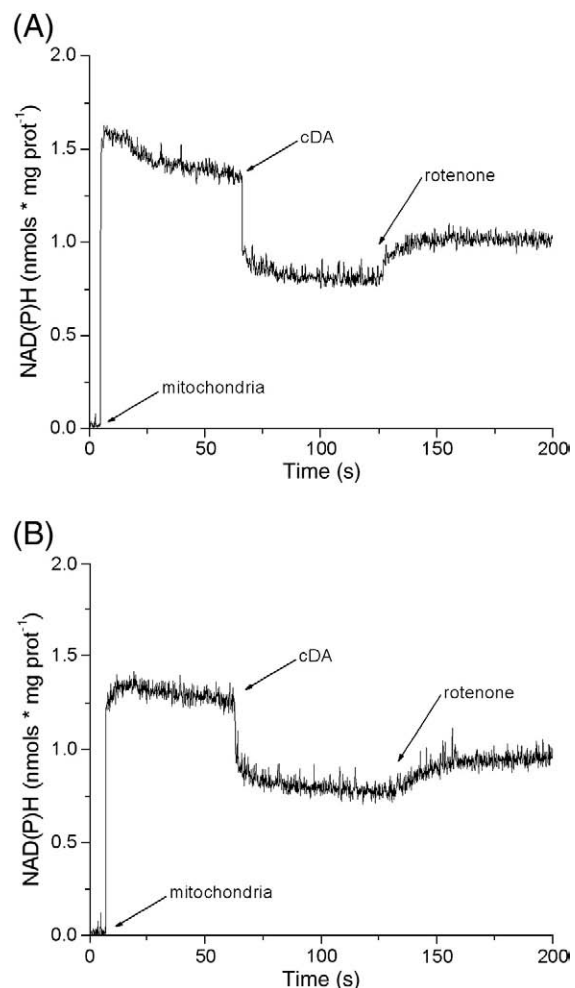


Fig. 5. Effect of cDA on mitochondrial NAD(P)H content using glutamate/malate (A) or succinate (B) as substrates. cDA (1.0 mM) was added to the medium containing the mitochondrial preparation (0.5 mg protein mL^{-1}) at the beginning of the assay. Rotenone (4 μM) was added at the end of the measurements. Traces are representative of four independent experiments and data were expressed as nmol NAD(P)H mg of protein $^{-1}$.

cis-4-decenoic acid induces mitochondrial cytochrome c release

Considering that permeabilization of mitochondrial membrane could result in cytochrome c release from the mitochondria, we determined the cytochrome c immunocontent inside the mitochondria in the presence of 1.0 mM cDA. We observed that cDA decreased (up to 20%) the mitochondrial cytochrome c content [$F(2,6)=196.5$; $P<0.001$] (Fig. 7), implying an augmented cytochrome c release from the mitochondria.

Discussion

Patients affected by MCADD present encephalopathic crises accompanied by cerebral abnormalities (Smith and Davis 1993; Ruitenberg et al. 1995; Mayatepek et al. 1997; Wilson et al. 1999; Mayell et al. 2007), whose pathogenesis is not yet defined. Lethargy that may progress to coma and death during episodes of metabolic decompensation was recently suggested to be due to the accumulation of toxic medium-chain fatty acids (MCFA) and their by-products (Gregersen et al. 2008).

Previous findings have shown that cis-4-decenoate (cDA), the pathognomonic compound accumulating in MCADD, impairs brain mitochondrial bioenergetics and causes oxidative damage to a higher

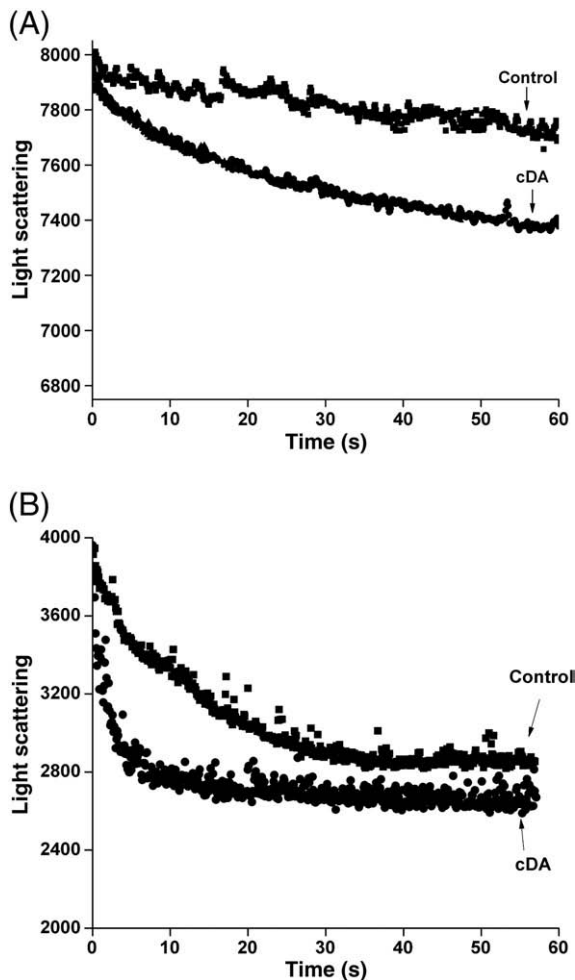


Fig. 6. Effect of cDA on mitochondrial swelling. cDA (1.0 mM) was added to the medium containing the mitochondrial preparation (0.5 mg protein mL⁻¹) and light scattering changes were assessed in the presence of KCl (A) or sucrose (B). Traces are representative of three to four independent experiments and were expressed as fluorescence arbitrary units (FAU).

extend and at lower doses than the effects elicited by octanoate (OA) and decanoate (DA), indicating that cDA is the most toxic accumulating compound in MCADD (Reis de Assis et al. 2004; Schuck et al. 2007, 2009a). cDA is structurally similar to *trans,trans*-2,4-decadienal, a promoter of non-selective inner mitochondrial membrane permeabilization (Sigolo et al. 2008). Therefore, in the present work we evaluated the effects of cDA on a wide spectrum of mitochondrial bioenergetic parameters determined by the rate of oxygen consumption, as well as citric acid cycle enzyme activities, mitochondrial membrane potential ($\Delta\Psi_m$), NAD(P)H content, mitochondrial swelling and cytochrome *c* release using rat brain mitochondrial preparations.

We first found that cDA significantly increased oxygen consumption in state 4 respiration mitochondria and reduced the ratios ADP/O and RCR with both substrates. The data is indicative that cDA behaves as an uncoupler of oxidative phosphorylation. In addition, state 3 respiration was markedly diminished by cDA with succinate as substrate. Interestingly, when succinate was used as substrate, the rate of oxygen consumption in state 4 respiration mitochondria markedly dropped at the highest cDA dose (1.0 mM) employed, as compared to 0.5 mM. This may have occurred due to an inhibition of complex II activity, limiting the flux of electrons from succinate through the respiratory chain, as previously demonstrated (Reis de Assis et al. 2004). Alternatively, a competition between cDA and succinate for mitochondrial dicarboxylate transport could possibly

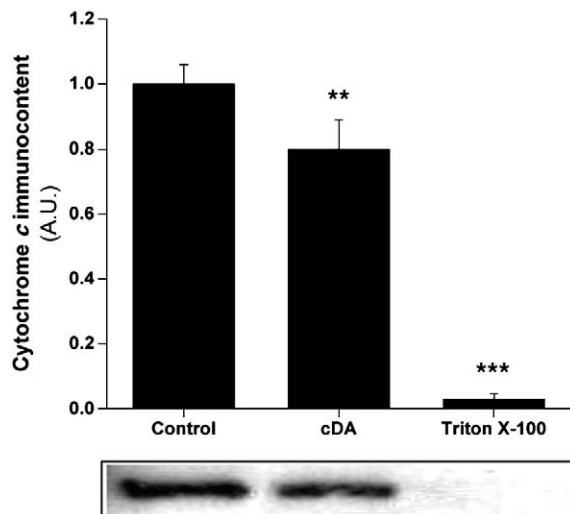


Fig. 7. Effect of cDA on mitochondrial cytochrome *c* immunocontent. cDA (1.0 mM) was added to the medium containing the mitochondrial preparation (0.5 mg protein mL⁻¹). Triton-X 100 was used as a positive control. A representative immunoblot of cytochrome *c* is also displayed. ANT was used as loading control. Values are means \pm standard deviation for three independent experiments and the results were expressed as arbitrary units (AU). ** $P<0.01$, *** $P<0.001$ compared to controls (Duncan multiple range test).

explain the results obtained with cDA at the highest concentration on states 3 and 4, but this is unlikely since cDA is a monocarboxylic acid and uses other mitochondrial carrier.

cDA also decreased $\Delta\Psi_m$ in state 4-respiring mitochondria to a similar extent as that of the classical uncoupler CCCP, supporting a strong uncoupling role for this organic acid. Another evidence that cDA acts as uncoupler of oxidative phosphorylation was the reduction of matrix NAD(P)H levels altering the mitochondrial redox state, a finding commonly provoked by uncoupling agents by stimulating NADH oxidation. Moreover, the complex I inhibitor rotenone, which prevents NADH oxidation, only partially reestablished the reduced equivalent pool in the presence of cDA, suggesting that the reduced equivalents may have been partially lost from the mitochondrial matrix. On the other hand, considering that the phosphorylation state of the cytosolic ATP pool is very sensitive to small changes in the mitochondrial membrane potential (Nicholls 2004), the marked depolarization of the mitochondrial membrane potential evoked by cDA might have severe consequences for long-term energy homeostasis in MCAD-deficient patients.

We also observed that the adenine nucleotide translocator (ANT) inhibitor atractyloside (ATC) did not prevent the increase in the rate of oxygen consumption in state 4-respiring mitochondria elicited by cDA, implying that the involvement of ANT in cDA-uncoupling effect, as previously shown for other fatty acids (Brustovetsky et al. 1990; Skulachev 1998; Samartsev et al. 2000), is unlikely. In this context, interaction with other anion transporters, with mitochondrial membrane phospholipids, or a distortion of the packing of the lipids in the inner mitochondrial membrane leading to alterations in fluidity and ion permeability (Kimmelberg and Pahadopoulous 1974; Lee 1976; Abeywardena et al. 1983; Schonfeld and Struy 1999; Skulachev 1999; Mokhova and Khailova 2005) may possibly underlie the uncoupling effect promoted by this compound. Our findings showing that cDA provoked a significant mitochondrial swelling reinforce the presumption that this compound increases mitochondrial membrane permeability. Furthermore, the observations that this effect was not blocked by cyclosporin A (CsA) rule out the participation of the mitochondrial permeability transition pore (MPTP). It is therefore presumed that the increased permeabilization of the inner mitochondrial membrane provoked by cDA possibly explains the partial loss of the reduced equivalents from the mitochondrial matrix through other

mechanisms than CsA-sensitive MPTP opening. In this scenario, since mitochondrial swelling elicited by cDA occurred with either KCl or sucrose in the incubation medium, a cDA-induced non-selective permeabilization of inner mitochondrial membrane may possibly explain our data.

We also found that cDA reduced mitochondrial matrix cytochrome *c* immunocontent, a finding that may be related to the increase of mitochondrial membrane permeability caused by this fatty acid. However, considering that cytochrome *c* release is part of the intrinsic apoptotic pathway (Li et al. 1997; Perkins et al. 2009), we cannot rule out that cDA induces apoptosis, but this should be investigated in further studies.

Although the pathophysiological relevance of our data is at present unknown since brain cDA concentrations in MCADD are not yet established, it should be stressed that cDA provoked an impairment of mitochondrial homeostasis at concentrations of 100 μM and higher. In this scenario, previous works reported that the average plasma cDA levels in MCADD patients may achieve 200 μM (controls: <0.4 μM) and that these concentrations significantly increase during crises of metabolic decompensation (Duran et al. 1988; Onkenhout et al. 1995; Martinez et al. 1997). Moreover, considering that the enzymes of fatty acid oxidation are expressed in the neural cells (Tyni et al. 2004) and that the tissue concentrations of the accumulating metabolites dramatically increase in these patients during metabolic crises due to accelerated lipolysis and the blockage of the enzymatic step catalyzed by MCAD (Martinez et al. 1997; Roe and Ding 2001), it is presumed that higher concentrations of this fatty acid occur in metabolic stress situations. It should be also emphasized that impairment of the transchoroidal clearance of fatty acids accumulating in MCADD and similar compounds from the brain occurs after *in vivo* administration of octanoic acid (Kim et al. 1983) and that the concentrations of organic acids in neural cells overcome those of plasma or CSF in various disorders of organic acid metabolism (Hoffmann et al. 1993). All these mechanisms may act synergistically contributing to the accumulation of MCFA in the brain and cerebral spinal fluid of patients affected by MCADD.

We have previously demonstrated that OA and DA, which also accumulate in MCADD, disturb energy production and oxidative phosphorylation. OA and DA at 1 mM or higher concentrations were demonstrated to inhibit the citric acid cycle and respiratory chain complexes activities, as well as to alter respiratory parameters and mitochondrial membrane potential (Reis de Assis et al. 2004; Schuck et al. 2009b). It should be emphasized that cDA effects on these parameters were more severe and occurred at much lower concentrations (0.1 mM and higher). Therefore, based on these findings showing that more pronounced effects were achieved with lower concentrations of cDA, as compared to OA and DA, and also considering the concentrations of these fatty acids in MCADD, we hypothesized that cDA is probably the most toxic metabolite in this disorder.

Conclusion

In conclusion, this is the first report showing that cDA acts as an uncoupler of oxidative phosphorylation. Based on the present observations that cDA at 1 mM significantly decreases state 3 respiration, causes a rapid drop in oxygen consumption in state 4 respiration with succinate and markedly inhibits aconitase activity, as well as CO₂ production and respiratory chain complexes activities (Reis de Assis et al. 2004), it is feasible that cDA also behaves as a metabolic inhibitor, therefore compromising mitochondrial energy homeostasis. Therefore, it is tempting to speculate that our present and previous findings indicate that impairment of brain bioenergetics may be involved in the neuropathology of MCAD-deficient patients (Egidio et al. 1989; Maegawa et al. 2008).

Conflict of interest statement

The authors declare that there are no conflicts of interest.

Acknowledgments

This work was supported by grants from CNPq, PRONEX II, FAPERGS, PROPESQ/UFRGS, FAPESP, FINEP research grant Rede Instituto Brasileiro de Neurociência (IBN-Net) # 01.06.0842-00 and INCT-EN.

References

- Abeywardena MY, Allen TM, Charnock JS. Lipid–protein interactions of reconstituted membrane-associated adenosine triphosphatases. *Biochimica et Biophysica Acta* 729, 62–74, 1983.
- Akerman KE, Wikström MK. Safranine as a probe of the mitochondrial membrane potential. *FEBS Letters* 68, 191–197, 1976.
- Brustovetsky NN, Dedukhova VI, Egorova MV, Mokhova EN, Skulachev VP. Inhibitors of the ATP/ADP antiporter suppress stimulation of mitochondrial respiration and H⁺ permeability by palmitate and anionic detergents. *FEBS Letters* 272, 187–189, 1990.
- Coates PM. New developments in the diagnosis and investigation of mitochondrial fatty acid oxidation disorders. *European Journal Pediatrics* 153, 49–56, 1994.
- de Assis DR, Maria RC, Ferreira GC, Schuck PF, Latini A, Dutra-Filho CS, Wannmacher CM, Wyse AT, Wajner M. Na⁺, K⁺ ATPase activity is markedly reduced by cis-4-decenoic acid in synaptic plasma membranes from cerebral cortex of rats. *Experimental Neurology* 197, 143–149, 2006.
- de Assis DR, Ribeiro CA, Rosa RB, Schuck PF, Dalcin KB, Vargas CR, Wannmacher CM, Dutra-Filho CS, Wyse AT, Briones P, Wajner M. Evidence that antioxidants prevent the inhibition of Na⁺, K⁺-ATPase activity induced by octanoic acid in rat cerebral cortex *in vitro*. *Neurochemical Research* 28, 1255–1263, 2003.
- Derkx TG, Reijngoud DJ, Waterham HR, Gerver WJ, van den Berg MP, Sauer PJ, Smit GP. The natural history of medium-chain acyl CoA dehydrogenase deficiency in the Netherlands: clinical presentation and outcome. *The Journal of Pediatrics* 148, 665–670, 2006.
- Duran M, Bruunvis L, Ketting D, de Klerk JB, Wadman SK. Cis-4-decenoic acid in plasma: a characteristic metabolite in medium-chain acyl-CoA dehydrogenase deficiency. *Clinical Chemistry* 34, 548–551, 1988.
- Egidio RJ, Francis GL, Coates PM, Hale DE, Roesel A. Medium-chain acyl-CoA dehydrogenase deficiency. *American Family Physician* 39, 221–226, 1989.
- Estabrook RW. Mitochondrial respiratory control and the polarographic measurement of ADP/O ratios. In: Estabrook, RW, Pullman, ME (Eds.), *Methods in Enzymology*. Academic Press, New York, pp. 41–47, 1967.
- Fischer JC, Ruitenberg W, Berden JA, Trijbels JM, Veerkamp JH, Stadhouders AM, Sengers RC, Janssen AJ. Differential investigation of the capacity of succinate oxidation in human skeletal muscle. *Clinica Chimica Acta* 153, 23–36, 1985.
- Gregersen N, Andresen BS, Pedersen CB, Olsen RK, Corydon TJ, Bross P. Mitochondrial fatty acid oxidation defects—remaining challenges. *Journal of Inherited Metabolic Disease* 31, 643–657, 2008.
- Hoffmann GF, Seppel CK, Holmes B, Mitchell L, Christen HJ, Hanefeld F, Rating D, Nyhan WL. Quantitative organic acid analysis in cerebrospinal fluid and plasma: reference values in a pediatric population. *Journal of Chromatography* 617, 1–10, 1993.
- Kim CS, O’Tuama LA, Mann JD, Roe CR. Effect of increasing carbon chain length on organic acid transport by the choroid plexus: a potential factor in Reye’s syndrome. *Brain Research* 259, 340–343, 1983.
- Kimmelberg H, Pahadjopoulos D. Effects of phospholipid acyl chain fluidity, phase transitions, and cholesterol on (Na⁺, K⁺)-stimulated adenosine triphosphatase. *The Journal of Biological Chemistry* 249, 1071–1080, 1974.
- Kitto GB. Intra- and extramitochondrial malate dehydrogenase from chicken and tuna heart. *Methods Enzymology* 13, 106–116, 1969.
- Kowaltowski AJ, Cosso RG, Campos CB, Fiskum G. Effect of Bcl-2 overexpression on mitochondrial structure and function. *The Journal of Biological Chemistry* 277, 42802–42807, 2002.
- Lai JC, Cooper AJ. Brain alpha-ketoglutarate dehydrogenase complex: kinetic properties, regional distribution, and effects of inhibitors. *Journal of Neurochemistry* 47, 1376–1386, 1986.
- Lee AG. Model for action of local anesthetics. *Nature* 262, 545–548, 1976.
- Li P, Nijhawan D, Budihardjo I, Srinivasula SM, Ahmad M, Alnemri ES, Wang X. Cytochrome *c* and dATP-dependent formation of Apaf-1/caspase-9 complex initiates an apoptotic protease cascade. *Cell* 91, 479–489, 1997.
- Lowry OH, Rosebrough NJ, Farr AL, Randall RJ. Protein measurement with the Folin phenol reagent. *The Journal of Biological Chemistry* 193, 265–275, 1951.
- Maegawa GH, Poplawski NK, Andresen BS, Olpin SE, Nie G, Clarke JT, Teshima I. Interstitial deletion of 1p22.2p31.1 and medium-chain acyl-CoA dehydrogenase deficiency in a patient with global developmental delay. *American Journal of Medical Genetics* 146, 1581–1586, 2008.
- Martinez G, Jiménez-Sánchez G, Divry P, Vianey-Sabán C, Riudor E, Rodés M, Briones P, Ribes A. Plasma free fatty acids in mitochondrial fatty acid oxidation defects. *Clinica Chimica Acta* 267, 143–154, 1997.
- Mayatepek E, Koch HG, Hoffmann GF. Hyperuricaemia and medium-chain acyl-CoA dehydrogenase deficiency. *Journal of Inherited Metabolic Disease* 20, 842–843, 1997.

- Mayell SJ, Edwards L, Reynolds FE, Chakrapani AB. Late presentation of medium-chain acyl-CoA dehydrogenase deficiency. *Journal of Inherited Metabolic Disease* 30, 104, 2007.
- Mokhova EN, Khailova LS. Involvement of mitochondrial inner membrane anion carriers in the uncoupling effect of fatty acids. *Biochemistry (Mosc.)* 70, 159–163, 2005.
- Morrison JF. The activation of aconitase by ferrous ions and reducing agents. *The Biochemical Journal* 58, 685–692, 1954.
- Nicholls DG. Mitochondrial membrane potential and aging. *Aging Cell* 3, 35–40, 2004.
- O'Hare MC, Doonan S. Purification and structural comparisons of the cytosolic and mitochondrial isoenzymes of fumarate from pig liver. *Biochimica et Biophysica Acta* 827, 127–134, 1985.
- Onkenhout W, Venizelos V, Van der Poel PF, Van der Heuvel MP, Poorthuis BJ. Identification and quantification of intermediates of unsaturated fatty acid metabolism in plasma of patients with fatty acid oxidation disorders. *Clinical Chemistry* 41, 1467–1474, 1995.
- Perkins G, Bossy-Wetzel E, Ellisman MH. New insights into mitochondrial structure during cell death. *Experimental Neurology* 218, 183–192, 2009.
- Plaut GWE. Isocitrate dehydrogenase from bovine heart. In: Lowenstein JM (Ed.), *Methods in Enzymology*, Vol. 13. Academic Press, New York, pp. 34–42, 1969.
- Reis de Assis D, Maria RC, Borba Rosa R, Schuck PF, Ribeiro CA, da Costa Ferreira G, Dutra-Filho CS, Terezinha de Souza Wyse A, Duval Wannmacher CM, Santos Perry ML, Wajner M. Inhibition of energy metabolism in cerebral cortex of young rats by the medium-chain fatty acids accumulating in MCAD deficiency. *Brain Research* 1030, 141–151, 2004.
- Rinaldo P, Raymond K, Al-Odaib A, Bennett M. Clinical and biochemical features of fatty acid oxidation disorders. *Current Opinion in Pediatrics* 10, 615–621, 1998.
- Roe CR, Ding J. Mitochondrial fatty acid oxidation disorders. In: Scriver, CR, Beaudet, AL, Sly, WS, Valle, D (Eds.), *The Metabolic and Molecular Bases of Inherited Disease*. McGraw-Hill, New York, pp. 1909–1963, 2001.
- Rosenthal RE, Hamud F, Fiskum G, Varghese PJ, Sharpe S. Cerebral ischemia and reperfusion: prevention of brain mitochondrial injury by lidoflazine. *Journal of Cerebral Blood Flow and Metabolism* 7, 752–758, 1987.
- Ruitenbeek W, Poels PJ, Turnbull DM, Garavaglia B, Chalmers RA, Taylor RW, Gabreels FJ. Rhabdomyolysis and acute encephalopathy in late onset medium chain acyl-CoA dehydrogenase deficiency. *Journal of Neurology, Neurosurgery and Psychiatry* 58, 209–214, 1995.
- Samartsev VN, Simonyan RA, Markova OV, Mokhova EN, Skulachev VP. Comparative study on uncoupling effects of laurate and lauryl sulfate on rat liver and skeletal muscle mitochondria. *Biochimica et Biophysica Acta* 145, 179–190, 2000.
- Schonfeld P, Struy H. Refsum disease diagnostic marker phytanic acid alters the physical state of membrane proteins of liver mitochondria. *FEBS Letters* 457, 179–183, 1999.
- Schuck PF, Ceolato PC, Ferreira GC, Tonin A, Leipnitz G, Dutra-Filho CS, Latini A, Wajner M. Oxidative stress induction by cis-4-decenoic acid: relevance for MCAD deficiency. *Free Radical Research* 41, 1261–1272, 2007.
- Schuck PF, Ferreira GC, Moura AP, Busanello EN, Tonin AM, Dutra-Filho CS, Wajner M. Medium-chain fatty acids accumulating in MCAD deficiency elicit lipid and protein oxidative damage and decrease non-enzymatic antioxidant defenses in rat brain. *Neurochemistry International* 54, 519–525, 2009a.
- Schuck PF, Ferreira GdA C, Tonin AM, Viegas CM, Busanello EN, Moura AP, Zanatta A, Klamt F, Wajner M. Evidence that the major metabolites accumulating in medium-chain acyl-CoA dehydrogenase deficiency disturb mitochondrial energy homeostasis in rat brain. *Brain Research* 1296, 117–126, 2009b.
- Sigolo CA, Di Mascio P, Kowaltowski AJ, Garcia CC, Medeiros MH. trans, trans-2, 4-decadienal induces mitochondrial dysfunction and oxidative stress. *Journal of Bioenergetics and Biomembranes* 40, 103–109, 2008.
- Skulachev VP. Uncoupling: new approaches to an old problem of bioenergetics. *Biochimica et Biophysica Acta* 1363, 100–124, 1998.
- Skulachev VP. Anion carriers in fatty acid-mediated physiological uncoupling. *Journal of Bioenergetics and Biomembranes* 31, 431–445, 1999.
- Smith Jr ET, Davis GJ. Medium-chain acylcoenzyme-A dehydrogenase deficiency. Not just another Reye syndrome. *The American Journal of Forensic Medicine and Pathology* 14, 313–318, 1993.
- Srere PA. Citrate synthase. *Methods Enzymology* 13, 3–11, 1969.
- Tretter L, Adam-Vizi V. Generation of reactive oxygen species in the reaction catalyzed by alpha-ketoglutarate dehydrogenase. *The Journal of Neuroscience* 24, 7771–7778, 2004.
- Tyni T, Paetau A, Strauss AW, Middleton B, Kivelä T. Mitochondrial fatty acid beta-oxidation in the human eye and brain: implications for the retinopathy of long-chain 3-hydroxyacyl-CoA dehydrogenase deficiency. *Pediatric Research* 56, 744–750, 2004.
- Wilson CJ, Champion MP, Collins JE, Clayton PT, Leonard JV. Outcome of medium chain acyl-CoA dehydrogenase deficiency after diagnosis. *Archives of Disease and Childhood* 80, 459–462, 1999.

***Saccharomyces cerevisiae coq10* null mutants are responsive to antimycin A**

Cleverson Busso¹, Erich B. Tahara², Renata Oguuscu², Ohara Augusto², Jose Ribamar Ferreira-Junior³, Alexander Tzagoloff⁴, Alicia J. Kowaltowski² and Mario H. Barros¹

¹ Departamento de Microbiologia, Instituto de Ciencias Biomedicas, Universidade de Sao Paulo, Brazil

² Departamento de Bioquimica, Instituto de Quimica, Universidade de Sao Paulo, Brazil

³ Escola de Artes, Ciências e Humanidades, Universidade de Sao Paulo, Brazil

⁴ Department of Biological Sciences, Columbia University, New York, NY, USA

Keywords

coenzyme Q; mitochondria;
Saccharomyces cerevisiae

Correspondence

M. H. Barros, Departamento de Microbiologia, Instituto de Ciencias Biomedicas, Universidade de Sao Paulo, Av. Professor Lineu Prestes, 1374, 05508-900, Sao Paulo, Brazil
Fax: 55 11 30917354
Tel: 55 11 30918456
E-mail: mariohb@usp.br

(Received 16 June 2010, revised 3 August 2010, accepted 3 September 2010)

doi:10.1111/j.1742-4658.2010.07862.x

Deletion of *COQ10* in *Saccharomyces cerevisiae* elicits a respiratory defect characterized by the absence of cytochrome *c* reduction, which is correctable by the addition of exogenous diffusible coenzyme Q₂. Unlike other *coq* mutants with hampered coenzyme Q₆ (Q₆) synthesis, *coq10* mutants have near wild-type concentrations of Q₆. In the present study, we used Q-cycle inhibitors of the coenzyme QH₂-cytochrome *c* reductase complex to assess the electron transfer properties of *coq10* cells. Our results show that *coq10* mutants respond to antimycin A, indicating an active Q-cycle in these mutants, even though they are unable to transport electrons through cytochrome *c* and are not responsive to myxothiazol. EPR spectroscopic analysis also suggests that wild-type and *coq10* mitochondria accumulate similar amounts of Q₆ semiquinone, despite a lower steady-state level of coenzyme QH₂-cytochrome *c* reductase complex in the *coq10* cells. Confirming the reduced respiratory chain state in *coq10* cells, we found that the expression of the *Aspergillus fumigatus* alternative oxidase in these cells leads to a decrease in antimycin-dependent H₂O₂ release and improves their respiratory growth.

Introduction

Coenzyme Q (ubiquinone) is an essential electron carrier of the mitochondrial respiratory chain whose main function is to transfer electrons from the NADH-coenzyme Q and succinate-coenzyme Q reductases to the coenzyme QH₂-cytochrome *c* reductase (*bc1*) complex [1]. Electron transfer in the *bc1* complex occurs through the Q-cycle [2–4], in which electrons from reduced coenzyme Q (QH₂) follow a branched path to the iron-sulfur protein and to cytochrome *bL* [4].

Biosynthesis of coenzyme Q in eukaryotes occurs in mitochondria. In *Saccharomyces cerevisiae*, the benzene ring of coenzyme Q₆ (Q₆) has a polypropenyl side

chain with six isoprenoid units [5]. The size of the isoprenoid chain varies among species, and affects coenzyme Q diffusion through cell membranes [6]. On the other hand, at least nine yeast nuclear genes [7–9] have been shown to be involved in the synthesis of Q₆. *COQ10* is not involved in the synthesis of Q₆ but, interestingly, the respective mutants have Q₆ respiratory deficiencies [10–12]. All products of *COQ* genes, including Coq10p, are located in the mitochondrial inner membrane [1]. There is genetic and physical evidence that enzymes of Q₆ biosynthesis, but not Coq10p, form part of a multisubunit complex [13–15].

Abbreviations

AOX, alternative oxidase; *bc1*, coenzyme QH₂-cytochrome *c* reductase; BN, blue native; GSH, reduced glutathione; GSSG, oxidized glutathione; Q₆, coenzyme Q₆; QH₂, reduced coenzyme Q; ROS, reactive oxygen species.

Coq10p is a member of the START domain superfamily [10,12]. Members of this family were shown to bind lipophilic compounds such as cholesterol [16]. When overexpressed in yeast, purified Coq10p contains bound Q₆ [10,11]. The inability of Q₆ in *coq10* mutants to promote electron transfer to the *bcl* complex suggests that Coq10p might function in the delivery of Q₆ to its proper site in the respiratory chain. A direct role of Coq10p in electron transfer is not completely excluded, although it appears to be unlikely, because of stoichiometric considerations [10]. The present studies were undertaken to assess the respiratory functionality of Q₆ in *coq10* mutants that are defective in the reduction of cytochrome *c*. Using *bcl* complex inhibitors, we observed that *coq10* mitochondria were responsive to antimycin A but not to myxothiazol, indicating an active Q-cycle and defective transfer of QH₂ to the *bcl* Rieske protein. EPR spectroscopic analysis also suggests that wild-type and *coq10* mitochondria have similar amounts of Q₆ semiquinone, even with a lower steady-state level of *bcl* complex. On the other hand, the expression of *Aspergillus fumigatus* alternative oxidase (AOX) [17], which transports electrons directly from QH₂ to oxygen, reduced H₂O₂ release in *coq10* cells and improved their respiratory growth.

Results

Effect of antimycin A and myxothiazol on semiquinone formation in the *coq10* mutant

Antimycin A and myxothiazol are well-known inhibitors of the *bcl* complex, acting, respectively, at the N-site and P-site of the Q-cycle [18–21]. Both inhibitors enhance the formation of oxygen radicals from the P-site [20,21]. Antimycin A binds to the N-site and blocks oxidation of cytochrome *b_H*, resulting in a reverse flow of electrons from cytochrome *b_L* to coenzyme Q to form the semiquinone (Fig. 1). Myxothiazol, on the other hand, binds to the P-site and prevents the reduction of cytochrome *b_L*, but allows slow reduction of the Rieske iron–sulfur protein [4,20]. An increase in the amount of myxothiazol-dependent semiquinone is thought to occur at the P-site, owing to incomplete inhibition of ubiquinone oxidation [20–22]. However, the existence of semiquinones at the P-site is still controversial [20,23].

The functionality of the P-site in a *coq10* mutant was studied by examining antimycin A-dependent or myxothiazol-dependent production of reactive oxygen species (ROS) by assaying for H₂O₂ [21,22]. Yeast strains with different respiratory capacities were also

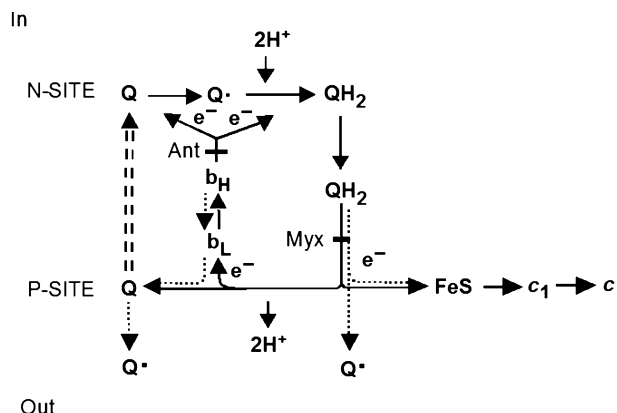


Fig. 1. Protonmotive Q-cycle of electron transfer and proton translocation in the *bc1* complex. The Q-cycle depicted schematically is based on Trumper *et al.* and Snyder *et al.* [4,32], showing the pathway of electron transfer from reduced QH₂ to cytochrome *c*. At the P-site, two electrons are transferred in a concerted manner from QH₂ to the iron–sulfur protein and to cytochrome *b_L*. Myxothiazol (Myx) binds to the P-site and prevents electron transfer to the Rieske protein. At the N-site, coenzyme Q (Q) is reduced by cytochrome *b_H*, first to the semiquinone and then to QH₂. This step is inhibited by antimycin (Ant), which binds to the N-site. The stippled arrows show the pathway of reduction of coenzyme Q to the semiquinone at the P-site in the presence of antimycin A or myxothiazol. The semiquinone formed in the presence of myxothiazol is the result of a slow leak of electrons to the iron–sulfur protein [21].

used as controls. Therefore, the effects of the two inhibitors were also tested in the parental wild-type strain, in a *coq2* mutant lacking Q₆ as a result of a deletion in the gene for *p*-hydroxybenzoate:polypropenyl transferase (which catalyzes the second step of coenzyme Q biosynthesis [24]), in a *bcs1* mutant arrested in assembly of the *bc1* complex [25], and in wild-type and *coq10* cells harboring the pYES2-AfAOX plasmid, expressing *A. fumigatus* AOX under the control of the *GAL10* promoter [17]. *A. fumigatus* AOX transfers electrons directly from QH₂ to oxygen [17].

Antimycin A increased H₂O₂ release in wild-type and *coq10* mitochondria. However, a clear myxothiazol-dependent increase occurred only in the wild type (Fig. 2A). On the other hand, the spontaneously high H₂O₂ release seen in the *coq2* and *bcs1* mutants suggests greater accumulation of flavin free radicals at the NADH and/or succinate dehydrogenase sites. Under conditions of Q₆ deficiency, when the oxidation of reduced Q₆ is blocked as a result of a defective *bc1* complex or respiratory inhibitor, keeping the FMN flavin reduced, NADH-coenzyme Q reductase (complex I) of mammalian and other mitochondria, including those of most yeast, has been shown to produce

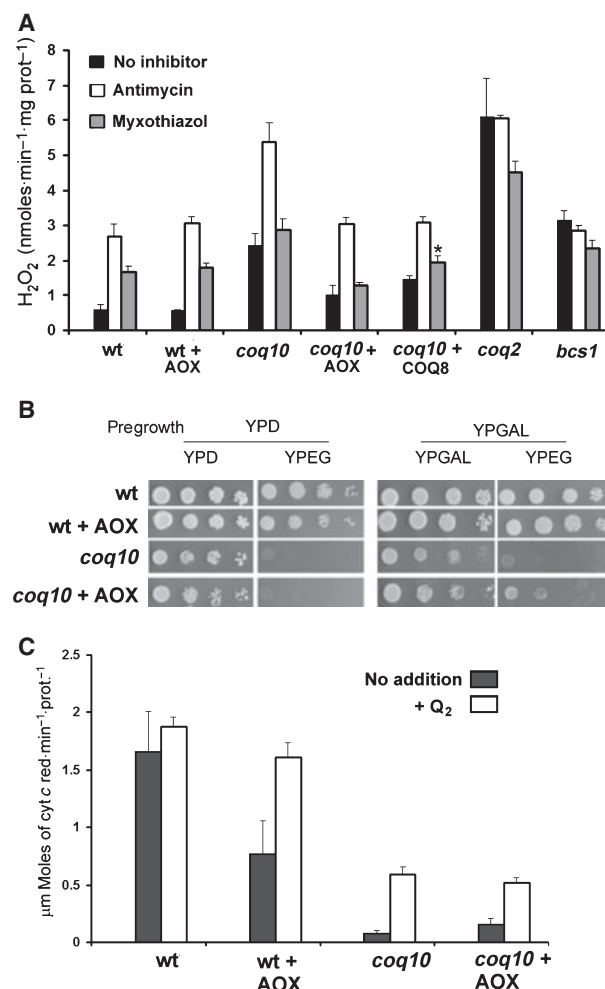


Fig. 2. Antimycin-dependent and myxothiazol-dependent production of H_2O_2 . Mitochondria were isolated from the following strains: wild-type W303-1A; the *coq* mutants aW303ΔCOQ2 (*coq2*) and aW303ΔCOQ10 (*coq10*); the *bcs1*-deficient mutant aW303ΔBCS1 (*bcs1*); and wild-type cells and *coq10* mutants transformed with pYES2-AfAOX (wt + AOX and *coq10* + AOX) and YEp352-COQ8 [10] (*coq10* + COQ8). (A) Mitochondria (100 µg of protein) were assayed as described in Experimental procedures for H_2O_2 release before and after the addition of 0.5 µg·mL⁻¹ antimycin A or myxothiazol at a final concentration of 0.5 µM. Both inhibitors increase the basal rate of single-electron reduction of oxygen, which generates the superoxide radical O_2^- [21], which then dismutates to H_2O_2 [30]. The vertical bars indicate ranges of four independent experiments. *P < 0.01 versus absence of inhibitor; statistical analysis and comparisons were performed with an unpaired Student's *t*-test, conducted by GRAPHPAD PRISM software. (B) Respiratory growth properties of wild-type cells, *coq10* mutants, and respective transformants with pYES2-AfAOX (wt + AOX, *coq10* + AOX) after pregrowth on glucose medium (YPD) or galactose medium (YPGal). (C) Measurements of NADH-cytochrome *c* reductase activity in isolated mitochondria from wild-type cells and *coq10* mutants and respective transformants with pYES2-AfAOX (wt + AOX, *coq10* + AOX), with or without the addition of 1 µM of synthetic coenzyme Q₂ (Q₂). The vertical bars indicate ranges of four independent experiments.

ROS [26]. NADH-coenzyme Q reductase of *S. cerevisiae* also contains FMN but is evolutionarily distinct from complex I. Even so, conditions that prevent reduction of Q₆ in *S. cerevisiae* may be expected to also favor increased production of H_2O_2 through accumulation of flavin semiquinones.

We reasoned that the presence of a bypass for reduced coenzyme Q might alleviate the production of ROS in the *coq10* mitochondria, and, indeed, we did observe less H_2O_2 in the mutant expressing the AOX of *A. fumigatus*.

Indeed, ROS production in the *coq10* mutant was enhanced by a factor of 4–6 (Fig. 2A), whereas in the *coq10*/AOX transformant, H_2O_2 release was only two times that observed in the wild-type cells. There was also a decrease in antimycin A-dependent release in the mutant strain expressing AOX. Antimycin A stimulation in the *coq10* mutant, however, was qualitatively different from that seen in the *coq2* or *bcs1* mutants. Antimycin A elicited a three-fold increase in ROS formation in the *coq10* mutant when normalized to the rate measured in the absence of inhibitor. In agreement with a previous report [21], antimycin A increased the rate of H_2O_2 release in wild-type and AOX transformants, but had no effect in the *coq2* and *bcs1* mutants over and above the rate seen without the inhibitor (Fig. 2B). The ability of antimycin A to stimulate ROS formation in the *coq10* mutant suggests that electron transfer from the low-potential cytochrome *b*_L to Q₆ at the P-site does not depend on Coq10p. Myxothiazol also increased H_2O_2 production in wild-type mitochondria, although the increase over the basal rate was less pronounced (three-fold). However, in the *coq10* mutant and in the *coq10*/AOX transformant, there were no significant effects on H_2O_2 release attributable to the addition of myxothiazol. Overexpression of COQ8 partially suppresses the *coq10* mutant respiratory defect [10]. Accordingly, we found that the presence of extra COQ8 in these experiments decreased the rate of H_2O_2 release, whereas antimycin A treatment promoted H_2O_2 levels similar to those in the wild-type strains and *coq10*/AOX transformant. On the other hand, we also observed that the COQ8-overexpressing strain showed a slight, but statistically significant, increase in H_2O_2 release when in the presence of myxothiazol.

The expression of the GAL10-AfAOX fusion in *coq10* cells also improved their respiratory growth when they were preincubated in media containing galactose (Fig. 2B). However, the specific enzymatic activity of NADH-cytochrome *c* reductase of *coq10*/AOX transformants did not change significantly (Fig. 2C). Curiously, wild-type cells harboring the

AOX plasmid had less NADH-cytochrome *c* reductase activity than untransformed cells, but the addition of synthetic Q₂ to wild-type/AOX mitochondria re-established the enzymatic activity to wild-type levels, indicating that the AOX electronic bypass is responsible for this decrease.

Detection of semiquinones by EPR spectroscopy and the steady-state level of *bc1* complex in the *coq10* mutant

The presence of Q₆ semiquinones in *coq10* mutants was checked by low-temperature EPR spectroscopy of wild-type, *coq10* and *coq1* mitochondria. The mitochondria of *coq1* mutants are completely devoid of Q₆, whereas *coq10* organelles have near wild-type levels of Q₆ [10]. Spectra were obtained from mitochondria with

membrane potentials maintained at 65 mV by the addition of extramitochondrial KCl [27] and with succinate as a respiratory substrate, to minimize the contribution of flavins to the semiquinone signal at $g \sim 2.005$ [28,29]. Under these conditions, the magnitude of the $g \sim 2.005$ signal was comparable in wild-type and *coq10* mitochondria, but was significantly lower in the *coq1* mutant (Fig. 3). Because of the absence of Q₆ in the *coq1* mutant, this signal is most likely derived from flavin semiquinones (Fig. 3A). Semiquinone concentrations in these samples were estimated by double integration of the EPR spectrum and comparison with the standard 4-hydroxy-2,2,6,6-tetramethyl-1-piperidinyloxy solution scanned under the same conditions. The calculated value for the wild-type mitochondria was 1.3 nmol·mg protein⁻¹, whereas that for the *coq10* mutant was 1.7 nmol·mg protein⁻¹.

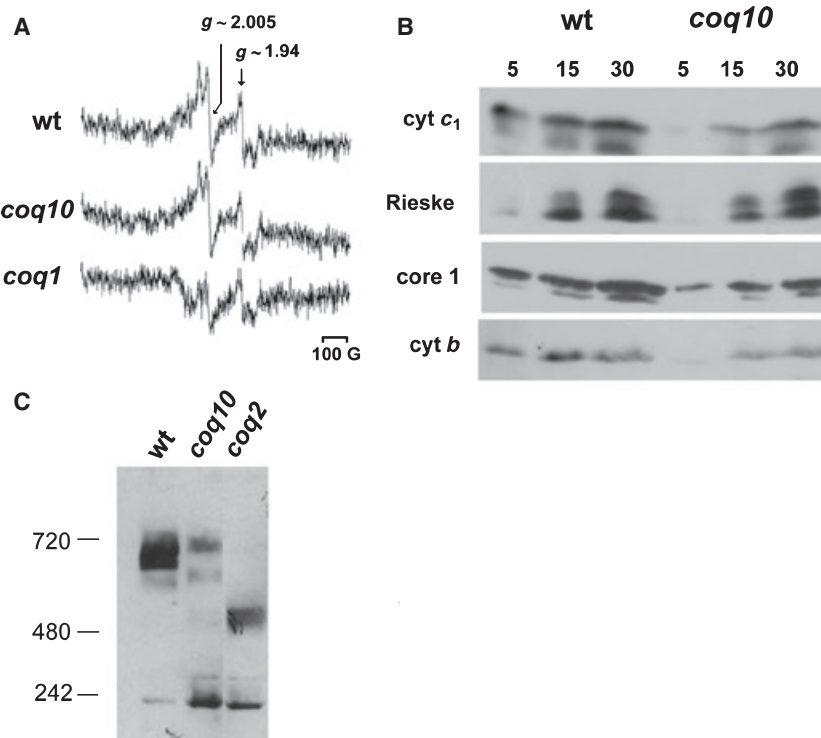


Fig. 3. Detection of semiquinone by EPR spectroscopy and *bc1* steady-state level. (A) Representative low-temperature EPR spectra of mitochondria isolated from W303 wild-type cells (wt) and *coq10* and *coq1* mutants maintained at 65 mV by the addition of KCl and succinate. The experimental conditions were as described in Experimental procedures. Spectra were obtained with a microwave power of 10 mW, a modulation amplitude of 5 G, a time constant of 81.920 ms, and a scan rate of 5.96 G s⁻¹. The receiver gain was 1.12×10^5 . Arrows correspond to the expected signal peaks for semiquinones ($g \sim 2.004$) and iron–sulfur centers ($g \sim 1.94$). (B) Western blot of *bc1* complex subunit polypeptides. Mitochondrial proteins from wild-type cells (wt) and *coq10* mutants (5, 15 and 30 µg) were separated on a 12% polyacrylamide gel as indicated. The proteins were transferred to nitrocellulose, and separately probed with antisera against Rieske iron–sulfur protein, core 1, cytochrome *c*₁, and cytochrome *b*. (C) Mitochondria from wild-type cells (wt) and *coq10* and *coq2* mutants were isolated with 2% digitonin, and samples representing 250 mg of starting mitochondrial protein were analyzed by BN-PAGE, the immunoblot of which was probed with antisera against cytochrome *b*. Estimated molecular masses are indicated, and were based on the migration of F₀/F₁-ATPase dimmers and monomers [42].

The semiquinone concentration in the *coq1* mutant was not calculated, because the spectrum obtained for this mutant contained a depression close to the semiquinone signal, precluding quantification by double integration. The signals detected at $g \sim 1.94$, corresponding to the iron–sulfur centers, were similar in the two mutants. Approximately half of the *coq10* ρ^+ cells and one-fifth of the *coq1* ρ^+ cells were converted to ρ^- and ρ^0 after cell growth for mitochondrial preparation. There are a number of cellular events that lead to mitochondrial DNA instability in yeast [30]. We can speculate that changes in the mitochondrial redox state may trigger the observed instability in these *coq* mutants. Nevertheless, this fact could also explain their lower iron–sulfur signal as compared with wild-type mitochondria. In order to evaluate the presence of the *bcl* complex in the *coq10* mutant mitochondria, the steady-state concentrations of some *bcl* subunits were checked and compared with those of wild-type mitochondria, using different amounts of mitochondrial proteins for quantitative evaluation (Fig. 3B). Western blot analyses with subunit-specific antibodies revealed six-fold less cytochrome *b*, and half to two orders of magnitude decreases in the amounts of cytochrome *c*₁, Rieske iron–sulfur and core 1 proteins in the *coq10* mitochondria, probably as a consequence of the *coq10* mitochondrial DNA instability. On the other hand, in a *coq2* mutant, the steady-state levels of these *bcl* complex proteins were one-quarter lower than that of the wild type (not shown). Accordingly, the addition of diffusible Q₂ to the *coq10* mitochondria restored less than half of the NADH-cytochrome *c* reductase activity of the wild type (Fig. 2C), which is also observed in other *coq* mutants [9,14,24]. In agreement with this lower concentration of *bcl* complex subunits in the *coq10* mutant, Fig. 3C shows one-dimensional blue native (BN)-PAGE of wild-type, *coq10* and *coq2* mitochondrial digitonin extracts, immunodetected with apocytochrome *b*. The predominant signal indicates the presence of high molecular mass complexes in the wild-type and in the *coq10* mitochondrial digitonin extracts, but with altered size in the *coq2* extract, as detected previously in a *coq4* point mutant [31]. These high molecular mass complexes correspond to respiratory supercomplexes, which in yeast should involve the association of cytochrome *c* oxidase and *bcl* complex dimer [32]. Immunodetection with antibodies against Cox4p also revealed the same high molecular mass complexes at the same size and intensity (not shown). It is noteworthy that *coq10* mitochondrial extracts revealed complexes of apparently the same size as those of the wild type, but much less abundant. Altogether, the EPR spectra and *bcl* complex steady-state

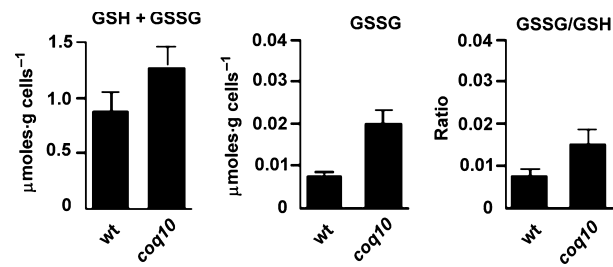


Fig. 4. Whole-cell glutathione in wild-type cells and *coq10* mutants. (A) GSSG and total glutathione were assayed in whole cells as previously described [33]. Briefly, total glutathione was determined with 76 μM 5,5'-dithiobis(2-nitrobenzoic acid) in the presence of 0.27 mM NADPH and 0.12 U·mL⁻¹ glutathione reductase. The GSSG level was estimated by incubation of cells for 1 h in the presence of 5 mM *N*-ethylmaleimide at pH 7. The concentration of GSH was calculated from the difference between total glutathione and GSSG, and used to express the GSSG/GSH ratio. The values reported are averages of three independent measurements with the ranges indicated by the vertical bars.

levels suggest that even with less active *bcl* complex in the *coq10* mitochondria, they accumulate semiquinone concentrations similar to those of the wild type.

Superoxide anion formation and redox state of *coq* mutants

Leakage of electrons emanating from NADH and succinate reduce oxygen to the superoxide anion, which is dismutated to H₂O₂ [33]. As already noted, the H₂O₂ assays indicated substantially higher rates of superoxide production in the *coq10* mutant and in the *coq2* mutant (lacking Q₆) (Fig. 3B). Measurements of cellular glutathione, a natural ROS scavenger, were used to further assess the redox state of mutants blocked in electron transfer at the level of the *bcl* complex. The increased oxidant production in *coq10* and *coq2* mutants was supported by their significantly greater content of oxidized glutathione (GSSG) than of reduced glutathione (GSH) and total glutathione (Fig. 4).

Discussion

The yeast *COQ10* gene codes for a mitochondrial inner membrane protein that binds Q₆ and is essential for respiration [10–12]. Unlike *coq1–9* mutants, which fail to synthesize Q₆ [7–9], yeast *coq10* mutants have normal amounts of Q₆, but respiration is completely restored by the addition of the more diffusible Q₂ [10,12].

The ability of Coq10p to bind Q₆ suggested that one of its functions might be the delivery/exchange of Q₆

between the *bc1* complex and the large pool of free Q₆ during electron transport [10]. This idea was supported by the homology of Coq10p to the reading frame CC1736 of *Caulobacter crescentus*, which codes for a member of the START superfamily [10,12] that is implicated in the delivery of polycyclic compounds such as cholesterol. These compounds bind to a hydrophobic tunnel that is a structural hallmark of this protein family. Another possible function of Coq10p was proposed to be in the transport of Q₆ from its site of synthesis to its active sites in the *bc1* complex, which would also require Coq10p binding to Q₆.

To better understand the function of Coq10p, we tested the reducibility of Q₆ in a *coq10* null mutant in the presence of inhibitors that block Q₆ binding to the P (o)-site and N (i)-site of the *bc1* complex. Reduction of Q₆ was also examined by comparing the EPR signals associated with semiquinone radicals in wild-type and mutant mitochondria, and by measuring their concentrations of GSSG and GSH. As glutathione is an effective scavenger of ROS, the ratio of GSSG to GSH serves as an index of redox state.

Inhibition of respiration in mammalian and yeast mitochondria with antimycin A has previously been shown to increase the rate of coenzyme Q reduction to form oxygen radicals [20,21]. In agreement with these data, addition of antimycin A and myxothiazol to respiratory-competent yeast mitochondria was found to stimulate oxygen radical formation by six-fold and three-fold, respectively, as inferred by the rate of H₂O₂ released. A significant (three-fold) antimycin A-dependent increase in ROS production was also observed in the *coq10* mutant. The stimulation by antimycin A was not observed in a *bc1* mutant or in mutants lacking Q₆, and was much lower in the *coq10* mutant when myxothiazol was used. The increase in ROS production in the presence of antimycin A indicates that the mutant is capable of transferring an electron from cytochrome *b*_L to Q₆ at the P-site. Coq10p is therefore not required for the accessibility of Q₆ to the cytochrome *b*_L center at the P-site. Moreover, the presence of the *A. fumigatus* AOX [17] as a bypass for reduced coenzyme Q alleviates H₂O₂ release from the *coq10* mutant, and even improves respiratory growth. These results are also supported by EPR spectroscopy of mitochondria. The signal at *g* ~ 2.005 corresponds to semiquinones, and had a lower magnitude in *coq1* mitochondria. As this mutant lacks Q₆, the residual signal at *g* ~ 2.005 is most likely contributed by flavin semiquinone. Because of the lower steady-state level of *bc1* complex in the *coq10* mitochondria, the real magnitude of the EPR signal should be larger in the mutant than in wild-type cells.

The possible myxothiazol-dependent reduction of Q₆ to the semiquinone at the P-site has been proposed to result from incomplete inhibition of electron transfer to the iron–sulfur protein [19,20,34]. In the strains tested, the presence of myxothiazol elevated H₂O₂ release only in the wild-type cells and in the *coq10* mutant overexpressing *COQ8*.

The Q₆-deficient mitochondria of the *coq2* mutant had a higher basal rate of ROS production than the wild type. The sources of the extra ROS are probably NADH and succinate dehydrogenase-associated flavins. Similar results were reported for a Q₆-deficient *coq7* mutant, but only when the mitochondria were assayed at 42 °C [35]. As the assays in the present study were performed at 30 °C, the difference in ROS production may stem from the genetic background of the W303 strain used in the present study, which could engender a feebler oxidative stress response [36]. Our experiments do not distinguish between flavin and Q₆ as the source of the increased free radicals in the *bc1* mutant. It is worth emphasizing that even though the *coq2* and *bc1* mutants both displayed higher basal rates of ROS production, these were not further enhanced by the addition of antimycin A, as was the case with wild-type and *coq10* mutant mitochondria.

Experimental procedures

Yeast strains and growth media

The genotypes and sources of the yeast strains used in this study are listed in Table 1. The compositions of YPD, YPEG and minimal glucose medium have been described elsewhere [10].

Oxygen consumption

Mitochondrial and spheroplast oxygen consumption was monitored on a computer-interfaced Clark-type electrode at 30 °C with 1 mM malate/glutamate, 2% ethanol or 1 μmol of NADH as substrate in the presence of mitochondria at 400 μg·mL⁻¹, or spheroplasts at 600 μg·mL⁻¹ total cell protein. All measurements were carried out in the presence of 0.002% digitonin. In order to block cytochrome *c* oxidase respiration, 1 mM KCN was added at the end of the trace.

H₂O₂ production

H₂O₂ formation in mitochondria was monitored for 10 min at 30 °C in a buffer containing 50 μM Amplex Red (Invitrogen, Carlsbad, CA, USA), 0.5 U·mL⁻¹ horseradish

Table 1. Genotypes and sources of *S. cerevisiae* strains.

Strain	Genotype	Source
W303-1 ^a	<i>MATa ade2-1, trp1-1, his3-115, leu2-3,112 ura3-1 p+, canR</i>	R. Rothstein, Columbia University
aW303ΔCOQ1	<i>MATa ade2-1 his3-1,15 leu2-3,112 trp1-1 ura3-1 coq1::LEU2</i>	[14]
aW303ΔCOQ2	<i>MATa ade2-1 his3-1,15 leu2-3,112 trp1-1 ura3-1 coq2::HIS3</i>	[23]
aW303ΔCOQ10	<i>MATa ade2-1 his3-1,15 leu2-3,112 trp1-1 ura3-1 coq10::HIS3</i>	[10]
aW303ΔBCS1	<i>MATa ade2-1 his3-1,15 leu2-3,112 trp1-1 ura3-1 bcs1::HIS3</i>	[24]

^a R. Rothstein, Department of Human Genetics, Columbia University, New York, NY, USA.

peroxidase (Sigma, St. Louis, MO, USA), 2% ethanol, 1 mM malate, 6 mM glutamate and 100 µg·mL⁻¹ mitochondrial protein. Resorufin production was recorded with a fluorescence spectrophotometer at 563 nm excitation and 587 nm emission. A calibration curve of known amounts of H₂O₂ was used to convert fluorescence to concentration of H₂O₂. Antimycin A and myxothiazol were added to final concentrations of 0.5 µg·mL⁻¹ and 0.5 µM, respectively.

Glutathione assays

GSSG, GSH and total glutathione were determined in late stationary phase with the 5,5'-dithiobis(2-nitrobenzoic acid) colorimetric assay [37].

EPR spectroscopy

EPR spectra were recorded at 77 K with a Bruker EMX spectrometer equipped with an ER4122 SHQ 9807 high-sensitivity cavity. For these experiments, 8 mg of mitochondrial protein suspended in 0.6 M sorbitol, 10 mM Tris/HCl (pH 7.5) and 1 mM EDTA were maintained at 65 mV by incubation for 2 min with KCl (12.4 mM), valinomycin (0.1 µg·mL⁻¹) and succinate (1 mM final) [27]. The samples were immediately transferred to a 1 mL disposable syringe, frozen, and stored in liquid nitrogen until analysis. Spectra were acquired by extrusion of the samples from the syringe into a finger-tip Dewar flask containing liquid nitrogen, and were examined at 77 K in the region of *g* ~ 2.000 [38]. The spectra shown here were corrected by baseline subtractions. The spectrum of 1,1-diphenyl-2-picrylhydrazyl (*g* = 2.004), and those of known concentrations of 4-hydroxy-2,2,6,6-tetramethyl-1-piperidinyloxy, acquired under the same conditions, were used as standards for determining the *g*-values and semiquinone concentrations, respectively.

Miscellaneous procedures

Measurements of respiratory enzymes were performed as described previously [39]. Mitochondria were prepared from yeast grown in rich media containing galactose as a carbon source [40]. Western blot quantifications were performed with 1DSCAN EX software (Scanalytics, Fairfax, VA, USA). For BN-PAGE, mitochondrial proteins were extracted with

a 2% final concentration of digitonin, and separated on a 4–13% linear polyacrylamide gel [41]. Proteins were transferred to a poly(vinylidene difluoride) membrane and probed with rabbit polyclonal antibodies against yeast cytochrome *b*. The antibody–antigen complexes were visualized with the SuperSignal chemiluminescent substrate kit (Pierce Thermo Scientific, Rockford, IL, USA).

Acknowledgements

We thank C. F. Clarke (University of California) for providing yeast strains, and T. Magnanini and S. A. Uyemura (Universidade de São Paulo) for the *A. fumigatus* AOX plasmid. We are indebted to E. Linares (IQ-USP) and F. Gomes (ICB-USP) for technical assistance. This work was supported by grants and fellowships from the Fundação de Amparo à Pesquisa de São Paulo (FAPESP – 2007/01092-5; 2006/03713-4), Conselho Nacional de Desenvolvimento Científico e Tecnológico (CNPq 470058/2007-2), and INCT de Processos Redox em Biomedicina-Redoxoma (CNPq-FAPESP/CAPES), and Research Grant HL022174 from the National Institutes of Health.

References

- Hatefi Y (1985) The mitochondrial electron transport and oxidative phosphorylation system. *Annu Rev Biochem* **54**, 1015–1069.
- Mitchell P (1975) The protonmotive Q cycle: a general formulation. *FEBS Lett* **59**, 137–139.
- Trumper BL (1990) The protonmotive Q cycle. Energy transduction by coupling of proton translocation to electron transfer by the cytochrome bc₁ complex. *J Biol Chem* **265**, 11409–11412.
- Trumper BL (2002) A concerted, alternating sites mechanism of ubiquinol oxidation by the dimeric cytochrome bc(1) complex. *Biochim Biophys Acta* **1555**, 166–173.
- Gloer U & Wiss O (1958) The biosynthesis of ubiquinone. *Experientia* **14**, 410–411.
- Marchal D, Boireau W, Laval JM, Moiroux J & Bourdillon C (1998) Electrochemical measurement of

- lateral diffusion coefficients of ubiquinones and plastoquinones of various isoprenoid chain lengths incorporated in model bilayers. *Biophys J* **74**, 1937–1948.
- 7 Tzagoloff A & Dieckmann CL (1990) PET genes of *Saccharomyces cerevisiae*. *Microbiol Rev* **54**, 211–225.
 - 8 Tran UC & Clarke CF (2007) Endogenous synthesis of coenzyme Q in eukaryotes. *Mitochondrion*, **7S**, S62–S71.
 - 9 Johnson A, Gin P, Marbois BN, Hsieh EJ, Wu M, Barros MH, Clarke CF & Tzagoloff A (2005) COQ9, a new gene required for the biosynthesis of coenzyme Q in *Saccharomyces cerevisiae*. *J Biol Chem* **280**, 31397–31404.
 - 10 Barros MH, Johnson A, Gin P, Marbois BN, Clarke CF & Tzagoloff A (2005) The *Saccharomyces cerevisiae* *COQ10* gene encodes a START domain protein required for function of coenzyme Q in respiration. *J Biol Chem* **280**, 42627–42635.
 - 11 Cui TZ & Kawamukai M (2009) Coq10, a mitochondrial coenzyme Q binding protein, is required for proper respiration in *Schizosaccharomyces pombe*. *FEBS J* **276**, 748–759.
 - 12 Busso C, Bleicher L, Ferreira-Junior JR & Barros MH (2010) Site-directed mutagenesis and structural modeling of Coq10p indicate the presence of a tunnel for coenzyme Q6 binding. *FEBS Lett* **584**, 1609–1614.
 - 13 Hsieh EJ, Gin P, Gulmezian M, Tran UC, Saiki R, Marbois BN & Clarke CF (2007) *Saccharomyces cerevisiae* Coq9 polypeptide is a subunit of the mitochondrial coenzyme Q biosynthetic complex. *Arch Biochem Biophys* **463**, 19–26.
 - 14 Gin P & Clarke CF (2005) Genetic evidence for a multi-subunit complex in coenzyme Q biosynthesis in yeast and the role of the Coq1 hexaprenyl diphosphate synthase. *J Biol Chem* **280**, 2676–2681.
 - 15 Tauche A, Krause-Buchholz U & Rödel G (2008) Ubi-quinone biosynthesis in *Saccharomyces cerevisiae*: the molecular organization of O-methylase Coq3p depends on Abc1p/Coq8p. *FEMS Yeast Res* **8**, 1263–1275.
 - 16 Soccio RE, Adams RM, Romanowski MJ, Sehayek E, Burley SK & Breslow JL (2002) The cholesterol-regulated StarD4 gene encodes a StAR-related lipid transfer protein with two closely related homologues, StarD5 and StarD6. *Proc Natl Acad Sci USA* **99**, 6943–6948.
 - 17 Magnani T, Soriani FM, Martins VP, Nascimento AM, Tudella VG, Curti C & Uyemura SA (2007) Cloning and functional expression of the mitochondrial alternative oxidase of *Aspergillus fumigatus* and its induction by oxidative stress. *FEMS Microbiol Lett* **271**, 230–238.
 - 18 Wikström MK & Berden JA (1972) Oxidoreduction of cytochrome b in the presence of antimycin. *Biochim Biophys Acta* **283**, 403–420.
 - 19 von Jagow G, Ljungdahl PO, Graf P, Ohnishi T & Trumper BL (1984) An inhibitor of mitochondrial respiration which binds to cytochrome b and displaces quinone from the iron-sulfur protein of the cytochrome bc1 complex. *J Biol Chem* **259**, 6318–6326.
 - 20 Starkov AA & Fiskum G (2001) Myxothiazol induces H2O2 production from mitochondrial respiratory chain. *Biochem Biophys Res Commun* **281**, 645–650.
 - 21 Dröse S & Brandt U (2008) The mechanism of mitochondrial superoxide production by the cytochrome bc1 complex. *J Biol Chem* **283**, 21649–21654.
 - 22 Muller F, Crofts AR and Kramer DM (2002) Multiple Q-cycle bypass reactions at the Qo site of the cytochrome bc1 complex. *Biochemistry* **41**, 7866–7874.
 - 23 Zhang H, Chobot SE, Osyczka A, Wraight CA, Dutton PL & Moser CC (2008) Quinone and non-quinone redox couples in complex III. *J Bioenerg Biomembr* **40**, 493–499.
 - 24 Ashby MN, Kutsunai SY, Ackerman S, Tzagoloff A & Edwards PA (1992) COQ2 is a candidate for the structural gene encoding para-hydroxybenzoate: polyphenyltransferase. *J Biol Chem* **267**, 4128–4136.
 - 25 Nobrega FG, Nobrega MP & Tzagoloff A (1992) BCS1, a novel gene required for the expression of functional Rieske iron–sulfur protein in *Saccharomyces cerevisiae*. *EMBO J* **11**, 3821–3829.
 - 26 St-Pierre J, Buckingham JA, Roebuck SJ & Brand MD (2002) Topology of superoxide production from different sites in the mitochondrial electron transport chain. *J Biol Chem* **47**, 44784–44790.
 - 27 Kowaltowski AJ, Cocco RG, Campos CB & Fiskum G (2002) Effect of Bcl-2 overexpression on mitochondrial structure and function. *J Biol Chem* **277**, 42802–42807.
 - 28 Ruzicka FJ, Beinert H, Schepler KL, Dunham WR & Sands RH (1975) Interaction of ubisemiquinone with a paramagnetic component in heart tissue. *Proc Natl Acad Sci USA* **72**, 2886–2890.
 - 29 Seddiqi N, Meunier B, Lemesle-Meunier D & Brasseur G (2008) Is cytochrome b glutamic acid 272 a quinol binding residue in the bc1 complex of *Saccharomyces cerevisiae*? *Biochemistry* **47**, 2357–2368.
 - 30 Contamine V & Picard M (2000) Maintenance and integrity of the mitochondrial genome: a plethora of nuclear genes in the budding yeast. *Microbiol Mol Biol Rev* **64**, 281–315.
 - 31 Marbois B, Gin P, Gulmezian M & Clarke CF (2009) The yeast Coq4 polypeptide organizes a mitochondrial protein complex essential for coenzyme Q biosynthesis. *Biochim Biophys Acta* **1791**, 69–75.
 - 32 Zhang M, Mileykovskaya E & Dowhan W (2005) Cardiolipin is essential for organization of complexes III and IV into a supercomplex in intact yeast mitochondria. *J Biol Chem* **280**, 29403–29408.
 - 33 Boveris A & Chance B (1973) The mitochondrial generation of hydrogen peroxide. General properties and effect of hyperbaric oxygen. *Biochem J* **134**, 707–716.

- 34 Snyder CH, Gutierrez-Cirlos EB & Trumper BL (2000) Evidence for a concerted mechanism of ubiquinol oxidation by the cytochrome bc₁ complex. *J Biol Chem* **275**, 13535–13541.
- 35 Davidson JF & Schiestl RH (2001) Mitochondrial respiratory electron carriers are involved in oxidative stress during heat stress in *Saccharomyces cerevisiae*. *Mol Cell Biol* **24**, 8483–8489.
- 36 Veal EA, Ross SJ, Malakasi P, Peacock E & Morgan BA (2003) Ybp1 is required for the hydrogen peroxide-induced oxidation of the Yap1 transcription factor. *J Biol Chem* **278**, 30896–30904.
- 37 Monteiro G, Kowaltowski AJ, Barros MH & Netto LE (2004) Glutathione and thioredoxin peroxidases mediate susceptibility of yeast mitochondria to Ca(2+) -induced damage. *Arch Biochem Biophys* **425**, 14–24.
- 38 Giorgio S, Linares E, Ischiropoulos H, Von Zuben FJ, Yamada A & Augusto O (1998) *In vivo* formation of electron paramagnetic resonance-detectable nitric oxide and of nitrotyrosine is not impaired during murine leishmaniasis. *Infect Immun* **66**, 807–814.
- 39 Tzagoloff A, Akai A, Needleman RB & Zulch G (1975) Assembly of the mitochondrial membrane system. Cytoplasmic mutants of *Saccharomyces cerevisiae* with lesions in enzymes of the respiratory chain and in the mitochondrial ATPase. *J Biol Chem* **250**, 8236–8242.
- 40 Herrmann JM, Foelsch H, Neupert W & Stuart RA (1994) Isolation of yeast mitochondria and study of mitochondrial protein translation. In *Cell Biology: A Laboratory Handbook*, Vol. I (Celis JE ed), pp 538–544. Academic Press, San Diego, CA.
- 41 Wittig I, Braun HP & Schägger H (2006) Blue native PAGE. *Nat Protoc* **1**, 418–428.
- 42 Rak M & Tzagoloff A (2009) F1-dependent translation of mitochondrially encoded Atp6p and Atp8p subunits of yeast ATP synthase. *Proc Natl Acad Sci USA* **106**, 18509–18514.

Respiratory and TCA cycle activities affect *S. cerevisiae* lifespan, response to caloric restriction and mtDNA stability

Erich B. Tahara · Kizzy Cezário ·
Nadja C. Souza-Pinto · Mario H. Barros ·
Alicia J. Kowaltowski

Received: 18 May 2011 / Accepted: 27 June 2011 / Published online: 21 July 2011
© Springer Science+Business Media, LLC 2011

Abstract We studied the importance of respiratory fitness in *S. cerevisiae* lifespan, response to caloric restriction (CR) and mtDNA stability. Mutants harboring mtDNA instability and electron transport defects do not respond to CR, while tricarboxylic acid cycle mutants presented extended lifespans due to CR. Interestingly, mtDNA is unstable in cells lacking dihydrolipoyl dehydrogenase under CR conditions, and cells lacking aconitase under standard conditions (both enzymes are components of the TCA and mitochondrial nucleoid). Altogether, our data indicate that respiratory integrity is required for lifespan extension by CR and that mtDNA stability is regulated by nucleoid proteins in a glucose-sensitive manner.

Keywords Aging · Calorie restriction · Mitochondria · Respiration · Yeast · Krebs cycle

Abbreviations

CR	calorie restriction
CLS	chronological lifespan
ETC	mitochondrial electron transport chain
mtDNA	mitochondrial DNA
TCA	tricarboxylic acid
YPD	yeast extract, peptone and glucose (dextrose) media
YPEG	yeast extract, peptone, ethanol and glycerol media

E. B. Tahara · N. C. Souza-Pinto · A. J. Kowaltowski (✉)
Departamento de Bioquímica, Instituto de Química,
Universidade de São Paulo,
Cidade Universitária, Av. Prof. Lineu Prestes, 748,
São Paulo, SP, Brazil 05508-000
e-mail: alicia@iq.usp.br

K. Cezário · M. H. Barros
Departamento de Microbiologia, Instituto de Ciências
Biomédicas, Universidade de São Paulo,
São Paulo, Brazil

Introduction

Aging is a complex, multifactorial, process in which biological systems undergo progressive changes in their metabolic functions, efficiency and behavior over time, generally associated with a decline in stress responses, fertility and, ultimately, increased age-dependent mortality (Kenyon 2001; Jazwinski 2002a, b). The use of simpler systems such as the budding yeast *Saccharomyces cerevisiae* has vastly added to the understanding of the more relevant hallmarks and molecular mechanisms involved in the aging process (Sinclair et al. 1998; Jazwinski 2000a, b; Bitterman et al. 2003; Fabrizio et al. 2005; Piper 2006; Barros et al. 2010).

S. cerevisiae has proven to be a convenient model organism for aging studies, and attracted intense interest after Jiang et al. (2000) and Lin et al. (2000) independently demonstrated that this yeast was responsive to calorie restriction (CR), a dietary intervention capable of increasing the lifespan of a large number of organisms (Fontana et al. 2010). The replicative lifespan of *S. cerevisiae*—i.e., the number of daughter cells generated by a single mother cell—was shown to be significantly enhanced by decreasing the initial glucose content in YPD media from the usual 2.0% to 0.5% (Jiang et al. 2000; Lin et al. 2000; Barros et al. 2010). Subsequent work indicated that this protocol was also capable of increasing chronological lifespan (CLS) in this yeast (Reverter-Branchat et al. 2004; Barros et al. 2004; Smith et al. 2007), or the period of time that a single *S. cerevisiae* cell remains metabolically active when in the stationary growth phase (Müller et al. 1980; MacLean et al. 2001; Fabrizio and Longo 2003).

S. cerevisiae is a Crabtree-positive yeast, capable of simultaneously fermenting and respiring under conditions of high glucose concentration (Gancedo 1998; Klein et al.

1998; Gombert et al. 2001). Interestingly, Oliveira et al. (2008) verified that *Kluyveromyces lactis*, a Crabtree-negative yeast in which respiratory carbon metabolism occurs independently of glucose availability (Schaffrath and Breunig 2000) is not responsive to CR. This gives rise to the idea that the effects of CR may be related to a phenotype promoted by the mitigation of glucose signaling in *S. cerevisiae* (Oliveira et al. 2008).

A characteristic of batch cultures—in which aging studies using yeast are carried out—is the limited availability of substrates. Interestingly, in both standard and CR media, glucose is expected to be exhausted within the first culture day (Goldberg et al. 2009), while *S. cerevisiae* cells remain viable for several weeks (Sinclair et al. 1998; Reverter-Branchat et al. 2004; Fabrizio and Longo 2003). After glucose exhaustion, the remaining substrates present in the initial media, such as aminoacids, and those formed during the metabolism of glucose, such as ethanol, acetic acid and glycerol, can be metabolized only through aerobic pathways (MacLean et al. 2001; Frick and Wittmann 2005). Therefore, respiratory fitness is an expected requirement for *S. cerevisiae* survival during the stationary growth phase (MacLean et al. 2001; Fabrizio and Longo 2003; Samokhvalov et al. 2004). Currently, however, there is little information about the importance of specific aerobic bioenergetic pathways in the chronological aging of *S. cerevisiae*, as well in its responsiveness to CR.

Here we describe the impact of tricarboxylic acid (TCA) cycle and mitochondrial electron transport chain (ETC) components in CLS and the responsiveness to CR in *S. cerevisiae*, since both are determinant for the aerobic utilization of glucose as an energetic substrate. We further verified the role of mitochondrial DNA (mtDNA) stability in these responses because, in this yeast, seven proteins encoded by this genome are involved in mitochondrial electron transport, proton pumping and oxidative phosphorylation (Foury et al. 1998). Our results demonstrate the importance of mtDNA integrity and functionality, as well long-term respiratory ability in *S. cerevisiae* responsiveness to CR. Finally, we uncover a concentration-dependent role of glucose in regulating proteins responsible for maintaining mtDNA integrity in this yeast.

Materials and methods

S. cerevisiae

S. cerevisiae parental cells (WT), *aco1Δ* (Gangloff et al. 1990), *icl1Δ* (Fernández et al. 1992), *kgd1Δ* (Repetto and Tzagoloff 1989), *lpd1Δ* (Dickinson et al. 1986), *sdh1Δ* (Chapman et al. 1992), *mdh1Δ* (McAlister-Henn and Thompson 1987), *cyt1Δ* (Sadler et al. 1984), *atp2Δ*

(Saltzgaber-Muller et al. 1983), *abf2Δ* (Diffley and Stillman 1992; Newman et al. 1996) and ρ^0 mutants used in this study were BY4741 strains (MAT α ; *his3Δ1*; *leu2Δ0*; *met15Δ0*; *ura3Δ0*; Brachmann et al. 1998).

Media and cell culture

Media used for this study were liquid YPD (1.0% yeast extract, 2.0% peptone and 2.0% for standard or 0.5% glucose for CR) or solid YPD (standard liquid YPD supplemented with 2.0% bacteriological agar) and solid YPEG (1.0% yeast extract, 2.0% peptone, 2.0% ethanol, 2.0% glycerol and 2.0% bacteriological agar), sterilized for 20 min at 121 °C. Cell cultures (50–80 mL) were carried out in aseptic cotton-stopped 250 mL Erlenmeyer flasks with continuous orbital shaking at 200 rpm, at 30 °C. The number of pre-growth cells inoculated per mL of fresh media to initiate the cultures was set at $1 \cdot 10^5$ for all strains tested. Differences in colony counts at 16 h and later (as described below) therefore reflect changes in survival. Plates containing solid media were also incubated at 30 °C.

ρ^0 mutant identification, isolation and characterization

S. cerevisiae ρ^0 mutants were obtained spontaneously after growth of WT cells cultured for 20 h in 2.0% liquid YPD. 100 cells were plated onto solid YPD and after 72 h, this plate was replicated onto YPEG, a respiratory-selective medium. After 48 h of incubation, respiratory incompetent colonies were identified and isolated from the YPD plate. The ρ^0 phenotype of selected colonies was confirmed by mating them with *S. cerevisiae* mit⁻ strains containing point mutations in the mitochondrial genes *cox1*, *cob1* and *atp6* (Slonimski and Tzagoloff 1976). After diploid selection based on heterozygous auxotrophy complementations, no reversion of respiratory incompetence was observed after mitotic segregation of the resultant diploids, confirming the ρ^0 phenotype. We then selected one isolated colony and further characterized it by following its growth curve (which did not exhibit pos-diauxic biomass formation) and by monitoring the exhaustion of aerobic metabolites from culture media. The elected ρ^0 mutant was not able to consume glucose-derived aerobic metabolites such as ethanol, acetic acid and glycerol and presented a decreased rate of growth when compared to WT cells (data not shown).

CLS determination

CLS was accessed through colony-forming ability over time. After 16 h and 7, 14, 21 and 28 days of growth, we transferred a 2 mL aliquot from each culture to a sterile

centrifuge conic tube and added 3 mL of sterile ultra-purified distilled water. The suspension was centrifuged for 1 min at $1000 \times g$, 25 °C, and the supernatant was discarded. The washing procedure was repeated. The cells were resuspended in 2 mL of sterile ultra-purified distilled water and the absorbance at 600 nm (Abs_{600}) was determined. Serial dilutions to a final Abs_{600} of 0.2, 0.02, 0.002 and 0.0002 were conducted and 50 µL of the last dilution (containing 100 cells) were added to YPD plates and incubated for 72 h to promote cellular growth, after which the number of colonies was counted (Tahara et al. 2007). Results are indicated as the absolute number of colonies counted, and were not corrected for survival percentages at 16 h, in order to reflect the true differences in behavior of each strain studied.

Long-term respiratory growth capacity

Long-term respiratory growth capacity was determined after 7 days of growth over solid media. *S. cerevisiae* were cultured for 16 h in standard YPD media and the same procedures described above were repeated, substituting a series of final dilutions described above with Abs_{600} of 1.0, 0.1, 0.01, 0.001 and 0.0001. 5 µL of each dilution were added to YPD and YPEG plates.

mtDNA stability

The loss of *S. cerevisiae* mtDNA leads to a lack of respiratory ability (Tzagoloff et al. 1975) and can be accessed through respiratory competence. To do so, YPD plates obtained from CLS determinations were replicated onto YPEG solid media in the manner described above, and the percentage of respiratory-competent or -incompetent colonies (ρ^+ and ρ^0 , respectively) was determined. This determination provides a snapshot of the presence of ρ^0 over time in culture, although it does not determine the cumulative numbers of ρ^0 cells formed during chronological aging. However, it should be noted that ρ^0 cells are capable of surviving extended periods in the absence of added glucose, as demonstrated in Fig. 1, Panel c. Since *lpd1Δ* mutants exhibit marked respiratory incompetence due to the absence of pyruvate and α -ketoglutarate dehydrogenase activities, the YPEG plates where these mutants were replicated contained a layer of the ρ^0 tester strain $\alpha\text{KL14}\rho^0$ cells (Foury and Tzagoloff 1976) previously grown in YPD liquid media for 16 h, in order to provide short-term respiratory ability to the resulting diploids and allow for colony counts after 48 h.

Graph generation and statistical analysis

Graphs were generated and statistical analysis was performed using GraphPad Prism 5.00 software. The results

are expressed as means \pm standard errors. Student's *t*-test (for paired comparisons) or Two-Way ANOVA (for multiple comparisons) were used.

Results

TCA cycle enzymes are not essential for CR effects and long-term respiratory growth capacity in *S. cerevisiae*

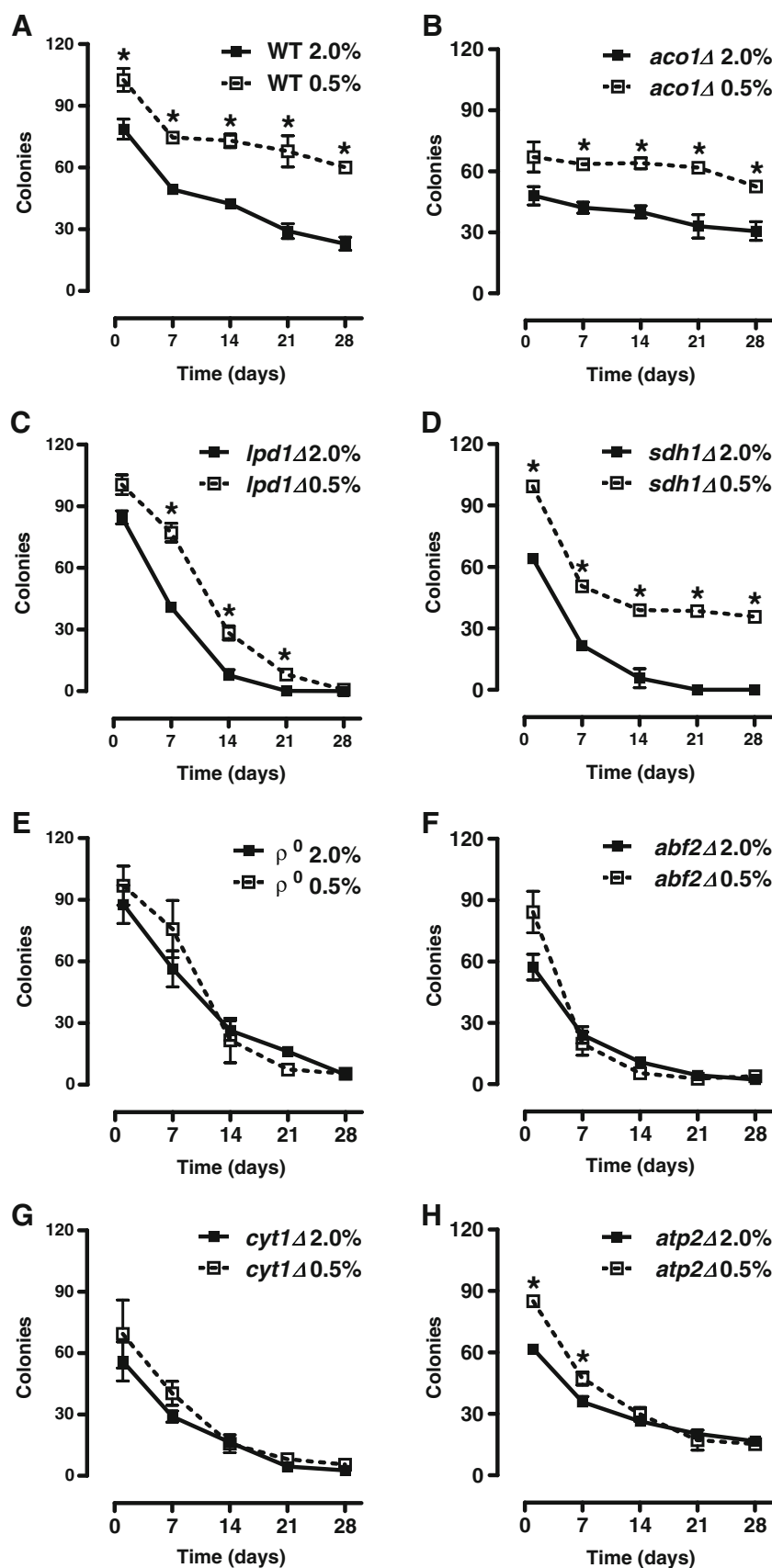
During the diauxic shift, *S. cerevisiae* drastically change the expression of TCA cycle enzymes and components of the mitochondrial electron transport chain (DeRisi et al. 1997). Genes related to aerobic metabolism become derepressed as glucose is consumed, and aerobic metabolism prevails during the stationary phase (MacLean et al. 2001; Fabrizio and Longo 2003; Samokhvalov et al. 2004). In order to evaluate the importance of TCA cycle activity in both CLS and the response to CR, as well in long-term respiratory growth capacity, we selected *S. cerevisiae* mutants harboring inactivations in aconitase (*aco1Δ*), dihydrolipoyl dehydrogenase (*lpd1Δ*)—a subunit of α -ketoglutarate dehydrogenase complex—and the flavoprotein subunit of succinate dehydrogenase (*sdh1Δ*; see Scheme 1).

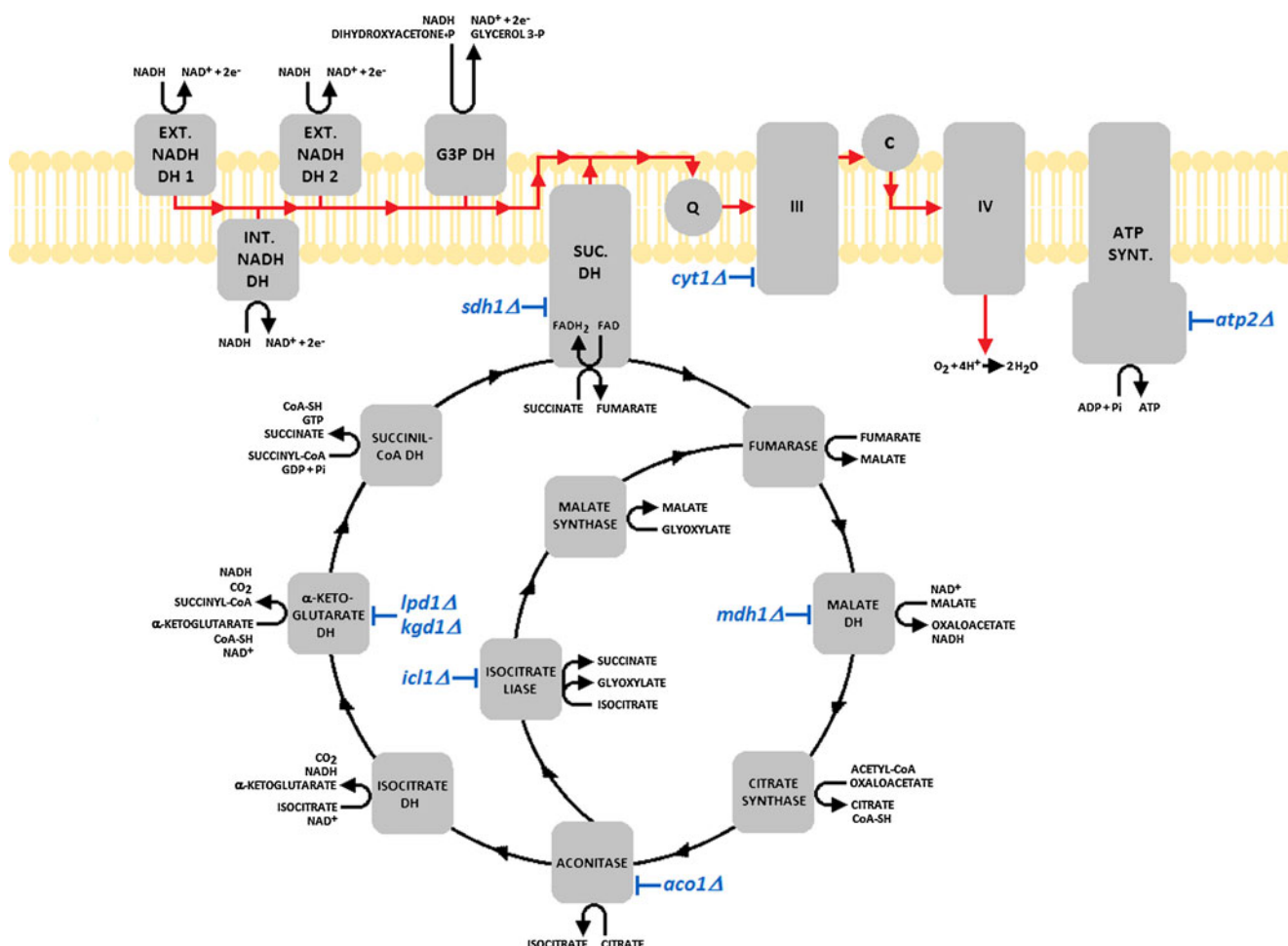
Interestingly, although *lpd1Δ* and *sdh1Δ* mutants presented decreased CLS compared to the WT strain, neither of these mutants had their response to CR affected (Fig. 1, Panels a, c and d). Moreover, *aco1Δ* cell CLS was similar to WT, and also responded to CR (Panel B). In addition, *kgd1Δ* and *mdh1Δ* mutants—lacking α -ketoglutarate and malate dehydrogenase activities—presented statistically significant increases in CLS when cultured under CR conditions (results not shown). *S. cerevisiae* TCA mutants usually show impaired growth in media containing only non-fermentable carbon sources (Tzagoloff and Dieckmann 1990). Probably due to small amounts of TCA intermediates in rich media, NADH and FADH₂ can be slowly generated in the TCA cycle reactions up or downstream of the disruptions, or even during glycolysis and conversion of pyruvate into acetyl-CoA, and oxidized by the intact ETC. Therefore, in long-term incubations, TCA cycle mutants were capable of growing on solid YPEG media, even though they exhibited a lower growth capacity than WT cells (Fig. 2).

Loss of mtDNA suppresses CR-mediated CLS extension and long-term respiratory growth capacity in *S. cerevisiae*

Next, we used ρ^0 and *abf2Δ* mutants to investigate if electron transport chain and ATP synthase integrity were essential toward CR effects. Since seven proteins encoded by *S. cerevisiae* mtDNA are components of the oxidative phosphorylation system, namely cytochrome *c* subunits I, II and III, ATP synthase subunits 7, 8 and 9, and apocyto-

Fig. 1 TCA cycle-deleted, but not respiratory-deficient *S. cerevisiae*, present increased CLS when grown under CR conditions. The colony-forming ability of WT (a), *aco1Δ* (b), *lpd1Δ* (c), *sdh1Δ* (d), ρ^0 (e), *abf2Δ* (f), *cyt1Δ* (g) and *atp2Δ* (h) mutants was assessed after 16 h and 7, 14, 21 and 28 days of culture either under standard (filled squares) or CR conditions (open squares). The number of colonies formed from 100 cells plated onto solid media over time was assessed as CLS, as described in “Materials and Methods”. Panel a: * $p<0.05$ vs. 2.0% WT; Panel b: * $p<0.05$ vs. 2.0% *aco1Δ*; Panel c: * $p<0.05$ vs. 2.0% *lpd1Δ*; Panel h: * $p<0.05$ vs. 2.0% *atp2Δ*





Scheme 1 Aerobic metabolic pathways in *S. cerevisiae* mitochondria. ETC, TCA and glyoxylate cycle components are depicted in grey. Electron transfers are represented in red. Mutants used in this study

are highlighted in blue. C cytochrome *c*; DH dehydrogenase; G3P glycerol 3 phosphate; Q coenzyme Q; Suc succinate

chrome *b* (Foury et al. 1998), mutants lacking mtDNA *per se* or harboring a defect in mtDNA maintenance exhibit substantial impairments in aerobic metabolism. *abf2Δ* cells (defective in the *ars* binding protein, a member of mitochondrial high mobility group of proteins important for mtDNA replication, recombination and stability; Diffley and Stillman 1991, 1992) do not grow in respiratory-selective medium when previously cultured in glucose (Zelenaya-Troitskaya et al. 1995).

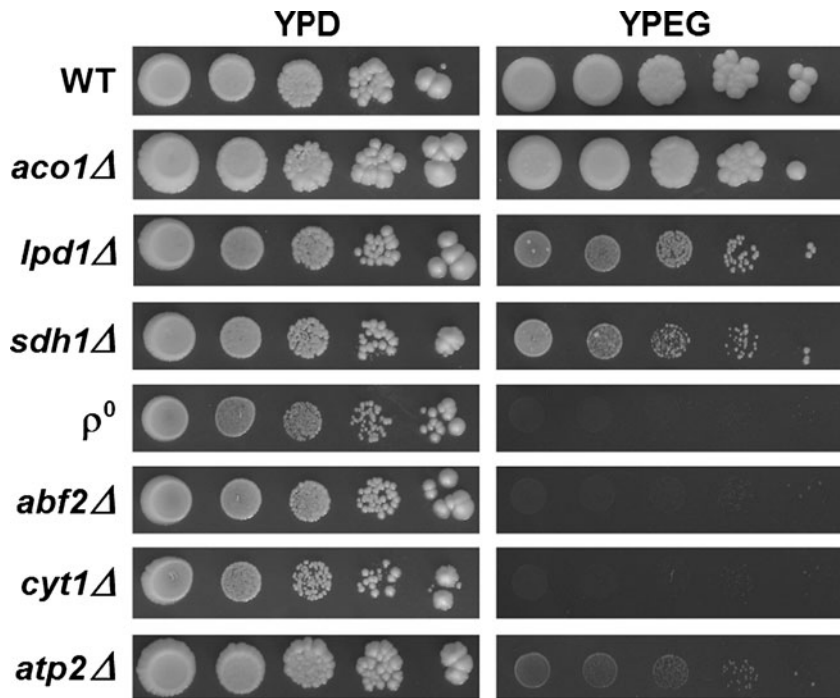
We observed that loss of mitochondrial DNA, either in ρ^0 mutants or due to the *abf2Δ* mutation, which results in the respiration-deficient *petite* phenotype (Kao et al. 1993), completely suppressed the response to CR (Fig. 1, Panels e and f), as well long-term respiratory growth capacity (Fig. 2). These observations directly demonstrate that disruption of mitochondrial electron flow, and the consequences thereof, such as loss of oxidative phosphorylation, mitochondrial membrane potential and protein import impairment (Baker and Schatz 1991; Stuart et al. 1994),

totally abrogate CR-mediated CLS extension in *S. cerevisiae*. In addition, the inability of ρ^0 and *abf2Δ* mutants to maintain long-term respiratory growth under the experimental conditions used here clearly associates mtDNA integrity and maintenance as key features for *S. cerevisiae* aerobic growth in rich media (Fig. 2).

Nuclearly-encoded respiratory chain components are necessary for CR effects and long-term respiratory growth capacity

Mitochondrial functionality requires a concerted interaction between both nuclear and mitochondrial genomes (Linnane et al. 1972; Falkenberg et al. 2007). Since the absence of mtDNA abolishes CR-mediated CLS extension (Fig. 1, Panels e and f) and aerobic growth in respiratory selective media (Fig. 2), we decided to investigate whether the lack of a specific subunit of the ETC encoded by nuclear DNA could promote the same phenotypes. CLS under control and

Fig. 2 Long-term respiratory growth capacity in *S. cerevisiae* mutants. The respiratory capacity of WT and mutant cells was assessed performing serial dilutions. Growth was recorded after 7 days in culture at 30 °C over solid YPD and YPEG media, as described in “Materials and Methods”. The figure is a representative image of at least 4 equal repetitions



CR conditions, and long-term respiratory growth capacity were measured in *cyt1Δ* mutants, which lack cytochrome *c*₁, a component of the multicomplex ubiquinol-cytochrome *c* reductase, the first proton pump in the *S. cerevisiae* ETC (Sidhu and Beattie 1983). We verified that *cyt1Δ* cells do not respond to CR with CLS extension (Fig. 1, Panel g) nor present long-term respiratory growth capacity (Fig. 2). These findings further support the idea that respiratory integrity is essential for CR-mediated lifespan extension, and are in line with our previous results obtained in ρ^0 and *abf2Δ* mutants (Fig. 1).

ATP synthase defects partially abolish the response to CR and long-term respiratory growth ability in *S. cerevisiae*

Our results so far indicate that integrity of the ETC is required for CR effects in CLS extension (Fig. 1, Panels e, f and g; Fig. 2). However, ρ^0 cells also present defects in the ATP synthase (Foury et al. 1998). Thus, we tested whether *atp2Δ* mutants, which lack the β -subunit of F₁ in F₁F_O ATP synthase (Saltzgaber-Muller et al. 1983), respond to CR in a similar fashion. We observed that CR significantly increased cellular viability only up to the 7th day of culture in these mutants. From the 14th day on, CLS did not vary significantly between control and CR cells (Fig. 1, Panel h). Furthermore, *atp2Δ* mutants also presented the lowest long-term respiratory growth capacity between all mutants that exhibited positive growth in YPEG (Fig. 2).

mtDNA stability is dependent on initial glucose concentrations

While conducting CLS experiments using the mutants described above, we noticed that these strains presented different tendencies to form spontaneous *petite* colonies, almost exclusively related to mtDNA instability (Linnane et al. 1989; Ferguson and von Borstel 1992). We thus further determined the percentage of respiratory-competent (ρ^+) colonies in *aco1Δ* and *lpd1Δ* mutants cultured in standard and CR conditions over time, since both aconitase and dihydrolipoyl dehydrogenase have dual roles as TCA cycle enzymes and structural components of mitochondrial nucleoids in *S. cerevisiae* (Chen et al. 2005). These nucleoproteic structures, formed by the interaction between double-stranded DNA and packaging proteins (Rickwood et al. 1981), promote physical stability and functionality to the mitochondrial genome (Rickwood et al. 1981; Miyakawa et al. 1984; Newman et al. 1996; Brewer et al. 2003; Chen et al. 2005). The number of ρ^+ colonies was assessed by replicating the YPD solid plates from CLS determinations onto YPEG, as described in “Materials and Methods”.

Although there is no significant difference in the percentage of ρ^+ colonies between standard and CR conditions in WT cells and in *aco1Δ* mutants, we observed an increased percentage of ρ^+ colonies as the culture time advances (Fig. 3, Panels a and b). This is probably due to the loss of ρ^0 cells replicating in the absence of fermentative substrates; since ρ^0 cells do not exhibit significantly

different mortality rates from WT cells until the 14th day of culture (Fig. 1), and WT cells present ethanol-supported growth but ρ^0 mutants do not, we infer that the number of these mutants in batch cultures becomes proportionally reduced as culture times advance.

Interestingly, culture condition was a determinant factor for mtDNA stability in *lpd1Δ* mutants, which exhibited a higher percentage of ρ^+ colonies during the early culture days, when in standard media (Fig. 3, Panel c). *lpd1Δ* mutants cultured under CR conditions also showed a significant decrease in mtDNA stability when compared to WT cells during the early culture days. Finally, *aco1Δ* cells cultured under standard conditions present lower ρ^+ counts relative to WT at the 1st day of culture (Fig. 3, Panel b).

Taken together, these results indicate that, under standard culture conditions, aconitase is a determinant player in *S. cerevisiae* mtDNA stability when glucose is still present in the media [glucose from both standard and CR culture media is exhausted within the first day (Goldberg et al. 2009)]. On the other hand, dihydrolipoyl dehydrogenase, under CR, is necessary to promote this same phenotype both before and after glucose exhaustion.

Discussion

Although respiratory metabolism plays a central role in *S. cerevisiae* lifespan and is involved in the beneficial effects of CR (MacLean et al. 2001; Fabrizio and Longo 2003; Samokhvalov et al. 2004), little is known about the role in aging of specific oxidative metabolism components. As a result, we evaluated the separate roles of the TCA cycle, electron transport chain and the ATP synthase in CLS and its response to CR.

We measured CLS in a series of TCA and ETC mutants, and verified if there is a correlation between long-term respiratory fitness and CLS extension due to CR. As expected, most of these metabolic mutants have lower

CLS than WT cells (Fig. 1). We observed distinct responses relative to respiratory deficiency phenotypes: TCA cycle mutants (*aco1Δ*, *lpd1Δ* and *sdh1Δ*) were capable of growing in respiratory selective-media, while cells lacking mtDNA (ρ^0) or exhibiting marked mitochondrial genome instability (*abf2Δ*) were not (Fig. 2). In fact, mtDNA encodes several proteins required for respiratory fitness in *S. cerevisiae*, and its functional impairment completely abolishes respiratory growth (Tzagoloff et al. 1975). On the other hand, TCA cycle components are not crucial for growth in YPEG (Fig. 2), since this medium contains TCA intermediates, and reduced NAD and FAD can be reoxidized by the ETC in their absence. Interestingly, all TCA cycle mutants studied here also responded to CR with CLS extension (Fig. 1), an effect not observed in ρ^0 , *abf2Δ* mutants or *cyt1Δ* cells (Fig. 1). Furthermore, although enzymes from the glyoxylate cycle are activated during CLS (Samokhvalov et al. 2004), this pathway is not required for a response to CR, as indicated by experiments using *icl1Δ* cells (deficient in isocitrate lyase), which also present enhanced CLS when cultured under CR conditions (results not shown). Another mutant in which these respiratory activity and CLS correlate is *atp2Δ*, which grows very poorly in respiratory media and responds marginally to CR. The lack of ATP synthase activity does not energetically impair cells in the logarithmic growth phase, when *S. cerevisiae* rely on glycolysis to generate the bulk of their ATP, but may be important for mitochondrial protein import and ATP generation in the stationary phase (Baker and Schatz 1991; Stuart et al. 1994). Thus, a strong correlation between CR responsiveness in CLS and ability to exhibit long-term respiratory growth is evident.

Interestingly, although our results indicate that the ability to metabolize respiratory substrates through a functional electron transport chain is required for the beneficial effects of CR in CLS, previous results show that respiratory mutants may exhibit enhanced replicative life span when cultured under CR conditions (Kaeberlein et al. 2005; Lin

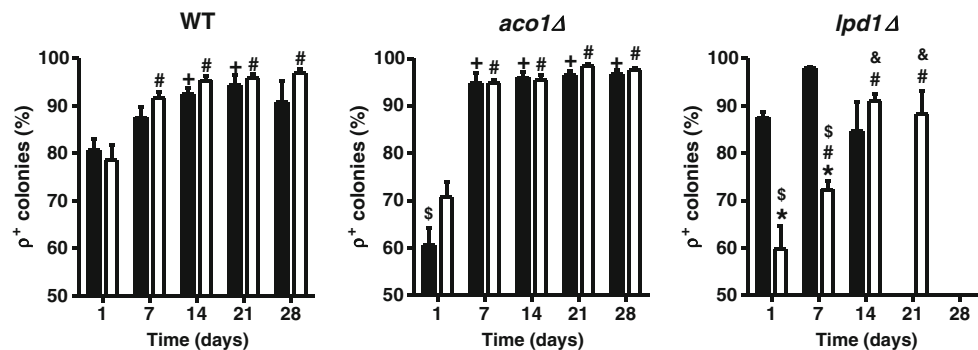


Fig. 3 mtDNA stability is modulated by aconitase and dihydrolipoyl dehydrogenase in a glucose-sensitive manner. The percentage of ρ^+ colonies from WT, *aco1Δ* and *lpd1Δ* cells was assessed over time, as

described in “Materials and Methods”. ${}^{\#}p<0.05$ vs. 16 h 0.5%; ${}^{+}p<0.05$ vs. 16 h 2.0%; $*p<0.05$ vs. time-matched 2.0%; ${}^{\$}p<0.05$ vs. WT, $&p<0.05$ vs. 7 days

and Guarente 2006). This demonstrates that despite many similar properties of RLS and CLS, some conditions affect each aspect of yeast lifespan differently (Barea and Bonatto 2009; Barros et al. 2010). ETC integrity is strongly dependent on the stability of mtDNA, since it encodes for key components of the respiratory chain (Foury et al. 1998). mtDNA differs from nuclear DNA, as it (i) lacks protective histones, (ii) has different repair mechanisms (Lipinski et al. 2010) and (iii) presents mutagenesis rates of 10^{-1} to 10^{-3} , against 10^{-7} to 10^{-8} , for nuclear DNA mutation rates (Linnane et al. 1989; Ferguson and von Borstel 1992). Interestingly, mtDNA is physically associated with mitochondrial proteins, most of which have primary metabolic functions, forming a nucleoproteic complex known as nucleoid (Rickwood et al. 1981; Chen et al. 2005). Recent studies have focused on specific nucleoid proteins such as aconitase, suggesting these may participate in the maintenance of mtDNA stability, in addition to their well-established metabolic roles (Chen et al. 2005). Here, we further dissect the role of nucleoid proteins in mtDNA stability in *S. cerevisiae* by showing that the lack of aconitase and dihydrolipoyl dehydrogenase affect mtDNA stability differently depending on culture conditions (Fig. 3). In the early stages of the cultures, when glucose is still present, *aco1Δ* cells present fewer ρ^+ colonies, indicating that aconitase is important to maintain mtDNA stability in the presence of glucose. On the other hand, *lpd1Δ* cells cultured under CR conditions present high mtDNA instability, indicating that dihydrolipoyl dehydrogenase is important for mtDNA maintenance under low glucose culture conditions. Dihydrolipoyl dehydrogenase is also important for mtDNA stability in the early stages of the aging process, as indicated by low quantities of ρ^+ *lpd1Δ* cells at 7 days of culture under CR. Overall, we provide support for the finding that the metabolic state of *S. cerevisiae* may remodel the nucleoid, thus changing mtDNA stability (Kucej et al. 2008).

Although results using *S. cerevisiae* as a model organism cannot be immediately extended to more complex life forms, some parallels with aging studies in animals have already been demonstrated. For example, CR has been shown to increase maximal respiratory capacity in rodents by promoting mitochondrial biogenesis (Nisoli et al. 2005; López-Lluch et al. 2006; Cerqueira et al. 2011), an effect also observed in other animal models with enhanced lifespans such as fat-specific insulin knockout mice (Katic et al. 2007). Furthermore, the accumulation of lesions to mtDNA leads to premature aging (Trifunovic et al. 2004).

Overall, we demonstrate using *S. cerevisiae* as a model system that mtDNA and electron transport integrity are essential for CR-mediated CLS extension while, surprisingly, TCA and glyoxylate cycle activity are not. Interestingly, CR itself impacts mtDNA maintenance, since the levels of

glucose in the media differentially affect the roles of two nucleoid proteins, aconitase and dihydrolipoyl dehydrogenase, in maintaining mtDNA stability. These results strengthen the idea that CR, respiratory activity and mtDNA integrity are key players in the aging process.

Acknowledgements The authors would like to thank Dr. Luis Eduardo Soares Netto and Simone Vidigal Alves for the kind donation of *S. cerevisiae* mutants and Dr. José Ribamar dos Santos Ferreira Júnior for stimulating and highly helpful discussions. We are also indebted with Camille Cristine Caldeira Ortiz, Edson Alves Gomes and Doris Dias de Araújo for excellent technical assistance. This work was supported by grants from the Fundação de Amparo à Pesquisa do Estado de São Paulo (FAPESP), Conselho Nacional de Desenvolvimento Científico e Tecnológico (CNPq), Instituto Nacional de Ciência e Tecnologia de Processos Redox em Biomedicina (INCT Redoxoma) and The John Simon Guggenheim Memorial Foundation. EBT and KC are supported by FAPESP and CNPq fellowships, respectively.

References

- Baker KP, Schatz G (1991) Nature 349:205–208
- Barea F, Bonatto D (2009) Mech Ageing Dev 130:444–460
- Barros MH, Bandy B, Tahara EB, Kowaltowski AJ (2004) J Biol Chem 279:49883–49888
- Barros MH, da Cunha FM, Oliveira GA, Tahara EB, Kowaltowski AJ (2010) Mech Ageing Dev 131:494–502
- Bitterman KJ, Medvedik O, Sinclair DA (2003) Microbiol Mol Biol Rev 67:376–399
- Brachmann CB, Davies A, Cost GJ, Caputo E, Li J, Hieter P, Boeke JD (1998) Yeast 14:115–132
- Brewer LR, Friddle R, Noy A, Baldwin E, Martin SS, Corzett M, Balhorn R, Baskin RJ (2003) Biophys J 85:2519–2524
- Cerdeira FM, Laurindo FR, Kowaltowski AJ (2011) PLoS One 31: e18433
- Chapman KB, Solomon SD, Boeke JD (1992) Gene 118:131–136
- Chen XJ, Wang X, Kaufman BA, Butow RA (2005) Science 307:714–717
- DeRisi JL, Iyer VR, Brown PO (1997) Science 278:680–686
- Dickinson JR, Roy DJ, Dawes IW (1986) Mol Gen Genet 204:103–107
- Diffley JF, Stillman B (1991) Proc Natl Acad Sci USA 88:7864–7868
- Diffley JF, Stillman B (1992) J Biol Chem 267:3368–3374
- Fabrizio P, Longo VD (2003) Aging Cell 2:73–81
- Fabrizio P, Li L, Longo VD (2005) Mech Ageing Dev 126:11–16
- Falkenberg M, Larsson NG, Gustafsson CM (2007) Annu Rev Biochem 76:679–699
- Ferguson LR, von Borstel RC (1992) Mutat Res 265:103–148
- Fernández E, Moreno F, Rodicio R (1992) Eur J Biochem 204:983–990
- Fontana L, Partridge L, Longo VD (2010) Science 328:321–326
- Foury F, Tzagoloff A (1976) Eur J Biochem 68:113–119
- Foury F, Roganti T, Lecrenier N, Purnelle B (1998) FEBS Lett 440:325–331
- Frick O, Wittmann C (2005) Microb Cell Fact 4:30
- Gancedo JM (1998) Yeast carbon catabolite repression. Microbiol Mol Biol Rev 62:334–361
- Gangloff SP, Marguet D, Lauquin GJ (1990) Mol Cell Biol 10:3551–3561
- Goldberg AA, Bourque SD, Kyryakov P, Gregg C, Boukh-Viner T, Beach A, Burstein MT, Machkalyan G, Richard V, Rampersad S, Cyr D, Milijevic S, Titorenko VI (2009) Exp Gerontol 44:555–571

- Gombert AK, Moreira dos Santos M, Christensen B, Nielsen J (2001) *J Bacteriol* 183:1441–1451
- Jazwinski SM (2002a) *Exp Gerontol* 37:1141–1146
- Jazwinski SM (2002b) *Annu Rev Microbiol* 56:769–792
- Jiang JC, Jaruga E, Repnevskaya MV, Jazwinski SM (2000) *FASEB J* 14:2135–2147
- Kaeberlein M, Hu D, Kerr EO, Tuchiya M, Westman EA, Dang N, Fields S, Kennedy BK (2005) *PLoS Genet* 1:e69
- Kao LR, Megraw TL, Chae CB (1993) *Proc Natl Acad Sci USA* 90:5598–5602
- Katic M, Kennedy AR, Leykin I, Norris A, McGettrick A, Gesta S, Russell SJ, Bluhm M, Maratos-Flier E, Kahn CR (2007) *Aging Cell* 6:827–839
- Kenyon C (2001) *Cell* 105:165–168
- Klein CJ, Olsson L, Nielsen J (1998) *Microbiology* 144:13–24
- Kucej M, Kucejova B, Subramanian R, Chen XJ, Butow RA (2008) *J Cell Sci* 121:1861–1868
- Lin SJ, Guarente L (2006) *PLoS Genet* 2:e33
- Lin SJ, Defossez PA, Guarente L (2000) *Science* 289:2126–2128
- Linnane AW, Haslam JM, Lukins HB, Nagley P (1972) *Annu Rev Microbiol* 26:163–198
- Linnane AW, Marzuki S, Ozawa T, Tanaka M (1989) *Lancet* 25:642–645
- Lipinski KA, Kaniak-Golik A, Golik P (2010) *Biochim Biophys Acta* 1797:1086–1098
- López-Lluch G, Hunt N, Jones B, Zhu M, Jamieson H, Hilmer S, Cascajo MV, Allard J, Ingram DK, Navas P, de Cabo R (2006) *Proc Natl Acad Sci USA* 103:1768–1773
- MacLean M, Harris N, Piper PW (2001) *Yeast* 18:499–509
- McAlister-Henn L, Thompson LM (1987) *J Bacteriol* 169:5157–5166
- Miyakawa I, Aoi H, Sando N, Kuroiwa T (1984) *J Cell Sci* 66:21–38
- Müller I, Zimmermann M, Becker D, Flömer M (1980) *Mech Ageing Dev* 12:47–52
- Newman SM, Zelenaya-Troitskaya O, Perlman PS, Butow RA (1996) *Nucleic Acids Res* 24:386–393
- Nisoli E, Tonello C, Cardile A, Cozzi V, Bracale R, Tedesco L, Falcone S, Valerio A, Cantoni O, Clementi E, Moncada S, Carruba MO (2005) *Science* 310:314–317
- Oliveira GA, Tahara EB, Gombert AK, Barros MH, Kowaltowski AJ (2008) *J Bioenerg Biomembr* 40:381–388
- Piper PW (2006) *Yeast* 23:215–226
- Repetto B, Tzagoloff A (1989) *Mol Cell Biol* 9:2695–2705
- Reverter-Branchat G, Cabisco E, Tamarit J, Ros J (2004) *J Biol Chem* 279:31983–31989
- Rickwood D, Chambers JA, Barat M (1981) *Exp Cell Res* 133:1–13
- Sadler I, Suda K, Schatz G, Kaudewitz F, Haid A (1984) *EMBO J* 3:2137–2143
- Saltzgaber-Muller J, Kunapuli SP, Douglas MG (1983) *J Biol Chem* 258:11465–11470
- Samokhvalov V, Ignatov V, Kondrashova M (2004) *Biochimie* 86:39–46
- Schafffrath R, Breunig KD (2000) *Fungal Genet Biol* 30:173–190
- Sidhu A, Beattie DS (1983) *J Biol Chem* 258:10649–10656
- Sinclair D, Mills K, Guarente L (1998) *Annu Rev Microbiol* 52:533–560
- Slonimski PP, Tzagoloff A (1976) *Eur J Biochem* 61:27–41
- Smith DL Jr, McClure JM, Matecic M, Smith JS (2007) *Aging Cell* 6:649–662
- Stuart RA, Gruhler A, van der Klei I, Guiard B, Koll H, Neupert W (1994) *Eur J Biochem* 220:9–18
- Tahara EB, Barros MH, Oliveira GA, Netto LE, Kowaltowski AJ (2007) *FASEB J* 21:274–283
- Trifunovic A, Wredenberg A, Falkenberg M, Spelbrink JN, Rovio AT, Bruder CE, Bohlooly-Y M, Gidlöf S, Oldfors A, Wibom R, Törnell J, Jacobs HT, Larsson NG (2004) *Nature* 429:417–423
- Tzagoloff A, Dieckmann CL (1990) *Microbiol Rev* 54:211–225
- Tzagoloff A, Akai A, Needleman RB (1975) *J Biol Chem* 250:8236–8242
- Zelenaya-Troitskaya O, Perlman PS, Butow RA (1995) *EMBO J* 14:3268–3276

SÚMULA CURRICULAR

DADOS PESSOAIS

Nome: Erich Birelli Tahara

Local e data de nascimento: Mogi das Cruzes, 5 de fevereiro de 1980.

1.EDUCAÇÃO

Colégio Bandeirantes de Mogi das Cruzes, Mogi das Cruzes, 1997.

Universidade de São Paulo, São Paulo, 2006.

Farmacêutico-Bioquímico.

2.OCUPAÇÃO

Bolsista de Doutorado da Fundação de Amparo à Pesquisa do Estado de São Paulo, de Novembro de 2006 a Outubro de 2011.

3.PUBLICAÇÕES (Artigos Completos e Resumos em Congressos)

ARTIGOS

Tahara, E.B.; Cezário, K.; Souza-Pinto, N.C.; Barros, M.H.; Kowaltowski, A.J. (2011) Respiratory and TCA cycle activities affect *S. cerevisiae* lifespan, response to caloric restriction and mtDNA stability. *J. Bioenerg. Biomembr.* **43**:483-491.

Busso, C., Tahara, E.B., Ogușcu, R., Augusto, O., Ferreira-Junior, J.R., Tzagoloff, A., Kowaltowski, A.J., Barros, M.H. (2010) *Saccharomyces cerevisiae* coq10 null mutants are responsive to antimycin A. *FEBS J.* **277**:4530-4538.

Schuck, P.F., Ferreira, G., Tahara, E.B., Klamt, F., Kowaltowski, A.J., Wajner, M. (2010) cis-4-decenoic acid provokes mitochondrial bioenergetic dysfunction in rat brain. *Life Sci.* **87** 139-146.

Barros, M.H., da Cunha, F.M., Oliveira, G.A., Tahara, E.B., Kowaltowski, A.J. (2010) Yeast as a model to study mitochondrial mechanisms in ageing. *Mech. Ageing Dev.* **131**:494-502.

Tahara, E.B.; Navarete, F.D.T.; Kowaltowski, A.J. (2009) Tissue-, substrate-, and site-specific characteristics of mitochondrial reactive oxygen species generation. *Free Rad. Biol. Med.* **46**: 1283-1297.

Oliveira, G.A.; Tahara, E. B.; Gombert, A.K.; Barros, M.H.; Kowaltowski, A.J. (2008) Increased aerobic metabolism is essential for the beneficial effects of caloric restriction on yeast life span. *J. Bioenerg. Biomembr.* **40**:381-388.

Tahara, E.B.; Oliveira, G.A.; Barros, M.H.; Netto, L.E.S.; Kowaltowski, A.J. (2007) Dihydrolipoyl dehydrogenase as a source of reactive oxygen species inhibited by caloric restriction and involved in *Saccharomyces cerevisiae* aging. *FASEB J.* **21**:274-283.

Barros, M.H.; Bandy, B.; Tahara, E.B.; Kowaltowski, A.J. (2004) Higher Respiratory Activity Decreases Mitochondrial Reactive Oxygen Release and Increases Life Span in *Saccharomyces cerevisiae*. *J. Biol. Chem.* **279**:49883-49888.